

Report Number CCEER-08-02

**Seismic Time History Analysis  
And Instrumentation of the  
Galena Creek Bridge**

Michael S. Taylor  
David H. Sanders

---

**Center for Civil Engineering Earthquake Research**  
Department of Civil Engineering/258  
University of Nevada  
Reno, NV 89557

April 2008

## **Acknowledgements**

This report is based on a Master's Thesis research project funded by the Nevada Department of Transportation (NDOT). The conclusions and recommendations presented in this report are those of the authors only and should not be construed to be endorsed by NDOT.

The authors wish to thank NDOT engineers Troy Martin, Bernard Ponte, and Cole Mortensen for their assistance throughout the duration of this project.

The authors would also like to give acknowledgement to the numerous hours and assistance provided by Patrick Laplace and Paul Lucas of the University of Nevada, Reno's Department of Civil & Environmental Engineering.

Numerous others provided their time and expertise throughout the duration of this project, including Hilliard Bond and Raul Vega of Parsons Corporation; Kevin Almer and Eric Monzon, Ph.D candidates at the University of Nevada, Reno; and Professors Ian Buckle and John Anderson of the University of Nevada, Reno.

## Abstract

The behavior of complex and irregular structures during construction and in a seismic event is often not well understood by practicing design engineers. The focus of this research is centered around a comprehensive examination of the Galena Creek Bridge, both during construction and under seismic loading. The original arch design of the Galena Creek Bridge featured an innovative steel pilot truss, which supported the arch during construction and supplied the supporting framework for concrete casting. To examine its behavior during construction, an instrumentation plan was developed that consisted of a series of strain gages attached to the pilot truss, conventional arch reinforcing, and embedded in the pilot truss grout and arch concrete. The instrumentation plan allows researchers to monitor the arch in real-time through the construction sequence. The instrumentation plan also featured accelerometers attached to the arch frame to monitor the response of the structure to dynamic loading.

To further understand the behavior of the structure to earthquake loading, a non-linear time history analysis of the structure was performed, and then compared to traditional elastic response spectrum techniques. Peak structure displacements, moments, and base shears formed the basis for the comparison. Seismology experts were consulted to select seven acceleration time histories from earthquake records with similar seismology as the active faults located near the Galena Creek Bridge. Recommendations by the Federal Emergency Management Agency (FEMA) were used to scale the seven earthquake acceleration records which were used for the non-linear time history analysis.

The results of the analysis show reasonable agreement between the non-linear time history analysis and the elastic response spectrum analysis. With the proper selection of input ground motions, the non-linear time history analysis is effective as a performance-based evaluation tool for better understanding global bridge behavior and interactions.

## Table of Contents

<b>Chapter 1</b>	<b>Introduction</b>	<b>1</b>
1.1	Introduction	1
1.2	Research Scope and Goals	2
1.3	Bridge Background Information	2
<b>Chapter 2</b>	<b>Design and Description of the Galena Creek Bridge</b>	<b>5</b>
2.1	Basic Design	5
2.2	Design Criteria	5
2.3	Columns	5
2.4	Arch	6
2.5	Superstructure	7
2.6	Abutments	8
2.7	Hinges	8
2.8	Prestressing	9
2.9	Link Slab, Link Beams	9
2.10	Construction Sequence	10
<b>Chapter 3</b>	<b>Instrumentation</b>	<b>11</b>
3.1	Instrumentation Introduction	11
3.2	Instrumentation Overview	11
3.2.1	Layout	12
3.2.2	Truss Instrumentation	12
3.2.3	Concrete Instrumentation	13
3.2.4	Data Acquisition System	14
3.2.4	Installation	14
3.2.5	Seismic Instruments	15
3.3	Revised Instrumentation Plan	15
<b>Chapter 4</b>	<b>Seismic Time History Analysis Modeling</b>	<b>16</b>
4.1	AASHTO Standard Specifications	16
4.2	UNR Seismic Analysis	17
4.2.1	Scope	17
4.2.2	Acceleration Time History Selection and Scaling	17
4.2.3	Boundary Conditions and Modeling Considerations	20
4.2.4	Moment-Curvature Analysis	22
4.2.5	Time History Analysis	25
4.2.6	Elastic Analysis	26
<b>Chapter 5</b>	<b>Analysis Comparison</b>	<b>28</b>
5.1	Basis of Analysis Comparison	28
5.2	Modal Analysis	28
5.3	Analysis Results	29

5.3.1	Analysis Results, 475-Year Earthquake	29
5.3.1.1	Transverse Structure Response	29
5.3.1.2	Longitudinal Structure Response	31
5.3.2	Analysis Results, 2500-Year Earthquake	32
5.3.2.1	Transverse Structure Response	32
5.3.2.2	Longitudinal Structure Response	33
5.4	Analysis Discussion	34
5.4.1	Transverse Response	34
5.4.2	Longitudinal Response	36
5.5	Conclusions	39
<b>Chapter 6</b>	<b>Summary and Conclusions</b>	<b>42</b>
6.1	Summary of Report	42
6.2	Conclusions	43
	<b>REFERENCES</b>	<b>45</b>
	<b>TABLES</b>	<b>47</b>
	<b>FIGURES</b>	<b>63</b>
	<b>LIST OF CCEER PUBLICATIONS</b>	<b>125</b>

## List of Tables

### Chapter 4

4-1	Seismic Performance Category Based on Acceleration and Importance Classification	47
4-2	Site Soil Coefficients	47
4-3	AASHTO Response Modification Factors for Select Components	47
4-4	Selected Ground Motions	48
4-5	Scale Factors, 10% Probability of Exceedance in 50 Years	48
4-6	Scale Factors, 2% Probability of Exceedance in 50 Years	48
4-7	Abutment and Hinge Gap Openings (mm) at 21°C	49
4-8	Column Plastic Hinge Lengths (Paulay and Priestley)	49

### Chapter 5

5-1	Modal Periods and Mass Participation Ratios	50
5-2	Transverse Displacement Summary (475-Year EQ)	51
5-3	Transverse Base Shear Summary (475-Year EQ)	51
5-4	Transverse Moment Summary, Northbound Structure (475-Year EQ)	52
5-5	Transverse Moment Summary, Southbound Structure (475-Year EQ)	53
5-6	Longitudinal Displacement Summary (475-Year EQ)	54
5-7	Longitudinal Base Shear Summary (475-Year EQ)	54
5-8	Longitudinal Moment Summary, Northbound Structure (475-Year EQ)	55
5-9	Longitudinal Moment Summary, Southbound Structure (475-Year EQ)	56
5-10	Transverse Displacement Summary (2500-Year EQ)	57
5-11	Transverse Base Shear Summary (2500-Year EQ)	57
5-12	Transverse Moment Summary, Northbound Structure (2500-Year EQ)	58
5-13	Transverse Moment Summary, Southbound Structure (2500-Year EQ)	59
5-14	Longitudinal Displacement Summary (2500-Year EQ)	60
5-15	Longitudinal Base Shear Summary (2500-Year EQ)	60
5-16	Longitudinal Moment Summary, Northbound Structure (2500-Year EQ)	61
5-17	Longitudinal Moment Summary, Southbound Structure (2500-Year EQ)	62

## List of Figures

### Chapter 2

2-1	Overview of Galena Creek Bridge	63
2-2	Typical Column Section	64
2-3	Construction Sequence Figure 1	65
2-4	Construction Sequence Figure 2	66
2-5	Original Arch Section (Typical)	67
2-6	Concrete Arch Segment Layout	68
2-7	New Arch Cross Section (Typical)	69
2-8	Typical Superstructure Section	70
2-9	Hinge Restrainer Layout and Typical Section	71
2-10	Frame 1 Longitudinal Post-Tensioning	72
2-11	Frame 2 Longitudinal Post-Tensioning	73
2-12	Frame 3 Longitudinal Post-Tensioning	74
2-13	Transverse Post Tensioning Detail	75
2-14	Link Slab and Link Beam Detail	76

### Chapter 3

3-1	Instrumentation Locations (Strain Gages)	77
3-2	Pilot Truss Instrumentation	78
3-3	Concrete Strain Gage	78
3-4	Tube Gage View	79
3-5	Concrete Instrumentation	80
3-6	Superstructure Instrumentation Locations	81
3-7	Dynamic Instrumentation Locations	82
3-8	Revised Typical Instrumentation Cross Section	83

### Chapter 4

4-1	AASHTO Elastic Design Spectrum for Galena Creek Bridge	84
4-2	Fault Map in Vicinity of Galena Creek Bridge	84
4-3	Period Range of Interest	85
4-4	Deformed Shape, Fundamental Period of Vibration	86
4-5	Un-scaled Composite Spectrum vs. 475-Year AASHTO Spectrum	87
4-6	SRSS Response Spectrum, Bolu Ground Motion	87
4-7	SRSS Response Spectrum, Duzce Ground Motion	88
4-8	SRSS Response Spectrum,, KJMA Ground Motion	88
4-9	SRSS Response Spectrum,, Denali, Ground Motion	89
4-10	SRSS Response Spectrum, Parkfield Ground Motion	89
4-11	SRSS Response Spectrum, Centro 6 Ground Motion	90
4-12	SRSS Response Spectrum, Centro 7 Ground Motion	90
4-13	10% Probability of Exceedance in 50 Year Composite Spectrum	91
4-14	2% Probability of Exceedance in 50 Year Composite Spectrum	91
4-15	Abutment Cross Section	92
4-16	Sample Hysteretic Abutment Response	93

4-17	Abutment 1 Longitudinal Force-Displacement Model	93
4-18	Abutment 2 Longitudinal Force-Displacement Model	94
4-19	Hinge Restrainer Detail	94
4-20	Hinge 1 Longitudinal Force-Displacement Model	95
4-21	Hinge 2 Longitudinal Force-Displacement Model	95
4-22	Link Beam Model Diagram	96
4-23	Link Slab Model Diagram	96
4-24	Confined Concrete Curve, Column	97
4-25	Confined Concrete Curve, Arch	97
4-26	Moment-Rotation Response, Pier 1 Top, X-Axis Bending	98
4-27	Moment-Rotation Response, Pier 1 Top, Y-Axis Bending	98
4-28	Moment-Rotation Response, Pier 1 Bottom, X-Axis Bending	99
4-29	Moment-Rotation Response, Pier 1 Bottom, Y-Axis Bending	99
4-30	Moment-Rotation Response, Pier 2&3 Top, X-Axis Bending	100
4-31	Moment-Rotation Response, Pier 2&3 Top, Y-Axis Bending	100
4-32	Moment-Rotation Response, Pier 2&3 Bottom, X-Axis Bending	101
4-33	Moment-Rotation Response, Pier 2&3 Bottom, Y-Axis Bending	101
4-34	Moment-Rotation Response, Pier 4 Top, X-Axis Bending	102
4-35	Moment-Rotation Response, Pier 4 Top, Y-Axis Bending	102
4-36	Moment-Rotation Response, Pier 4 Bottom, X-Axis Bending	103
4-37	Moment-Rotation Response, Pier 4 Bottom, Y-Axis Bending	103
4-38	Moment-Rotation Response, Pier 5 Top, X-Axis Bending	104
4-39	Moment-Rotation Response, Pier 5 Top, Y-Axis Bending	104
4-40	Moment-Rotation Response, Pier 5 Bottom, X-Axis Bending	105
4-41	Moment-Rotation Response, Pier 5 Bottom, Y-Axis Bending	105
4-42	Moment-Rotation Response, Pier 6 Top, X-Axis Bending	106
4-43	Moment-Rotation Response, Pier 6 Top, Y-Axis Bending	106
4-44	Moment-Rotation Response, Pier 6 Bottom, X-Axis Bending	107
4-45	Moment-Rotation Response, Pier 6 Bottom, Y-Axis Bending	107
4-46	Moment-Rotation Response, Arch Crown Top, X-Axis Bending	108
4-47	Moment-Rotation Response, Arch Crown Top, Y-Axis Bending	108
4-48	Moment-Rotation Response, Arch Segment 0&0A Bottom, X-Axis Bending	109
4-49	Moment-Rotation Response, Arch Segment 0&0A Bottom, Y-Axis Bending	109
4-50	Flexural Hinge Modeling Diagram	110
4-51	Arch Transverse Displacement History, 2500-Year Centro 6 Ground Motion	110
4-52	Arch Longitudinal Displacement History, 2500-Year Centro 6 Ground Motion	111
4-53	Pier 1 Northbound Longitudinal Moment-Rotation Response, 2500-Year Centro 6 Ground Motion	111
4-54	Pier 1 Northbound Transverse Moment Rotation Response, 2500-Year Centro 6 Ground Motion	112

## Chapter 5

5-1	Longitudinal Abutment Response Comparison Frame 1 Northbound,	113
-----	---	-----

	2500-Year KJMA Ground Motion	
5-2	Longitudinal Abutment Response Comparison, Frame 1 Southbound, 2500-Year KJMA Ground Motion	114
5-3	Longitudinal Moment-Rotation Response, Pier 1 Northbound, 2500-Year KJMA Ground Motion	114
5-4	Longitudinal Moment-Rotation Response, Pier 1 Southbound, 2500-Year KJMA Ground Motion	115
5-5	Moment Time History, Pier 1 Northbound, 2500-Year KJMA Ground Motion	115
5-6	Moment Time History, Pier 1 Southbound, 2500-Year KJMA Ground Motion	116
5-7	Transverse Displacement Comparison, Northbound Structure, 475-Year Earthquake	116
5-8	Transverse Displacement Comparison, Southbound Structure, 475-Year Earthquake	117
5-9	Transverse Displacement History, Pier 3 Northbound & Pier 2 Southbound, 2500-Year Centro 7 Ground Motion	117
5-10	Longitudinal Displacement Comparison, Northbound Structure, 475-Year Earthquake	118
5-11	Longitudinal Displacement Comparison, Southbound Structure, (475-Year Earthquake)	118
5-12	Abutment Displacement Comparison, (Toward Back-wall), 475-Year Earthquake	119
5-13	Moment Time History, (Piers 4&6) vs. Abutment Reaction, Northbound Structure, 475-Year Centro 6 Ground Motion	119
5-14	Abutment Displacement Comparison (Towards Back-wall) 2500-Year Earthquake	120
5-15	Abutment 2 NB Hysteresis Response, 2500-Year Centro 6 Ground Motion	120
5-16	Relative Hinge Displacement Comparison (Towards), 475-Year Earthquake	121
5-17	Relative Hinge Displacement Comparison (Away), 475-Year Earthquake	121
5-18	Peak Non-Linear Displacement vs. Gap Opening Over Time, Hinge 1	122
5-19	Peak Non-Linear Displacement vs. Gap Opening Over Time, Hinge 2	122
5-20	Moment Time History, Crown 2 SB, Comparing Effect of Vertical Acceleration	123
5-21	Moment Time History, Pier 3 Top SB, Comparing Effect of Vertical Acceleration	123
5-22	Moment Time History, Arch Segment 0 SB, Comparing Effect of Vertical Acceleration	124

# Chapter 1

## Introduction

### 1.1. Introduction

The expansion of the I-580 Freeway in northwestern Nevada led to the design of the Galena Creek Bridge, a 525-m reinforced concrete cathedral arch bridge. For practicing engineers, it is important to understand the global behavior of a complex and unique structure such as the Galena Creek Bridge both during construction and in a seismic event.

To help engineers better understand the behavior of the Galena Creek Bridge during construction, an instrumentation plan was developed to monitor the state of stress within the concrete arch during the construction sequence. The original arch design featured a unique steel pilot truss that supports the arch during construction, and is used as a framework for casting the concrete for the arch. Strain gages attached to the steel pilot truss, on conventional reinforcement, and embedded in the concrete would be used to gather data in real-time, allowing engineers to monitor the bridge throughout the duration of construction.

The understanding of the response of bridge structures in a seismic event is of interest to practicing engineers in order to design safe and cost efficient structures. Different methods exist in which the effect of seismic loading on structure response can be accounted for in design and analysis. Modern design codes use simplified methods of analysis to determine seismic forces and displacements. These methods are most generally linear-elastic methods, and do not account for global structure and material nonlinearity.

In the American Association of State and Highway Transportation Officials (AASHTO) Standard Specifications for Highway Bridges, the standard design code for highway structures prior to 2007, response spectrum techniques using modal superposition are used for seismic analysis. Structure response quantities (forces and displacements), are found by using various rules for combining maximum effects due to a spectral acceleration response spectrum. These various earthquake spectra are generated by inputting a acceleration coefficient that corresponds to the location of the structure, and a local site soil profile. Acceleration coefficients are generated for each geographic region based on probabilities of a certain level earthquake happening in a given time period. The AASHTO specifications classify the design earthquake as one with a return period of 475-years, or roughly a 10% probability of exceedance in 50 years. This design level earthquake is intended to prevent collapse of the structure in a large seismic event, and keep the structure operational for emergency vehicles and security/defense purposes (AASHTO, 2002).

With the advance of computers, the technology is now available to perform more in-depth, complicated methods of analysis for use in the design of structures. The Federal Emergency Management Agency (FEMA) provides guidance for other methods of analysis, including non-linear seismic time history analysis. In one such method, acceleration time histories are selected from records representing similar fault characteristics as those near the structure; these records are then applied to the structure

as time-varying acceleration loads. Several time histories are selected, and are scaled based on the design response spectrum. If at least seven time histories are used, the overall design force effects and displacements are found as the average of the response of each time selected time history. In using this method for the seismic design of structures, the effects of structure non-linearity can be accounted for and more realistic force effects and displacements can be determined.

## **1.2. Research Scope and Goals**

The scope and goals of this research project centers around a comprehensive examination of the structural behavior of the Galena Creek Bridge. The original scope of the project revolved around the instrumentation of the southbound concrete arch. The interaction of the unique steel pilot truss, erected to create a self-supporting arch frame, and the concrete arch body presented an interesting research opportunity to understand the interaction of these elements. Through a comprehensive instrumentation plan that detailed strain gages placed in strategic areas on the arch, the state of stress in the arch could be monitored during the construction sequence in real time. Additional aspects of this instrumentation plan included the installation of fifteen accelerometers at various places on the arch frame to capture the response of the structure to dynamic loading.

Due to unforeseen delays in the construction of the Galena Creek Bridge, the installation of the strain gage instrumentation has been trimmed from the scope of this research. Future research will be done to follow through on the instrumentation plan. Delays in construction have yielded an alternative arch design that omits the pilot truss completely; due to the omission of the pilot truss, a simplified instrumentation plan has been proposed that eliminates some gages and adds accelerometers to the arch span of the bridge. The addition of the accelerometers will allow for opportunities to further understand the structural behavior of the structure under seismic loading in conjunction with the strain gages.

To understand and examine the response of the structural to seismic loading, finite element models of the bridge were constructed and a non-linear time history analyses of the bridge was performed. The results of this analysis were then compared to traditional response spectrum techniques and were used to support the placement of the arch accelerometers. Designers can justify these more elaborate methods in special circumstances when dealing with unusual or irregular structures, as well as those structures located near active earthquake faults. The Galena Creek Bridge is a multi-span structure, with a main reinforced concrete arch span. This bridge is also located near a known active fault, making it an excellent candidate for more refined methods of seismic analysis.

## **1.3. Bridge Background Information**

The Galena Creek Bridge is a major component of the State of Nevada's I-580 Freeway Extension Project, currently under construction in Washoe Valley, located to the south of Reno, Nevada. Plans to extend the existing portion of I-580 from the Mt. Rose Highway Interchange to the southern end of Carson City, Nevada, have been in the works since the 1950s. When completed, I-580 will effectively join Reno and Carson City with a six line divided freeway. Major construction on I-580 is divided between two sections;

the northern section stretches from the Mt. Rose Interchange to Bower's Mansion, and the southern section extends from north Carson City to US 50. Portions of the completed freeway will share the existing US 395 alignment through southern Washoe Valley.

The I-580 Freeway Extension Project covers the construction between the Mt. Rose Interchange and Bowers Mansion. Specific project details include the construction of nine new structures, various retaining walls, and a large amount of earthwork and grading. The construction was originally broken down into two main construction packages, so called Package A and Package B. Package A consisted of the construction of the Galena Creek Bridge, the Brown's Creek Bridge, grade separations spanning Parker Ranch Road and St. James Parkway, retaining walls, and rough grading. A technical dispute between the Package A contractor and NDOT regarding wind loading on the Galena Creek Bridge steel pilot truss, ultimately resulted in the termination of the Package A contract. Work left to be completed included the construction of both Galena arches, and minor work on the other three Package A structures. The remaining work was re-bundled into the Package B contract, awarded to Fischer Sand and Gravel in November of 2006. Details of Package B details include the construction of the remaining five bridges including interchanges at Mt. Rose and Bower's Mansion, as well as mass grading and paving along the extent of the new alignment. After termination of the original Package A contract, NDOT proposed modifications to the Galena Creek structure, namely a stiffer pilot truss as well as provisions to allow the contractor to construct the arch on falsework and omit the pilot truss completely.

The original arch design featured a steel-pilot truss, which serves as the supporting framework for the arch during construction. Upon erection of the pilot truss, a concrete traveler form would be used to cast the concrete section. C.C. Myers, subcontractor under Fischer Industries, is the contractor responsible for construction of the I-580 structures. C.C. Myers elected to omit the pilot-truss and to erect the arches using a falsework system supported on temporary fill over Galena Creek. Initial project schedules anticipated finishing the I-580 Freeway Extension project in 2011.

The University of Nevada, Reno was contracted by the Nevada Department of Transportation in 2004 to instrument the southbound Galena Creek Bridge arch to monitor the structure during the construction sequence. Structural monitoring would be live during construction, and would extend for a period of two years during post-construction. The response, as recorded by the instrumentation system, would then be compared to the analytical results that were found during design. The adequacy of the design assumptions could then be verified. In addition to the structural monitoring, accelerometers would be incorporated into the instrumentation to capture the response of structure to transient loading.

As the focus of the research shifted towards the seismic analysis of the Galena Creek Bridge, seismology experts at the University of Nevada, Reno were consulted to select seven acceleration time histories that are considered representative of the active strike/slip fault near the Galena Creek Bridge. Structural modeling of the structure uses moment-curvature backbone curves to represent the plastic-hinging behavior of the substructure components, specifically the reinforced concrete columns and arch. The moment-rotation response of these substructure components use Takeda hysteresis models to account for response degradation to cyclic loading. Gap and hook elements are

used in the expansion joint hinges and abutments to capture the non-linear response of these components. The recommendations found in FEMA 356 are then used to scale the time histories and perform the non-linear time history analysis of the structure. The results of this analysis are then compared to the response spectrum techniques that were used by the bridge designers.

Chapter 2 of this thesis gives a brief description of the Galena Creek Bridge and details of its design. Chapter 3 discusses the instrumentation plan originally developed as the primary scope of this research, as well as the alterations to that plan that have been for the current design of the structure. Chapter 4 discusses in detail the seismic analysis of the bridge, and Chapter 5 provides the results of that analysis. Chapter 6 serves as the summary and conclusions chapter.

## Chapter 2

### Design and Description of the Galena Creek Bridge

#### 2.1. Basic Design

The Galena Creek Bridge is a 525-meter long reinforced concrete cathedral arch bridge (Figure 2-1). The bridge is actually two separate structures, one carrying northbound traffic on I-580, the other carrying southbound traffic. Each structure is seven spans long, with a 200-meter main arch span, roughly 100 meters above Galena Creek. Six single column bents support the bridge superstructure. Two internal hinges 15 meters either side of the arch span divide the structure into three frames. The superstructure of the bridge is a two-cell post-tensioned box girder, featuring a transversely post-tensioned deck.

The original arch design is comprised of a steel-pilot truss, which serves as the frame-work for casting the concrete arch section. Erected first, the pilot-truss is used to support rebar and formwork for casting the concrete arch. Cable-stays extending from adjacent piers help support the pilot truss during the erection sequence. The new arch design is similar to the original design, with the steel pilot-truss being replaced by additional longitudinal reinforcement.

Several different structure types were considered in the design of the Galena Creek Bridge. A reinforced concrete cathedral arch bridge was eventually selected for its simple aesthetics and minimal visual impact. Local property owners were concerned with construction of a structure that stood out and lobbied for a structure that complimented the surrounding environment. Two alternate designs of the structure were made available to contractors in the original bidding process. The original contractor, Edward Kraemer and Sons, bid the pilot-truss alternative, as it was the less expensive of the two designs and considered easier to construct.

#### 2.2. Design Criteria

The selected design of the Galena Creek Bridge was designed by the Nevada Department of Transportation using the AASHTO “Standard Specifications for Highway Bridges,” Sixteenth Edition 1996, Interims thru 2000. Standard HS25-44 loading was used for structure live load. Overload design was based on the California “Standard Permit Design Vehicles” with a maximum allowable overload of the P-13 truck. The seismic design was based on an acceleration coefficient of 0.4g with a Type I soil. This corresponds to a 475-year earthquake, or roughly a 10% probability of exceedance in 50 years.

#### 2.3. Columns

Each of the two Galena Creek Structures is comprised of seven spans, supported on six single column piers and the main arch span. Each column is hollow rectangular and measures 3 m by 6 m (Figure 2-2). The columns strong axis is oriented to resist transverse bending. The open core of each column measures 4 m by 1.8 m, with 150-mm fillets in each corner.

Each of the columns is detailed based on its respective flexural and shear demand. A varying number of longitudinal bars and shear/confinement steel is found depending on the location within each column. Piers 1 and 6 for both structures are detailed the same. Within the plastic hinge region at the bottom of each of these columns is a 6 m length in which the spacing of the shear/confinement steel is detailed at 100 mm. The top of each column is detailed the same as the bottom for the first 3.2 meters. In between these two plastic hinge zones, the shear/confinement steel is at a 200-mm spacing. As Piers 1 and 6 are the shortest columns on the structure, they are detailed with additional #22M longitudinal bars for increased flexural capacity. Horizontal confinement ties are #16M bars, which are tied around each longitudinal bar set. The main shear reinforcement is comprised primarily of #19M bars, with the exception of two #16M headed bars in the top and bottom section; these bars are oriented for shear in the transverse direction.

Piers 2 and 3 southbound (SB) and northbound (NB) are detailed very similarly as Piers 1 and 6, described above. The plastic hinge region flexural detailing is somewhat different in that they are detailed with the 100-mm shear/confinement steel spacing for 6.5 meters at both the top and bottom of each section. Additionally, the supplemental longitudinal bars in the plastic hinge zone are #29M bars, larger than the #22M bars found in the detailing for Piers 1 and 6.

Piers 4 and 5 have the greatest height difference between the northbound and southbound structure. Here, the northbound structure features taller columns due to the native topography. All four of these columns do not contain any supplemental longitudinal reinforcement in the plastic hinge zones. Rather, they maintain the same number of longitudinal bars from the top to the bottom. Shear/confinement steel detailing stays consistent with the other piers. Each maintains 100-mm spacing for 6 m at the bottom of each column. The tops of the columns see slightly different treatment, where the two southbound columns have the plastic hinge detailing for 4 meters at the top of each column, while the northbound columns have the plastic hinge detailing for 6 meters at the top of each column.

With the exception of Piers 2 and 3 which are founded on the arch thrustblocks, each column is situated on 14 m (wide) by 13.42 m (long) by 2.75 m (deep) pile caps. Twelve Cast-In-Drilled-Hole (CIDH) piles are found around the perimeter of each pile cap. The depth of each CIDH is different, depending on the depth to competent material (bedrock). Each pile has a steel-embedment length of 2.6 meters. Piles are detailed with tighter spiral pitches within their 4.6 m plastic hinge zone.

#### **2.4. Arch**

The original arch design for the Galena Creek Bridge consisted of a steel pilot truss that supported conventional steel for the final concrete arch. A key component of the construction sequence, the pilot truss allowed the arch to be self supporting during construction and permitted the construction of a concrete arch without falsework. Figures 2-3 and 2-4 show various steps in the erection of the steel pilot truss. The pilot truss was designed and fabricated into ten segments. Temporary cable stays anchored in the Pier 1 and 4 footings and passing through the tops of Piers 2 and 3, respectively, helped support the truss during the erection sequence. After the closure segment was in place, the hollow

structural tube sections that serve as the main structural members in the pilot truss are grouted, providing extra stiffness to the section.

Standard AISC HSS sections comprise the majority of structural steel sections in the pilot truss. The four main chords are HSS 406x406x16 sections, and are spaced at 2.994 m vertically and 5.394 m horizontally. Lateral bracing in the vertical and horizontal planes are provided by HSS 203x152x16 sections, with bolted connections to the main chords. The splice locations for alternating truss segments are joined together with a contractor option of a bolted splice detail or field welds.

After erection and grouting of the steel pilot truss, the truss serves as a working platform and framework for the concrete arch. Conventional steel is tied to the pilot truss, and the concrete placement operations can begin. The completed concrete section measures 6 m by 3.6 m, with 400 mm walls. 350 mm fillets are provided in each corner. Sixteen longitudinal bars are provided in the top and bottom mats of the top and bottom arch slabs. In each of the arch side walls, eight longitudinal bars are distributed on each face. The concrete arch is divided into 19 different segments (Figure 2-6), nine on a side with a closure segment at the arch crown. Shear and confinement steel varies in spacing from 100 mm at the bottom of the arch, to 300 mm in the middle of arch, and back to 150 mm near the arch crown. The first segments on either side of the arch span, designated Segment 0 (south side) and Segment 0A (north side) are cast as solid sections.

In the revised plans that came out as the second phase of the I-580 Freeway Extension project as NDOT Contract 3292, the plans provided provisions to omit the steel pilot truss and construct the arch on traditional falsework. In place of the steel pilot truss, roughly every longitudinal bar in the arch would be doubled to provide an adequate structural section (Figure 2-7). C.C. Myers, the I-580 structures sub-contractor, elected to construct the arch under this provision. The Value Engineering Proposal (VEP) for this option with the actual proposed structural arch section has not been received by NDOT at the time of this publication. A sample revised arch section is provided by NDOT in the Conformed Special Provisions, with essentially bundled #29M bars in place of each longitudinal bar in the original pilot-truss arch section.

## **2.5. Superstructure**

The superstructure of the Galena Creek Bridge is a two cell box girder (Figure 2-8). The total structure with measures 18.9 meters wide, allowing room for three 3.6-m travel lanes and two 3.6 m shoulders. The bridge deck is transversely post-tensioned, with -strands spaced at 400 mm. The deck is 200 mm thick, with a 125 mm by 1.2-m fillet on either side of the interior girder. At the exterior girders, the deck thickens to 375 mm. All three girders are 325 mm thick, with the exterior girders sloped at 48 degrees from horizontal. The overhangs on either side of the superstructure measure 3.59 meters, and support standard concrete barrier rail with a height of 1.07 meters.

Main transverse deck reinforcement is comprised of #13M bars at 300 mm. Longitudinal distribution steel is comprised of #13M bars at 300 mm on the top, and #16M bars in the main deck spans. In the fillets and thickened portions outside the exterior webs, #13M bars are used. Due to anticipation of using the southbound structure for hauling material during construction, the east cell of the southbound structure contains additional #16M longitudinal bars at 150 mm to provide sufficient strength for

the overweight haul trucks. Skin reinforcement of #13M at 300 mm on each face is provided in each of the three girders. The soffit contains #13M bars at 200 mm, alternating bars between the top of the slab and the bottom of the slab. Concrete cover to the top layer of steel in the deck is specified at 65 mm. Permissible construction joints are located at the top of the soffit slab, and the tops of each girder.

Numerous diaphragms are provided throughout the length of the structure. 1.6 meter thick end diaphragms are provided at both abutments. Intermediate diaphragms 250 mm thick are provided at mid-span of each typical structure span. In the arch span, four diaphragms are detailed. 500-mm fillet diaphragms are specified where the arch and superstructure merge. 6.75 meters on either side of the center of the arch span are 300 mm crown diaphragms. An additional 250-mm intermediate diaphragm is provided halfway between the arch-superstructure merge area and the nearest column on either side of the arch span.

## **2.6. Abutments**

Seat type abutments are provided on each end of the structure. A single abutment stem wall and footing system are used to support both the northbound and southbound structures. Each abutment is founded on a 6.1 m wide footing, supported on CIDH piles. Due to the side slope at each abutment, a three step footing is detailed. Transverse shear keys are provided on the exterior of each structure, with an additional shear key provided between the two structures. A 300-mm back-wall is provided to retain soil and support the adjacent approach slabs. A gap is provided between the end diaphragm of each structure and the back-wall. Polystyrene is specified in the gap to prevent debris from accumulating and restricting movement. The total provided seat width for the superstructure is 1.2 meters, and each girder is supported on elastomeric bearings.

## **2.7. Hinges**

Two expansion joint hinges are provided along the length of the structure, dividing the structure into 3 frames (Figure 2-1). Each hinge is located 15 m to the outside of the arch span, measured from the centerline of the adjacent column to the centerline of the hinge. Diaphragms are provided on the upper and lower portions of each hinge to accommodate the necessary amount of conventional reinforcement and prestressing found in each hinge. Transverse shears keys are provided to restrict relative transverse displacement and unseating in the case of a seismic event. Elastomeric bearings are provided under each girder to allow for movements due to temperature, creep, and shrinkage. Seismic restrainers are provided in the longitudinal direction to prevent unseating under seismic loading. Each 36-mm post-tensioned restrainer bar is placed in a 50-mm steel sleeve, and anchored at one end. The other end is fixed with a rubber fender with a 150-mm gap. This gap permits some movement due to temperature, creep, and shrinkage before engaging the restrainer system. The restrainers are detailed in two different configurations: a 1 bar restrainer assembly, and a 2 bar restrainer assembly. In Hinge 1, 2-2PT bar units and 16-1PT bar units are specified, while in hinge 2, 10-2PT bar units and 16-1PT bar units are specified. The typical hinge restrainer layouts are shown in Figure 2-11. If seismic displacements become large enough to close the initial

gap, eight rectangular rubber fenders are provided in each hinge to protect the superstructure from damage due to pounding.

## **2.8. Prestressing**

Each of the three frames in the Galena Creek Bridge have slightly different post-tensioning details. As part of the design criteria, all longitudinal post-tensioning in the structure is based on a 10-mm anchor set, with a coefficient of friction of 0.2 and a wobble factor of 0.00066/m.

Frame 1 specifies the use of 9-0.6" 27 strand tendons, equally distributed between the three girders. The specified total jacking force is 48300 KN (1420 MPa), with estimated total losses due to friction, creep and shrinkage of concrete, relaxation of steel, and elastic shortening of 179 MPa. The typical tendon path has anchorages at Abutment 1 and in Hinge 1. Tendons are specified to be jacked from Abutment 1. The post-tensioning layout for Frame 1 is shown in Figure 2-10.

Frame 2 contains both internal and external longitudinal post-tensioning. The external post-tensioning runs from each hinge back to the nearest pier. The main internal post-tensioning consists of 18-0.6" 27-strand tendons, equally distributed between girders. Anchorages for Frame 2 are found in the two hinges. A jacking force of 101300 KN (1420 MPa) is specified, with an estimation of 276 MPa of total losses. The jacking sequence requires jacking from both ends simultaneously. The post-tensioning layout for Frame 2 is shown in Figure 2-11.

Post-tensioning in Frame 3 consists of 12-0.6" 27 strand tendons. A total jacking force of 64200 KN (1420 MPa) is specified. Anchorages are found in Hinge 2 and Abutment 2, with jacking specified from the hinge. The post-tensioning layout for Frame 3 is shown in Figure 2-12.

Transverse post-tensioning in the deck consists of single 0.6" four strand tendons spaced at 400 mm. The specified jacking force for each tendon is 812 KN (1450 MPa); tendons are to be alternately stressed from each side of the superstructure. The typical superstructure cross section with the transverse post tensioning layout is shown in Figure 2-13.

## **2.9. Link Slab, Link Beams**

Seismic analysis during design revealed that tying the northbound and southbound Galena Creek structures together reduced seismic forces and displacements. Over the length of Frame 2, the two structures are linked together with a 200 mm thick link slab that joins the two structure's overhangs. Reinforcement in the link slab is the same as the main deck spans, with #13M transverse bars spaced at 300 mm top and bottom, and #13M bars at 300 mm serving as distribution steel in the longitudinal direction.

The two arch thrust blocks are linked together with a link beam, cast after the thrust blocks have been poured. The link beam connects the middle portion of the northbound and southbound thrustblocks. The link beams acts as a rigid link, and forces the foundations for the two arches to act together in a seismic event. Figure 2-14 shows the link slab and link beam.

## **2.10. Construction Sequence**

The construction sequence for the Galena Creek Bridge centers around the overall project schedule for successful completion of the new I-580 freeway alignment. The southbound structure is to be used to haul material from one end of the project to the other, and is hence a key critical path item.

The first step in the construction process is the completion of the substructure. Drilling and casting of the CIDH piles for the abutment and column footings is the first milestone. Once the footings are cast, each column and abutment can be formed and cast. Depending on the height of an individual pier, the pier may need to be cast in multiple sections due to crane and form limitations. Abutment stem walls and wingwalls can be cast monolithically, but an optional construction joint is specified in the plans.

Construction of the concrete arch warrants special consideration to balance the arch dead loads. To help relieve form pressures and concrete placement issues, permissible construction joints are detailed at the bottom and top of the arch walls. Load balancing is done by pouring a segment, or portion of a segment, on one side of the arch span and then duplicating the pour on the other side until reaching the crown. Ahead of each forming and casting operation, the arch rebar is tied to allow for continuous construction.

Once the arch is completed, the three frames that comprise the bridge superstructure can be constructed. After falsework to support the superstructure is in place, the soffit slabs of each span can be cast, followed by the webs and deck sections. Prior to casting the hinges, post-tensioning of each frame is completed. After post-tensioning, the hinges are formed and cast. Once both structures are complete, the link slab joining the two structures and the link beams at each thrust block can be cast. Construction of the concrete barrier rail and approach slabs marks the last step in the construction process.

## **Chapter 3 Instrumentation**

### **3.1. Instrumentation Introduction**

Due to the complexity of the structure and uncertainty in construction loads on the steel pilot truss, the University of Nevada, Reno was contracted to instrument the southbound Galena Creek Arch. A formal instrumentation plan was developed in which a series of 108 strain gages would be placed in specific areas of interest on the arch. Faculty at the University, along with the NDOT designers, met to decide on locations in which stress/strain data were deemed important. Two different kind of strain gages were to be used in the selected locations. For the steel pilot truss and longitudinal arch reinforcement, welded steel strain gages were to be used. Concrete strain gages were also to be used, to instrument the grout in the steel tubes comprising the pilot truss, and to instrument the actual arch concrete.

The original plan was developed for the arch designed with a steel pilot truss. As mentioned previously, the design of the arch was changed in between contractors, and is now a more conventional reinforced concrete structure due to the omission of the steel pilot truss. The following instrumentation overview is given as an example of a potential instrumentation plan.

### **3.2. Instrumentation Overview**

The instrumentation of the Galena Creek Bridge creates a unique research opportunity for researchers at the University. By creating a system capable of streaming data in real-time, the effect of the construction sequence and schedule on the state of stress in the structure will be analyzed and compared to design loads. As part of the instrumentation, comparison work between captured data and existing models of the bridge will be compared. With careful consideration, the adequacy of current methods of design and analysis will be examined and recommendations for future design could be made.

To create a feasible instrumentation plan numerous considerations need to be taken into account. First and foremost, the impact on the contractor should be minimized. With this in mind, as much work as possible would be done at the University, or before erection of the steel pilot truss. Due to the exposure conditions of the bridge and the Northern Nevada climate, strains due to thermal effects must be accounted for. Thermisters on each gage are needed to isolate temperature strains induced by environmental conditions. Additionally, strains due to creep and shrinkage of the concrete structure must be understood to further reduce the number of variables skewing the strain gage results. To isolate the strains due to creep and shrinkage, creep frames with 6" x 12" cylinders will be located on site and instrumented.

To facilitate the instrumentation plan, a strain gage data acquisition system capable of taking real-time readings from the various gages was designed. Included in the data acquisition system is a built-in wire-less transmitter for sending data to researchers at the University for analysis. A comprehensive plan was also developed to help minimize the impact of the instrumentation on the contractor's construction activities.

Staging the instrumentation plan with the construction sequence is of vital importance in order to be able to capture the state of stress in the structure during the construction sequence. The proposed instrumentation plan has the gage packages being pre-assembled at the university to minimize the impact on the contractor. Each gage will be fitted with a lead-cable that brought each instrument cable in a given arch section to the same general location. The data acquisition box will be assembled into a weather-proof steel box, with leads that ran up the arch from its primary location at the south thrust block. Each lead wire from the individual instruments and the main cable runs will be fitted with a d-sub connector to allow the cables to be connected easily and quickly.

To help document and monitor the construction process, two digital cameras have been set up on either side of the arch span. These cameras take pictures of the structure on 15 minute intervals. Each camera is powered with two solar panels. Power for the instrumentation data acquisition system is provided by hooking up to the camera solar panels. An on-board battery insures that the instrumentation will stay active if solar power is temporarily interrupted.

### **3.2.1. Layout**

Figure 3-1 shows the layout and location of the instrumentation sections. Specific areas of interest include the interface between the arch footing (thrust block) and start of the arch; the arch crown region; and portions of the arch between the thrust block and crown. In each section, the pilot truss, arch concrete, and arch longitudinal reinforcement are instrumented. All of the instrumentation is set in the southern portion of the southbound Galena Creek arch. Additional areas to be instrumented include the soffit and deck in the area of span 2 directly above the arch crown region.

### **3.2.2. Truss Instrumentation**

The first step in the instrumentation sequence for the Galena Creek Bridge is the truss instrumentation (Figure 3-2). The truss instrumentation will be tack welded into place prior to the pilot truss erection. To fully understand the composite stresses in the pilot truss, this instrumentation is divided up into grout instrumentation, and the structural steel instrumentation.

One basic assumption made in the design phase was that full composite action existed between the structural steel tubes, and the internal grout. By instrumenting both the grout and the steel, any differential strain can be examined to verify this assumption.

Special concrete strain gages were selected for installation in the tube (Figure 3-3). Brackets were designed to keep the gage in place, and to ensure proper orientation of the gage within the tube (Figure 3-4). Two 10-mm diameter holes 130.8 mm apart would be drilled in the inside face of each structural tube, located approximately 250 mm from the end of each instrumented-truss section. By locating the gage as far into the tube as feasible possible, impact from the field welding and bolting operations during truss erection would be minimal. A third hole would be drilled to allow the belden-cable lead to pass out of the section and continue to the junction location. The grouting operations will be performed from the low end of the truss section, on the opposite end from the instrumentation. This further helps protect the gage and to ensure its integrity during grouting.

Steel strain gages will be installed in approximately the same location as the corresponding concrete strain gage. The surface of each tube will be prepared by light grinding of the surface to ensure a smooth, uniform finish for tack welding. Tack welding equipment will be brought on site, and each gage welded onto the steel tube. The leads from the pre-prepared belden cables will then be soldered to the connection on each strain gage and strain relieved to prevent the connection from being damaged during construction.

All of the truss instrumentation will be installed prior to truss erection. As each subsequent truss segment is erected, the steel strain gages will be connected to the data acquisition system at the south thrust block, and real-time data gathered. After the grouting operations, data can be gathered from the concrete gages within the structural tubes.

As each chord in the pilot truss would be instrumented at a given section, data about the forces present on the section could be determined. By looking at the difference in strain from the top members to the bottom members, longitudinal bending moments could then be determined. Similarly, differences in strain between opposite sides of the pilot truss would reveal the transverse bending of the pilot truss from any lateral loading.

The total strain ( $\epsilon_t$ ) for a system due to the combined effect of axial load and uniaxial bending moment is given by  $\epsilon_t = \epsilon_{axial} + \epsilon_{flexure}$ . Given that the member is symmetric about the axis of bending,  $\epsilon_{flexure}$  is equal but opposite sign for the extreme tension ( $\epsilon_{tension}$ ) and compression ( $\epsilon_{compression}$ ) fibers. For the given uniaxial bending case, it can be shown that  $\epsilon_{axial} = \frac{\epsilon_{tension} + \epsilon_{compression}}{2}$ , and that  $\epsilon_{flexure} = \epsilon_t - \epsilon_{axial}$ . The given bending moment and axial force can then be found by equations (1) and (2) below.

$$(1) P = \epsilon_{axial} \cdot A \cdot E$$

$$(2) M = \frac{I \cdot E \cdot \epsilon_{flexure}}{\bar{y}}$$

Where: A = Gross cross sectional area

I= Moment of inertia about axis of bending

E= Elastic modulus

$\bar{y}$  = Distance from neutral axis to area of interest

Under dead loads and post-tensioning loads, the arch should not experience any significant transverse bending; this would permit the use of the above equations.

### 3.2.3. Concrete Instrumentation

The second portion of the original instrumentation plan is the instrumentation of the arch conventional reinforcement and concrete (Figure 3-5). The same two types of gages will be used for this instrumentation. In each proposed cross section on the arch, a minimum of two longitudinal bars in the top and bottom arch slab will be instrumented, along with two concrete gages imbedded in the middle of both the top and bottom arch slabs.

Conventional steel strain gages will be tack welded to 1.8-meter #16M bars. By tack welding to supplemental bars, impact on the contractor is minimized. After the longitudinal steel is tied for a given arch section, this #16M “sister-bar” can be brought to the site and tied in the appropriate place in the steel mat. The use of a 1.8 meter bar allows adequate development length in both tension and compression, as required by ACI 318 (ACI, 2005). Cable leads will also be pre-soldered prior to installation; cables will be strapped along the unexposed face of the steel mat and run to the connection location in the arch wall. The concrete strain gages will be tied in between the mats of longitudinal bars.

In the instrumented arch sections near the arch crown, additional strain gages are planned (Figure3-5). To understand the behavior of the merge area (Arch Segment 6), strain gages are placed in the region that connects the arch rib to the frame 2 superstructure. Additionally, areas of the frame 2 superstructure above the merge area are also instrumented, including main longitudinal bars in the deck and soffit slabs in three different locations.

#### **3.2.4. Data Acquisition System**

The data acquisition system for the Galena Creek Bridge instrumentation consists of a series of National Instrument 32-channel multiplexers that are used to collect and store data. Four multiplexers are located at the south Pier 2 thrust block, which collect all of the data from the instrumentation Sections 1-6 (Figure 3-1). The gages are section 7 as well as the accelerometers are connected to a multiplexer that is to be installed at the top of the arch.

#### **3.2.5. Installation**

The installation of each gage follows a specific instrumentation plan that is designed to minimize the impact on the contractor’s construction activities. In the case of the steel pilot truss, each gage could be tack welded to the pilot truss prior to truss erection. Each section of the pilot truss is assembled on site once fabricated, which provides an opportunity of installation of these gages without impacting the contractor. Additionally, the truss-grout gages can be installed simultaneously as the truss steel strain gages by drilling the necessary holes for the gage bracket system and inserting the concrete gage. After erection of a particular instrumented segment, the gages would then be connected to the data acquisition system to start gathering data via cable leads carried in PVC conduit that connect the gages to the data acquisition system at the south thrust block.

In the case of the concrete instrumentation, more careful consideration is needed to properly sequence the installation of the gages with the construction schedule. The first step in this process is the installation of PVC conduit carrying cable leads from the data acquisition system to each instrumented section. Once the reinforcing steel is in place for an instrumented segment, the gages are brought on site and installed. The instrumented longitudinal “sister bars” are tied into the reinforcing mat, and the concrete gages placed between steel layers. Cable leads from each gage are connected to the cable leads from the thrust block. This allows for real time data streaming during the casting sequence.

Gages in the frame 2 superstructure are installed in a similar matter, with the gages live during casting.

### **3.2.6. Seismic Instruments**

The final type of instrumentation planned for the Galena Creek Bridge is the addition of 15 accelerometers. Due to inclusion of two expansion joint hinges 15 meters outside of both ends of the arch span, the Galena Creek Bridge is composed of three separate frames that can behave somewhat uniquely from one another in a seismic event. The behavior of Frame 2, the arch span, is of interest due to presence of the arch. Five locations were selected in this frame, with three accelerometers in each location. Figure 3-7 shows the locations of the dynamic instrumentation. Two of the accelerometers in each location will be placed in the horizontal plane to capture both the longitudinal and transverse response of the frame. The other will be oriented vertically to capture any vertical acceleration in a seismic event.

The top of the two columns and thrust blocks on either end of the arch span will be instrumented. By instrumenting the top of each column and the thrust blocks, relative movements along the length of each column can be captured. Additionally, the movement of the bottom of the arch on either end of the span is also captured. The final location for the dynamic instrumentation is the crown of the arch. The combination of the response of each of the five gage locations should yield good results as to the response of Frame 2 to dynamic loading.

### **3.3. Revised Instrumentation Plan**

Due to unforeseen construction delays, the scope of the original instrumentation plan has been slightly altered. Additionally, the election of the current Galena Creek Bridge contractor to construct the bridge on falsework and omit the steel pilot-truss, simplifies the construction sequence and removes a great deal of complexity regarding the arch design and behavior. The need for an extensive instrumentation package that gathers data in real-time is hence not warranted.

A revised instrumentation plan has since been developed, to try and incorporate the financial resources that have already been used on developing and assembling the gage packages and data acquisition system. There is still interest in monitoring the state of stress in the arch and Frame 2 superstructure post-construction. The objective is to monitor the effect of long term creep and shrinkage, and the response of the arch to live loading and potential earthquake motions. The revised typical arch instrumentation layout is shown in Figure 3-8.

## Chapter 4

### Seismic Time History Analysis Modeling

#### 4.1. AASHTO Standard Specifications

The Galena Creek Bridge was designed according to the requirements of the American Association of State and Highway Transportation Officials (AASHTO) Standard Specifications for Highway Bridges. The AASHTO Code provides four methods of analysis for determining seismic load effects. Each method is a linear-elastic technique and hence does not account for geometry and material non-linearity. The four methods presented in the Standard Specifications are the i.) Uniform Load Method, ii.) the Single-Mode Spectral Method, iii.) the Multimode Spectral Method, and iv.) the Time History Method. The AASHTO Standard Specifications set minimum requirements for the selection of the proper analysis method based on a Seismic Performance Category (Table 4-1) and a bridge classification, based on the “regularity” of a bridge structure. A regular bridge is classified as one with less than seven spans and without unusual changes in geometry, weight, or stiffness throughout the length of the structure. Based on a site acceleration coefficient and an Importance Classification, a Seismic Performance Category is assigned. With the Seismic Performance Category and bridge irregularity as input parameters, minimum analysis requirements are specified. Based on the irregularity of the Galena Creek Bridge and its Seismic Performance Category of “D”, the code requires a minimum analysis requirement of the Multimode Spectral Method.

The Multimode Spectral Method is a method of dynamic analysis by which various modes of vibration are found for a structure and an elastic response spectrum are used in determining design member forces and displacements. The AASHTO Standard Specifications provides guidelines on developing an adequate computational model for use in the Multimode Spectral Method. The code specifies the development of a three-dimensional bridge model that is adequately discretized to capture the stiffness and inertia effects of the bridge structure. Each node within the computational model should have six degrees of freedom (DOF): three translational and three rotational. Additionally, an adequate number of modes should be used in the analysis to ensure adequate mass participation; generally 90% mass participation is sufficient.

Once the modes of vibration and their corresponding periods are known, force effects are found by using an elastic-response spectrum, which is developed based on a probabilistic site acceleration coefficient and a constant damping ratio. Response quantities for the structure are then found by combining the responses of the individual modes using the Complete Quadratic Combination (CQC) method, as required by the Standard Specifications.

The elastic response spectrum specified in AASHTO (Figure 4-1) is constructed by the equation

$$C_s = \frac{1.2 \cdot A \cdot S}{T_m^{2/3}}$$

Where: A: Probabilistic acceleration coefficient  
S: Dimensionless site soil coefficient  
T<sub>m</sub>: Period of the nth mode of vibration

### C<sub>s</sub>: Spectral Acceleration

The site soil coefficient is based on four soil profile types (Table 4-2). Type I corresponds to rock or a stiff soil condition; Type II is for stiff clays or deep cohesionless soils; Type III is for soft to medium-stiff clays and sands; Type IV is for soft clays and silts. Values of S are 1.0, 1.2, 1.5, and 2.0 for Types I, II, III, and IV soils, respectively.

Two different design load cases are specified for seismic design. Load Case I corresponds to 100% of the force effect in the longitudinal direction and 30% of the force effect in the transverse direction; Load Case II corresponds to 100% of the force effect in the transverse direction and 30% of the force effect in the longitudinal direction. Response Modification Factors (Table 4-3) are used to reduce the design forces in certain structure components in order to force any inelastic action in the presence of seismic loading to specified areas in the structure. This helps simplify the repair and inspection after an earthquake. In general, yielding should not occur in the superstructure, but rather be concentrated in substructure components such as columns. Detailing to provide sufficient ductility helps prevent collapse of the structure.

## **4.2. UNR Seismic Analysis**

### **4.2.1. Scope**

Due to the complexity of the Galena Creek Bridge and its close proximity to a known active fault, it was decided to conduct a more detailed seismic analysis than was originally conducted by the Nevada Department of Transportation (NDOT) as described in Section 1.1. A detailed finite element model was developed that employed structural material and geometric non-linearity to more accurately predict member forces and displacements. Different methods of analysis were explored and evaluated based on their accuracy, efficiency, and practical use for future bridge design. Ultimately, a non-linear time history analysis was selected and was compared and contrasted to traditional linear-elastic methods, such as the multi-modal spectral response method. To perform the non-linear time history analysis, the Department of Seismology at the University of Nevada, Reno's was contacted to select ground motions that reflected characteristics of active faults that lie near the Galena Creek Bridge.

### **4.2.2. Acceleration Time History Selection and Scaling**

The first step in performing the non-linear time history analysis of the Galena Creek Bridge was the selection and scaling of appropriate acceleration time histories. The recommendations of the Federal Emergency Management Agency (FEMA) 356 were used in the selection and scaling of seven unique ground motions. As per FEMA recommendations, an expert in the field of seismology was contacted to select ground motions that reflected characteristics of active faults with a close proximity to the Galena Creek Bridge.

Selecting proper ground motions that are representative of local seismology is complicated for a number of reasons. The major active fault near the Galena Creek bridge is the Mt. Rose Fault, located within 6 km of the bridge site. This fault system is classified as a normal fault. Research done by Ramelli and dePolo and compiled by

Sawyer (1999) into the Mt. Rose Fault system indicates that there have been two earthquakes from this fault in the last 1700 years. There are several splays extending from this fault system that are within a few km of the Galena Creek Bridge. Figure 4-2 shows a fault map of the area around the bridge. Evidence shows that the fault system dips to the east underneath the structure, placing the bridge on the hanging wall of a normal fault.

In selecting representative ground motions for this site, it should be noted that there are no near-field records from sites on the hanging wall of normal fault with a representative Richter magnitude as the Mt. Rose fault system. In order to obtain earthquake records that included near-field effects such as velocity pulses, records from strike-slip faults were ultimately selected. It should also be noted that there is evidence to support the presence of strike-slip faults near the bridge. Due to this fact and the necessity of selecting earthquakes from sites in the near-field, the use of strike-slip motions is justifiable and appropriate. The characteristics of near-field motions such as large velocity pulses and higher accelerations at higher periods illustrate an important drawback or over simplification of traditional response spectrum techniques.

As recommended in FEMA 356, if seven or more pairs of time history cases are used, force effects can be determined as the average of the seven unique responses to these time histories. Each selected pair has three orthogonal acceleration histories; two horizontal components, and one vertical. In order to achieve a probabilistic earthquake level when using non-linear time history techniques, scaling of the individual records is necessary. FEMA recommends scaling the motions based on an average weighted composite response spectrum developed from the selected ground motions. In this method, the average composite spectrum is not to fall below 1.4 times design spectrum (target spectrum) within the period range of interest. The period range of interest is defined as the range bounded by 1.5 times the fundamental period of vibration, and 0.2 times the fundamental period of vibration (Figure 4-3). Preliminary modal analyses of the Galena Creek Bridge yielded values for the bridge's fundamental period of vibration. For the two structures tied together, the fundamental period is around 1.85 seconds; this vibration mode corresponds to a transverse response of the bridge dominated by lateral translation of Frame 2 (Figure 4-4).

Once the time histories were selected, response spectrums were developed for the two horizontal components of motion using the software SeismoSignal (Seismosoft, 2005). The response quantities for period ranging from 0 to 1.5  $T_n$  were tabulated for the two horizontal components of each record, where  $T_n$  is the fundamental period of vibration. For each time history, an SRSS response spectrum,  $Z$ , is determined as follows:

$$Z = \sqrt{X^2 + Y^2}$$

Where: X: Response spectrum for longitudinal component of motion  
 Y: Response spectrum for transverse component of motion  
 Z: SRSS response spectrum

The composite response spectrum used in scaling each motion is then developed by using the Square-Root-of-the-Sum-of-the-Squares (SRSS) response spectrums,  $Z$ , from each unique time history. The weighted average is developed as follows:

$$Z_{composite} = \frac{f_1 \cdot Z_{EQ1} + f_2 \cdot Z_{EQ2} + f_3 \cdot Z_{EQ2} + \dots + f_n \cdot Z_{EQn}}{n}$$

- Where:  $f_n$ : Scale factor for motion “n”  
 $Z_{EQn}$ : Response quantity for SRSS combination of two horizontal components of each ground motion  
 $Z_{composite}$ : Response quantity for composite spectrum

To determine the “f” factors for each ground motion, an iterative process was used. Figure 4-5 shows the composite response spectrum plotted against the scaled design 425-year earthquake spectrum. Various values for the “f” factors for each motion were input to try and match the composite spectrum with the design spectrum. Different motions dominated different portions of the composite curve; by iteratively changing each ‘f’ value, a smoothed spectrum is achieved that closely approximates the design curve. It should be noted that there is no “correct” value for these scale factors. Trial and error adjustment of the scale factors ultimately lead to the values used in the analysis. Engineering judgment is necessary to develop a reasonable curve

For purposes of analysis, two sets of “f” factors were developed for each set of ground motions: one for a 10% Probability of Exceedance in 50 Years, and 2% Probability of Exceedance in 50 Years. These factors are used to scale each ground motion (both horizontal components as well as vertical) when running the analysis. After the analysis is complete, force effects and displacements are found as the average of the absolute maximum quantities for each ground motion.

Consulting with the Seismology Department at the University of Nevada, Reno yielded the selection of seven ground motions for use in the analysis. Each selected ground motion seismograph corresponds to an earthquake from a strike/slip fault. As discussed previously, in order to capture near field effects, the selection of records based on strike-slip fault behavior was the primary criteria in the selection of appropriate ground motions. The selected ground motions and their respective Richter magnitudes are summarized in Table 4-4. It should be noted that the filtering criteria used in processing the acceleration time histories for each selected motion did not affect the frequency content within the range of frequencies corresponding to the modes of vibration of the structure. The selected ground motions will hence be referred to by their general station identification, as several of the records are from the same seismic event. Table 4-4 additionally lists the station designation along with the parent earthquake event. Figures 4-6 thru 4-12 show the un-scaled SRSS-averaged response spectrums for each selected motion.

Once the motions were selected and response spectrums generated for each motion, appropriate scale factors were determined following the FEMA recommendations. The target spectrum was plotted first, and the composite average spectrum was superimposed. Scale factors were iteratively input to produce the composite spectrum. The developed scale factors for each record for the 10% PE in 50 Year earthquake is shown in Table 4-5, and the scale factors for the 2% PE in 50 Year earthquake in Table 4-6. Plots of the composite response spectrums and target spectrum for both level earthquakes are shown in Figures 4-13 and 4-14.

### 4.2.3. Boundary Conditions and Modeling Considerations

Finite Element Analysis requires careful consideration of imposed boundary conditions for a structural model. In establishing appropriate boundary conditions for the Galena Creek Bridge model, consideration was given to boundary conditions used in the original NDOT design models. These conditions included the degree of fixity and flexibility of column and arch footings, and as well as the treatment of structure non-linearity at the abutments and expansion joint hinges. Ultimately, the same boundary conditions used in the original NDOT models were implemented in the UNR models.

Due to the absence of access to necessary soil information to develop six degree-of-freedom soil-spring models, the consideration of foundation flexibility was thought to be outside the scope of this project. Therefore, the foundations of the structure were assumed to be rigid-fixed. This assumption leads to conservative estimates of base shears and moments, but is un-conservative in determining structure displacements to applied lateral loads.

One basic assumption in the theory and design of reinforced concrete structures is that concrete does not have any capacity in tension. This assumption is referred to as “cracked-section” theory. To account for cracked concrete properties in a model, a reduced cross section moment of inertia is often times assumed, commonly known as the effective moment of inertia. Recommendations by Priestley, Seible, and Calvi were used to estimate the effective moment of inertia as  $0.4I_{gross}$  for the Galena Creek Bridge Columns (Priestley, 1996). These recommendations are a function of the longitudinal steel ratio and the axial load ratio for a given member. It should be noted that cracked concrete properties were only assumed for the columns of the structure. It is assumed that the post tensioning in the bridge superstructure should limit cracking, and hence permits the use of gross section properties. The high axial load in the concrete arch and high steel ratio led to the use of gross section properties for the arch.

To model the structure-abutment response interaction more realistically, non-linear elements were incorporated into the model. These elements allow explicit modeling of the gap between the abutment back-wall and superstructure end diaphragm (Figure 4-15). The conformance plan set developed for the Galena Creek Bridge by NDOT shows predicted gap opening at both abutments and at the expansion joint hinges at different ages after prestressing (Table 4-7). To incorporate these gaps into the model, the ultimate gap openings, approximately 1000 weeks after stressing, were used. The use of the predicted gaps at 1000 weeks after stressing was based on a probabilistic approach. If a 75-year service life is assumed for the bridge, a 425-year earthquake has a larger chance of occurring for years 20-75 than from years 0-20. For this reason, the 1000 week gap openings were assumed for the model.

Multi-linear link elements are used to model the non-linear behavior for the longitudinal degree of freedom at each abutment. Two link elements are modeled in series. The first is a multi-linear elastic element that models that provides no stiffness for displacements away from the abutment, allowing unrestrained movement. For displacements towards the abutment, an initial stiffness of zero is modeling until the displacement corresponding to the assumed abutment gap is reached. A large secondary stiffness is then modeled to transfer load to the second link element. The second link element is a multi-linear plastic element to model the soil response. This link provides

zero stiffness for movement away from the abutment back-wall, and models an elasto-perfectly-plastic soil response for movement towards the abutment back-wall. The initial stiffness models the abutment back-wall and soil stiffness. The secondary stiffness is zero, and corresponds to a perfectly plastic soil response. The soil link element uses a Takeda hysteresis model to account for cyclic degradation. A sample hysteretic response for the two link element longitudinal abutment model is shown in Figure 4-16. Provisions in the California Department of Transportation Seismic Design Criteria (Caltrans, 2006) were used to develop the multi-linear longitudinal abutment force- displacement model. The abutment response found in this guideline was developed from large scale abutment testing at the University of California, Davis. The results of this testing yield an estimate of back-wall/soil stiffness up to a maximum passive earth pressure of 239 kPa. Figures 4-17 and 4-18 show the force displacement backbone curve used for Abutments 1 and 2, respectively. Slight differences for the two abutment link models are noted because of different gaps openings for each abutment. Abutment 2 has a 15 mm larger gap than Abutment 1.

The bridge's seat-type abutments feature transverse shear keys; hence the structure was assumed to be fixed against translation transversely and vertically. The rotational degrees of freedom were modeled as unrestrained for rotation about the vertical and transverse axis, but were fixed for longitudinal axis/torsional rotation. In reality, some degree of flexibility would be present for the structure transversely, based on the transverse stiffness of the abutment piles and the passive soil pressures on the abutment wingwalls. Because of the large width of each abutment and the uniformly spaced CIDH piles, this transverse stiffness is large and is assumed to be fixed.

Structure non-linearity at the expansion joint hinges was also modeled with non-linear link elements. These link elements were used to model the design gap at each expansion joint, along with the restrainer system specified in the design to prevent unseating and restrict relative longitudinal motion between adjacent frames. For translation of the adjacent frames towards one another, zero stiffness is modeled up to the plan-specified gap; a secondary stiffness is then incorporated to model the closed gap. The secondary stiffness models the stiffness of the rubber bumpers incorporated in the design in series with the axial stiffness of the superstructure. For translation of the adjacent frames away from each other, zero stiffness is modeled for 150 mm to model the gap incorporated in to the expansion joint restrainer design (Figure 4-19). A secondary stiffness is then specified that is equal to the axial stiffness of the hinge-restrainer system. The expansion joint hinges feature transverse shear keys, and were subsequently modeled as being fixed transversely and vertically. Transverse and vertical rotations were assumed to be unrestrained; longitudinal axis/torsional rotation was assumed to be fixed. The longitudinal force displacement response for Hinge 1 and Hinge 2 (Figure 2-9) are shown in Figure 4-20 and 4-21 respectively.

As described in previous chapters, the Galena Creek Bridge is comprised of two separate structures, each comprised of three frames. The middle frame of each structure, containing the arch, is linked together by means of a link slab joining the adjacent overhangs, and beams connecting the thrust blocks. These unique design features warranted special consideration in developing the seismic model. To model the link beams at Piers 2 & 3 (Figure 2-14), special detail had to be given to model the thrust

blocks. For each thrust block the point of fixity was moved to the bottom of the footing. The middle section was modeled with a non-prismatic section to properly model the mass and stiffness of the section. An intermediate node on the mid-section element was inserted to provide a connection point for the link beam (Figure 4-22). Shell elements were used to model the 200 mm thick link slab. Because the Galena Creek Bridge model is a “beam-stick” model, the superstructure element is represented with a “line” that passes through the center of gravity (C.G.) of the section. Since the two structures are at different elevations and because the link slab joins the two structures’ overhangs, rigid links were modeled that extended from the (C.G.) of the superstructure to the theoretical point in space where the overhangs terminate (Figure 4-23). The shell elements modeling the link slab is then connected to these rigid links.

#### **4.2.4. Moment-Curvature Analysis**

The Galena Creek Bridge features tall and slender columns. The response of the structure due to flexural hinging therefore needs to be accounted for in the analysis. Since the columns are flexure-dominant, the effect of shear hinging can be safely neglected. The force-displacement response of various structure components was needed to develop the flexural-hinge models.

The first step in this analysis was to estimate the axial loads for each component to find the moment-curvature response. A linear-elastic analysis of the structure under the effects of dead loads and the post-tensioning loads was performed first. The results of this model yielded service-load axial force effects for the columns and arch. The axial load effects from live loading were neglected to yield a more conservative moment-curvature response. The software program XTRACT (Imbsen) was used to find the moment-curvature response of each structure component. Separate analyses were needed for the top and bottom of each column due to the varying axial loads along the column length. For the arch, the same process was used; the arch at Segment 0 near the thrust-block interface was modeled, as well as the portion of the arch rib adjacent to the crown/merge area.

The typical arch and column cross sections were used to develop confined concrete stress-strain models using the techniques recommended by Mander (1988). This method makes use of confining pressures to determine the confined concrete properties, which are primarily a function of the amount, size, and spacing of confining steel for a given section. Note that within the plastic hinge region at the top and bottom of each column, the steel reinforcement detailing is the same. The confined concrete curves for the column and arch are shown in Figures 4-24 and 4-25, respectively. The stress-strain relationship for the ASTM A706 reinforcing steel was based on the Park strain-hardening steel model (Computers and Structures, 2007). Once the stress-strain relationships for the materials in each section were known, the moment-curvature response was found for both of the primary axes of bending. A simplifying assumption that the axial loading remains fairly constant throughout the loading was made. This assumption allowed the use of a single hinge backbone curve for modeling the flexural hinges for each component. The XTRACT software program generates a bilinearized moment-curvature curve that can be input into the finite element software to generate the hinge backbone curve. Due to

limitations with the SAP2000 analysis software, the force displacement response for each degree of freedom is assumed to be uncoupled.

Once the moment-curvature relationship was determined for each component, an estimate of the plastic hinge length was needed. Recommendations by Paulay and Priestley (Paulay, 1992) were used to determine the effective plastic hinge length. From this, the plastic hinge length can be determined as

$$l_p = 0.08 \cdot l + 0.022 \cdot d_b \cdot f_y \quad (\text{MPa})$$

Where:  $l$ : Effective column length (m)  
 $d_b$ : Diameter of the longitudinal steel (m)  
 $f_y$ : Yield stress of longitudinal steel (MPa)

For typical beam and column proportions, this equation yields a plastic hinge length of 0.5 h, where h is the depth of the section. The Paulay and Priestley equation for plastic hinge length is a function of the effective column length, or equivalent cantilever length. As the columns on the Galena Creek Bridge have a wide range of column heights, a different plastic hinge length was determined for each column. Results from an elastic analysis revealed points of contra-flexure in the arch under the effect of dead loads and post-tensioning. This was used to determine the effective lengths necessary for determining the plastic hinge lengths for the arch.

Research performed at the University of California, San Diego (UCSD) has led to revised expressions for plastic hinge length that account for the member aspect ratio, crack angle, and shear ratio. The results of this research for unusual column shapes show a large discrepancy between the Paulay and Priestley expression for plastic hinge length and the actual measured value in laboratory tests (Dowell, 2002). The results also show that the difference between the two methods decreases as the ratio of plastic hinge length to effective column length decreases. The average Paulay & Priestley plastic hinge to effective column length ratios for the Galena Creek Bridge is around 0.1, roughly half of the smallest ratio found in the UCSD testing. Further examination of the UCSD testing shows that the two techniques for determining plastic hinge length diverge as the columns become more shear dominant. This suggests that for flexure dominant columns, the two methods more closely approximate each other. In the absence of experimental data regarding the plastic hinge length of the Galena Creek columns, the Paulay and Priestley method for plastic hinge length was determined to be acceptable. A simplifying assumption was made that the plastic hinge length remained constant for the two axes of bending for each component. The calculated plastic hinge lengths for each column and arch are given in Table 4-8. The resulting bilinearized moment-rotation curves for each component are shown in Figures 4-26 thru 4-49. The elastic-plastic bilinear response was determined in the XTRACT software program.

It should be noted that the simplifying assumptions made regarding the uncoupled moment-rotation response and plastic hinge lengths were selected to simplify the analysis. SAP2000, the finite element software used to perform the non-linear time history analysis, has several different methods for performing the analysis. Consideration is given to the fact that although the Galena Creek Bridge is a relatively complex structure, there exist relatively few areas of non-linearity within the structure for typical design level earthquakes. This is due to modern ductile design philosophies that encourage a limited number of supporting members undergo inelastic action. As a result, modal time history

methods of analysis become attractive for their efficiency and the certainty in which areas of non-linearity are known. SAP2000 uses a numerically efficient modal time history method called the Wilson Fast Non-Linear Analysis (FNA). This method uses load dependent Ritz vectors to represent static loads on the structure, and is used to determine the mode shapes for the active degrees of freedom in the model. The FNA method, using the Ritz Vectors, treats member forces of non-linear elements within in the model as unknowns that are solved at the end of each time step by iteration. The global elastic stiffness matrix does not include any stiffness from non-linear elements; “dummy” elastic stiffnesses are assumed for initial model stability prior to iterating (Wilson, 1997). In this method, flexural hinges are modeled with non-linear link elements. Different types of link elements provide different types of non-linear response. Multi-linear plastic link elements were used to model flexural hinges within the model. In the input data form for these link elements, the user can specify the active degrees of freedom for each component of deformation (three translational, three rotational) and whether the response or stiffness of these degrees of freedom is linear or non-linear. For the flexural hinge link elements, only the rotational degrees of freedom corresponding to flexure were active. In the non-linear definition for these link elements, the force-deformation curves are entered, and an assumed hysteresis type is specified. Takeda hysteresis models were assumed for all flexural hinges in the model to capture strength degradation with cyclic loading (Takeda, 1970). Within the actual model, these link elements were assigned as short segments (1 mm in length) within a component to represent the lumped-plasticity non-linear response for that region of the structure. For model stability, the corresponding nodes on either end of the link element were assigned a constraint that constrained the inactive degrees of freedom within the link definition. In the case of the flexural hinge-links, the nodes were constrained for the three translational DOF as well as the torsional DOF. A diagram of a typical flexural hinge within the finite element model is shown in Figure 4-50.

Other methods of dynamic analysis that use direct integration schemes can be used in SAP2000. These techniques may be extremely sensitive to the integration time step and, accuracy can vary. Additionally, analysis times are significantly longer than the Fast Non-Linear method. Several different methods can be used to capture the flexural-hinging behavior of structural components. The first method uses fiber-hinge models that are defined for each unique cross section. Using this technique, interacting axial loading/biaxial moment response can be found. The time required for analysis is quite long, and generates very large output files. This technique is not practical for typical design and analysis projects because of how intensive the process is. Without experimental data to support the results, it is hard to judge the accuracy of the method and to justify its use in conventional applications. Other methods of capturing the flexural yielding response exist that are more efficient than generating the response by using a fiber hinge model. Uncoupled non-linear response can be found by specifying backbone curves for the force-displacement relationship being modeled. These curves are assigned to specific locations within a frame element as a lumped-plasticity hinge. Alternative methods use non-linear link elements to model local non-linearities and solves for the structural response with a direct integration method.

The Fast Non-Linear method was chosen for this study as it resulted in relatively accurate response predictions. Attempts were made to analyze the structure using the various direct integration techniques. Runs using fiber models would not converge for the entire structure, regardless of the time step used. To simplify the structure, Frame 2 was isolated and successful runs were achieved. Direct Integration methods are considered to be more exact than the Fast Non-Linear method. For this reason, Direct Integration runs were used to analyze models using non-linear link elements that captured plastic hinging behavior. The results of these runs were compared to Fast Non-Linear runs, and good correlation was noted. Figures 4-51 and 4-52 show a comparative displacement time history of the arch span for the 2500-year Centro 6 record in the transverse and longitudinal directions, respectively. A comparison of the moment-rotation response for the bottom of Pier 1 northbound for the same 2500-year Centro 6 ground motion also shows good correlation between the two methods; the longitudinal plot is found in Figure 4-53 and the transverse plot in Figure 4-54. Due to the good correlation between these two methods, the Fast Non-Linear method was deemed acceptable in yielding accurate results for the Galena Creek Bridge model and was used for the remainder of the analysis.

Further simplifying assumptions were made regarding inherent structural damping. SAP2000 allows different methods of introducing damping within a model. For modal time history analysis, damping can be assumed to be constant for each mode, or the user can specify mass or stiffness proportional damping. Initial models comparing direct integration and modal time history methods of analysis showed excellent correlation when stiffness and mass proportional damping was used, and assumed constant for all periods. For the purpose of this research, a constant 5 percent proportional damping was assumed, which is a reasonable assumption for reinforced concrete structures (Chopra, 2001.) It should be noted that the response spectrums used for scaling the applied ground motions were generated assuming 5 percent damping.

#### **4.2.5. Time-History Analysis**

As discussed previously, the time-history analysis made use of SAP2000's Fast Non Linear Analysis using load dependent Ritz Vectors. A beam-stick model was developed for the structure using frame elements for the various structural components. The SAP2000 section designer was used to develop equivalent section properties for the superstructure elements. Each component in the beam-stick model was meshed into approximately 3-m long elements. Tendon-elements were used to model the applied post-tensioning force in each span. The specified losses due to creep, shrinkage, steel relaxation, elastic shortening, friction, and anchor set were all considered in modeling the post-tensioning loads, as well as the stressing pattern (one end stressing vs. two end stressing). Rigid links are used in the merge area between the superstructure and the arch rib to establish connectivity. To account for the additional mass from the integral barrier rail in the bridge superstructure, a line mass of 1.3 KN-s<sup>2</sup>/m was applied to each superstructure element. Additionally, a distributed load of 13.4 KN/m was applied to each superstructure element to account for the additional dead load from the barrier rail.

Non-linear link elements were used to model flexural hinges. Each of these link elements were placed into the model as short elements; the two adjacent nodes for each link were modeled with constraints that constrained the three translational and torsional

degree of freedoms of each node. The response of the two rotational degrees of freedom came from non-linear moment-rotation curves entered for each component. Each of these links was modeled as being 1-mm in length to generate a lumped-plasticity non-linear flexural response.

For the Ritz modal analysis, a total of 220 structural vibration modes (544 total modes) were found for use in the modal time history analysis. The use of this many modes provided for roughly 95 percent mass participation for the three translational degrees of freedom for all 8500 active degrees of freedom in the model. Mass moments of inertia were ignored in the model, as per recommendations by the software documentation (Computers and Structures, 2007). For the Ritz Modal analysis case within SAP2000, the program was specified to account for the structural stiffness at the end of a non-linear dead load case that considered the effects of dead loads and post-tensioning loads. Starting load vectors for the Ritz Modal analysis included all non-linearity in model links, accelerations in the global longitudinal, transverse, and vertical directions, as well as the structure dead load and post-tensioning loads.

As Ritz modal analyses ignore cross-coupling between modes, an Eigen modal analysis was run to confirm that significant cross-coupling did not exist within the model. The results of the Eigen analysis confirmed that no significant cross-coupling existed. It should be noted that the developed finite element analysis model is a beam stick model. Because of this, the lack of cross coupling between modes is then not entirely unexpected due to the lumping of masses to the center of gravity of the section being modeled. The spatial distribution of masses within a cross section is not considered.

The first step in running the earthquake dynamic modal time histories was running a dead-load time modal history analysis in which the structure dead loads and post-tensioning loads were applied using a ramp function. The duration of the ramp function was sufficiently slow so as not to induce vibrations in the structure that would influence later load cases. To further ensure that that all vibrations were damped out, a plateau of constant load was applied for 10 seconds after the load had reached 100 percent. The earthquake modal histories then ran from the end state of dead-load modal history, and considered all loads active in the requisite load case. The three orthogonal acceleration time histories for each selected earthquake were then applied as acceleration loads in the global longitudinal, transverse, and vertical directions. The predetermined scale factors (“F”), determined as per FEMA 356 recommendations, for each ground motion were specified for the three acceleration components. An output time step size of 0.01 seconds was specified, along with constant modal damping of 5 percent for each ground motion. Force effects and displacements were taken as the average of the absolute maximum for each ground motion. The results of the non-linear time history analysis are presented in Chapter 5.

#### **4.2.6. Elastic Analysis**

In order to compare the non-linear time history analysis with traditional analysis methods as required in the AASHTO Standard Specifications and Load and Resistance Factor Design, an elastic response spectrum analysis was performed. The same basic model used for the non-linear time history analysis was used, with all points of non-linearity removed. The abutments were assumed to be free for longitudinal translation,

and fixed vertically and transversely; the rotational degrees of freedom were modeled as unrestrained for rotation about the vertical and transverse axis, but were fixed for longitudinal axis/torsional rotation. For the expansion joint hinges, the model was assumed to be unrestrained longitudinally, and fixed transversely and vertically. Transverse and vertical rotations were assumed to be unrestrained; longitudinal axis/torsional rotation was assumed to be fixed. Similarly as the non-linear model, cracked concrete properties were assumed, and were also based on the recommendations by Priestley et.al. The response spectrum analysis used the same 220 Ritz modes used for the non-linear analysis. The complete quadratic combination (CQC) method was used to determine force effects and displacements. Damping was assumed to be constant at 5 percent. The results of the elastic analysis are presented in Chapter 5.

## **Chapter 5**

### **Analysis Comparison**

#### **5.1. Basis of Analysis Comparison**

As discussed in previous chapters, the ultimate focus of this research project was to compare the methods of analysis used in the design of the Galena Creek Bridge with more refined methods. The analysis used in the design of the structure made use of response spectrum techniques based on an earthquake with a recurrence interval of 475-years. The refined analysis performed as part of the scope of this research used non-linear time history techniques to better estimate structure displacements and member forces. The comparison of the two techniques is based on the comparison of peak displacements and member forces.

#### **5.2. Modal Analysis**

Modal analysis is the first step necessary in performing analyses that are based on modal superposition techniques, such as response spectrum analysis and the so-called Fast Non-Linear analysis. Typical response spectrum analyses use mode shapes and frequencies found through an Eigen analysis of the characteristic equation of motion. The characteristic equation is a function of the structure mass and stiffness matrices. The corresponding eigenvalues and eigenvectors represent the natural frequencies and corresponding mode shapes for the structure. Once these values are known, modal contribution factors are then determined to find the contribution of each mode to determine a desired response quantity (Chopra, 2001). Various rules exist for combining response quantities for each mode of vibration to determine peak structure displacements and forces. The default modal combination rule used in the SAP2000 Software is called the complete quadratic combination (CQC) rule. If modal damping is present, this rule accounts for the coupling of closely spaced modes. When modal damping is zero, this method essentially becomes the square-root-of-the-sum-of-squares (SRSS) method.

The non-linear analysis performed as part of this research uses a different technique for finding the vibration modes of the Galena Creek Bridge. Ritz Modal Analysis is used, which differs from Eigen Modal analysis in that it takes into account the spatial distribution of the dynamic loading on the structure. Research has shown this to be more accurate in representing the vibration response of a structure (Wilson, 1982). To maintain consistency between the non-linear time history analysis and the elastic response spectrum analysis, the Ritz Modes were used for the both analyses. As would be expected, slight differences were noted between the two modal-analysis methods. The primary difference between the two is roughly 5%-7% longer periods for the Ritz analysis. Table 5-1 shows a summary of the structural periods of vibration and mass participation ratios for the three translational degrees of freedom for the first 17 modes of vibration for the Galena Creek Bridge. Note the relatively low mass participation after 17 structural modes, only 55.5 percent, 63.4 percent, and 32.5 percent for the global X, Y, and Z directions respectively.

### **5.3. Analysis Results**

In this section of the report, the results of the analysis are presented by comparing the elastic response spectrum analysis and the non-linear time history analysis at several key locations on the structure. Superstructure displacements at the top of each column and at mid-span of the arch are given to compare the drift at each of these locations. Peak displacements are also given at the two expansion joint hinges and at each abutment. Total base shear is given at the base of each column, as well as at the arch/thrust block interface. Peak moments are given at the top and bottom of each column, as well as at the arch/thrust block interface and the crown of the arch, adjacent to the superstructure merge area. For comparison of the two methods, ratios of response quantities are also reported; these results are expressed as the ratio of the non-linear value to elastic value. The results of the two analyses to the 475-year earthquake are presented first, followed by the results of the analyses to the 2500-year earthquake.

#### **5.3.1. Analysis Results, 475-Year Earthquake**

##### **5.3.1.1. Transverse Structure Response**

The transverse response of the Galena Creek Bridge to the 475-Year earthquake loading shows marked differences between the two analysis methods. Reasonable agreement between the non-linear time history analysis and the elastic response spectrum analysis are shown within Frame 1 and 2 for the northbound and southbound structures. Frame 3 shows the largest discrepancies between the analyses, where the non-linear analysis predicts higher displacements, shears, and moments.

Shown in Table 5-2 is a summary of peak structure displacements at the top of each column within the structures, as well as at mid-span of the arch. The non-linear analysis predicts slightly lower displacements for Pier 1, Pier 2, and mid-span of the arch in both the northbound and southbound structures. In Frame 3, the non-linear analysis shows much larger displacements than the elastic analysis, with the largest differences being in Piers 5 and 6 in both structures. Frames 1 and 3 also show differences in peak displacements between corresponding columns in the northbound and southbound structures. The southbound structure sees slightly lower peak displacements (but comparable drifts) due to the shorter column heights throughout the length of the structure.

The behavior of Frame 2 differs from the other two frames in the Galena Creek Bridge due to the connectivity that exists between the northbound and southbound structures. The two structures are joined throughout the length of the frame by a link slab that joins the two structures' overhangs. Additionally, the large link beams at both thrust blocks help to transfer load between the two structures. These two design features force common locations within the northbound and southbound structures to undergo the same transverse displacements due to the rigid nature of the joining elements for the transverse direction of loading.

Other general trends that are noted when comparing the results of the non-linear time history analysis and the elastic response spectrum analysis are the larger differences between the two analysis methods for the southbound structure as compared to the northbound structure. It should be noted that both structures remain elastic with the

exception of the bottom of Pier 4 northbound, and the bottoms of Pier 4 and Pier 5 southbound. Possible explanations for the larger differences in peak displacements between the two analysis methods for the southbound structure likely originate in the fact that the southbound structure has shorter, stiffer columns than the corresponding columns in the northbound structure.

The results of the two analyses vary throughout the length of the structure when comparing predicted base shears. Table 5-3 shows a summary of transverse base shears for the 475-year earthquake loading. As seen in the comparison of peak displacements between the two analysis methods, there is wide variation in the results depending on the frame being considered, and between the northbound and southbound structures. For Frame 1, both structures show reasonable agreement with each other as do the non-linear and elastic analyses. For both structures, the non-linear analysis predicts slightly larger transverse base shears. Frame 2 shows good correlation between the northbound and southbound structures. The elastic analysis predicts larger base shears for Piers 2 and 3 in both structures than the non-linear analysis, while the non-linear analysis predicts larger base shears than the elastic analysis for the base of arch at each thrust block in each structure. Frame 3 of the structure generally shows larger base shears for the non-linear analysis as compared to the elastic analysis. Similar trends as shown in the displacement comparison are noted, with the shorter columns of the southbound structure showing slightly larger discrepancies between the two analysis methods than the northbound columns.

Comparing the results of the structure to flexural demand from the non-linear analysis and the elastic analysis reveal similar trends as noted in the comparison of displacements and base shears. Tables 5-4 and 5-5 show a summary of transverse moments for the northbound and southbound structures, respectively. Once again, distinct differences are noted depending on the frame being considered. The non-linear analysis predicts larger moments than the elastic analysis for the top and bottom of each column within Frames 1 and 3; that is, Piers 1, 4, 5, and 6. For Frame 2, the elastic analysis predicts larger moments than the non-linear analysis for the top and bottom of Piers 2 and 3, as well as the base of arch (Segment 0 and 0A). For the arch crown region, the non-linear analysis predicts higher moments than the elastic analysis. Note that “arch crown” followed by the number “2” designates the region closer to Pier 2; similarly, “arch crown” followed by the number “3” designates the region closer to Pier 3.

Due to transverse shear keys that fuse the three frames of the structure together, there is significant interaction between each frame on the total structure response. The largest discrepancies in key response quantities between the non-linear time history analysis and the elastic response spectrum analysis are in prediction of force effects in the arch, and in peak displacements within Frame 3. Note that very limited yielding is predicted by the non-linear analysis, which would ordinarily suggest better correlation between the two methods. However, the non-linear analysis seems to show load shedding to Frame 3 and the arch, as shown in the much larger non-linear displacements, shears and moments.

Recall that the reported force effects from the non-linear analysis are an average of seven unique time histories. Examining the results of each ground motion shows a greater tendency for Piers 3, 4, and 5 to yield as compared to other locations within the

bridge. For example, yielding is predicted by all seven ground motions at the bottom of Pier 4 southbound, and by six ground motions for the bottom of Pier 4 northbound. Force effects from five of the seven ground motions cause yielding at the bottom of Pier 3 in both structures. Due to the averaging of force effects, overall peak moments might not exceed the yield capacity of the column, but it does reveal insight into the distribution of loads to the concrete arch and Frame 3.

#### **5.3.1.2. Longitudinal Structure Response**

The longitudinal response of the Galena Creek Bridge is heavily dependent on the consideration given in modeling the imposed boundary conditions. For the non-linear analysis, structure non-linearity exists not only through flexural hinge formation, but also through non-linear response at the abutments and expansion joint hinges. However, the effects of the abutment and expansion joint hinge non-linearity is dependent on imposed displacements, and only effect the results when force effects are large enough to close design gaps, or engage the restrainer system incorporated into the expansion joint hinge design.

To examine the effect of the longitudinal abutment boundary conditions, three different abutment models were incorporated into analysis runs to examine the effect of abutment longitudinal stiffness on overall bridge response. The first abutment model is considered the most comprehensive of the three, as it discretely models the soil-structure interaction at the abutment back-wall. As described in section 4.2.3, the model uses two multi-linear plastic link elements in series, one to model the abutment gap, and the other to model an elastic perfectly-plastic soil response. The second abutment model considers just the design gap at the abutment, with a rigid soil mass behind the back-wall. The third abutment model assumed as free longitudinal degree of freedom.

To illustrate the different response of each of these models and its effect on frame forces and displacements, the longitudinal displacement history of Frame 1 northbound and Frame 1 southbound to the 2500-year KJMA ground motion are shown in Figures 5-1 and 5-2, respectively. In comparing the response of the two frames, note a larger residual drift in Frame 2 northbound, which exhibited larger maximum displacements. The comprehensive abutment model allows for approximately 142 mm of displacement before the soil behaves plastically, allowing unrestrained longitudinal displacement.

Examination of the response of the bottom of Pier 1 in both frames shows higher moments and rotations for the two abutment models that discretely consider longitudinal stiffness. Note that larger peak displacements for movement away from the abutment are larger for the two abutment models that include some form of longitudinal stiffness. This increase in peak displacements allows for larger moments to be generated in the adjacent columns, and accounts for the larger residual drift at Pier 1 when compared to the simple abutment model. Figures 5-3 and 5-4 show the moment-rotation response for the 2500-year KJMA ground motion for the bottom of Pier 1 northbound and Pier 1 southbound, respectively. Figures 5-5 and 5-6 show the moment time history for the 2500-year KJMA ground motion for the bottom of Pier 1 northbound and Pier 1 southbound, respectively.

For the comparison of the non-linear time history analysis and the elastic response spectrum analysis, the non-linear time history analysis uses the comprehensive abutment model. Under the effect of the 475-year earthquake, peak displacements vary between the

northbound and southbound structure, and the location within the structure. A summary of longitudinal displacements for the 475-year earthquake is shown in Table 5-6. A general trend noted when comparing the results is the larger elastic displacements as compared to the non-linear analysis for the northbound structure; for the southbound structure, the non-linear analysis predicts larger displacements than the elastic analysis. In general, peak displacements between the two analysis methods are reasonably close for Frames 1 and 2. In Frame 3, larger discrepancies between the two methods are noted. Important to note is the larger differences in column heights between the two structures in Frame 3.

Comparison of the two analysis methods reveals more interesting trends when examining peak base shears and peak moments throughout the structure. Shown in Table 5-7 is peak longitudinal base shears for the 475-year earthquake. Note the larger elastic base shears as compared to the non-linear base shears for Frames 1 and 3 in both structures. Frame 2 shows just the opposite trends, with the non-linear analysis prediction larger base shears than the elastic analysis. Other general trends to note are the larger base shears in the southbound structure as compared to the northbound structure.

A comparison of peak moment demands for the northbound and southbound structures are shown Tables 5-8 and 5-9, respectively. As was shown in the comparison of base shears, the elastic analysis again controls over the non-linear analysis for Frames 1 and 3, while the non-linear analysis controls for Frame 3. Looking at the status of the flexural hinges at the top and bottom of each column as well as the arch shows no yielding in Frame 2, while the majority of the columns in Frames 1 and 3 in both structures show the formation of plastic hinges.

### **5.3.2. Analysis Results, 2500-Year Earthquake**

#### **5.3.2.1. Transverse Structure Response**

The response of the Galena Creek Bridge under the 2500-year earthquake shows similar trends as the response of the structure to 475-year earthquake loading. Key differences that change the distribution of forces is more widespread yielding within the structure in the transverse direction. Once again, similar trends are noted between the two structures. As would be expected, the shorter stiffer columns in the southbound structure have a tendency to exhibit larger forces than their corresponding columns in the northbound structure.

Peak transverse displacements under the 2500-year earthquake loading follow virtually the same trends and differences between the non-linear time history analysis and the elastic response spectrum analysis as was noted for the 475-year earthquake. Table 5-10 summarizes peak displacements for both analysis methods for the 2500-year earthquake loading. Frames 1 and 2 see larger elastic displacements as compared to the non-linear peak displacements. For Piers 3, 4, 5, and 6, non-linear displacements are larger than the elastic displacements, with larger discrepancies noted for the columns furthest from the arch span.

As was shown in the comparison of force effects from the 475-year earthquake, force effects for the 2500-year earthquake also show much larger differences between the two analysis methods for the concrete arch and Frame 3. Table 5-11 shows a summary of

peak transverse base shears for the 2500-year earthquake. As was noted previously, base shears in Piers 1, 2, 3, and 4 are larger for the elastic analysis as compared to the non-linear analysis. The largest differences occur in the columns adjacent to the arch span, Piers 2 and 3. Also interesting to note is the very large differences between the non-linear time history analysis and the elastic response spectrum analysis in the peak force effects in Pier 6 in both structures. Here, peak transverse base shears are more than two times as large for the non-linear analysis as compared the elastic analysis.

Comparison of the flexural demand for the 2500-year earthquake loading between the two analyses again show similar trends as was noted for the 475-year earthquake. Tables 5-12 and 5-13 show peak transverse moments for the northbound and southbound structures, respectively. When compared to the results of the 475-year earthquake, the first thing that is noted is more widespread yielding throughout the structure. Frame 1 under the lower earthquake loading remained elastic in the non-linear analysis, but shows slight yielding when subjected to the 2500-year earthquake loading. Limited yielding is noted in Frame 2, and Frame 3 shows slightly more yielding.

An important thing to note in looking at the peak flexural demands is the tendency for the arch crown to attract more load for the non-linear analysis as compared to the elastic analysis. The base of the arch at Segments 0 and 0A show larger elastic moment demands than the non-linear moments, even without with formation of plastic hinges at the base of the arch.

#### **5.3.2.2. Longitudinal Structure Response**

The longitudinal response of the Galena Creek Bridge to the 2500-year earthquake reveals larger differences between the two analysis methods than those noted in the response of the structure to 475-year earthquake loading. There is more widespread yielding throughout both structures, particularly in the southbound structure. Consequently, larger differences are noted in the peak force effects predicted by the non-linear time history analysis and the elastic response spectrum analysis.

A comparison of peak longitudinal displacements to the 2500-year earthquake is shown in Table 5-14. Recall that for longitudinal displacement of the structure, gaps at the expansion joint hinges allow a certain amount of relative displacement between adjacent frames in the structure. As such, peak displacements between the two structures and in adjacent frames can show large differences, unlike the forced interaction for transverse movement. For the northbound structure, each of the three frames has larger predicted non-linear displacements than elastic displacements. For the southbound structure, the controlling analysis case changes throughout the structure. Elastic displacements exceed the non-linear displacements at Pier 1 and Pier 3. Non-linear displacements exceed the predicted elastic displacements for the remaining locations in the structure, namely at Pier, Mid-Span of the Arch, and Piers 4, 5, and 6.

In comparing the two analyses in peak base shears, the same trends as were noted for the 475-year earthquake hold true. Table 5-15 shows a summary of peak longitudinal base shears for the 2500-year earthquake. Note that base shears in Frames 1 and 3 show higher elastic values than non-linear values, while Frame 2 shows higher non-linear base shears than elastic base shears. Also note that the magnitude of the ratio of the force effect from the two analyses shows larger differences than were seen under 475-year

earthquake loading. The results between corresponding columns in the two structure are similar, with the exception of Pier 4. For Pier 4 northbound, non-linear base shears are roughly 79 percent of the elastic shears; for Pier 4 southbound, non-linear base shears are roughly 35% of the elastic shears.

Flexural demands between the two analyses also show larger differences than were seen under the 475-year earthquake loading. Tables 5-16 and 5-17 show a summary of peak longitudinal moments for the 2500-year earthquake loading. In the southbound structure, the top and bottom of each column shows yielding, with the most extensive yielding showing at the bottoms of Pier 1 and Pier 6. Additionally, yielding is shown in the arch crown region, as well as the tops of the adjacent columns to the arch span, Piers 2 and 3. For the northbound structure, similar trends are noted; however, force effects at the tops of Piers 4 and 5 and the bottom of Pier 4 are about 98 percent of the yield moment. Also noted is the formation of plastic hinges in the arch crown region and the adjacent columns to the arch span, Piers 2 and 3.

## **5.4. Analysis Discussion**

### **5.4.1. Transverse Response**

The transverse response of the Galena Creek Bridge shows several interesting trends when comparing the non-linear time history analysis and the elastic time history analysis. It should be reminded that with the exception of the non-linear link elements used at the top and bottom of each column and the arch to model flexural hinges, no non-linearity exists within the model in the transverse direction. At the abutments and expansion joint hinges, transverse shear keys act to fuse the three frame of the structure together. This allows for redistribution of loads from one frame of the bridge to the other, creating distinct load paths as plastic hinges form.

Figures 5-7 and 5-8 show a comparison chart of transverse displacements for the 475-year earthquake for the northbound and southbound structures, respectively. Note the larger non-linear displacements for Piers 3, 4, 5 and 6 in both structures as compared to the elastic analysis. As discussed previously, in the absence of yielding, the non-linear analysis shows larger flexural and shear demands within Frames 1 and 3 than the elastic analysis. Load distribution within Frame 2 shows a tendency for the arch crown, also in the absence of yielding, to have larger non-linear force effects than elastic force effects. As shown in Table 5-5, the bottom of Piers 4 and 5 in the southbound structure see fairly significant yielding under the 475-year earthquake, with plastic rotations exceeding the yield rotation by 6.4 and 4.3 times, respectively. The redistribution of forces in the non-linear analysis due to this plastic hinging causes large peaks in the Arch Crown region, explaining the large differences between the two analysis methods. Results of the analysis of the 2500-year earthquake also show this phenomenon.

The effect of plastic hinging within Frame 3 of the southbound structure also works to increase peak displacements, and accounts for the large differences between the two analyses for Piers 3, 4, 5 and 6. For the same input acceleration and in the absence of yielding, it would be expected that both the non-linear analysis and the elastic response spectrum analysis would predict roughly the same displacements. Additionally, common design theory maintains that even with yielding, elastic and non-linear displacements

should be approximately the same, due to the use of response modification factors. In this particular analysis, it would be expected that with little or no-yielding, the non-linear analysis would predict higher displacements than the elastic analysis due to the fact that the composite response spectrum curves from the used ground motions exceed the design spectrum within the periods of interest. What the non-linear dynamic analysis reveals is the effect of load path and force distribution on the system, an interaction not seen in traditional response spectrum techniques. Examination of the individual response of various components within the structure to each unique ground motion shows more consistent inelastic action within Piers 3, 4 and 5. The plastic hinging at these locations works to allow Frame 3 to “pull” the adjacent frames, increasing displacements within the non-linear analysis.

There are other key differences between the two methods of analysis that could also be affecting the results, in part explaining the non-uniform differences between the two analysis methods. As per the AASHTO recommendations, an elastic analysis for a given direction (transverse or longitudinal) considers 100% of the force effect in the primary direction, plus 30% of the force effect in the secondary direction. With the non-linear analysis, loading in all directions is considered simultaneously, which could potentially result in significant torsional effects. To illustrate this effect, Figure 5-9 shows a transverse displacement history for Pier 3 northbound and Pier 2 southbound for the 2500-year Centro 7 ground motion. Superimposed on the graph is the peak positive displacements predicted by the AASHTO Response Spectrum analysis. The non-uniform transverse displacement of these two columns, located on opposite corners of Frame 2, show the effect that torsion has on peak displacements within the structure. The difference between the two analysis methods becomes even more apparent after examination of this figure. While the elastic method does indeed predict a slight torsion effect, the torsion effect from the non-linear analysis is far more severe on the response of the structure. Other evidence of global torsional effects being more dominant in the non-linear analysis is the predicted transverse moments in the arch crown. For both levels of earthquake loading considered, the non-linear analysis predicted higher transverse moments. For the 475-year earthquake, the non-linear analysis shows 95% higher transverse moments at Crown 2 in the northbound structure and 99% higher moments for the southbound structure. The effects at Crown 3 are not as pronounced but still evident, with higher non-linear moments by 14% in the northbound structure and 56% in the southbound structure. This increase in moment at the top of the arch could also explain the differences in base shears noted at the bottom of the arch, as the non-linear analysis shows higher base shears for both thrust blocks in both structures, while the elastic analysis controls the response at both Pier 2 and 3.

Other discrepancies between the two analysis methods on the transverse response of the structure are revealed in the distribution of base shear between the various columns in the structure. Note that the difference between the two analysis methods is relatively low for Pier 1 northbound and southbound, with the non-linear analysis predicting slightly higher response quantities. For Frame 3, very large differences between the two methods are noted. Relative errors for Frame 2 are somewhat in the middle of the extremes shown in the Frame 1 response. These results demonstrate an apparent load path or force distribution that is exposed through the non-linear analysis, but not apparent

from the elastic analysis. Consequences of this unexpected interaction include the onset of yielding for transverse bending in the columns of Frame 3, adding further insight into the discrepancies between the two analysis methods and the interaction between adjacent frames. Also note that the non-linear analysis shows much larger base shears at the base of arch, and lower base shears in the adjacent columns (Piers 2 and 3). The exact reason for this distribution of base shear is unknown, but it shows a fundamental difference between the two methods. One possible explanation is through the interaction between the northbound and southbound structures due to the link beams and link slabs, presenting a stiffer load path through the concrete arch as opposed to the adjacent columns.

#### **5.4.2. Longitudinal Response**

Comparing the longitudinal response of the Galena Creek Bridge for the two analysis methods is complicated by the interaction of the structure at the expansion joint hinges and the abutments. While the elastic analysis neglects the gaps and the restrainer assemblies at the hinges as well as the gaps and soil-structure interaction at the abutments, the results of the non-linear analysis are heavily influenced by the effects of these interactions.

Peak structure displacements vary between the northbound and southbound structures, and demonstrate the effect of frame flexibility as well as the non-linear behavior at the hinges and abutments. Figures 5-10 and 5-11 show a comparison of peak structure displacements for the northbound and southbound structures, respectively, for the 475-year earthquake loading. For the northbound structure, predicted elastic displacements exceed the non-linear displacements for every column in the structure. The southbound structure shows slightly different behavior, with the non-linear displacements being larger for each column in the structure, with the exception of Pier 3. Examination of the longitudinal flexural response of each column shows several other significant details. While Frame 2 stays mostly elastic to the 475-year earthquake loading, yielding is noted in the non-linear analysis in both of the other frames. Yielding is predicted by the non-linear analysis at the base of Pier 1 in both structures. The response of Pier 6 is similar, with both the top and bottom of the column showing yielding in both structures. Pier 4 and Pier 5 show yielding at the top and bottom for the southbound structure but both remain elastic in the northbound structure.

Looking at the response of both structures at each abutment offers insight into this predicted behavior. Shown in Figure 5-12 is a comparison of non-linear and elastic displacements at each abutment for the two structures for the 475-year earthquake. The displacements shown are peak displacements in the direction of the abutment back-wall, which are limited in the non-linear analysis due to the consideration given to soil-structure interaction. The flexural response of the columns in Frame 3 show significant yielding in the southbound structure, with mostly elastic behavior in the northbound structure. Note that longitudinal displacements at Abutment 2 are larger for the northbound structure. One possible explanation for this behavior is in the effect the longitudinal reaction at the abutment has on the adjacent columns. A reaction introduced at the abutments generates an alternate load path for the inertial forces generated by the imposed earthquake. This reaction helps to relieve load that otherwise would have

generated large moments in the adjacent columns. Ultimately this results in lower peak moments for the adjacent columns.

The flexural response of Frame 3 offers a great illustration of this effect. In Figure 5-12, note the much larger inelastic action present in the northbound structure at the abutment, and consequently the larger reaction force generated within Frame 3. In Examining Table 5-8, slight yielding is noted at the top and bottom of Pier 6. Opposite from this is the response of the southbound structure. While total non-linear force effects from the 475-year earthquake are substantial enough to close the gap at the abutment, the total generated reaction force is less than a quarter of the reaction generated in the northbound structure. As shown in Table 5-9, yielding is noted at the top and bottom of each column within Frame 3. The reaction force at the abutment in Frame 3 northbound effectively caps the applied earthquake moment, allowing the majority of the columns to remain elastic. For the southbound structure, plastic hinges form at the top and bottom of each column. For the 2500-year earthquake loading, similar results are noted; in the northbound structure, more yielding is present at the bottom of the adjacent columns, while the tops of these columns remain elastic. In the southbound structure, plastic hinges are formed at the top and bottom of each column.

To further examine this behavior, the Centro 6 ground motion was selected, as predicted displacements show gap-closing at the abutment, but unrestrained displacement at Hinge 2. Shown in Figure 5-13 is a time history for the 475-Year Centro 6 ground motion plotting the moment at the base of Pier 4 northbound and Pier 4 southbound, and the longitudinal reaction at Abutment 2 for the northbound structure. Note the good correlation in peak moments for approximately the first 5 seconds of the record, and the large difference in peak moment between the two columns when the abutment reaction is introduced in the northbound structure. Pier 4 southbound shows the formation of a plastic hinge at around 7 seconds, which explains the dramatic difference in the moment time history for the two columns after yielding.

The interactions between peak column moments and abutment reactions are also perpetuated with an increase in the earthquake force. Figure 5-14 shows a comparison of non-linear and elastic displacements at each abutment for the 2500-year earthquake level. Note that at three of the four abutments, the soil is considered to be in a yielded state due to high longitudinal displacements. Abutment 2 northbound shows the highest non-linear peak displacement; correspondingly, it sees the highest elastic displacements as well. Looking at the flexural response of the adjacent columns in Frame 3 northbound shows the top and bottom of Pier 4 as well as the top of Pier 5 remaining elastic. Comparing the base shears, Pier 4 northbound shows the lowest relative error between the two analysis methods. This would suggest that Pier 4 remaining below its yield point is in part caused by the large reactions generated by the restraint at the abutment. Figure 5-15 shows the hysteretic response of the non-linear soil spring at Abutment 2 NB for the 2500-year Centro 6 ground motion. Note the increased gap opening in the second loading cycle that occurs as a consequence of soil yielding the first cycle.

In addition to displacements being limited in one direction for the two end frames due to the abutments, similar restraints are caused by the expansion joint hinges. As discussed in Chapter 3, relative translation between adjacent frames away from each other at each hinge is unrestrained up to a displacement of 150-mm. Displacement

beyond this threshold is limited by restrainer assemblies. For relative translation in adjacent frames towards each other, displacement is unrestrained up to 146-mm in Hinge 1 and 190-mm in Hinge 2. Shown in Figures 5-16 and 5-17 is a comparison of the two analysis methods in predicted displacements at the two expansion joint hinges for the 475-year earthquake. Figure 5-16 shows peak relative displacement between frames for translation away from each other; Figure 5-17 shows peak relative displacement between frames for translation towards each other. Note that in Figure 5-17 the compression gap is never “closed.” However, as shown in Figure 5-16, the hinge restrainers are engaged at each hinge. This shows a great example of the differences between the two models. Due to these imposed reactions that are neglected in the elastic response spectrum analysis, the effect of the interaction between frames is lost. As was noted in examination of the effect of longitudinal abutment reactions, these forces would have effects on the adjacent columns. Additionally, closing either the tension or compression gap at a given hinge would cause unintended interaction between adjacent frames.

To examine the effect of engaging the hinge restrainers on nearby columns, the 475-year Denali ground motion was selected and run through two models. One model considered the full non-linear behavior of the structure at the expansion joint hinges, while the other assumed a free longitudinal degree of freedom at the expansion joint hinges. Peak column moments at the bottom of Piers 4, 5 and 6 southbound were compared between the two models. While the hinge reaction did in fact reduce peak column moments, the change was very minor. Relative differences between the two models were only 0.7 percent for Pier 4, 0.3 percent for Pier 5, and 0.1 percent for Pier 6.

The relatively small stiffness of the restrainer system when compared to the longitudinal abutment stiffness is the likely explanation for the minor affect the engaged restrainers have on adjacent columns. Also important to note is the fact that in both models, peak moments exceed the yield moment of the adjacent columns. For a ground motion where the columns remained elastic, the force effects from non-linear interaction at the hinges might have a more significant impact on structural behavior. By engaging the hinge restrainers or closing the expansion joint hinge gap, load would be transferred to adjacent frames, reducing moment demands on the nearby columns.

It should be noted that the expansion joint hinge and abutment models considered in this analysis were for a specific temperature and time after prestressing. With a variation in temperature, the gap openings at these locations could be different, which would slightly change the results of the analysis. Similarly, in the time shortly after prestressing before significant creep-deformations are imposed on the structure, the gaps at the abutments and expansion joint hinges would be smaller, which would potentially affect the results of the analysis. As shown in the results of the non-linear analysis, impact at the hinges or abutments or engaging the restrainer assemblies does have an affect on nearby columns and could lead to an un-conservative estimate on peak force effects. Figures 5-18 and 5-19 show a plot of peak non-linear displacements against the predicted gap openings at discrete points in time after prestressing for Hinge 1 and Hinge 2, respectively. The predicted displacements for Hinge 2 in both structures show the initial gap to be sufficient for the design level earthquake. For Hinge 1, predicted non-linear displacements are larger than the gap opening until roughly 10 weeks after stressing.

One other key difference between the elastic response spectrum analysis and the non-linear time history analysis is the inclusion of the vertical component of acceleration in the non-linear analysis. It would be expected that the vertical acceleration would increase moments for longitudinal bending at the top of each column due to the vertical acceleration of the adjacent spans. To examine and quantify the effect that vertical acceleration has on moments in adjacent columns, the 2500-year Centro 6 ground motion was selected and run through the model in two analysis cases. The first case considered vertical acceleration, and the second neglected it. The Centro 6 record was selected for its large vertical accelerations. Figure 5-20 compares the moment response of Crown 2 southbound to vertical acceleration. Figure 5-21 compares the moment response of the top of Pier 3 southbound to vertical acceleration. Plotted against both moment histories is the vertical ground acceleration. The results of this analysis show that the effects of vertical acceleration can be quite significant, with local peak moments 1.7 times larger when vertical acceleration is considered (at approximately 2.6 sec into the time history). Note the large increase in moments that correspond to peaks in the vertical ground acceleration. As might be expected, this effect would widely vary depending on characteristics of a specific earthquake, local site conditions, and proximity to an earthquake fault.

Comparing the results of the non-linear analysis to the response spectrum analysis for Frame 2 confirms the effect of vertical acceleration when the components remain elastic. For the 475-year earthquake, longitudinal moments are larger for the non-linear analysis than for the elastic analysis; for this earthquake level Frame 2 remains elastic, with the exception of Crown 3 northbound. For the 2500-year earthquake, the results flip, with the non-linear analysis controlling when there is no yielding in a component, and with the elastic analysis controlling when yielding is predicted. This would suggest that the inclusion of vertical acceleration could potentially lead to the onset of yielding within components. In comparing the differences between Figure 5-20 and Figure 5-21, it becomes readily apparent that vertical acceleration has a much larger effect on moments in the arch, as opposed to the nearby columns. This is not entirely unexpected due to the large mass being supported at mid-span of the arch frame, near the merge area. This in part also explains the large relative errors between the non-linear analysis and the elastic analysis for the arch crown region. Moment behavior at the base of the arch (Segments 0 and 0A) is slightly more affected by vertical accelerations than moments at the tops of the adjacent columns, but isn't nearly as pronounced as the effect in the arch crown region. Figure 5-22 shows a moment time history comparing the effects of vertical acceleration for Segment 0 of the arch for the southbound structure.

## **5.5. Conclusions**

The results of the two analyses performed on the Galena Creek Bridge reveal insight into the behavior of the structure under dynamic loading. Several conclusions can be drawn after comparison of the two analysis methods. The elastic response spectrum technique, based on multi-modal superposition, in general offers reasonable estimates on structure forces and displacements. Through the use of response modification factors, the effects of yielding can be limited to certain structure components. This helps to ensure the safety and collapse prevention of the structure, assuming sufficient ductility exists

through proper detailing. However, to obtain a better grasp of the interaction of complex multi-frame structures, methods of analysis such as the non-linear time history analysis prove to be a more effective tool by accounting for localized non-linear behavior of the structure. The effects of yielding in one portion of the structure and the redistribution of loads is accounted for, allowing design engineers to better understand the global effects of load redistribution.

From a design-tool standpoint, a non-linear time history analysis may be impractical until the design of a structure is advanced to a certain point. The moment-curvature response of the bridge columns, for example, must be known in order to obtain accurate results. The magnitude of design dead loads, superimposed dead loads, and applied prestressing must also be known due to the non-linear response that is discretely accounted for. This being said, the non-linear time history analysis seems to be an effective tool to evaluate the seismic performance of the structure. The effect of design gaps in multi-frame bridges, for example, can be accounted for to ensure the behavior of the structure is as the designer intended.

In order to make a non-linear time history analysis feasible as a performance evaluation tool, simplifying assumptions need to be made. Some of these simplifications are necessitated based on limitations of the analysis software; others are based on time constraints that are undoubtedly a part of any bridge design. Chapter 4 discusses many of the simplifying assumptions that were made in consideration for this research. These include assumptions made about damping, the use of bilinearized moment-rotation curves, determination of plastic hinge length, uncoupled moment-rotation response, and the use of fixed foundations.

Other practical limitations on the use of non-linear time history analysis as a performance-based design tool are in the qualified selection of proper ground motions. In order to obtain realistic results using a non-linear time history analysis, local seismology needs to be carefully considered. The case for including multiple ground motions in an analysis (as per FEMA recommendations) is also strengthened, as it relieves the dependence on each unique ground motion by averaging results to obtain response quantities. This helps avoid cases when the response of a structure under consideration is dominated by a single ground motion.

Although FEMA recommendations were heeded by averaging the response to unique ground motions to generate design force effects, examination of the structure under a particular earthquake motion could potentially yield useful results. For instance, if a design engineer was interested in the effects of vertical acceleration, an earthquake motion with a particularly large vertical acceleration record could be used to study its effect on the structure.

As previously commented on, perhaps one of the most effective reasons for using an analysis tool such as a non-linear time history analysis is in sizing design gaps and designing restrainer-systems. This performance-based approach allows the designer to see the consequences of these features on global structure behavior. Due to the use of response-modification factors, actual peak structure displacements may not always be equal to elastic displacements. Additionally, the effect of yielding in one portion of the structure on other components is not accounted for. Using a performance based approach helps alleviate many of these issues.

It should be noted that other performance-based design methods exist, such as static push-over analysis. Further research could be performed to compare and contrast various performance-based methods of analysis.

One of the challenges in looking at methods, such as non-linear time history analysis, as a design tool is in evaluating and quantifying its level of conservatism on design. It can be argued that non-linear time history analysis is a more accurate method of analysis as it accounts for interactions that are not found in an elastic method of analysis. However, the careful consideration and scaling methods used for the input ground motions has a significant effect on the results of the analysis. Using the FEMA recommendations for example, scaling is performed based on a composite response spectrum and is recommended to exceed the design AASHTO spectrum by 40 percent. This fact alone would suggest a higher level of conservatism in the analysis due to higher force effects. Due to the vast differences between elastic methods of analysis and non-linear time history analysis, comparing the two based on a quantified level of conservatism seems inappropriate. Rather, it seems more prudent to compare the two based on the importance of a given structure, and the necessity for the designer to understand global behaviors and interactions in more sufficient detail.

## **Chapter 6**

### **Summary/Conclusions**

#### **6.1. Summary of Report**

During the design and construction of unique and unusual structures, it is important for engineers to understand the behavior and performance of the structure to different loading scenarios. For the Galena Creek Bridge, the understanding of the structure behavior both during the construction sequence and under earthquake loading is of particular interest, due to its unique and innovative design, and its close proximity to active earthquake faults.

The original arch design for the Galena Creek Bridge was comprised of a steel pilot truss that was used to support the bridge during construction. After truss erection, the pilot truss would be used to support traveling form work that would cast concrete to form the cathedral arch that supports the bridges' main span. The actual state of stress within the steel pilot truss, as well as the interaction between the pilot truss, conventional reinforcement, and concrete presented a unique opportunity for researchers. After being contracted by the Nevada Department of Transportation, the University of Nevada, Reno designed an instrumentation plan to monitor the arch in real time during construction and for a short period after the structure was completed.

The key feature of the instrumentation plan included the placement of gages on the pilot truss, on longitudinal reinforcement and embedded within the concrete at seven different locations on the southbound Galena Creek Arch and within the superstructure. A data acquisition system was designed to record data in real time, which would allow researchers to examine the behavior of the arch. Also included in the instrumentation plan was the inclusion of accelerometers within the arch span to capture the structure response to transient and seismic loading.

Due to unforeseen construction delays that included terminating the original construction contract, the design and method of construction of the bridge was slightly altered. The new contractor for the project elected to omit the steel pilot truss and construct the arch on falsework. The instrumentation plan was altered accordingly, with the pilot truss instrumentation allocated to other portions of the arch. Future research at the University of Nevada, Reno will carry out the revised instrumentation plan and analysis.

Due to the complex and irregular nature of the Galena Creek Bridge, as well as its' close proximity to an active earthquake fault, a non-linear time history analysis of the bridge was performed, and compared to conventional elastic response spectrum techniques. To perform the non-linear time history analysis, researchers consulted with seismologists at the University of Nevada, Reno to select seven earthquake time histories that featured characteristics similar to active faults near the location of the bridge. Using recommendations by the Federal Emergency Management Agency (FEMA), these seven earthquake motions were scaled based on the design response spectrum specified in the American Associations of State and Highway Transportation Officials (AASHTO) Standard Specifications for Highway Bridges. The scaled acceleration time histories were

input into finite element analysis models in SAP2000 as acceleration loads for the longitudinal, transverse, and vertical directions of motions. For comparison of the non-linear time history analysis with typical design methods, the specified AASHTO response spectrum analysis was also considered.

The finite element analysis models considered several types of structure non-linearity. Using the results of a moment-curvature analysis performed for each column in the structure, lumped-plasticity flexural hinges were defined at the top and bottom of each column and the top and bottom of the arch. The bridges' seat-type abutments were modeled with two springs in series; a gap element modeled the design gap between the end diaphragm and the abutment backwall, while an elastic-perfectly-plastic non-linear link element was used to model the soil response. At the expansion joint hinges adjacent to the arch span, gap and hook elements were used to model the design gap at the hinges and restrainer system, respectively.

The results of the analysis show different trends depending on the direction under consideration and the location on the structure. Due to the unique frequency content of each earthquake, the response of the structure is different for each ground motion used. As per FEMA recommendations, overall response quantities for the non-linear time history analysis are taken as the average of the response of the structure to each unique earthquake motion. The conclusions that were drawn from the comparison of the non-linear time history analysis and the elastic response spectrum analysis are summarized in section 6.2.

## **6.2. Conclusions**

After comparing the results of the non-linear time history analysis and the elastic response spectrum analysis, several conclusions were drawn.

### **A. The elastic response spectrum analysis method offers reasonable estimates on structure forces and displacements as compared to non-linear time history analysis.**

The results of the elastic response spectrum analysis and the non-linear time history analysis agree reasonably well. Due to the effects of plastic hinging in the non-linear analysis, force effects will not agree completely between the two analyses, assuming some yielding through the applied loads. Through the use of response modification factors, the effects of plastic hinging and local yielding are limited to certain locations of the structure, ensuring life safety and collapse prevention of the structure. As such, the use of elastic techniques is an effective design tool.

### **B. Non-linear time history analysis is an effective tool for performance-based evaluations of a structure.**

The use of techniques such as the non-linear time history analysis may be best suited as a performance-based analysis tool. Through the use of simplifying assumptions regarding structure performance, the use of such advanced techniques becomes more practical for irregular or unusual structures. Multi-frame bridges, for example, are an excellent candidate for use of more advanced seismic analysis tools. One of the more attractive reasons for using a technique such as non-linear time history analysis is in

better evaluating the interaction of adjacent frames due to design gaps and restrainer systems.

**C. Proper selection of input motions for a time-history analysis is a primary concern.**

As the primary goal of using an advanced technique such as a non-linear time history analysis is in understanding the behavior of a system under seismic loading that is reflective of the local seismology, the proper selection of input motions is extremely important. The use of multiple motions, as per FEMA recommendations, helps relieve the dependence on a single motion, but attempting to use motions that are not reflective of local seismology may provide unrealistic results.

**D. Non-linear time history analysis is best suited for understanding global behaviors and interactions.**

For the non-linear time history analysis performed for the Galena Creek Bridge, the most useful result of the analysis was in better understanding global behaviors and interactions. The effects of yielding in one portion of the structure and the redistribution of loads to other areas of the structure are better understood. For complex bridges, this becomes more and more attractive. Practical limitations for less complex, ordinary bridges may not justify the use of more elaborate seismic analyses.

## References

- AASHTO. "Standard Specifications for Highway Bridges, 17<sup>th</sup> Edition." American Association of State and Highway Transportation Officials. Washington, D.C. 2002.
- ACI 318-05. "Building Code Requirements for Structural Concrete and Commentary." American Concrete Institute. Farmington Hills, MI. 2005.
- Caltrans. "Seismic Design Criteria, Version 1.4." California Department of Transportation. Sacramento, CA. 2006.
- Chopra, A.K. "Dynamics of Structures: Theory and Applications to Earthquake Engineering." Prentice Hall. Upper Saddle River, New Jersey. 2001.
- Collins, M.P., and Mitchell, D. "Prestressed Concrete Structures." Prentice Hall. Englewood Cliffs, NJ. 1991.
- Computers and Structures, Inc. "SAP2000 Version 11.0.1 Non-Linear." Berkeley, CA.
- Computers and Structures, Inc. "SAP2000 Analysis Reference Manual." Computers and Structures, Inc. Berkeley, CA. 2007.
- Dowell, R.K., and Hines, E.M. "Plastic Hinge Length of Reinforced Concrete Bridge Columns." Proceedings of the Third National Seismic Conference and Workshop on Bridges and Highways. Portland, Oregon. 2002.
- FEMA 356. "Prestandard and Commentary for the Seismic Rehabilitation of Buildings." Federal Emergency Management Agency. Washington, D.C. 2000.
- Imbsen Software. "XTRACT." Sacramento, CA.
- Mander, J.B., Priestley, M.J.N., and Park, R. "Theoretical Stress-Strain Model for Confined Concrete." *Journal of Structural Engineering*, ASCE, V.114, No. 8, Aug. 1988.
- Paulay, T., and Priestley, M.J.N. "Seismic Design of Reinforced Concrete and Masonry Buildings." Wiley Interscience. New York. 1992.
- Priestley, M.J.N., Seible, F., and Calvi, G.M. "Seismic Design and Retrofit of Bridges." Wiley Interscience. New York. 1996.
- Sawyer, T.L. "Complete Report for Mount Rose Fault Zone (Class A) No. 1647." U.S. Geological Survey website, <http://earthquakes.usgs.gov/regional/qfaults>. (1999)
- Seismosoft, Inc. "Seismosignal, Version 3.2.0."

Takeda, T, Sozen, M.A., and Nielson, N.N. "Reinforced Concrete Response to Simulated Earthquakes." *Journal of Structural Engineering*, ASCE, V.96, No. 12, pp. 2257-2273, 1970

Wilson, E.L. "Three Dimensional Dynamic Analysis of Structures with Emphasis on Earthquake Engineering." Computers and Structures, Inc. Berkeley, CA. 1997

Wilson, E.L., Yuan, M.W., and Dickens, J.M.. "Dynamic Analysis by Direct Superposition of Ritz Vectors." *Earthquake Engineering and Structural Dynamics*, Vol. 10, pp. 813-823. 1982.

## Tables

**Table 4-1: Seismic Performance Category Based on Acceleration and Importance Classification**

Acceleration Coefficient	Importance Classification (IC)	
	I	II
A	I	II
$A \leq 0.09$	A	A
$0.09 < A \leq 0.19$	B	B
$0.19 < A \leq 0.29$	C	C
$0.29 < A$	D	C

**Table 4-2: Site Soil Coefficients**

Soil Profile Type	S
I	1.0
II	1.2
III	1.5
IV	2.0

**Table 4-3: AASHTO Response Modification Factors for Select Components**

Component	R
Single Columns	3
Multiple Column Bent	5
Vertical Reinforced Concrete Piles	3
Expansion Joints	0.8
Column-Superstructure Connection	1.0
Column-Foundation Connection	1.0

**Table 4-4: Selected Ground Motions**

<b>Earthquake</b>	<b>Station</b>	<b>Year</b>	<b>Magnitude</b>	<b>Description</b>
El Centro	Centro 6	1979	6.5	Strike Slip w/ Near Field Pulses
El Centro	Centro 7	1979	6.5	Strike Slip w/ Near Field Pulses
Denali	Denali	2002	7.8	Strike Slip w/ Near Field Pulses
Kobe	KJMA	1995	6.5	Strike Slip w/ Near Field Pulses
Parkfield	Parkfield	2004	6.0	Strike Slip w/ Near Field Pulses
Duzce	Duzce	1999	7.1	Fault Normal/Strike Slip
Duzce	Bolu	1999	7.1	Fault Normal/Strike Slip

**Table 4-5: Scale Factors, 10% Probability of Exceedance in 50 Years**

<b>Record</b>	<b>Scale Factor</b>
Centro 6	1.00
Centro 7	1.00
Denali	1.25
KJMA	0.70
Parkfield	0.90
Duzce	0.90
Bolu	0.90

**Table 4-6: Scale Factors, 2% Probability of Exceedance in 50 Years**

<b>Record</b>	<b>Scale Factor</b>
Centro 6	1.60
Centro 7	1.50
Denali	1.90
KJMA	1.00
Parkfield	1.15
Duzce	1.25
Bolu	1.25

**Table 4-7: Abutment and Hinge Gap Openings (mm) at 21°C**

<b>Time After Prestress (Weeks)</b>	<b>Abutment 1</b>	<b>Abutment 2</b>	<b>Hinge 1</b>	<b>Hinge 2</b>
2	55	55	100	100
3	56	57	108	108
6	59	61	117	123
12	61	65	131	142
30	64	70	145	162
52	67	75	160	182
1000	80	95	224	268

**Table 4-8: Column Plastic Hinge Lengths (Paulay and Priestley)**

<b>Column</b>	<b>Plastic Hinge Length (m)</b>
Pier 1 NB	1.181
Pier 2 NB	1.873
Pier 3 NB	1.909
Pier 4 NB	1.774
Pier 5 NB	1.609
Pier 6 NB	1.357
Pier 1 SB	1.080
Pier 2 SB	1.873
Pier 3 SB	1.909
Pier 4 SB	1.231
Pier 5 SB	1.278
Pier 6 SB	1.090

**Table 5-1: Modal Periods and Mass Participation Ratios**

Mode	Period (s)	Mass Participation Ratios			Cumm. Mass Participation Ratios		
		$U_x$	$U_y$	$U_z$	$\Sigma U_x$	$\Sigma U_y$	$\Sigma U_z$
1	1.85	0.0%	48.8%	0.0%	0.0%	48.8%	0.0%
2	1.71	9.6%	0.0%	0.0%	9.6%	48.8%	0.0%
3	1.65	11.0%	0.0%	0.0%	20.5%	48.8%	0.0%
4	1.25	5.9%	0.0%	0.0%	26.4%	48.8%	0.0%
5	1.07	4.2%	0.0%	0.0%	30.6%	48.8%	0.0%
6	1.05	13.0%	0.0%	0.0%	43.5%	48.8%	0.0%
7	0.93	0.0%	5.0%	0.0%	43.5%	53.8%	0.0%
8	0.86	0.0%	0.0%	3.1%	43.6%	53.8%	3.1%
9	0.73	0.2%	3.3%	0.0%	43.8%	57.2%	3.1%
10	0.72	5.4%	0.2%	0.2%	49.2%	57.3%	3.2%
11	0.67	0.0%	3.0%	0.0%	49.2%	60.3%	3.2%
12	0.66	0.0%	0.0%	5.6%	49.2%	60.3%	8.8%
13	0.53	1.1%	0.0%	12.4%	50.4%	60.7%	21.2%
14	0.50	4.3%	0.0%	5.2%	54.7%	60.7%	26.6%
15	0.42	0.2%	0.0%	4.3%	55.5%	61.1%	30.9%
16	0.38	0.0%	0.1%	1.4%	55.5%	61.9%	32.5%
17	0.38	0.0%	1.5%	0.0%	55.5%	63.4%	32.5%

**Table 5-2: Transverse Displacement Summary (475-Year EQ)**

	Location	Non-Linear		Elastic		Ratio
		Peak (m)	Drift	Peak (m)	Drift	
Frame 1	Pier 1 NB	0.061	0.27%	0.071	0.32%	0.868
	Pier 1 SB	0.058	0.29%	0.064	0.32%	0.907
Frame 2	Pier 2 NB	0.208	0.52%	0.233	0.59%	0.893
	Pier 2 SB	0.208	0.52%	0.233	0.59%	0.892
	Mid-Span Arch, NB	0.323	0.81%	0.355	0.89%	0.910
	Mid-Span Arch, SB	0.323	0.81%	0.355	0.89%	0.910
	Pier 3 NB	0.316	0.78%	0.302	0.74%	1.046
	Pier 3 SB	0.316	0.78%	0.301	0.74%	1.048
Frame 3	Pier 4 NB	0.237	0.64%	0.183	0.49%	1.299
	Pier 4 SB	0.164	0.70%	0.112	0.48%	1.461
	Pier 5 NB	0.172	0.52%	0.107	0.32%	1.609
	Pier 5 SB	0.129	0.52%	0.069	0.28%	1.872
	Pier 6 NB	0.067	0.25%	0.032	0.12%	2.099
	Pier 6 SB	0.052	0.26%	0.023	0.12%	2.245

**Table 5-3: Transverse Base Shear Summary (475-Year EQ)**

	Location	Non-Linear	Elastic	Ratio
		KN	KN	
Frame 1	Pier 1 NB	10145	9317	1.09
	Pier 1 SB	12150	11437	1.06
Frame 2	Pier 2 NB	10195	10712	0.95
	Pier 2 SB	10293	10781	0.95
	Arch Seg. 0, NB	5989	5014	1.19
	Arch Seg. 0, SB	5709	5115	1.12
	Arch Seg. 0A, NB	7729	6848	1.13
	Arch Seg. 0A, SB	6299	5377	1.17
	Pier 3 NB	10757	13952	0.77
	Pier 3 SB	10836	14016	0.77
Frame 3	Pier 4 NB	7275	6081	1.20
	Pier 4 SB	5334	6580	0.81
	Pier 5 NB	6477	4726	1.37
	Pier 5 SB	8854	6356	1.39
	Pier 6 NB	6477	2491	2.60
	Pier 6 SB	10142	3555	2.85

**Table 5-4: Transverse Moment Summary, Northbound Structure (475-Year EQ)**

Location	Non-Linear	Status	$\theta/\theta_{yield}$	Elastic	Ratio	
	KN-m			KN-m		
Frame 1	Pier 1 Bottom	176032	Elastic	0.92	166297	1.06
	Pier 1 Top	42920	Elastic	0.28	37550	1.14
	Pier 2 Bottom	201920	Elastic	0.84	221302	0.91
	Pier 2 Top	149071	Elastic	0.89	173025	0.86
	Arch Segment 0	168128	Elastic	0.48	180394	0.93
	Arch Crown 2	154406	Elastic	0.77	79012	1.95
	Arch Crown 3	165551	Elastic	0.82	144484	1.15
	Arch Segment 0A	229272	Elastic	0.66	237622	0.96
	Pier 3 Bottom	228424	Elastic	0.95	299372	0.76
	Pier 3 Top	165702	Elastic	0.99	233306	0.71
	Pier 4 Bottom	168702	Yielded	1.40	161347	1.05
	Frame 2	Pier 4 Top	34630	Elastic	0.23	30752
Pier 5 Bottom		158695	Elastic	0.99	113764	1.39
Pier 5 Top		19258	Elastic	0.13	14159	1.36
Pier 6 Bottom		136530	Elastic	0.75	50182	2.72
Pier 6 Top		18141	Elastic	0.13	7911	2.29
Frame 3						

**Table 5-5: Transverse Moment Summary, Southbound Structure (475-Year EQ)**

Location	Non-Linear	Status	$\theta/\theta_{yield}$	Elastic	Ratio	
	KN-m			KN-m		
Frame 1	Pier 1 Bottom	187982	Elastic	0.98	184833	1.02
	Pier 1 Top	44846	Elastic	0.30	38270	1.17
	Pier 2 Bottom	202418	Elastic	0.84	223084	0.91
	Pier 2 Top	148310	Elastic	0.88	174774	0.85
	Arch Segment 0	169976	Elastic	0.49	183992	0.92
	Arch Crown 2	168826	Elastic	0.84	84751	1.99
	Arch Crown 3	155717	Elastic	0.77	99621	1.56
	Arch Segment 0A	187018	Elastic	0.54	201235	0.93
	Pier 3 Bottom	228697	Elastic	0.95	301274	0.76
	Pier 3 Top	165540	Elastic	0.99	235205	0.70
	Pier 4 Bottom	189858	Yielded	6.36	258189	0.74
	Frame 2	Pier 4 Top	45823	Elastic	0.31	36507
Pier 5 Bottom		173324	Yielded	4.25	125748	1.38
Pier 5 Top		26342	Elastic	0.18	19964	1.32
Pier 6 Bottom		170311	Elastic	0.93	62131	2.74
Pier 6 Top		22621	Elastic	0.16	7852	2.88
Frame 3						

**Table 5-6: Longitudinal Displacement Summary (475-Year EQ)**

	Location	Non-Linear		Elastic		Ratio
		Peak (m)	Drift	Peak (m)	Drift	
Frame 1	Pier 1 NB	0.184	0.82%	0.187	0.84%	0.984
	Pier 1 SB	0.175	0.88%	0.146	0.74%	1.195
Frame 2	Pier 2 NB	0.093	0.23%	0.094	0.24%	0.990
	Pier 2 SB	0.104	0.26%	0.094	0.24%	1.114
	Mid-Span Arch, NB	0.056	0.14%	0.057	0.14%	0.982
	Mid-Span Arch, SB	0.059	0.15%	0.057	0.14%	1.035
	Pier 3 NB	0.097	0.24%	0.097	0.24%	0.995
	Pier 3 SB	0.094	0.23%	0.096	0.24%	0.970
Frame 3	Pier 4 NB	0.207	0.56%	0.270	0.73%	0.765
	Pier 4 SB	0.176	0.75%	0.149	0.63%	1.178
	Pier 5 NB	0.202	0.61%	0.257	0.78%	0.787
	Pier 5 SB	0.179	0.72%	0.138	0.56%	1.297
	Pier 6 NB	0.206	0.77%	0.264	0.99%	0.780
	Pier 6 SB	0.184	0.92%	0.148	0.73%	1.247

**Table 5-7: Longitudinal Base Shear Summary (475-Year EQ)**

	Location	Non-Linear	Elastic	Ratio
		KN	KN	
Frame 1	Pier 1 NB	10014	12561	0.80
	Pier 1 SB	10991	13346	0.82
Frame 2	Pier 2 NB	6847	5793	1.18
	Pier 2 SB	7068	5820	1.21
	Arch Seg. 0, NB	9650	8398	1.15
	Arch Seg. 0, SB	10629	8372	1.27
	Arch Seg. 0A, NB	9355	8592	1.09
	Arch Seg. 0A, SB	8685	8165	1.06
	Pier 3 NB	6588	5949	1.11
	Pier 3 SB	6774	5877	1.15
Frame 3	Pier 4 NB	5346	5742	0.93
	Pier 4 SB	4193	9240	0.45
	Pier 5 NB	5451	6822	0.80
	Pier 5 SB	7496	8145	0.92
	Pier 6 NB	8087	11935	0.68
	Pier 6 SB	10055	14856	0.68

**Table 5-8: Longitudinal Moment Summary, Northbound Structure (475-Year EQ)**

Location	Non-Linear	Status	$\theta/\theta_{yield}$	Elastic	Ratio
	KN-m			KN-m	
Frame 1					
Pier 1 Bottom	107140	Yielded	2.34	156360	0.69
Pier 1 Top	85116	Yielded	3.23	118499	0.72
Pier 2 Bottom	71061	Elastic	0.55	59714	1.19
Pier 2 Top	85695	Elastic	0.96	79090	1.08
Arch Segment 0	159976	Elastic	0.76	138816	1.15
Arch Crown 2	140001	Elastic	0.99	128941	1.09
Arch Crown 3	143286	Yielded	1.39	149951	0.96
Arch Segment 0A	160410	Elastic	0.77	141265	1.14
Pier 3 Bottom	66362	Elastic	0.51	60397	1.10
Pier 3 Top	82945	Elastic	0.92	76518	1.08
Pier 4 Bottom	73967	Elastic	0.83	98651	0.75
Pier 4 Top	68090	Elastic	0.84	86125	0.79
Pier 5 Bottom	76743	Elastic	0.90	109733	0.70
Pier 5 Top	68060	Elastic	0.85	94794	0.72
Pier 6 Bottom	99729	Yielded	1.10	167345	0.60
Pier 6 Top	79579	Yielded	2.78	141457	0.56
Frame 3					

**Table 5-9: Longitudinal Moment Summary, Southbound Structure (475-Year EQ)**

Location	Non-Linear	Status	$\theta/\theta_{yield}$	Elastic	Ratio
	KN-m			KN-m	
Frame 1	Pier 1 Bottom	111264	Yielded	150284	0.74
	Pier 1 Top	86528	Yielded	111122	0.78
	Pier 2 Bottom	69966	Elastic	59912	1.17
	Pier 2 Top	83306	Elastic	79122	1.05
	Arch Segment 0	170166	Elastic	138091	1.23
	Arch Crown 2	141962	Elastic	128135	1.11
	Arch Crown 3	139726	Elastic	128277	1.09
	Arch Segment 0A	158772	Elastic	139386	1.14
	Pier 3 Bottom	69120	Elastic	60212	1.15
	Pier 3 Top	83921	Elastic	76287	1.10
	Pier 4 Bottom	93164	Yielded	133328	0.70
	Pier 4 Top	84053	Yielded	102201	0.82
Frame 2	Pier 5 Bottom	88000	Yielded	100746	0.87
	Pier 5 Top	81742	Yielded	88072	0.93
	Pier 6 Bottom	107220	Yielded	159734	0.67
	Pier 6 Top	83053	Yielded	130801	0.63
Frame 3					

**Table 5-10: Transverse Displacement Summary (2500-Year EQ)**

	Location	Non-Linear		Elastic		Ratio
		Peak (m)	Drift	Peak (m)	Drift	
Frame 1	Pier 1 NB	0.096	0.43%	0.106	0.47%	0.907
	Pier 1 SB	0.090	0.45%	0.095	0.48%	0.942
Frame 2	Pier 2 NB	0.314	0.79%	0.349	0.88%	0.901
	Pier 2 SB	0.314	0.79%	0.349	0.88%	0.901
	Mid-Span Arch, NB	0.475	1.18%	0.531	1.32%	0.895
	Mid-Span Arch, SB	0.475	1.18%	0.531	1.32%	0.895
	Pier 3 NB	0.512	1.26%	0.452	1.11%	1.132
	Pier 3 SB	0.511	1.26%	0.452	1.11%	1.132
Frame 3	Pier 4 NB	0.348	0.93%	0.274	0.74%	1.271
	Pier 4 SB	0.266	1.13%	0.168	0.71%	1.581
	Pier 5 NB	0.242	0.73%	0.160	0.48%	1.514
	Pier 5 SB	0.184	0.74%	0.103	0.42%	1.781
	Pier 6 NB	0.093	0.35%	0.048	0.18%	1.947
	Pier 6 SB	0.072	0.36%	0.035	0.17%	2.085

**Table 5-11: Transverse Base Shear Summary (2500-Year EQ)**

	Location	Non-Linear	Elastic	Ratio
		KN	KN	
Frame 1	Pier 1 NB	12749	13966	0.91
	Pier 1 SB	14734	17148	0.86
Frame 2	Pier 2 NB	11949	16040	0.74
	Pier 2 SB	12033	16096	0.75
	Arch Seg. 0, NB	8502	7503	1.13
	Arch Seg. 0, SB	8165	7651	1.07
	Arch Seg. 0A, NB	10539	10246	1.03
	Arch Seg. 0A, SB	8710	8042	1.08
	Pier 3 NB	12755	20867	0.61
	Pier 3 SB	12890	20984	0.61
Frame 3	Pier 4 NB	8603	9106	0.94
	Pier 4 SB	7458	9858	0.76
	Pier 5 NB	7670	7089	1.08
	Pier 5 SB	9587	9532	1.01
	Pier 6 NB	8391	3736	2.25
	Pier 6 SB	12045	5332	2.26

**Table 5-12: Transverse Moment Summary, Northbound Structure (2500-Year EQ)**

Location	Non-Linear	Status	$\theta/\theta_{yield}$	Elastic	Ratio	
	KN-m			KN-m		
Frame 1	Pier 1 Bottom	205233	Yielded	3.17	249351	0.82
	Pier 1 Top	66432	Elastic	0.44	56193	1.18
	Pier 2 Bottom	238752	Elastic	0.99	331674	0.72
	Pier 2 Top	170261	Yielded	1.53	258697	0.66
	Arch Segment 0	238999	Elastic	0.69	270020	0.89
	Arch Crown 2	185339	Elastic	0.92	117727	1.57
	Arch Crown 3	201100	Yielded	1.10	215637	0.93
	Arch Segment 0A	302657	Elastic	0.87	355534	0.85
	Pier 3 Bottom	265338	Yielded	4.11	447969	0.59
	Pier 3 Top	186618	Yielded	5.33	348560	0.54
	Pier 4 Bottom	183291	Yielded	4.82	241617	0.76
	Frame 2	Pier 4 Top	53201	Elastic	0.35	45958
Pier 5 Bottom		174444	Yielded	4.52	170593	1.02
Pier 5 Top		25001	Elastic	0.17	21220	1.18
Pier 6 Bottom		170696	Elastic	0.93	75267	2.27
Pier 6 Top		26086	Elastic	0.18	11854	2.20
Frame 3						

**Table 5-13: Transverse Moment Summary, Southbound Structure (2500-Year EQ)**

Location	Non-Linear	Status	$\theta/\theta_{yield}$	Elastic	Ratio	
	KN-m			KN-m		
Frame 1	Pier 1 Bottom	248620	Yielded	10.29	277243	0.90
	Pier 1 Top	68537	Elastic	0.45	57267	1.20
	Pier 2 Bottom	239062	Elastic	1.00	333324	0.72
	Pier 2 Top	169357	Yielded	1.32	260456	0.65
	Arch Segment 0	245771	Elastic	0.71	275505	0.89
	Arch Crown 2	189980	Elastic	0.95	126037	1.51
	Arch Crown 3	186212	Elastic	0.93	148256	1.26
	Arch Segment 0A	262028	Elastic	0.75	301383	0.87
	Pier 3 Bottom	267064	Yielded	4.32	451446	0.59
	Pier 3 Top	187329	Yielded	5.49	351664	0.53
	Pier 4 Bottom	215172	Yielded	12.30	387027	0.56
	Frame 3	Pier 4 Top	71853	Elastic	0.48	54682
Pier 5 Bottom		186366	Yielded	7.42	188612	0.99
Pier 5 Top		35842	Elastic	0.24	29891	1.20
Pier 6 Bottom		195742	Yielded	3.21	93176	2.10
Pier 6 Top		30907	Elastic	0.22	11769	2.63

**Table 5-14: Longitudinal Displacement Summary (2500-Year EQ)**

	Location	Non-Linear		Elastic		Ratio
		Peak (m)	Drift	Peak (m)	Drift	
Frame 1	Pier 1 NB	0.237	1.06%	0.277	1.24%	0.854
	Pier 1 SB	0.213	1.07%	0.216	1.09%	0.985
Frame 2	Pier 2 NB	0.123	0.31%	0.123	0.31%	0.997
	Pier 2 SB	0.138	0.35%	0.123	0.31%	1.124
	Mid-Span Arch, NB	0.083	0.21%	0.085	0.21%	0.976
	Mid-Span Arch, SB	0.089	0.22%	0.085	0.21%	1.047
	Pier 3 NB	0.123	0.30%	0.127	0.31%	0.975
	Pier 3 SB	0.119	0.29%	0.125	0.31%	0.948
Frame 3	Pier 4 NB	0.283	0.76%	0.398	1.07%	0.710
	Pier 4 SB	0.239	1.01%	0.219	0.93%	1.095
	Pier 5 NB	0.279	0.84%	0.385	1.16%	0.724
	Pier 5 SB	0.243	0.98%	0.206	0.83%	1.175
	Pier 6 NB	0.278	1.04%	0.391	1.46%	0.712
	Pier 6 SB	0.249	1.24%	0.216	1.07%	1.155

**Table 5-15: Longitudinal Base Shear Summary (2500-Year EQ)**

	Location	Non-Linear	Elastic	Ratio
		KN	KN	
Frame 1	Pier 1 NB	11040	18780	0.59
	Pier 1 SB	12376	19957	0.62
Frame 2	Pier 2 NB	9336	7892	1.18
	Pier 2 SB	9531	7934	1.20
	Arch Seg. 0, NB	12495	10745	1.16
	Arch Seg. 0, SB	13130	10753	1.22
	Arch Seg. 0A, NB	11994	10964	1.09
	Arch Seg. 0A, SB	11228	10482	1.07
	Pier 3 NB	9057	8208	1.10
	Pier 3 SB	9407	8101	1.16
Frame 3	Pier 4 NB	6551	8326	0.79
	Pier 4 SB	4651	13339	0.35
	Pier 5 NB	6912	10204	0.68
	Pier 5 SB	8161	12214	0.67
	Pier 6 NB	9731	17646	0.55
	Pier 6 SB	10702	21584	0.50

**Table 5-16: Longitudinal Moment Summary, Northbound Structure (2500-Year EQ)**

Location	Non-Linear	Status	$\theta/\theta_{yield}$	Elastic	Ratio
	KN-m			KN-m	
Frame 1	Pier 1 Bottom	113486	Yielded	232400	0.49
	Pier 1 Top	87743	Yielded	176991	0.50
	Pier 2 Bottom	90440	Elastic	76918	1.18
	Pier 2 Top	92288	Yielded	99696	0.93
	Arch Segment 0	198318	Elastic	186079	1.07
	Arch Crown 2	156996	Yielded	164495	0.95
Frame 2	Arch Crown 3	156626	Yielded	187786	0.83
	Arch Segment 0A	192684	Elastic	189636	1.02
	Pier 3 Bottom	84989	Elastic	78646	1.08
	Pier 3 Top	91552	Yielded	97702	0.94
	Pier 4 Bottom	87032	Elastic	143353	0.61
	Pier 4 Top	79685	Elastic	123172	0.65
Frame 3	Pier 5 Bottom	87519	Yielded	164099	0.53
	Pier 5 Top	78752	Elastic	141736	0.56
	Pier 6 Bottom	106116	Yielded	247316	0.43
	Pier 6 Top	82735	Yielded	209029	0.40

**Table 5-17: Longitudinal Moment Summary, Southbound Structure (2500-Year EQ)**

Location	Non-Linear	Status	$\theta/\theta_{yield}$	Elastic	Ratio	
	KN-m			KN-m		
Frame 1	Pier 1 Bottom	131452	Yielded	12.73	223228	0.59
	Pier 1 Top	88960	Yielded	5.59	165712	0.54
	Pier 2 Bottom	88428	Elastic	0.68	77216	1.15
	Pier 2 Top	92051	Yielded	2.34	99765	0.92
	Arch Segment 0	207409	Elastic	0.99	185687	1.12
	Arch Crown 2	154493	Yielded	4.78	163650	0.94
	Arch Crown 3	153451	Yielded	4.46	162122	0.95
	Arch Segment 0A	196213	Elastic	0.94	188084	1.04
	Pier 3 Bottom	88874	Elastic	0.68	78408	1.13
	Pier 3 Top	92634	Yielded	2.67	97387	0.95
	Pier 4 Bottom	96679	Yielded	5.35	196065	0.49
	Frame 2	Pier 4 Top	87878	Yielded	5.35	143941
Pier 5 Bottom		91653	Yielded	4.60	151048	0.61
Pier 5 Top		84845	Yielded	4.33	132104	0.64
Pier 6 Bottom		112994	Yielded	6.94	231941	0.49
Pier 6 Top		86899	Yielded	7.64	189798	0.46
Frame 3						

# Figures

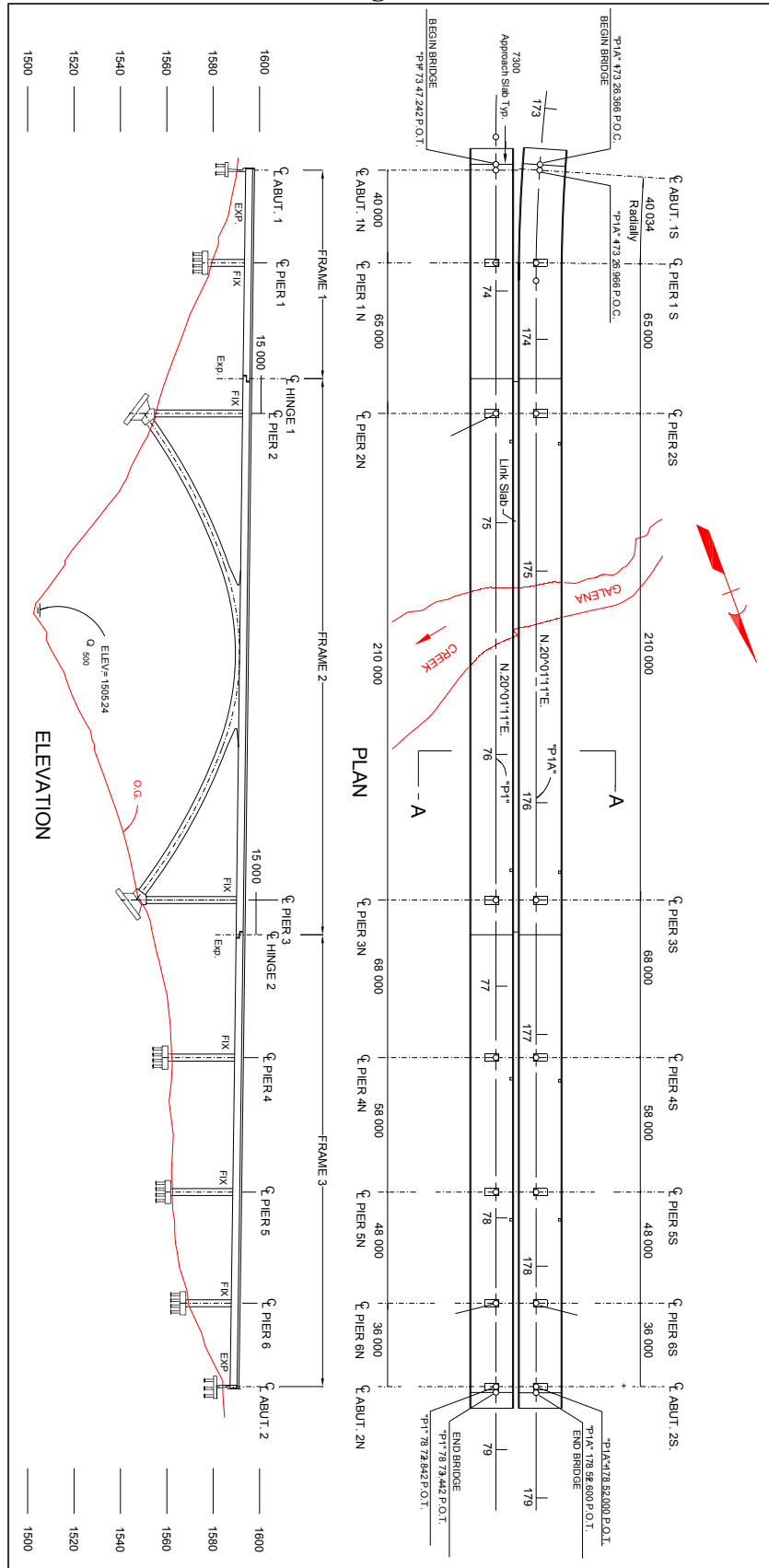
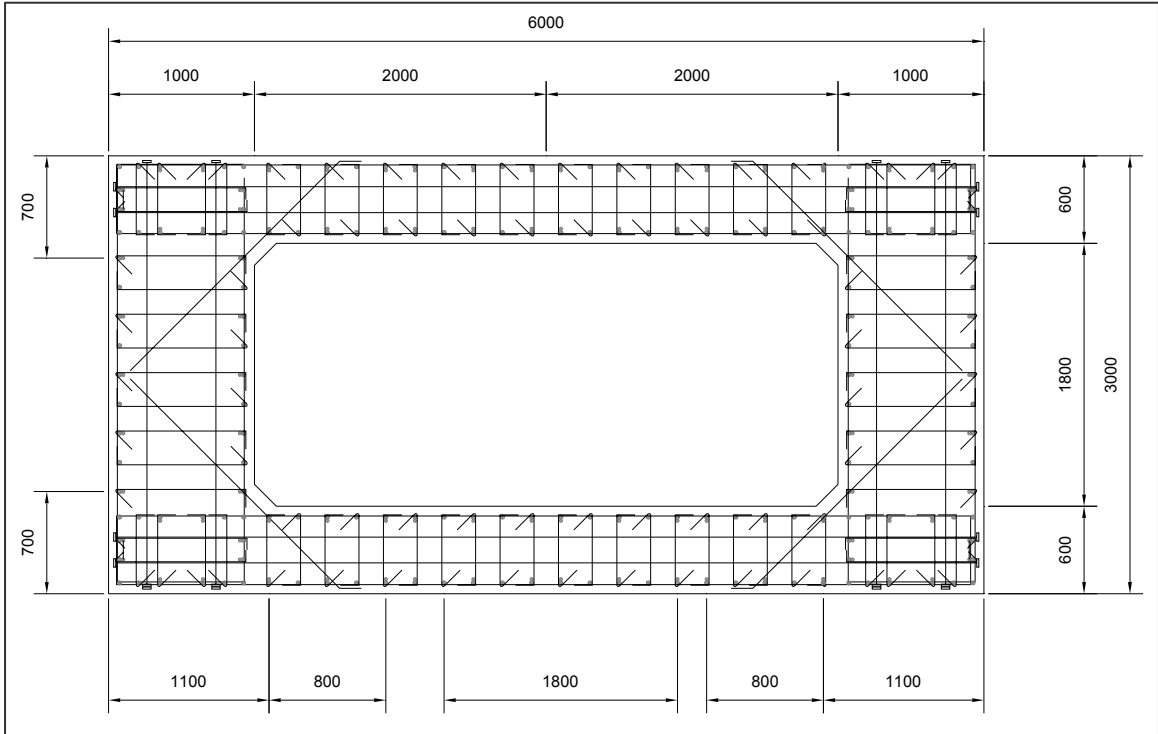


Figure 2-1: Overview of the Galena Creek Bridge



**Figure 2-2: Typical Column Section**

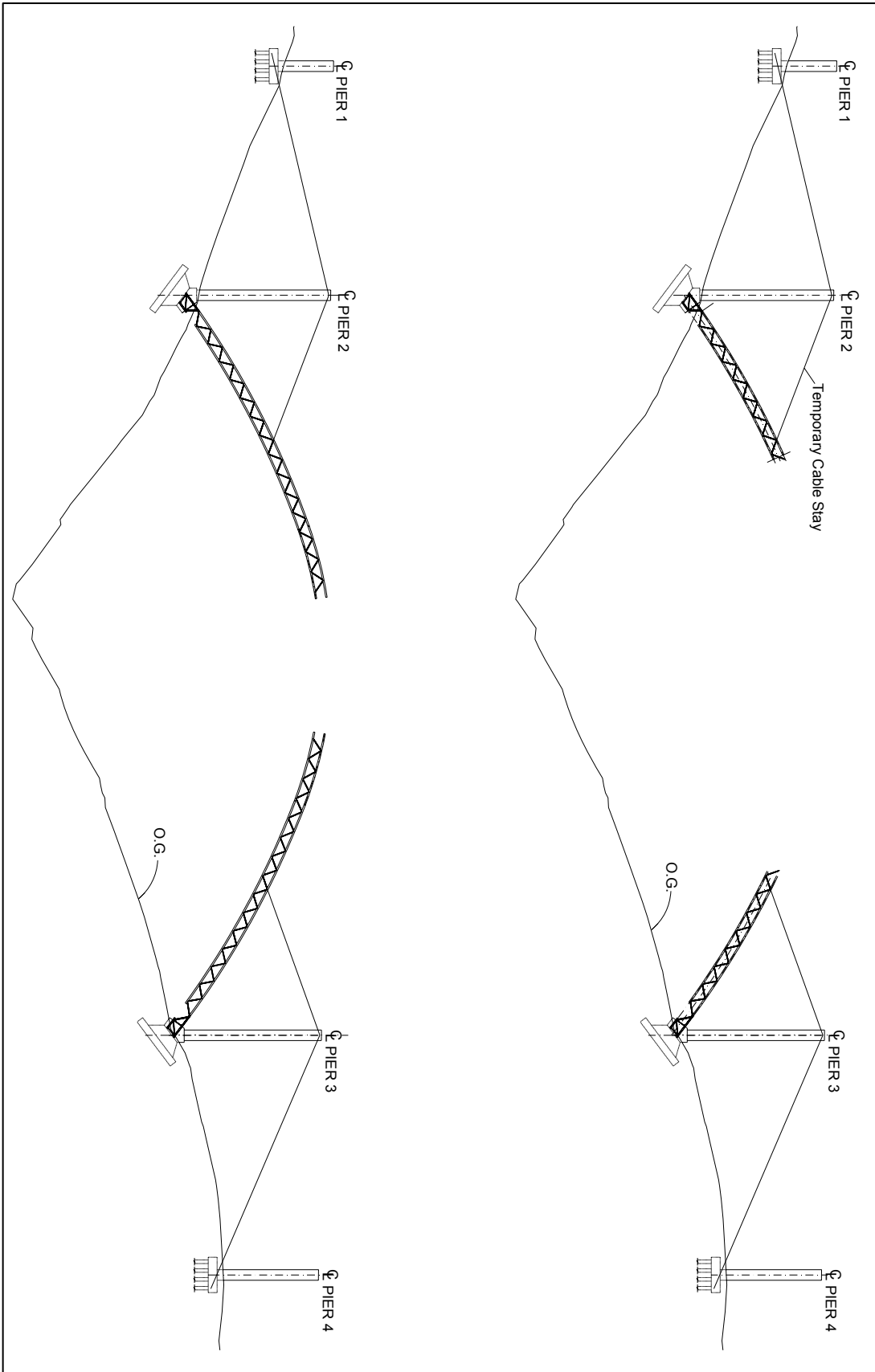
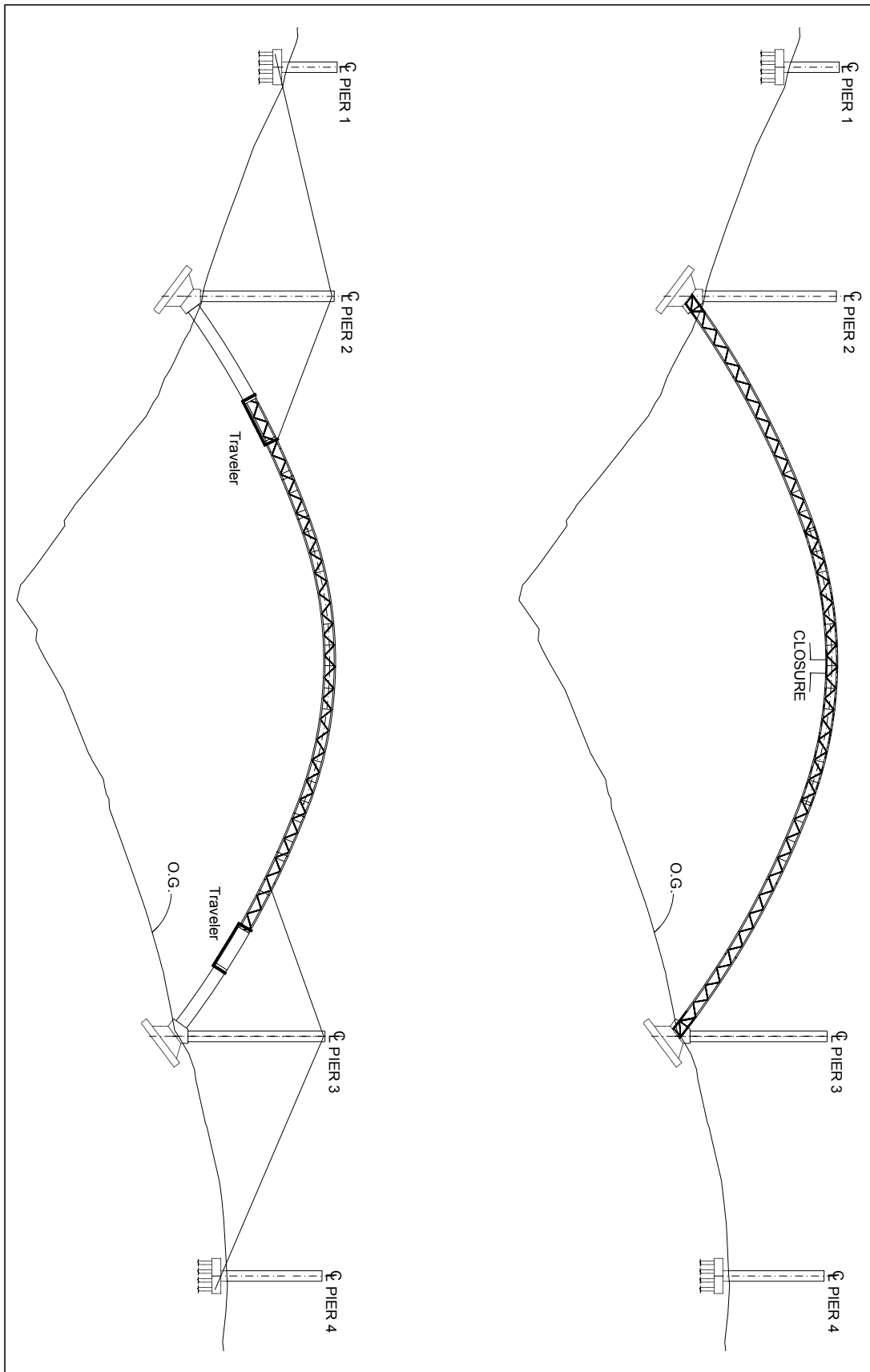
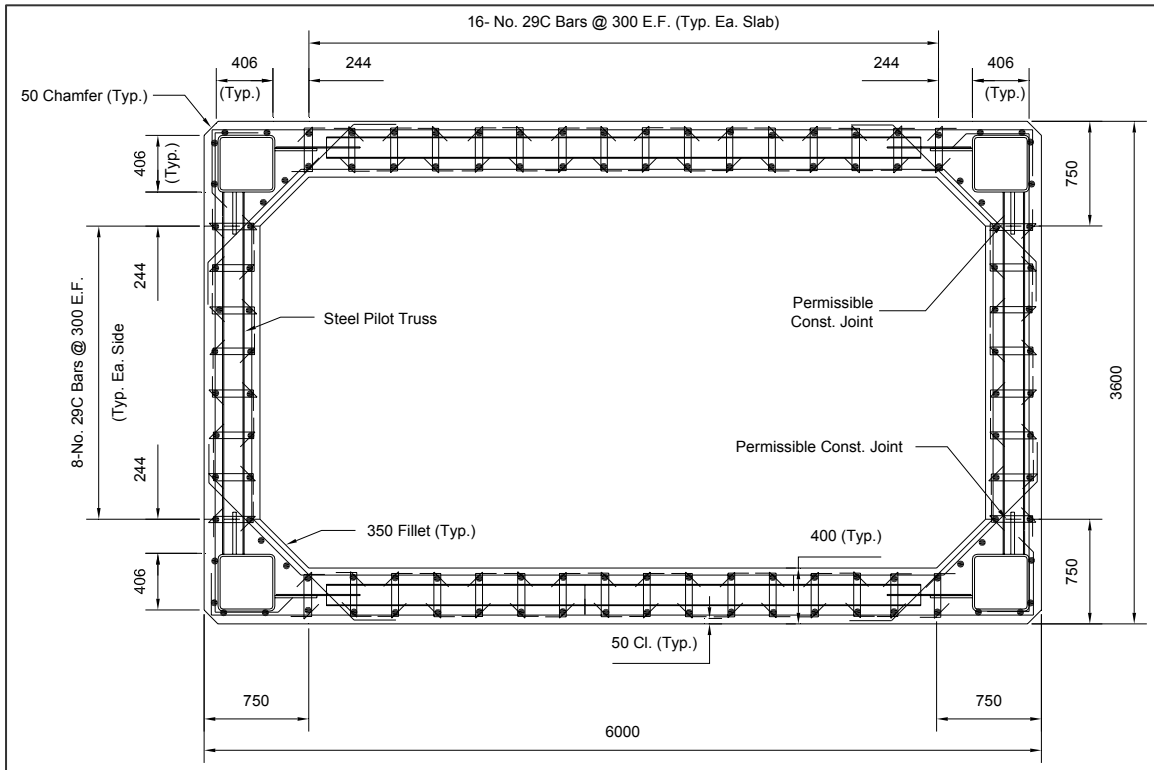


Figure 2-3: Construction Sequence: Pilot Truss Erection



**Figure 2-4: Construction Sequence: Pilot Truss Closure, and Form Traveler**



**Figure 2-5: Original Arch Section (Typical)**

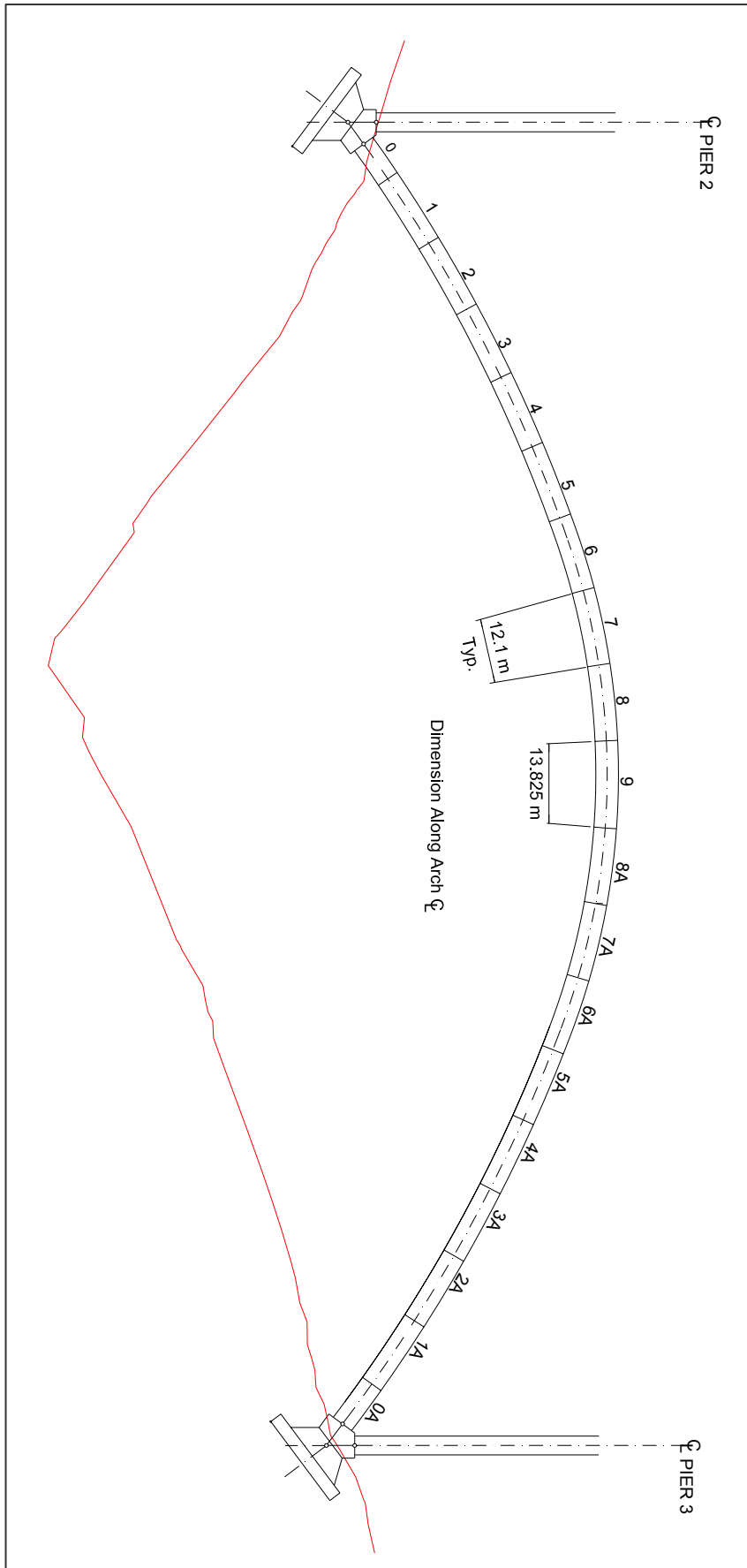
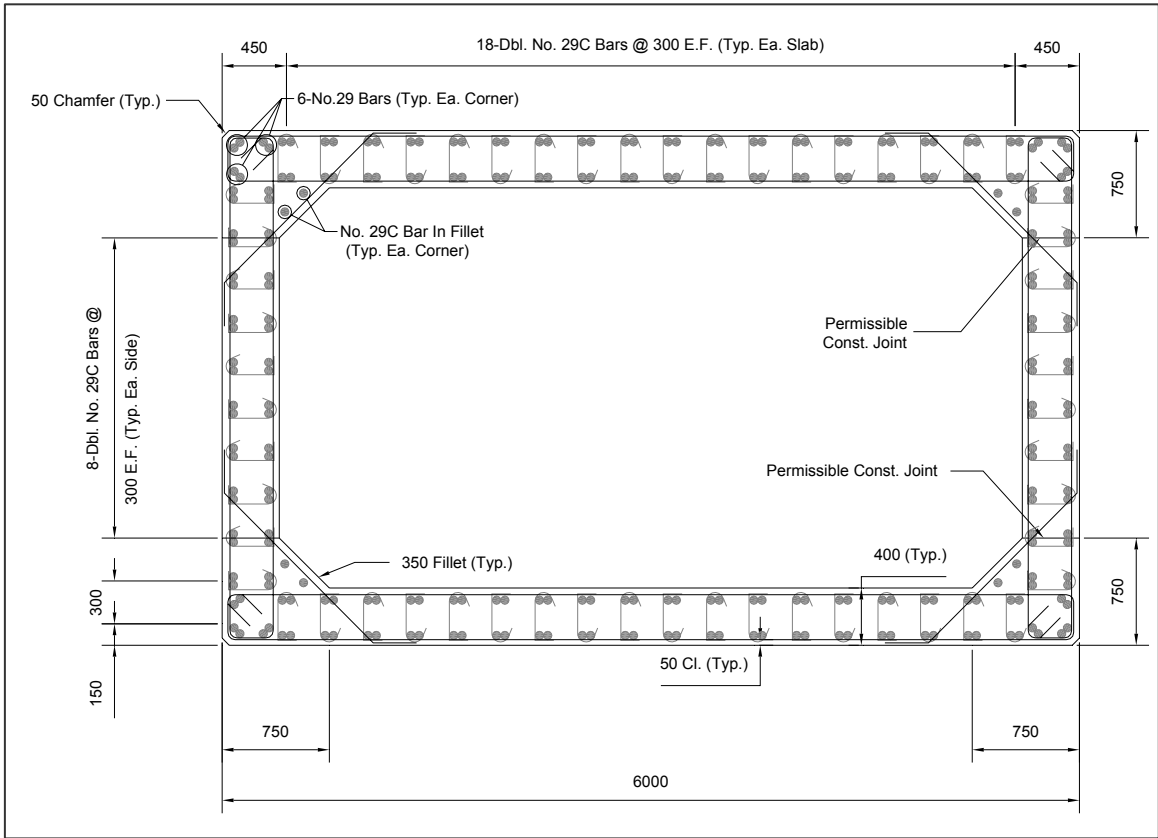


Figure 2-6: Concrete Arch Segment Layout



**Figure 2-7: New Arch Section (Typical)**

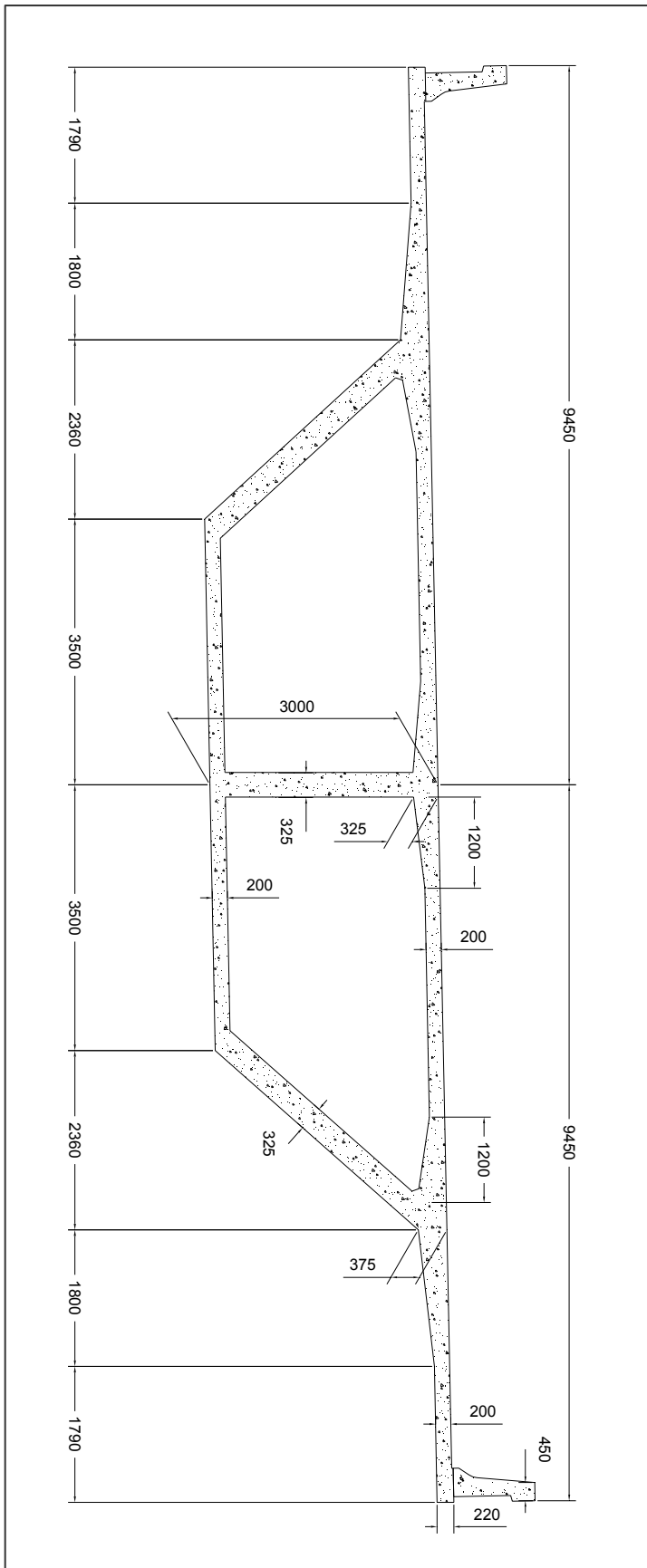
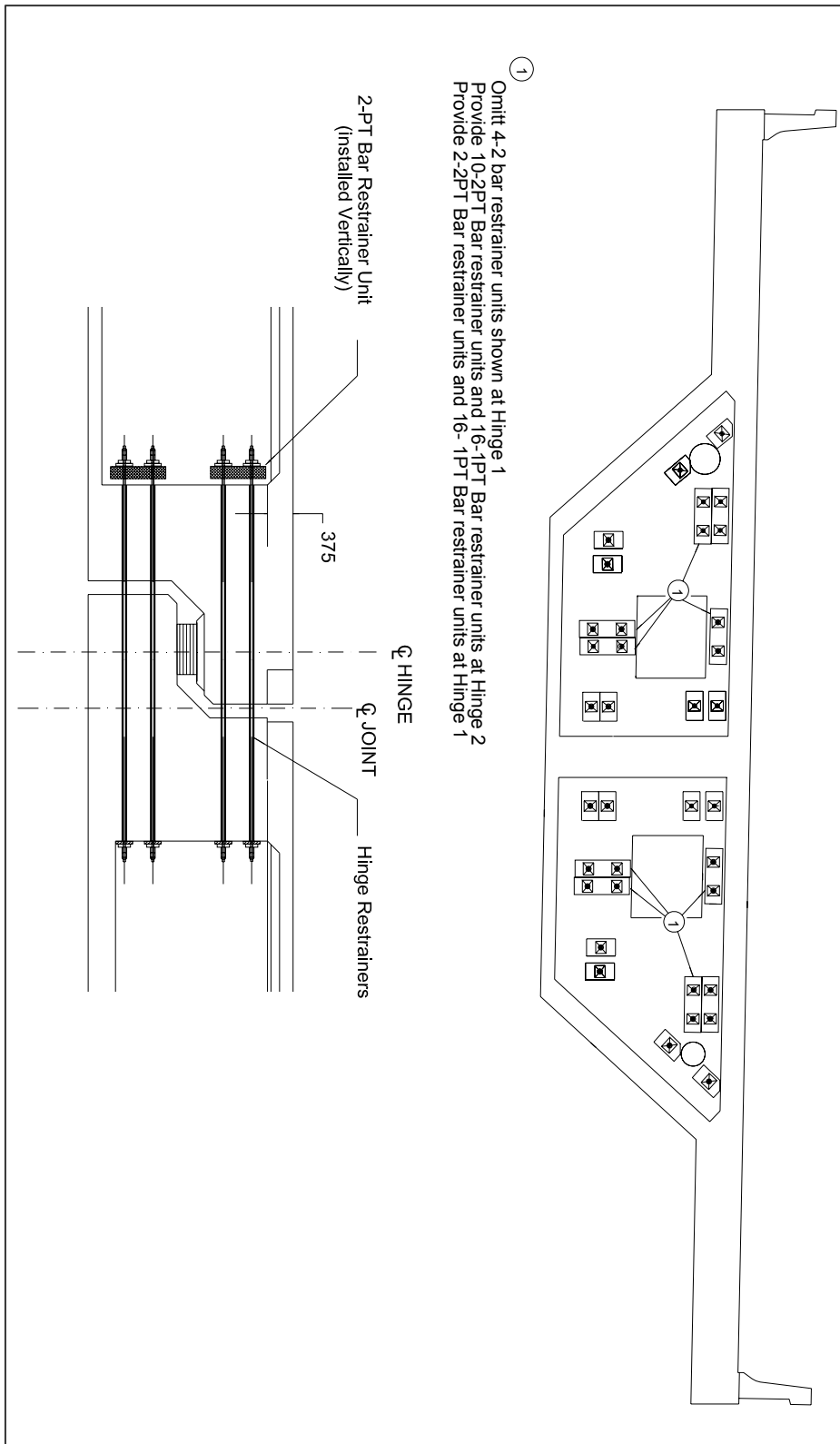


Figure 2-8: Typical Superstructure Section



**Figure 2-9: Hinge Restrainer Layout and Typical Section**

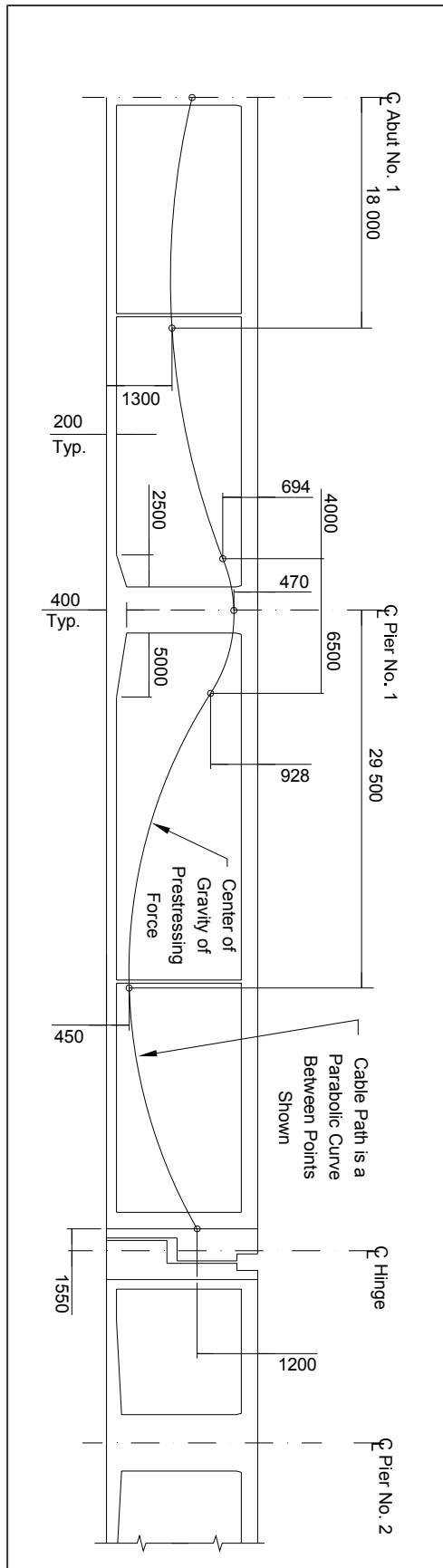


Figure 2-10: Frame 1 Longitudinal Post-Tensioning

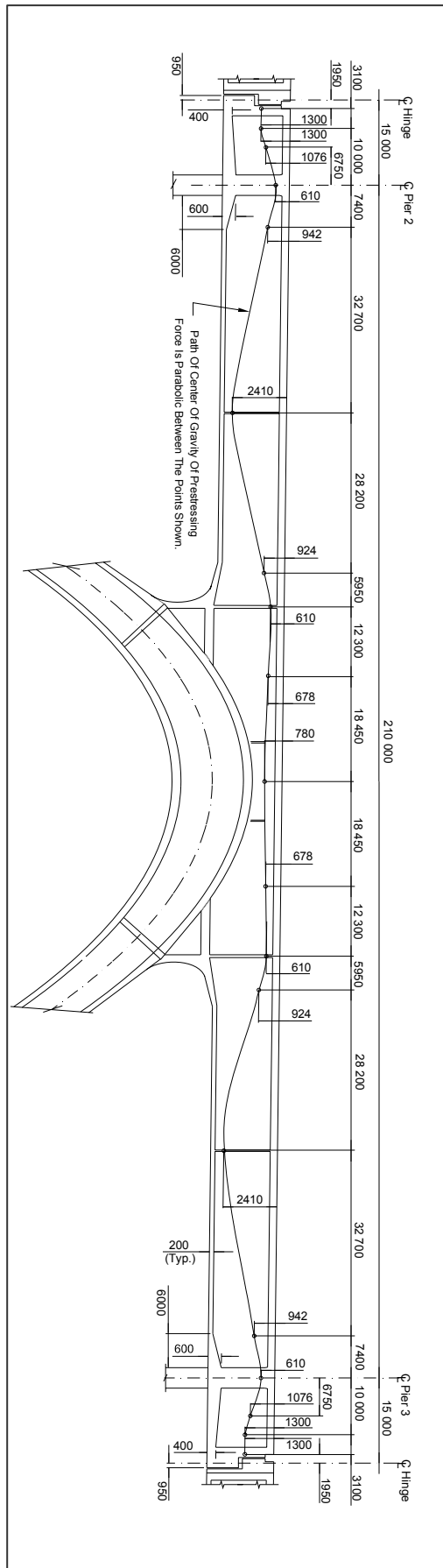


Figure 2-11: Frame 2 Longitudinal Post-Tensioning

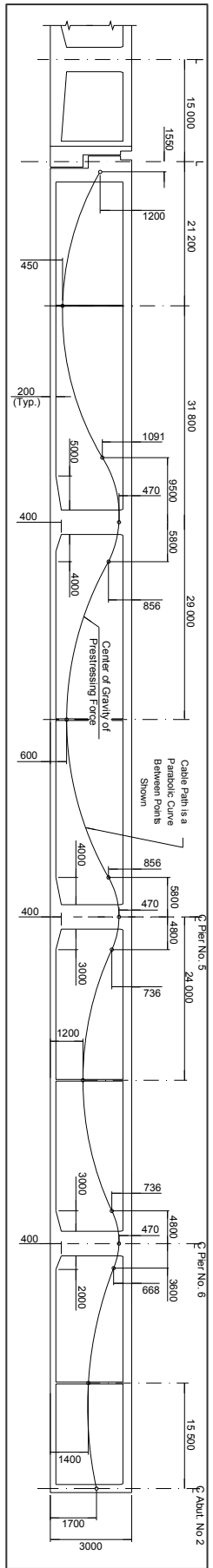


Figure 2-12: Frame 3 Longitudinal Post-Tensioning

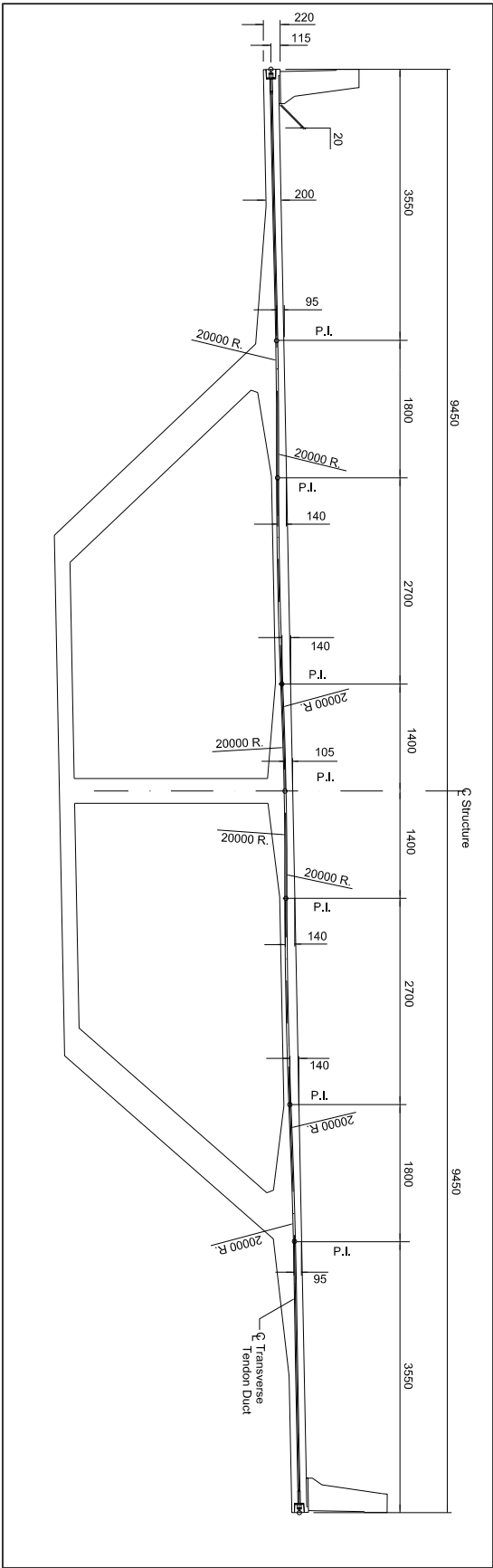
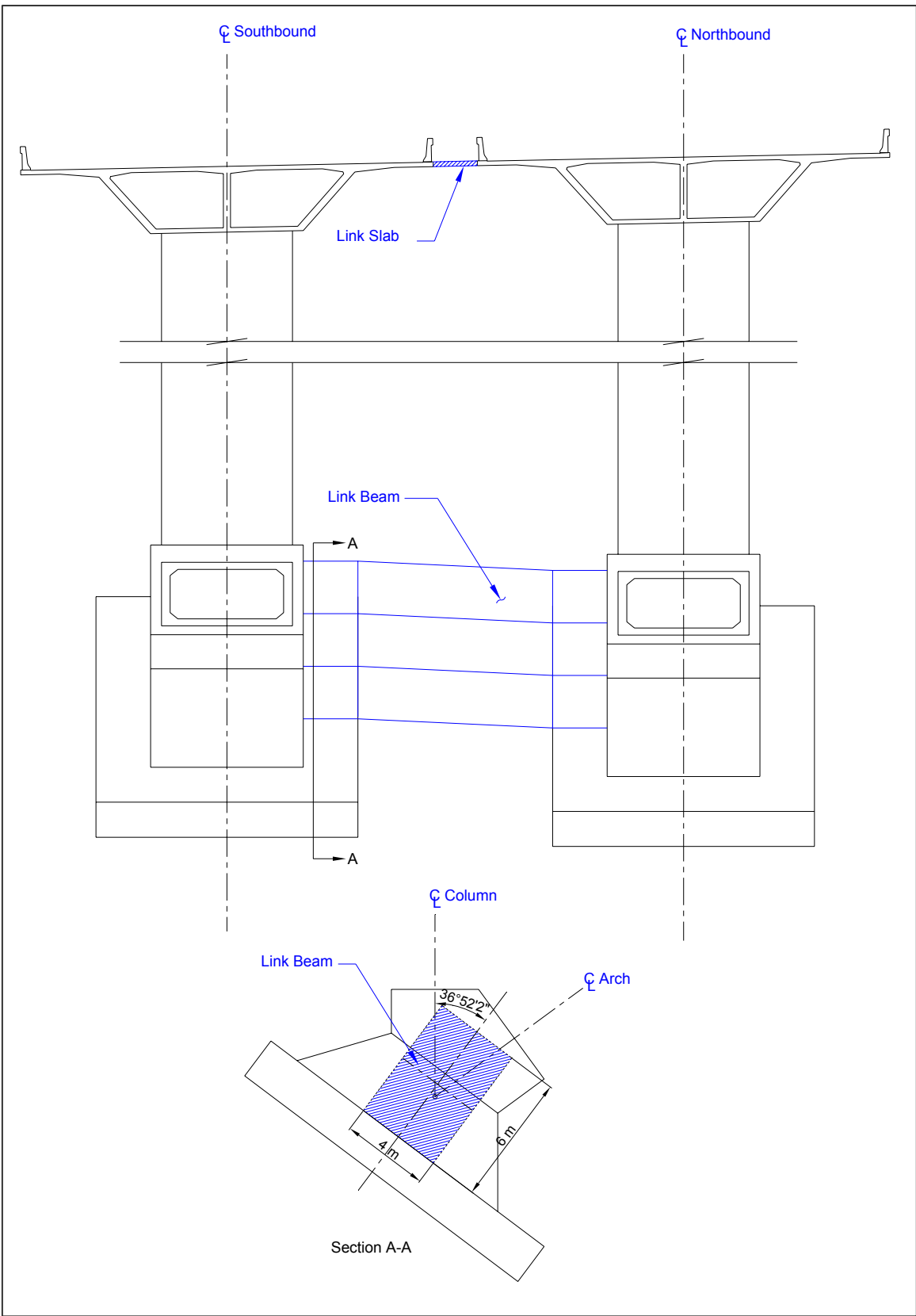


Figure 2-13: Transverse Post-Tensioning Detail



**Figure 2-14: Link Slab and Link Beam Detail**

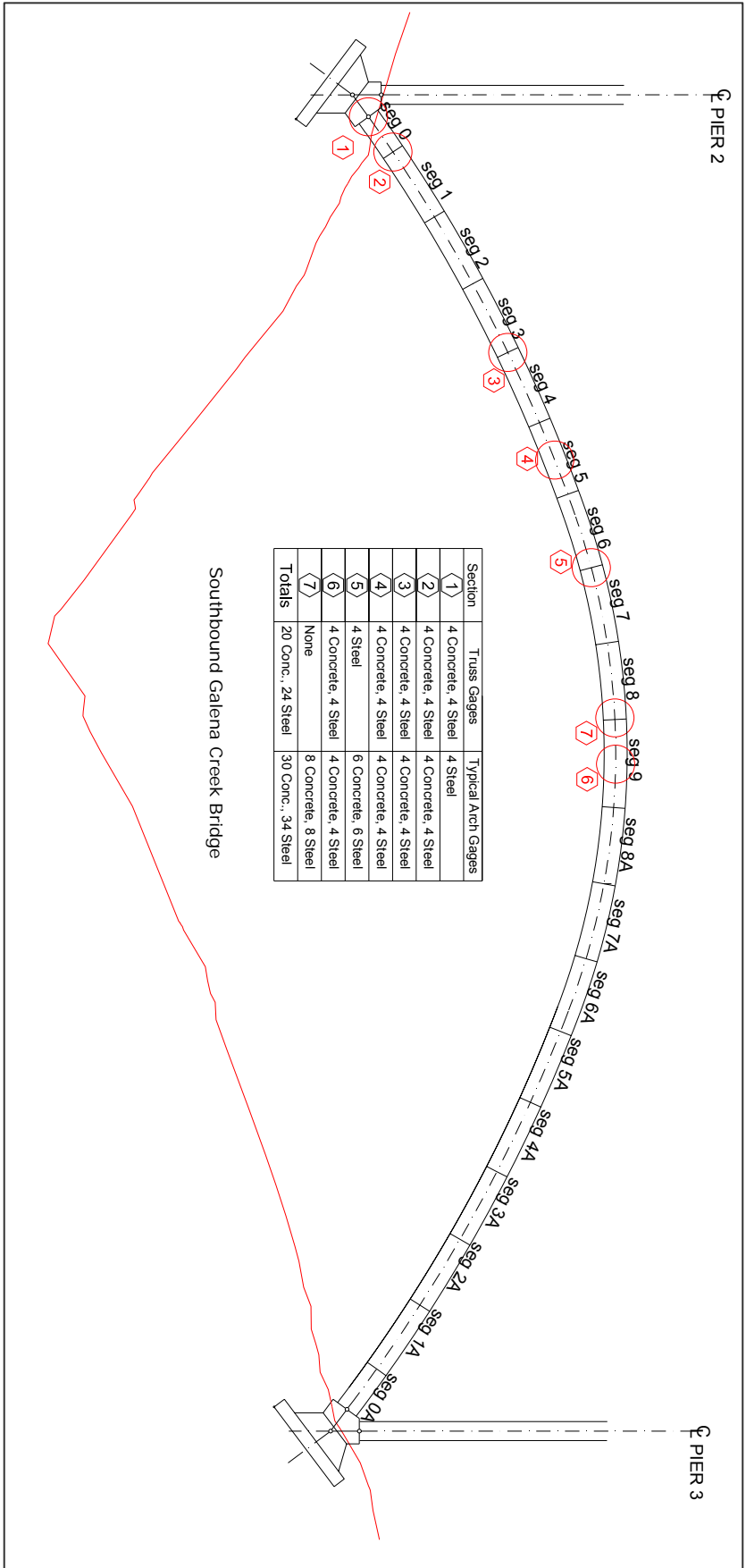


Figure 3-1: Instrumentation Locations (Strain Gages)

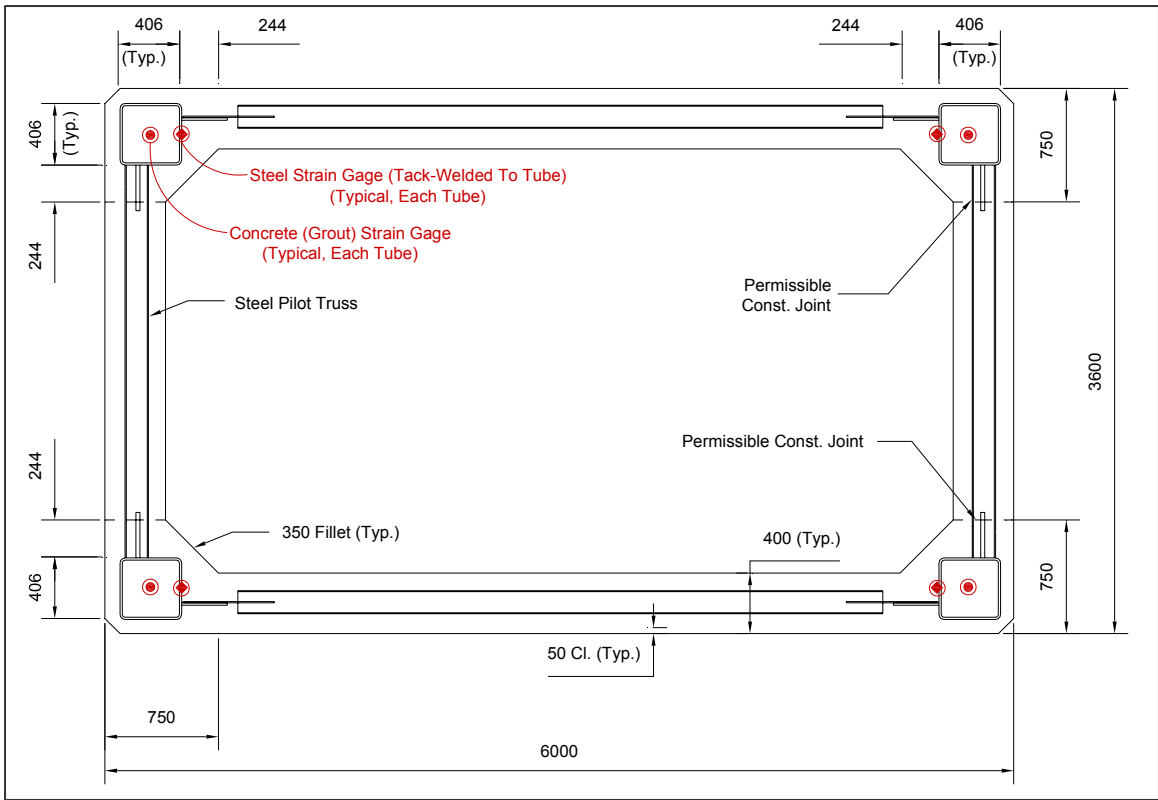
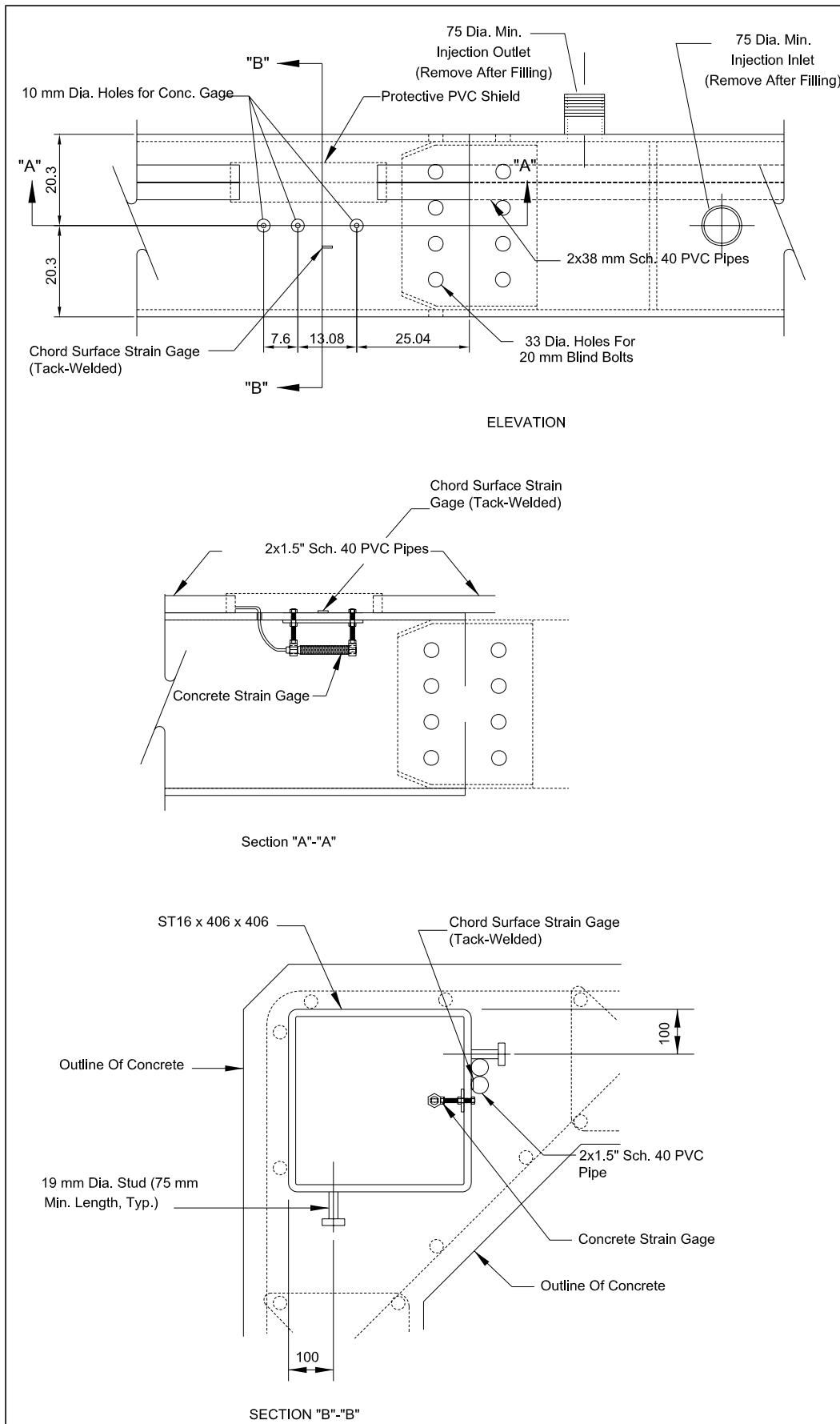


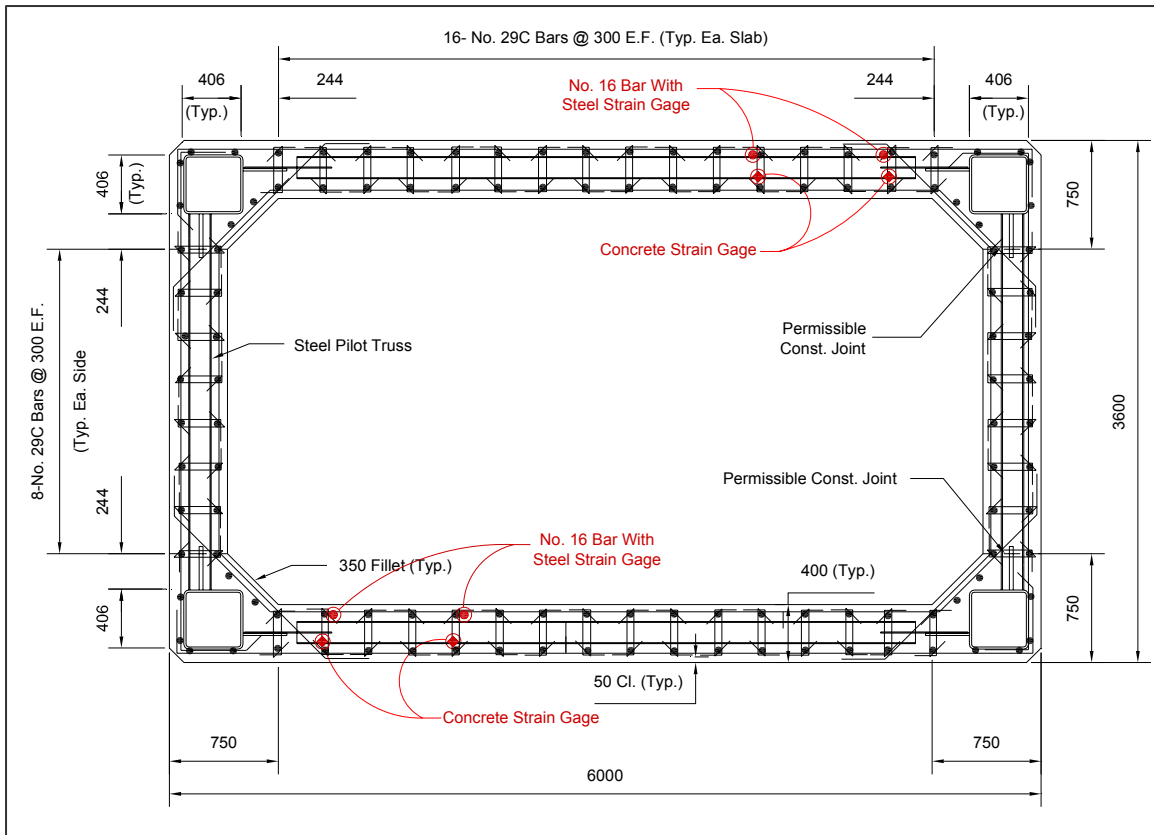
Figure 3-2: Pilot Truss Instrumentation



Figure 3-3: Concrete Strain Gage



**Figure 3-4: Steel Tube Instrumentation Details**



**Figure 3-5: Concrete Instrumentation**

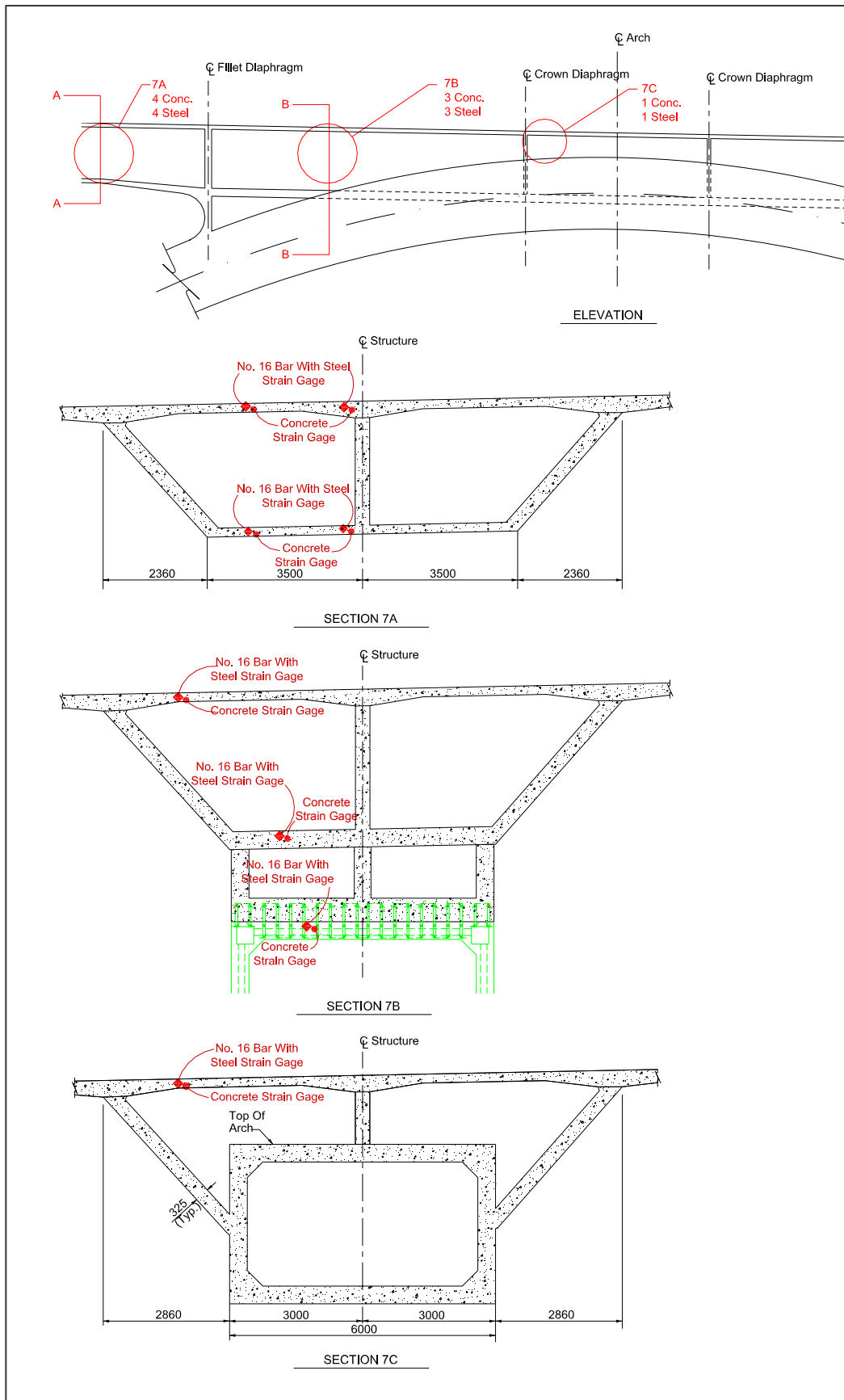
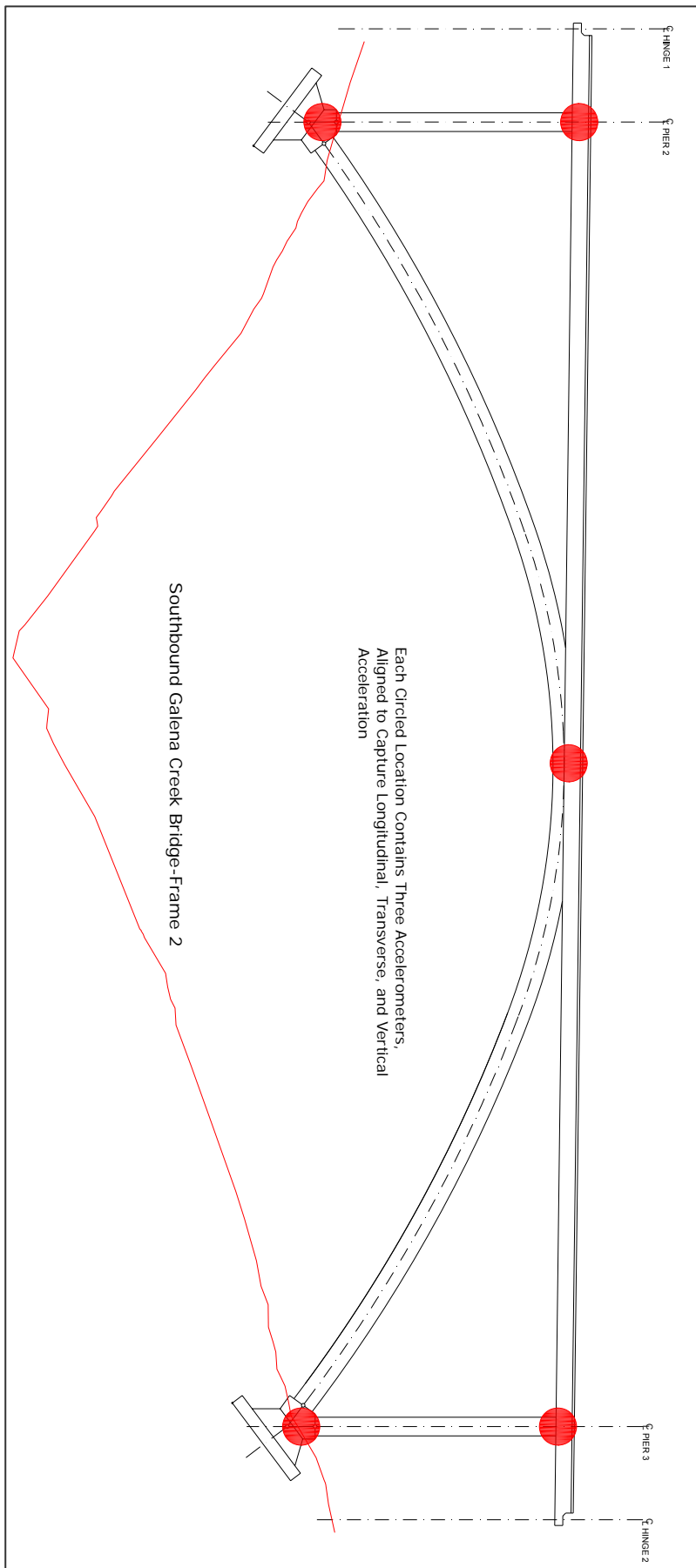
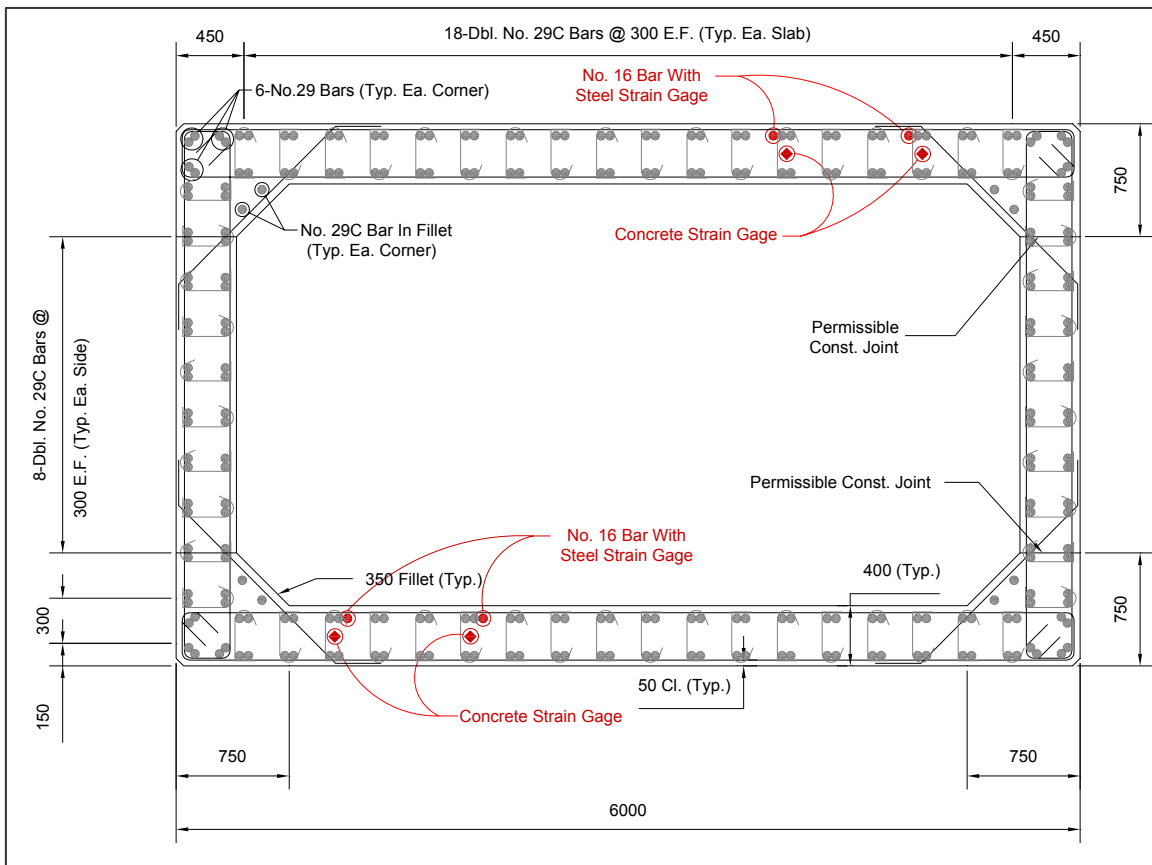


Figure 3-6: Superstructure Instrumentation Locations



**Figure 3-7: Dynamic Instrumentation Locations**



**Figure 3-8: Revised Typical Instrumentation Cross Section**

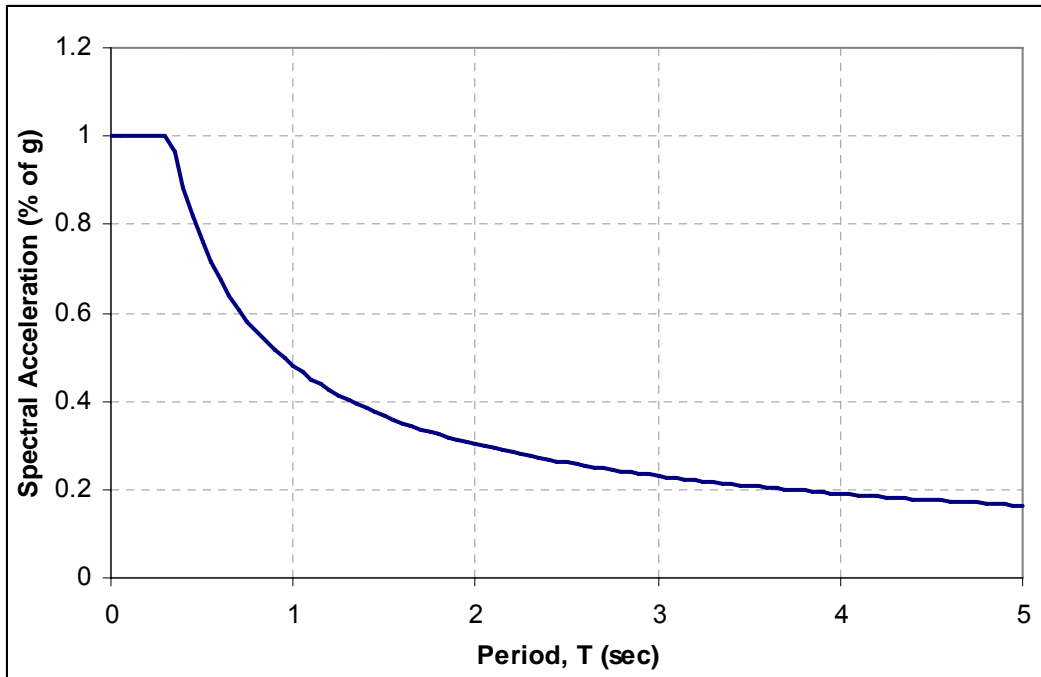


Figure 4-1: AASHTO Elastic Design Spectrum for Galena Creek Bridge

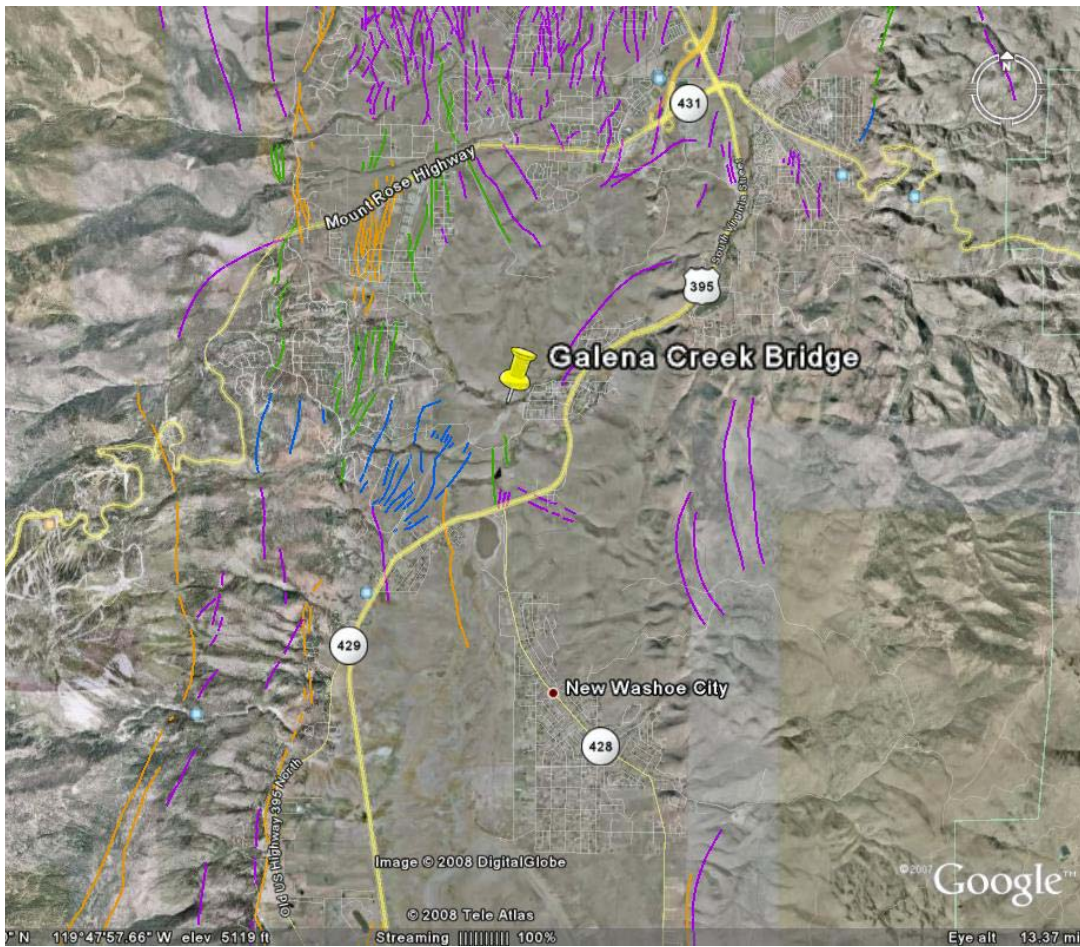


Figure 4-2: Fault Map in Vicinity of Galena Creek Bridge

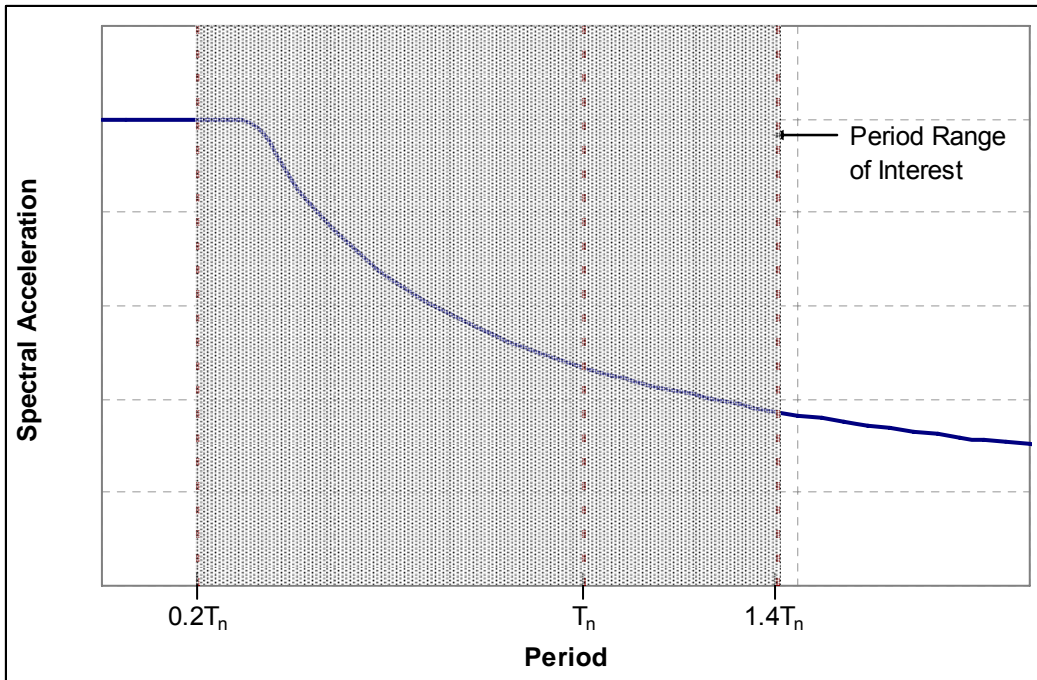
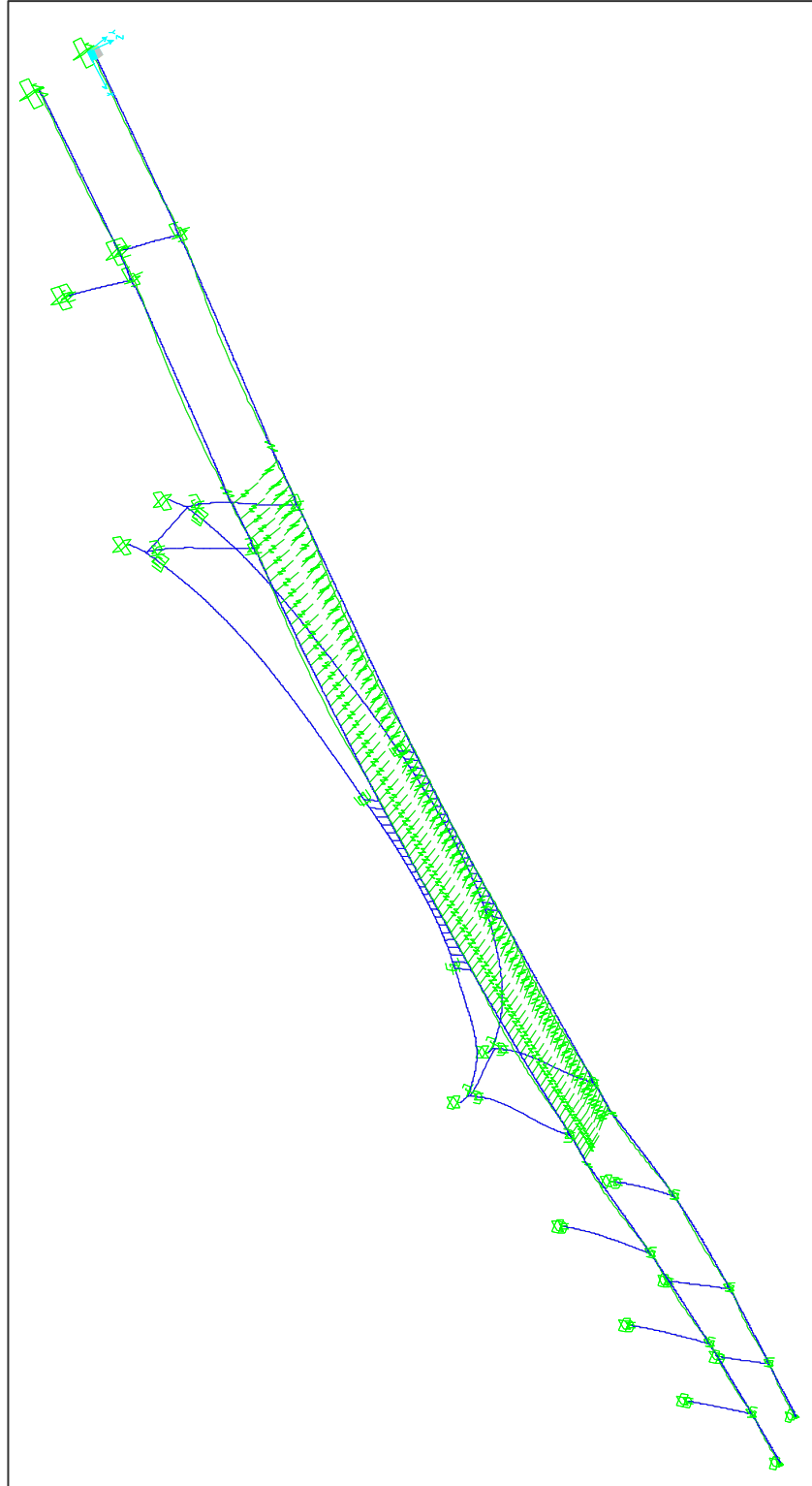


Figure 4-3: Period Range of Interest



**Figure 4-4: Deformed Shape, Fundamental Period of Vibration**

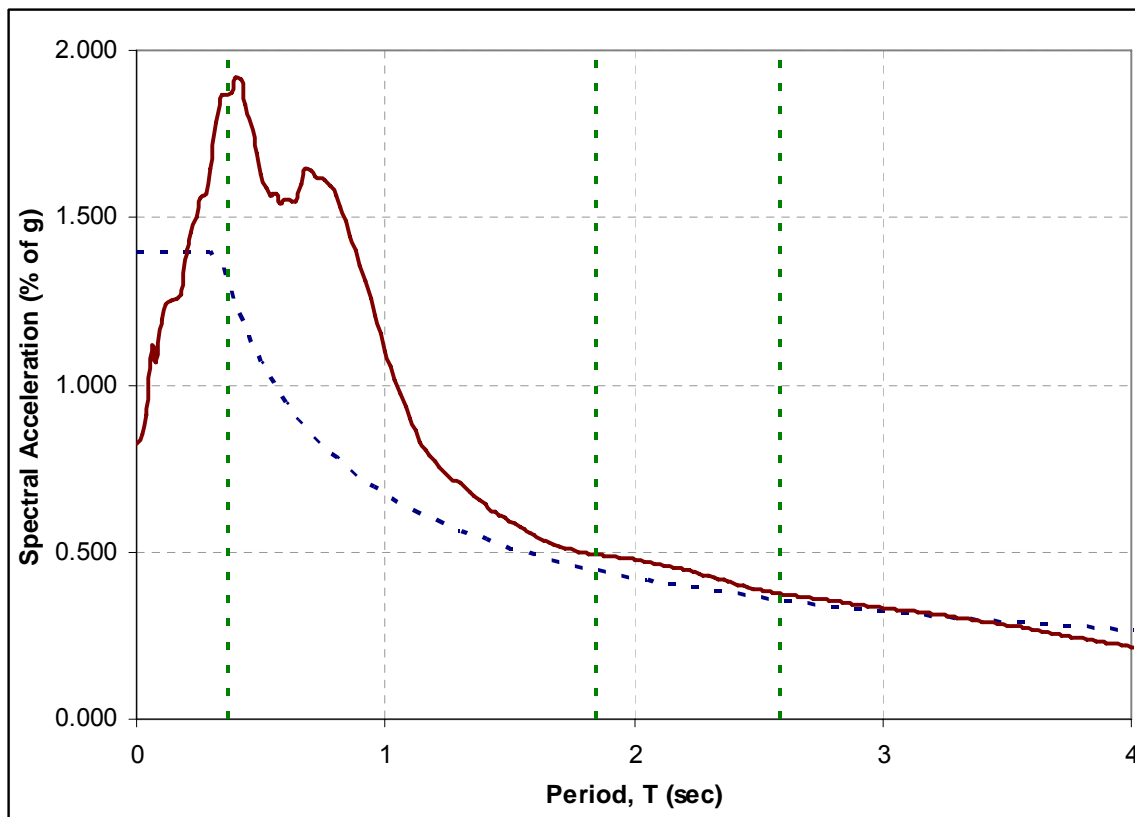


Figure 4-5: Un-scaled Composite Spectrum vs. 475-Year AASHTO Spectrum

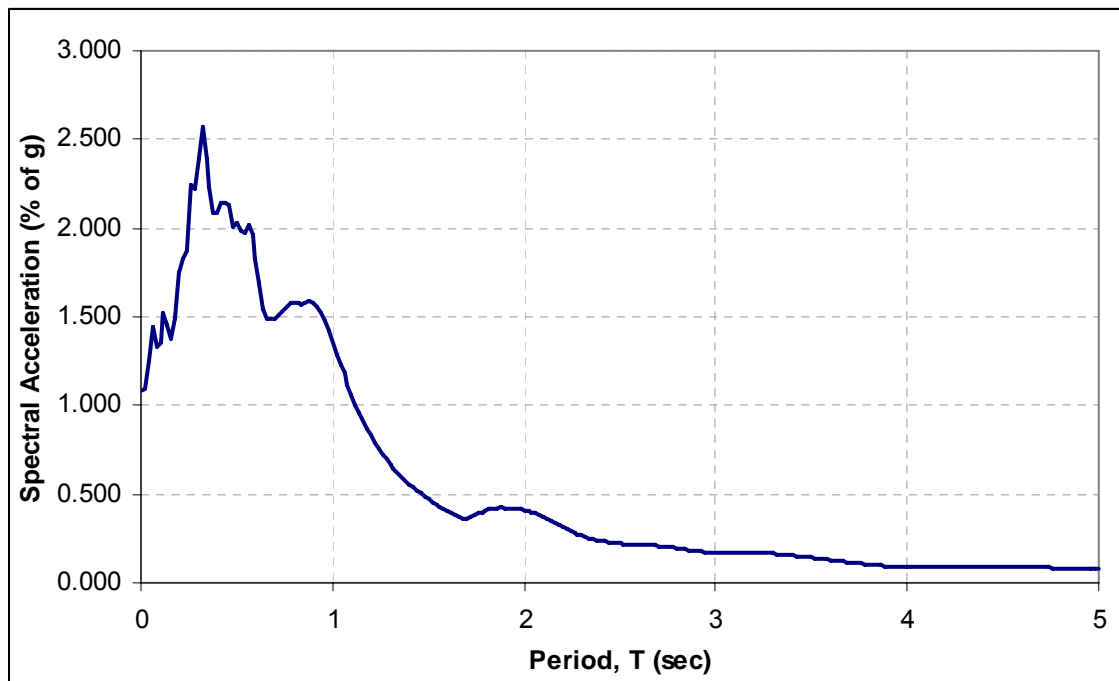


Figure 4-6: Un-scaled SRSS Response Spectrum, Bolu Ground Motion

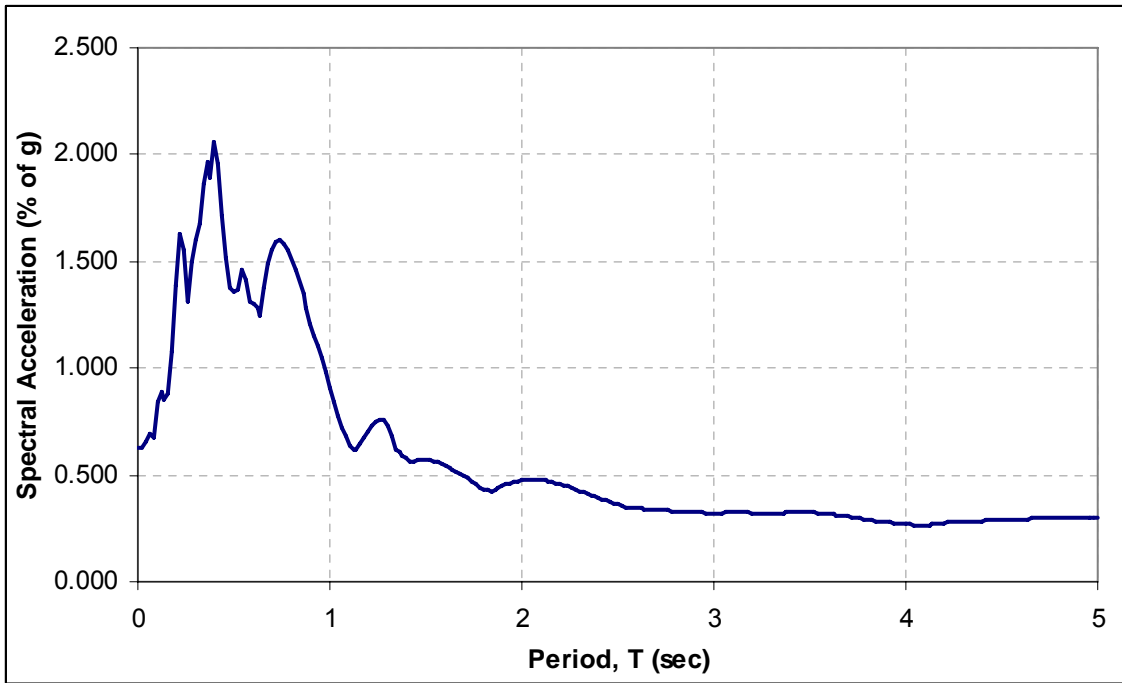


Figure 4-7: Un-scaled SRSS Response Spectrum, Duzce Ground Motion

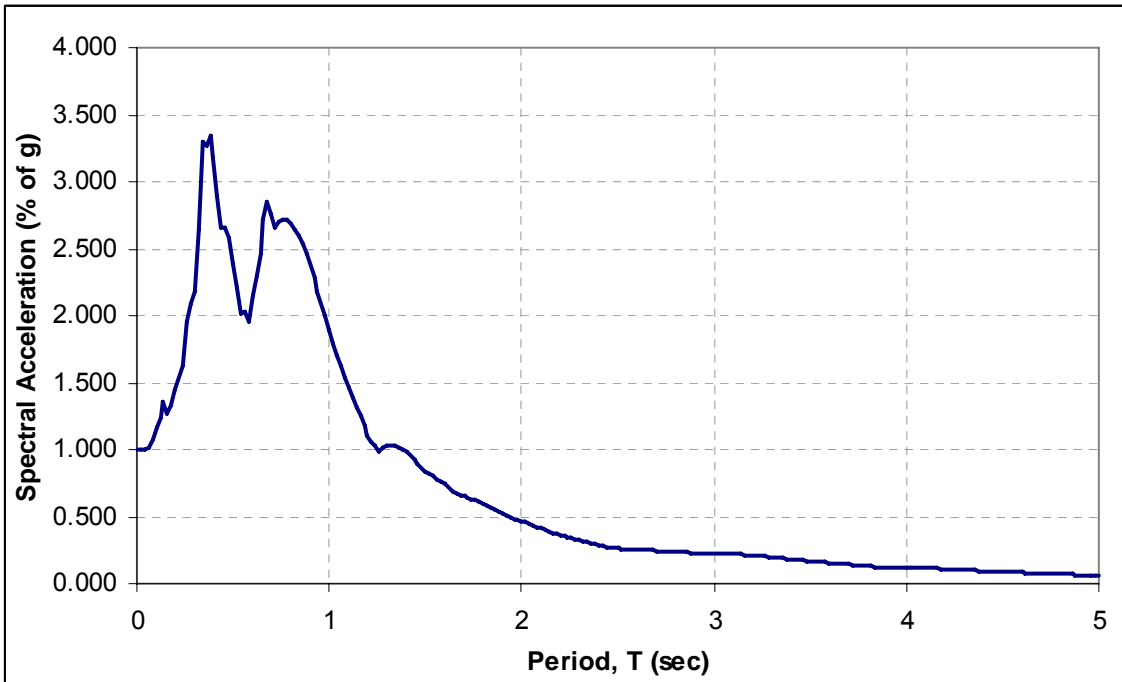


Figure 4-8: Un-scaled SRSS Response Spectrum, KJMA Ground Motion

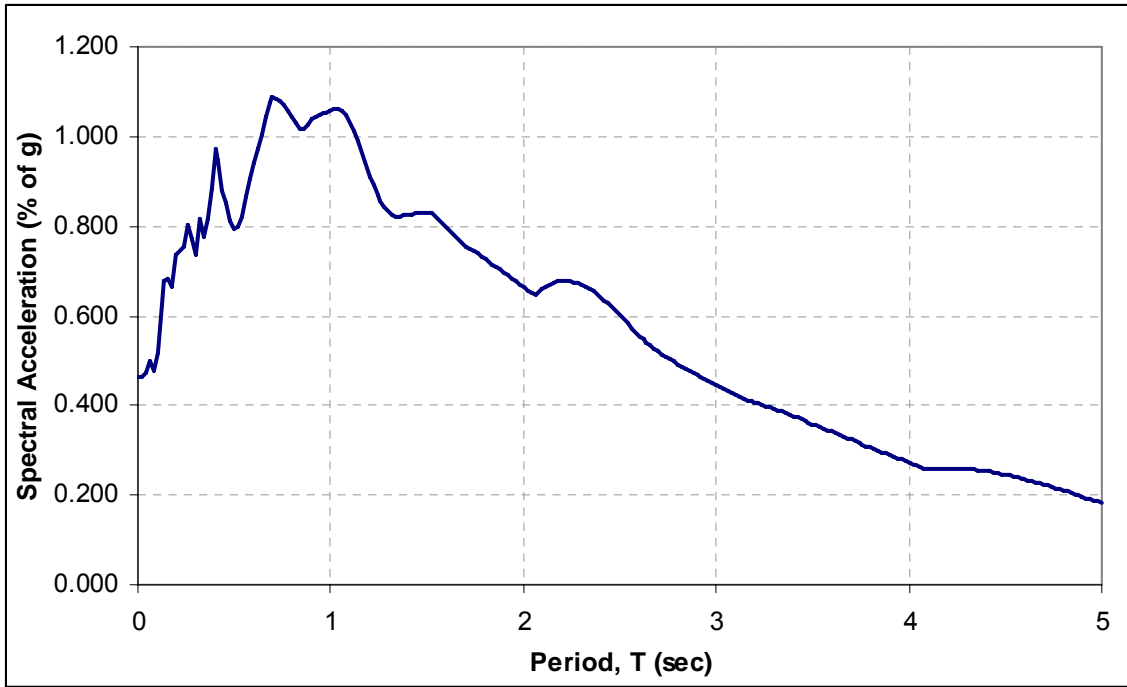


Figure 4-9: Un-scaled SRSS Response Spectrum, Denali Ground Motion

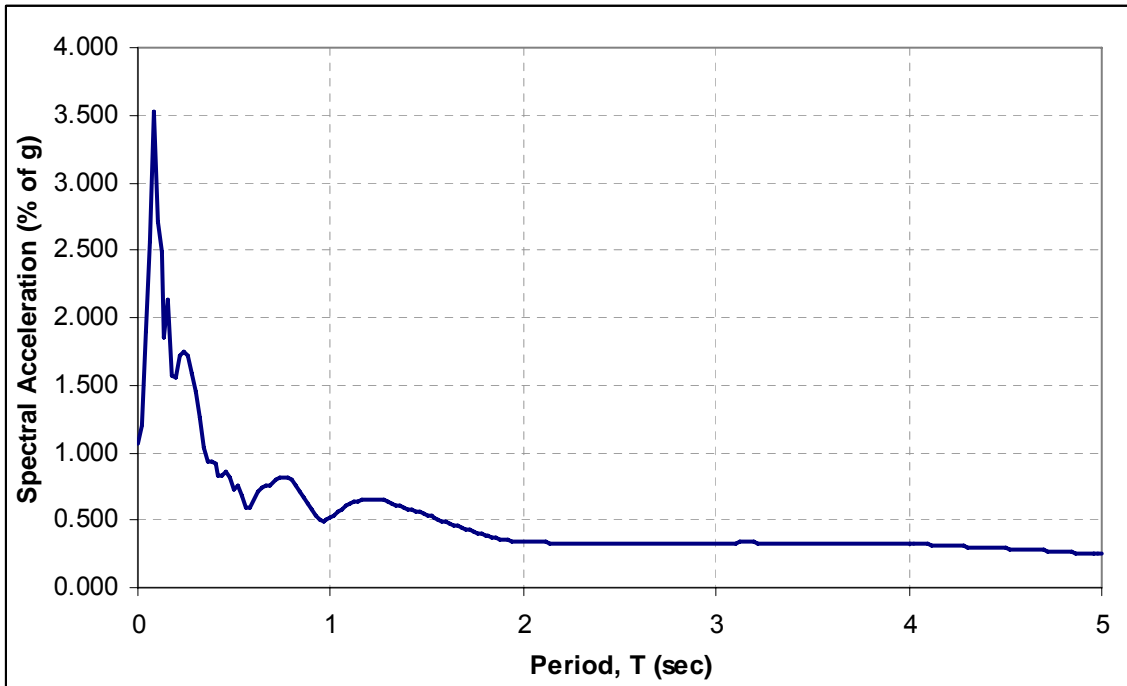


Figure 4-10: Un-scaled SRSS Response Spectrum, Parkfield Ground Motion

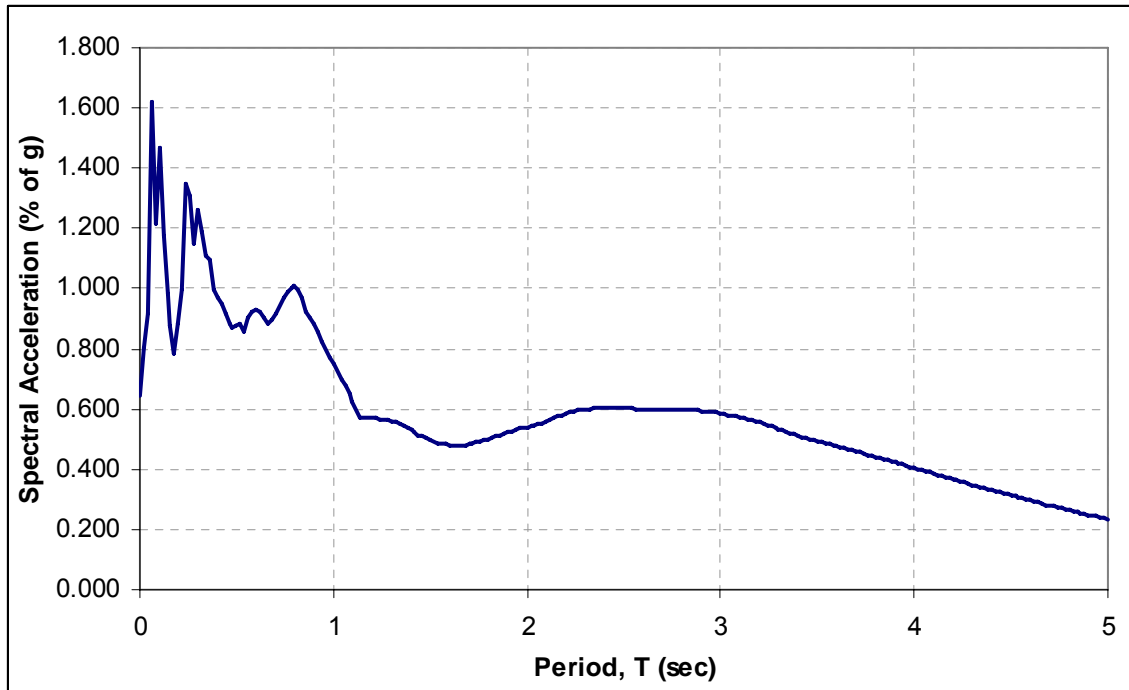


Figure 4-11: Un-scaled SRSS Response Spectrum, Centro 6 Ground Motion

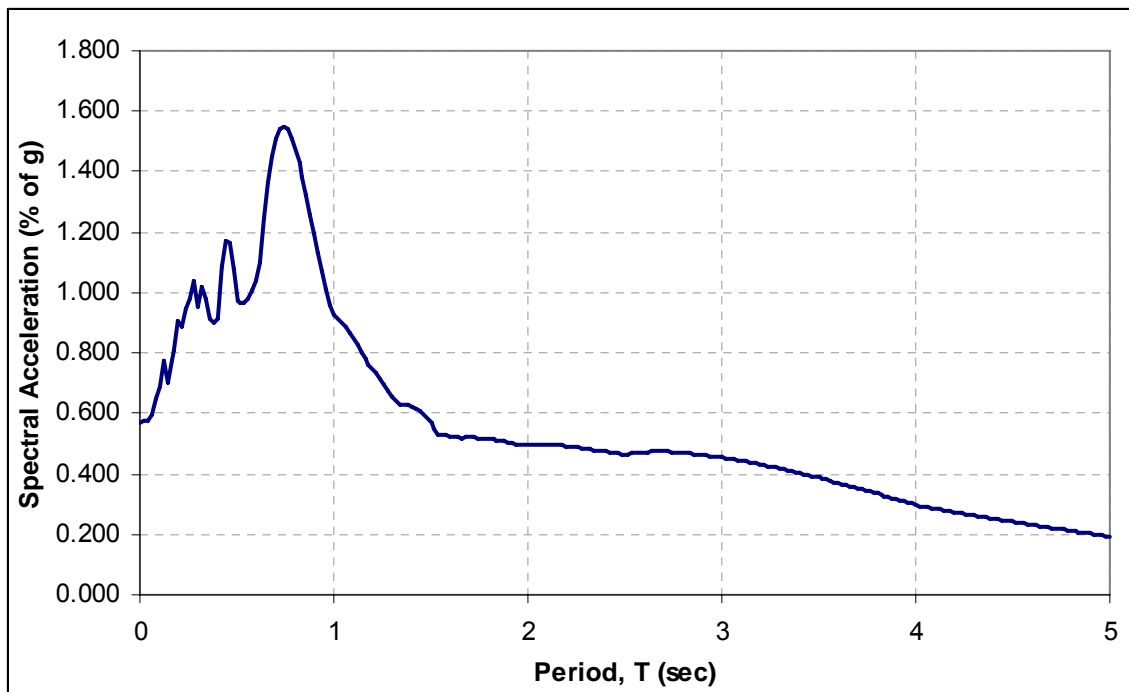


Figure 4-12: Un-scaled SRSS Response Spectrum, Centro 7 Ground Motion

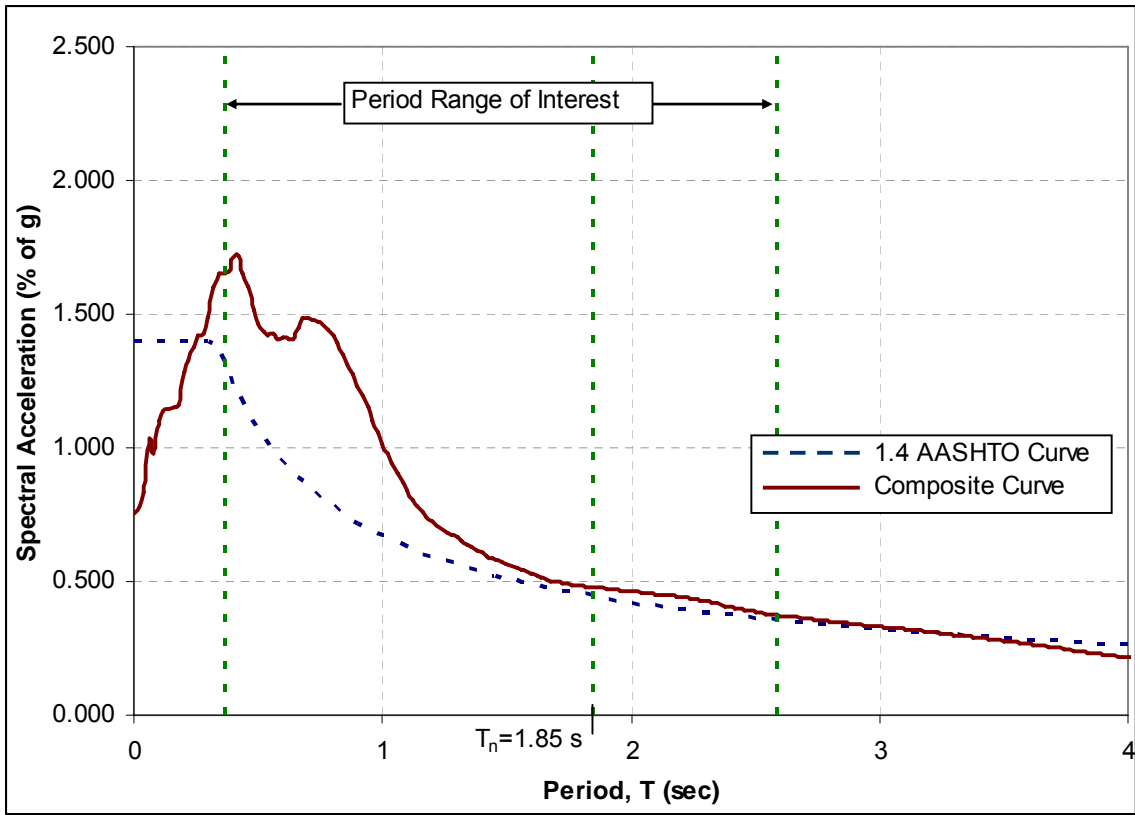


Figure 4-13: 10% Probability of Exceedance in 50 Years Composite Spectrum

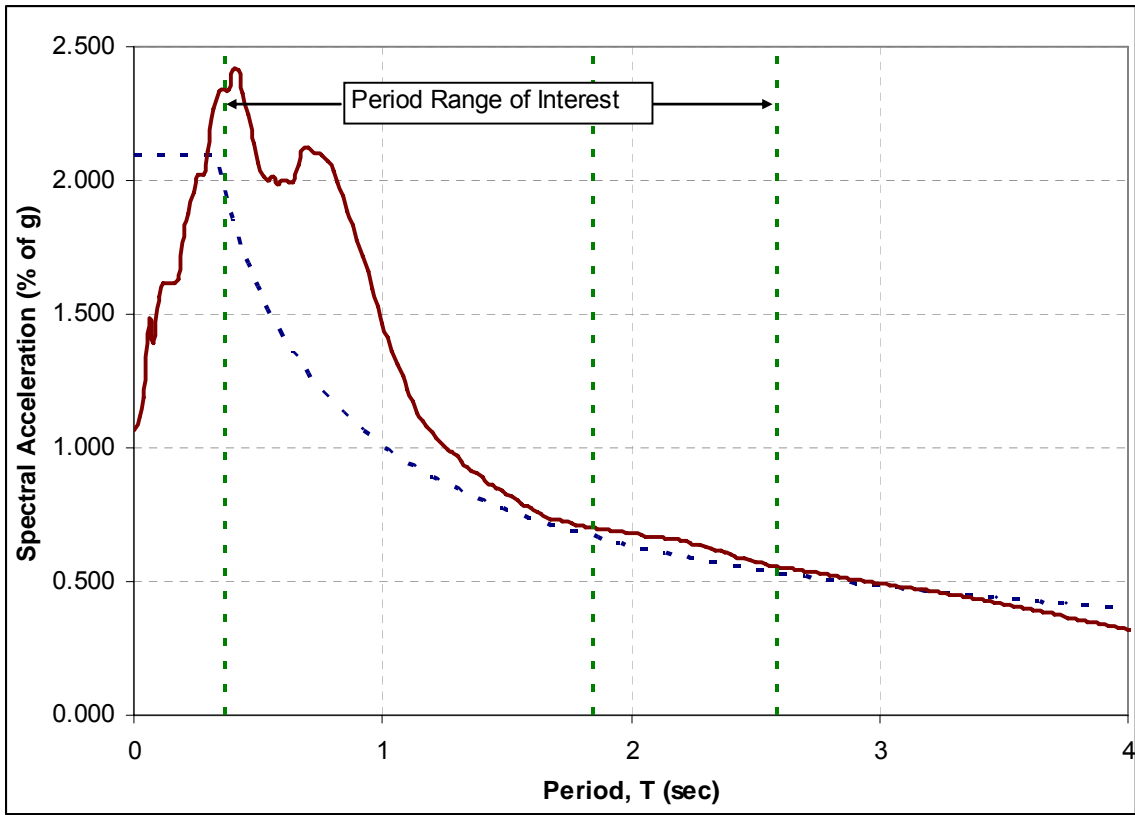
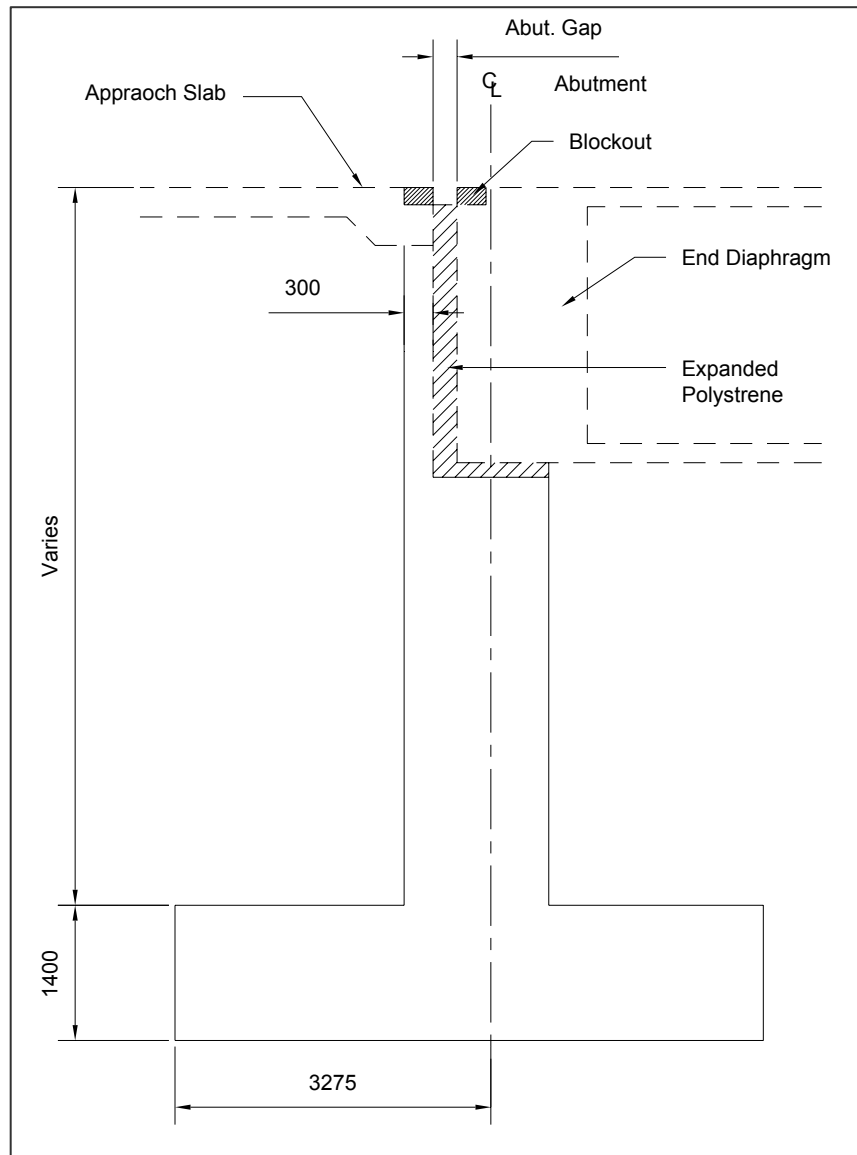


Figure 4-14: 2% Probability of Exceedance in 50 Years Composite Spectrum



**Figure 4-15: Typical Abutment Section**

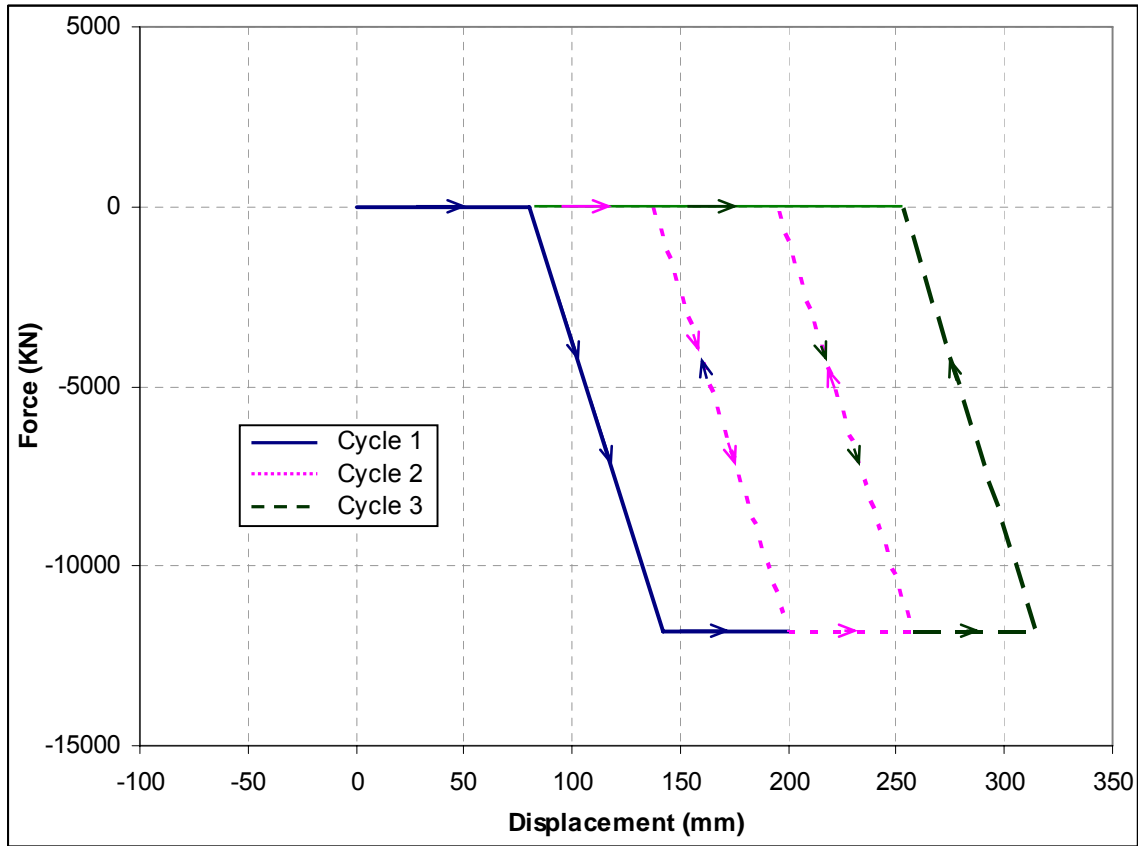


Figure 4-16: Sample Hysteretic Abutment Response

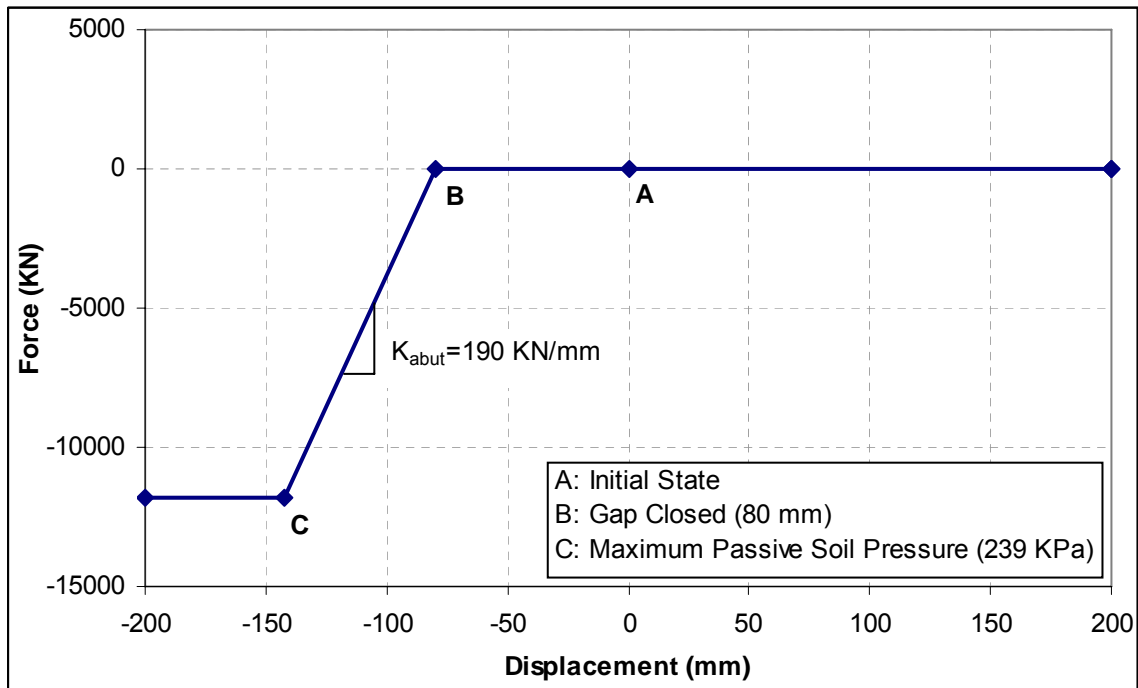


Figure 4-17: Abutment 1 Longitudinal Force Displacement Model

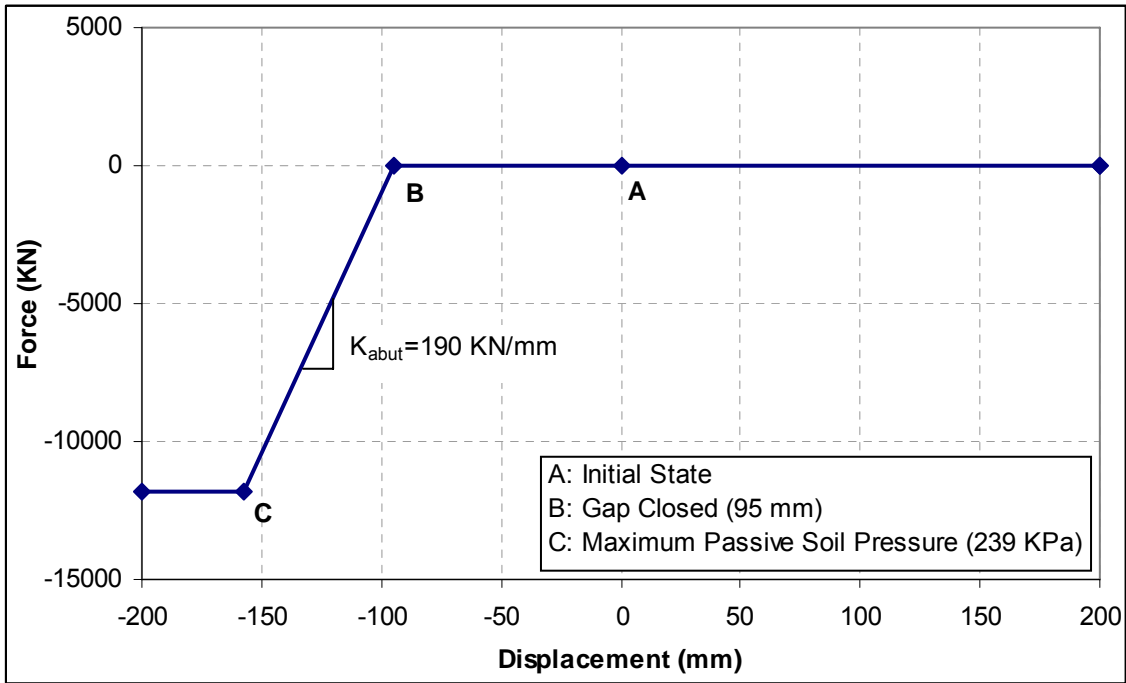


Figure 4-18: Abutment 2 Longitudinal Force Displacement Model

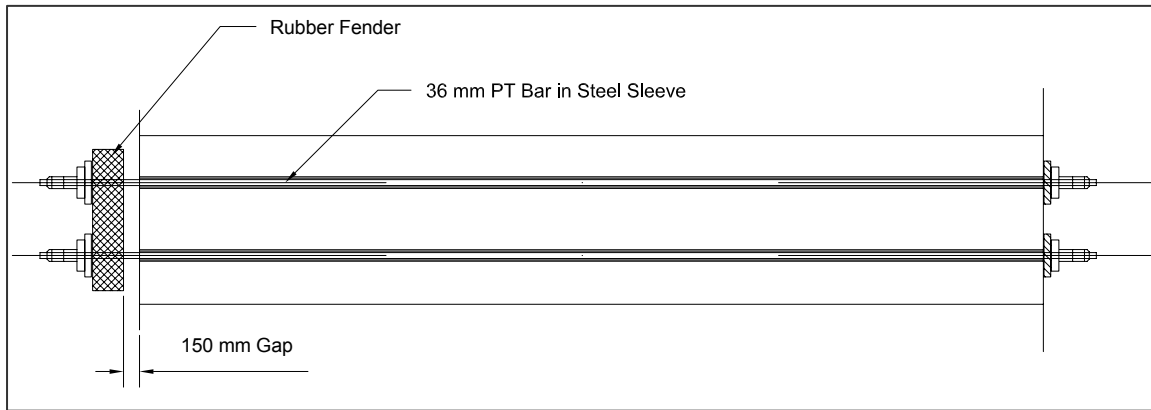


Figure 4-19: Hinge Restrainer Detail with Gap

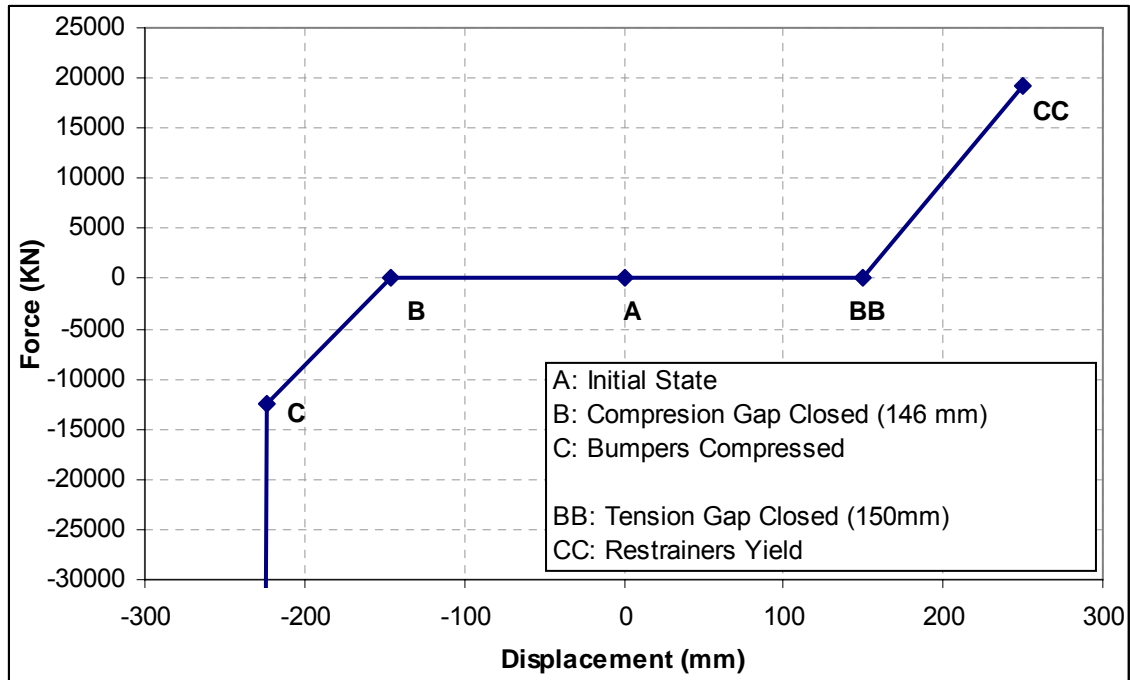


Figure 4-20: Hinge 1 Longitudinal Force Displacement Model

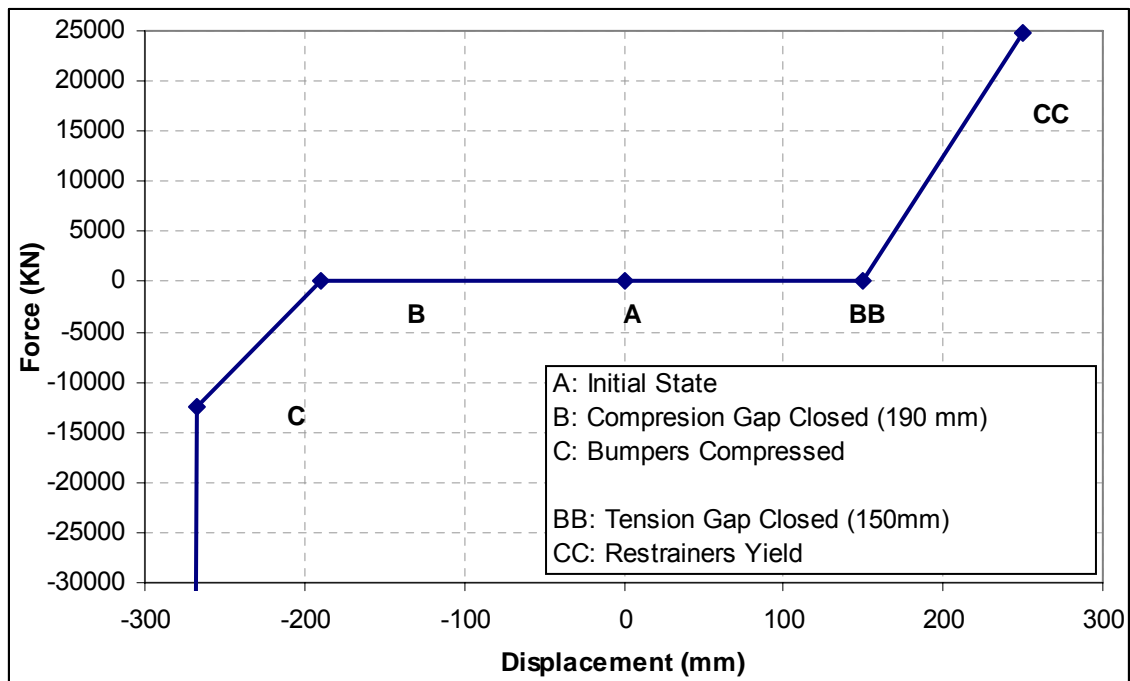
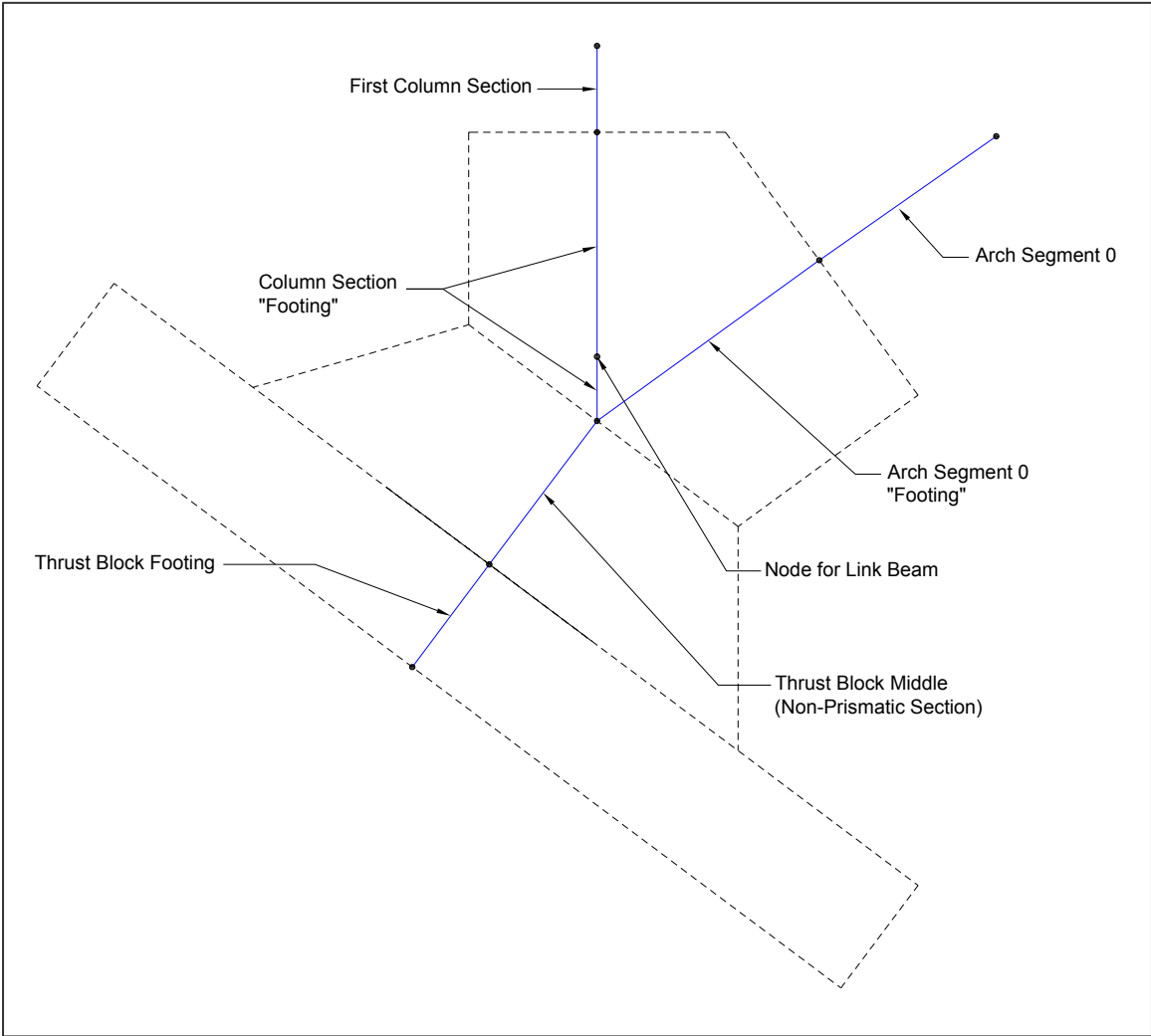
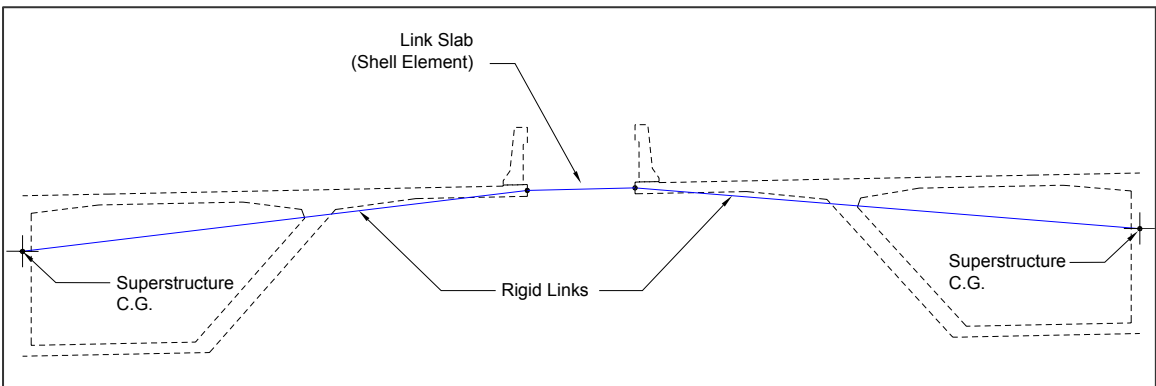


Figure 4-21: Hinge 2 Longitudinal Force Displacement Model



**Figure 4-22: Link Beam Model Diagram**



**Figure 4-23: Link Slab Model Diagram**

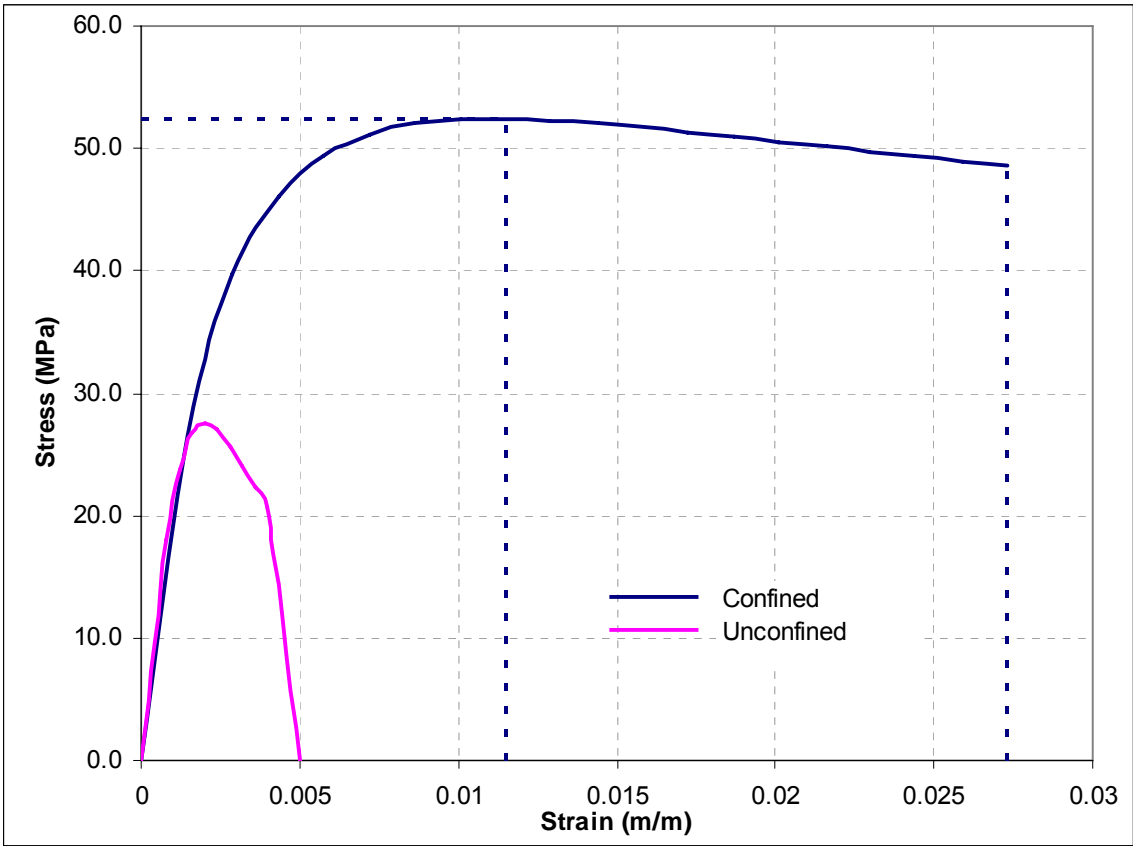


Figure 4-24: Column Confined Concrete Curve

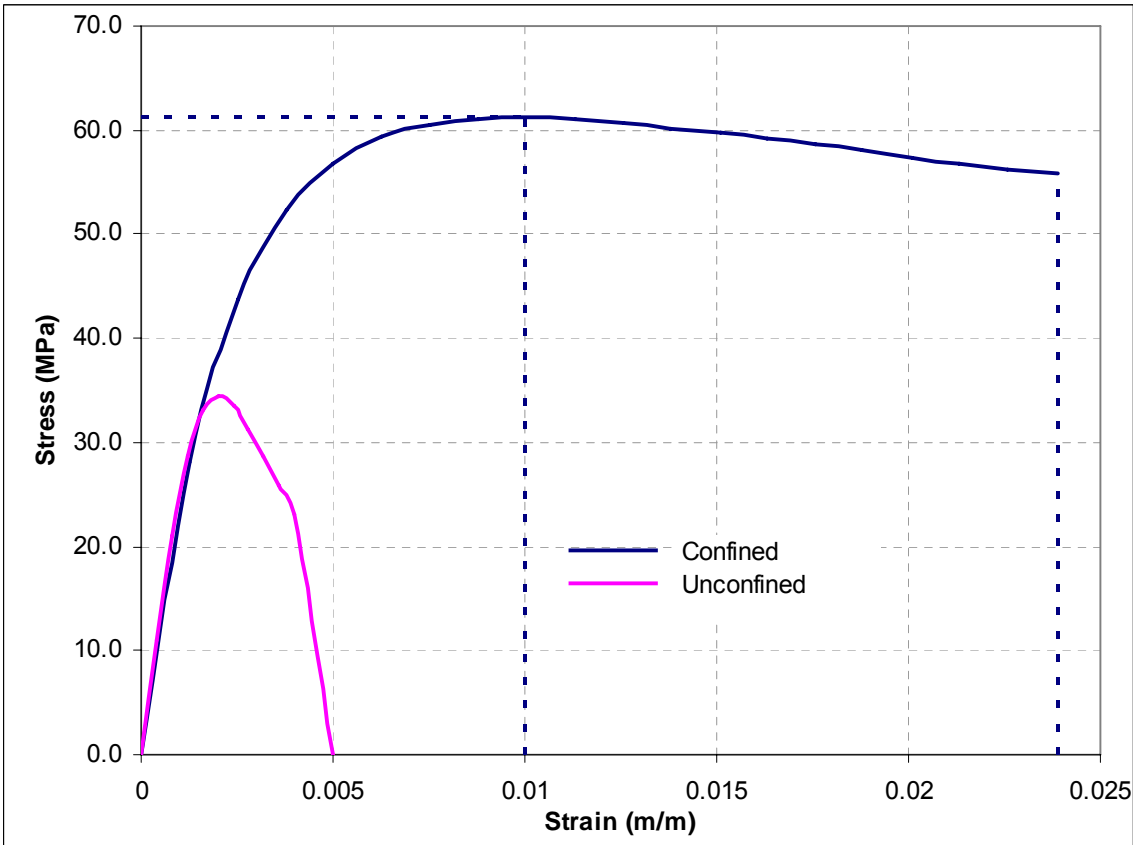


Figure 4-25: Arch Confined Concrete Curve

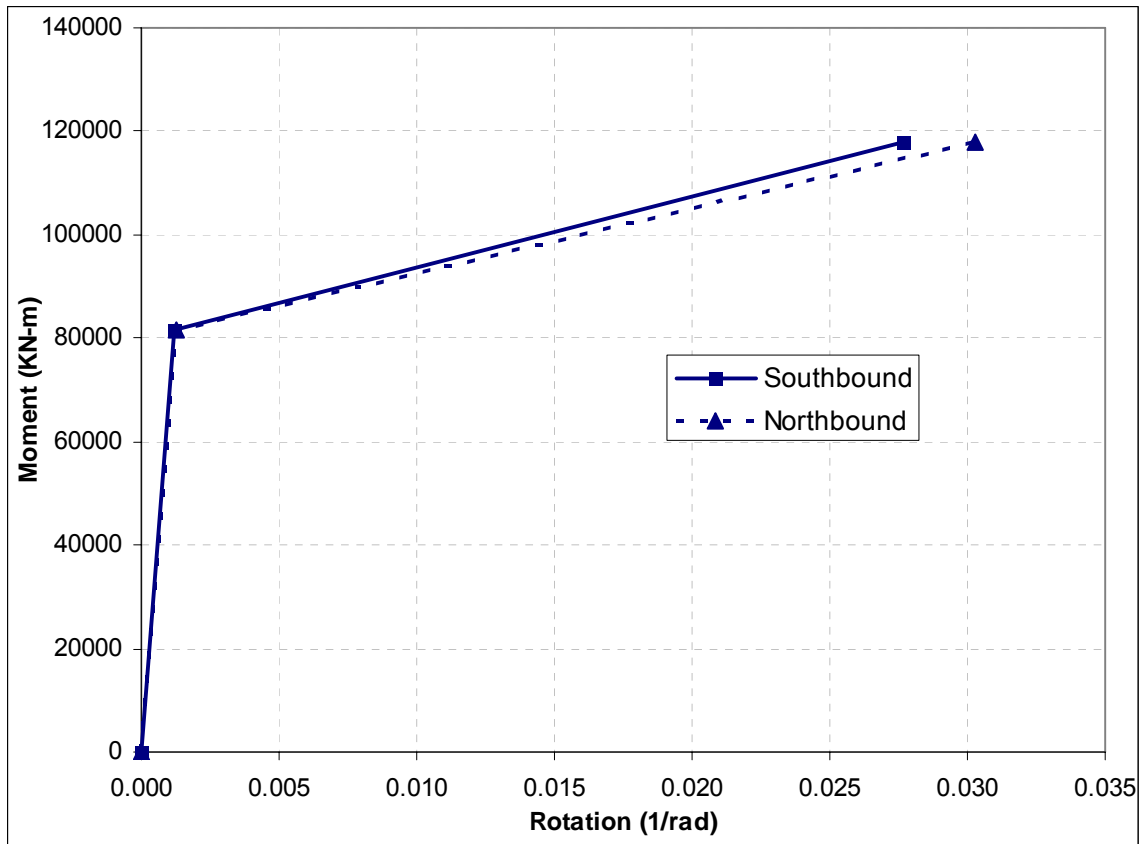


Figure 4-26: Moment-Rotation Response, Pier 1 Top, X-Axis Bending

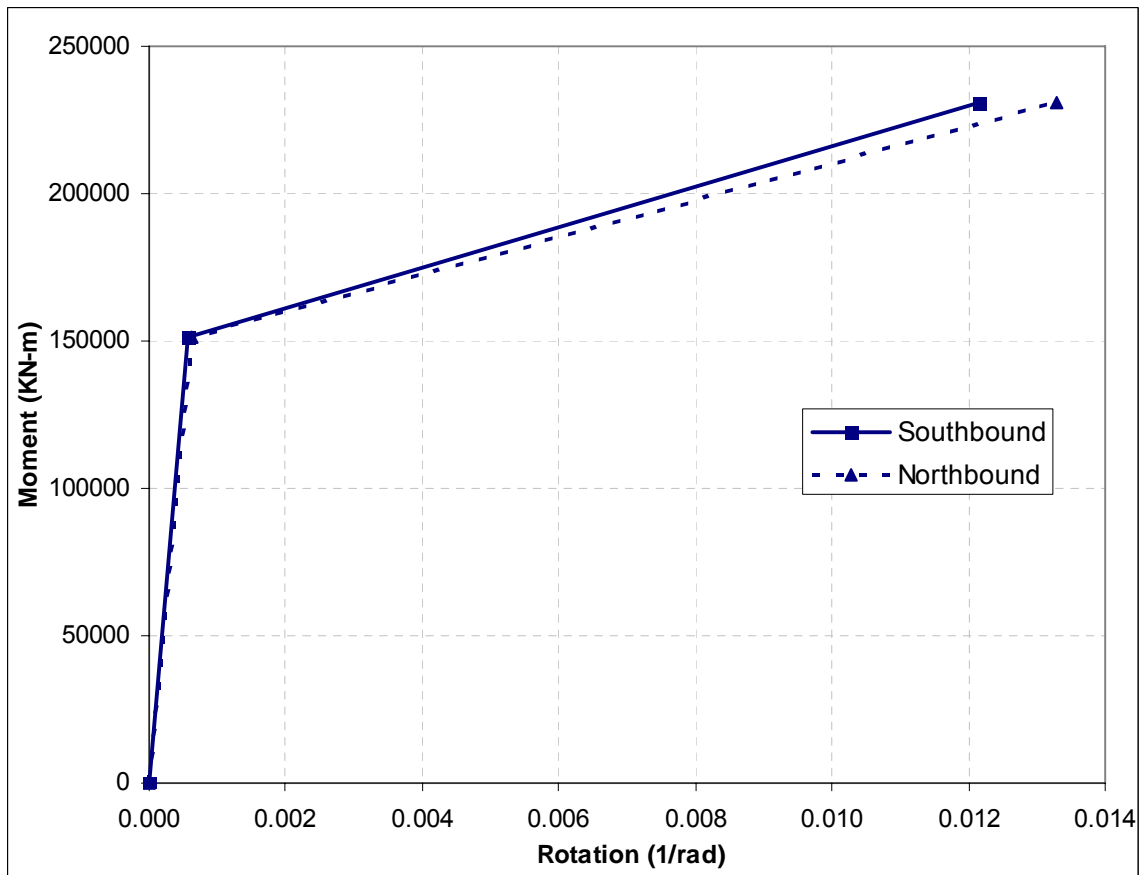


Figure 4-27: Moment-Rotation Response, Pier 1 Top, Y-Axis Bending

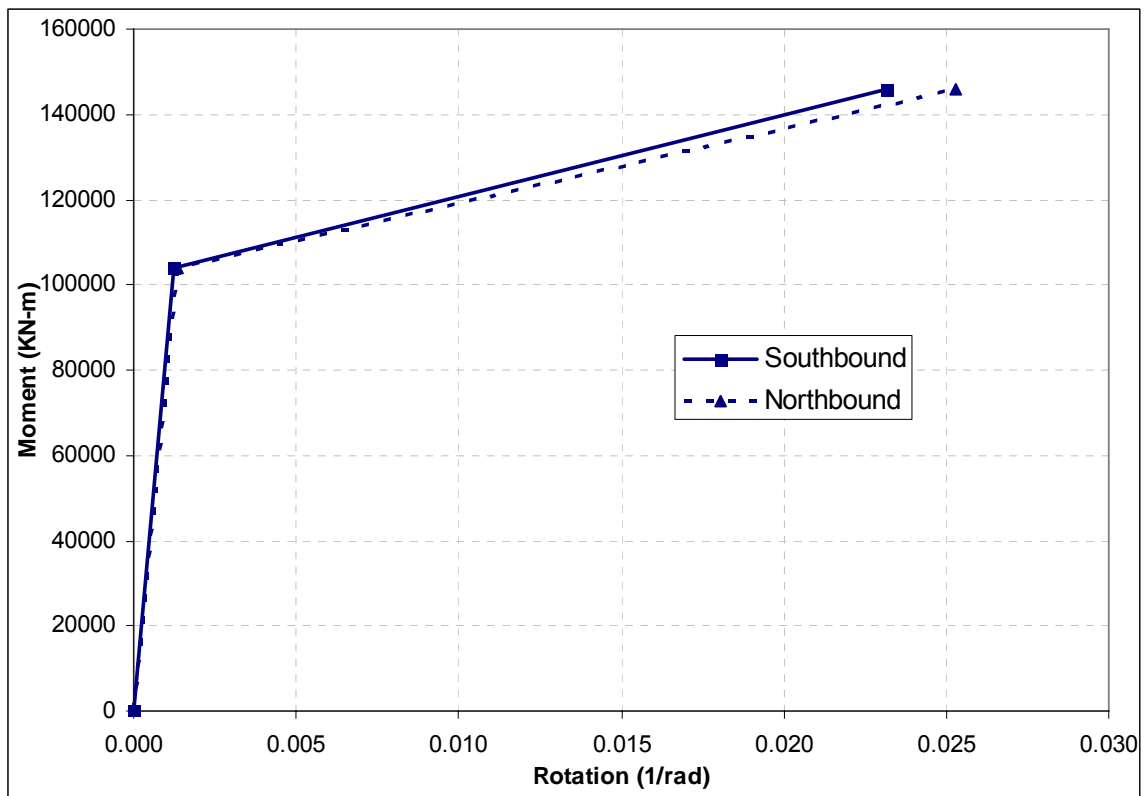


Figure 4-28: Moment-Rotation Response, Pier 1 Bottom, X-Axis Bending

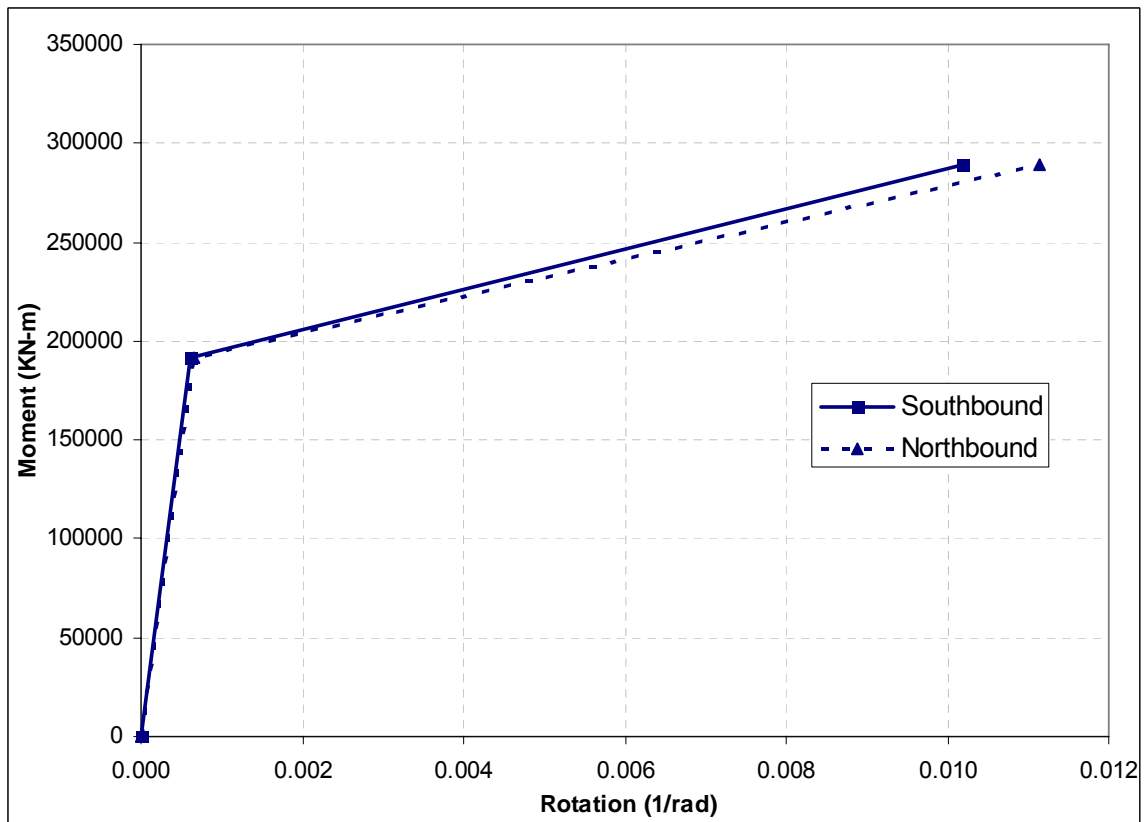


Figure 4-29: Moment-Rotation Response, Pier 1 Bottom, Y-Axis Bending

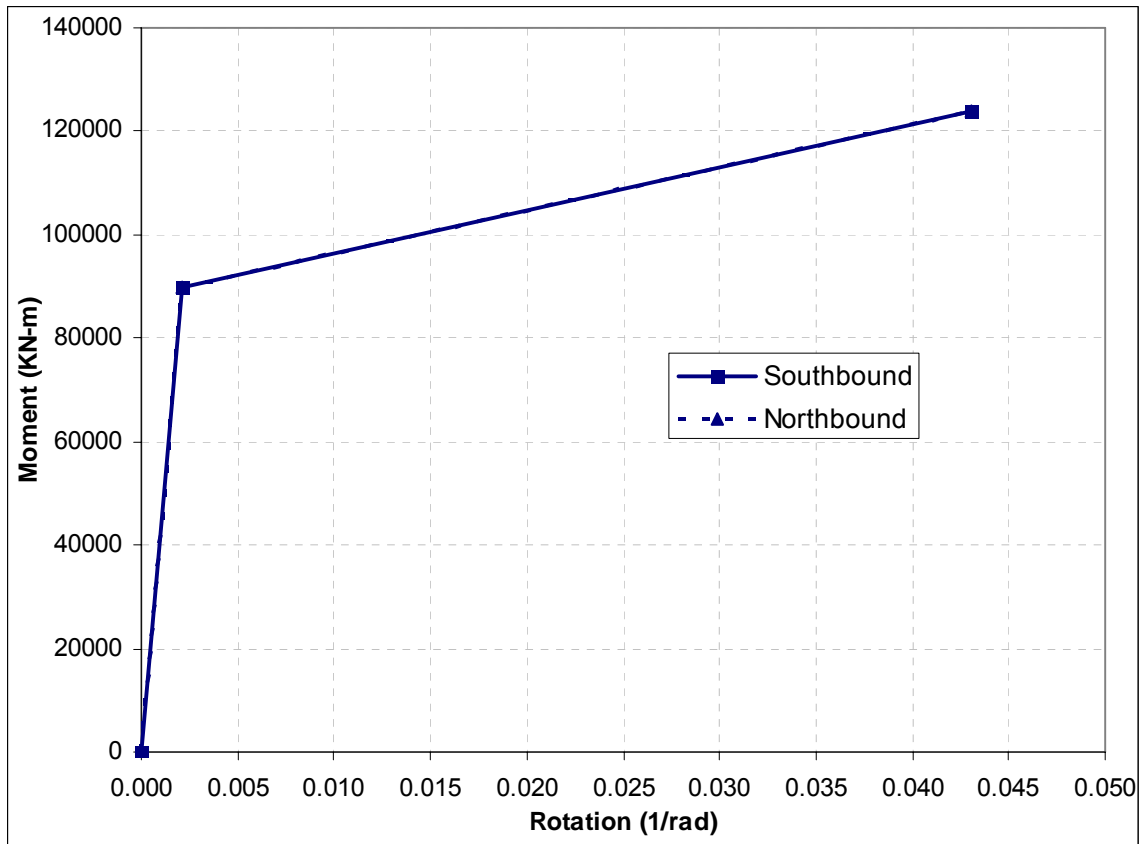


Figure 4-30: Moment-Rotation Response, Pier 2&3 Top, X-Axis Bending

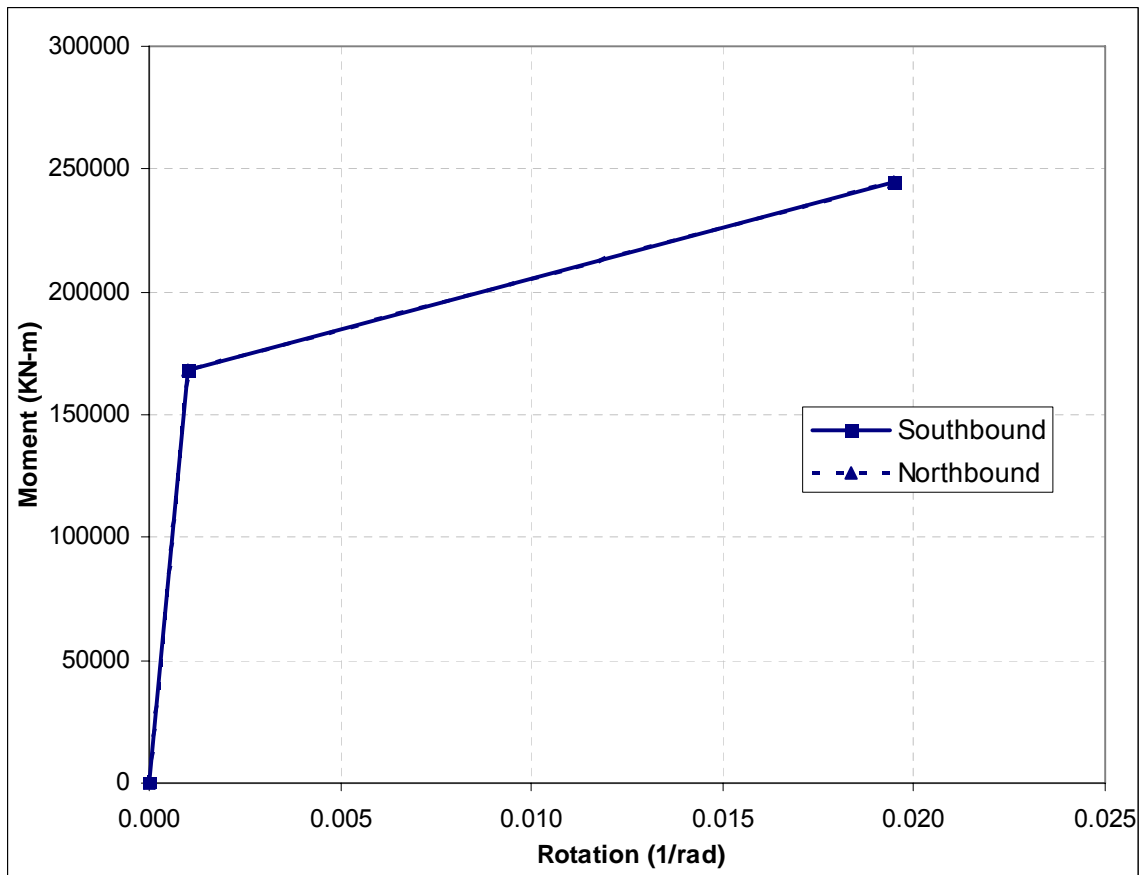


Figure 4-31: Moment-Rotation Response, Pier 2&3 Top, Y-Axis Bending

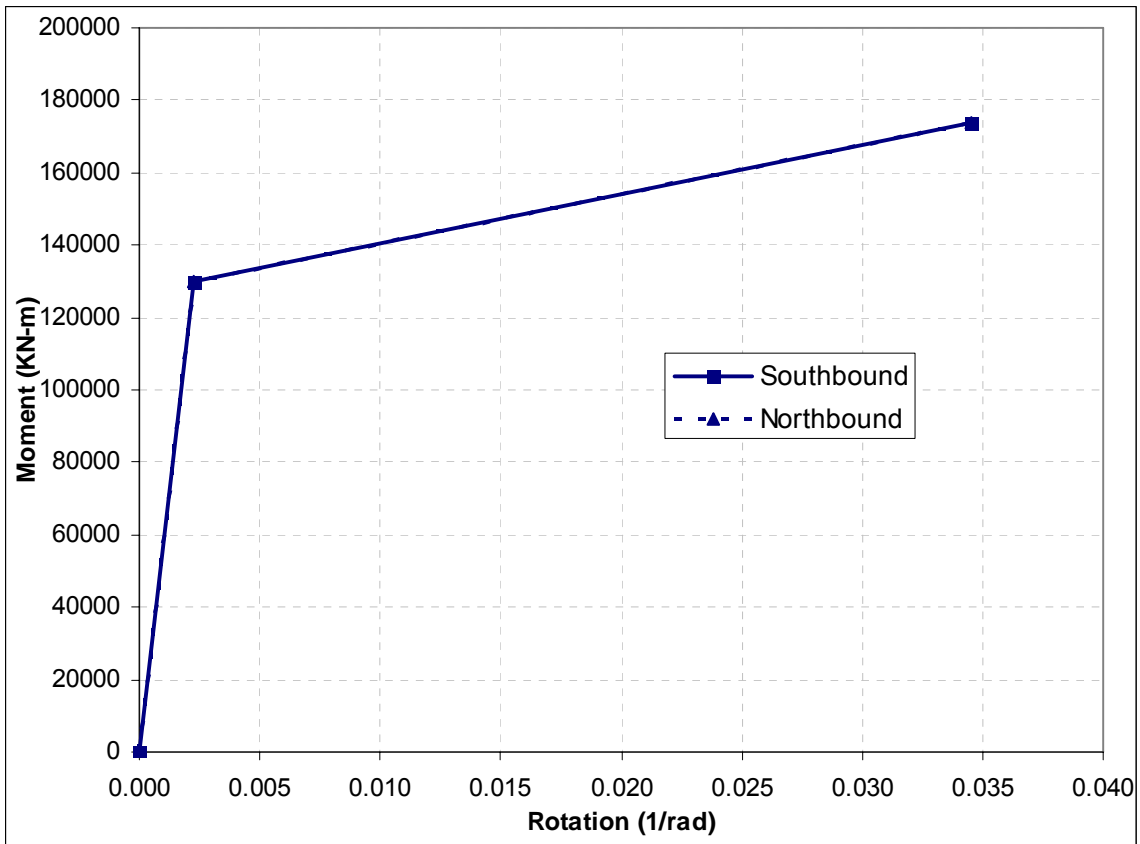


Figure 4-32: Moment-Rotation Response, Pier 2&3 Bottom, X-Axis Bending

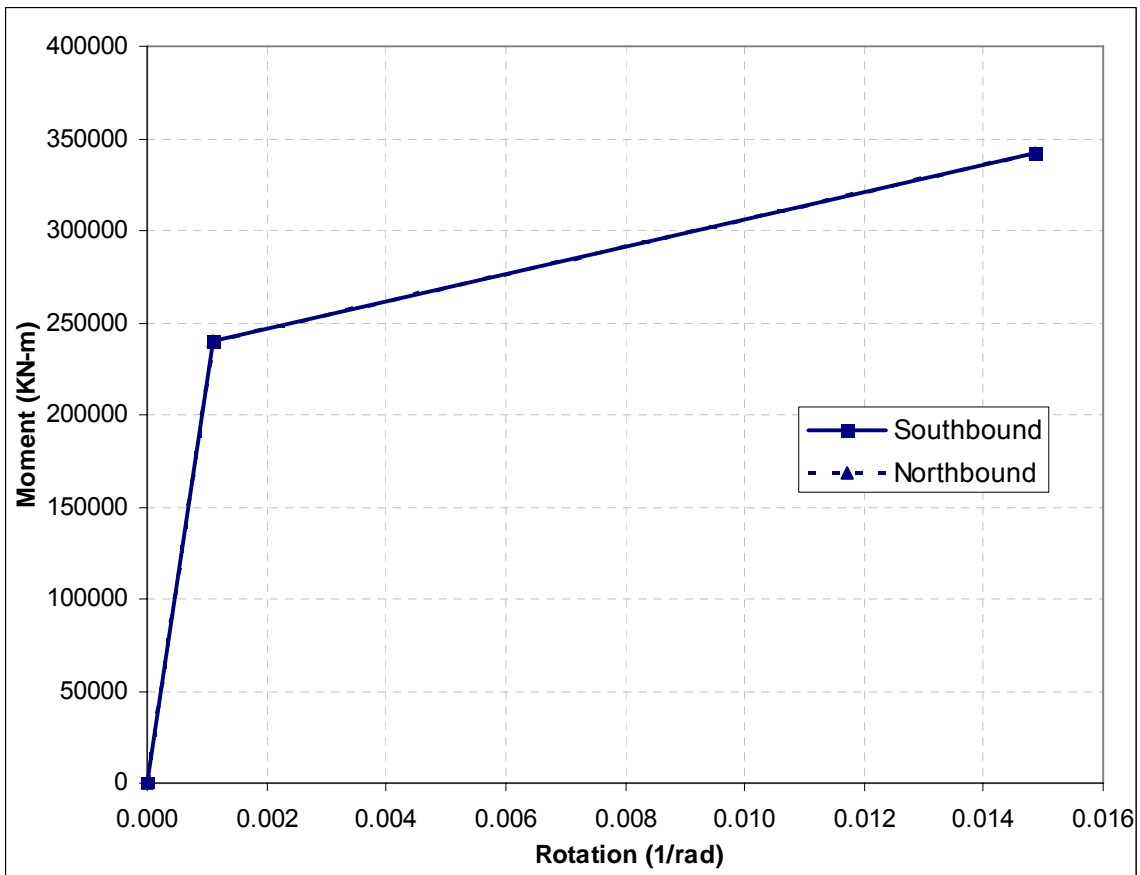


Figure 4-33: Moment-Rotation Response, Pier 2&3 Bottom, Y-Axis Bending

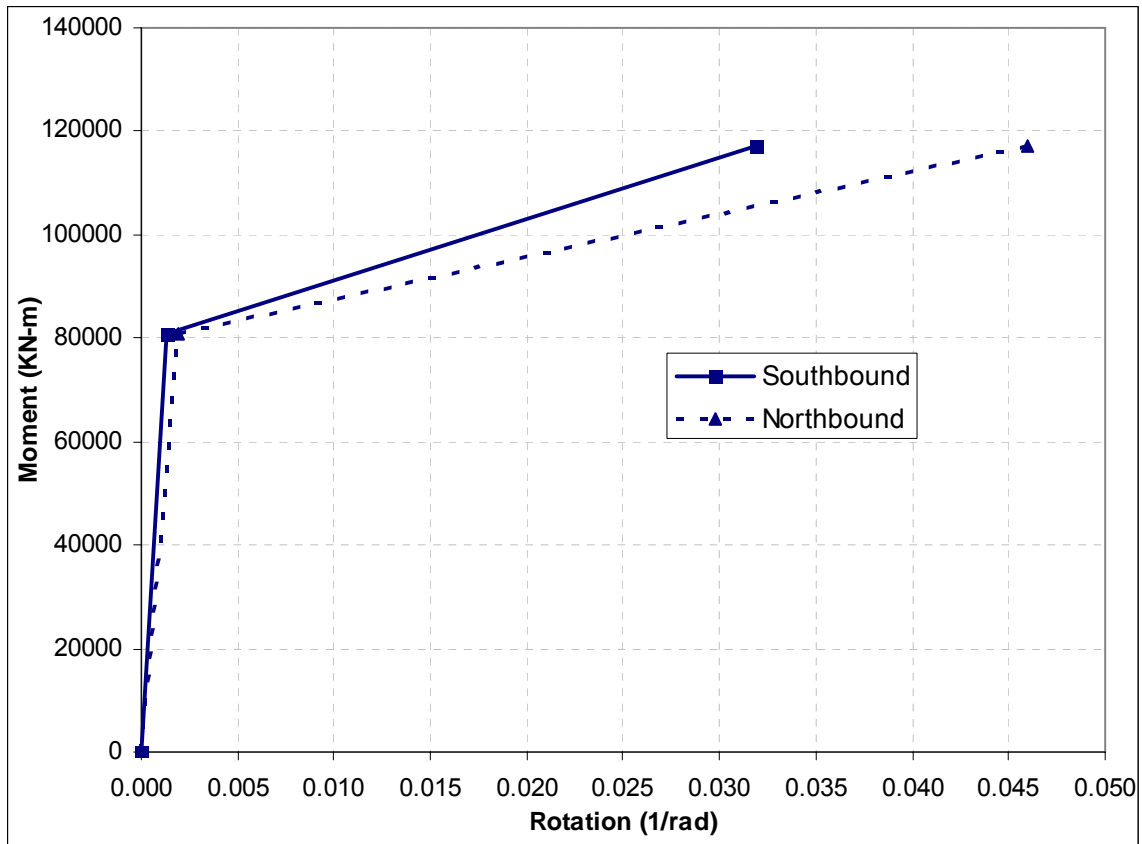


Figure 4-34: Moment-Rotation Response, Pier 4 Top, X-Axis Bending

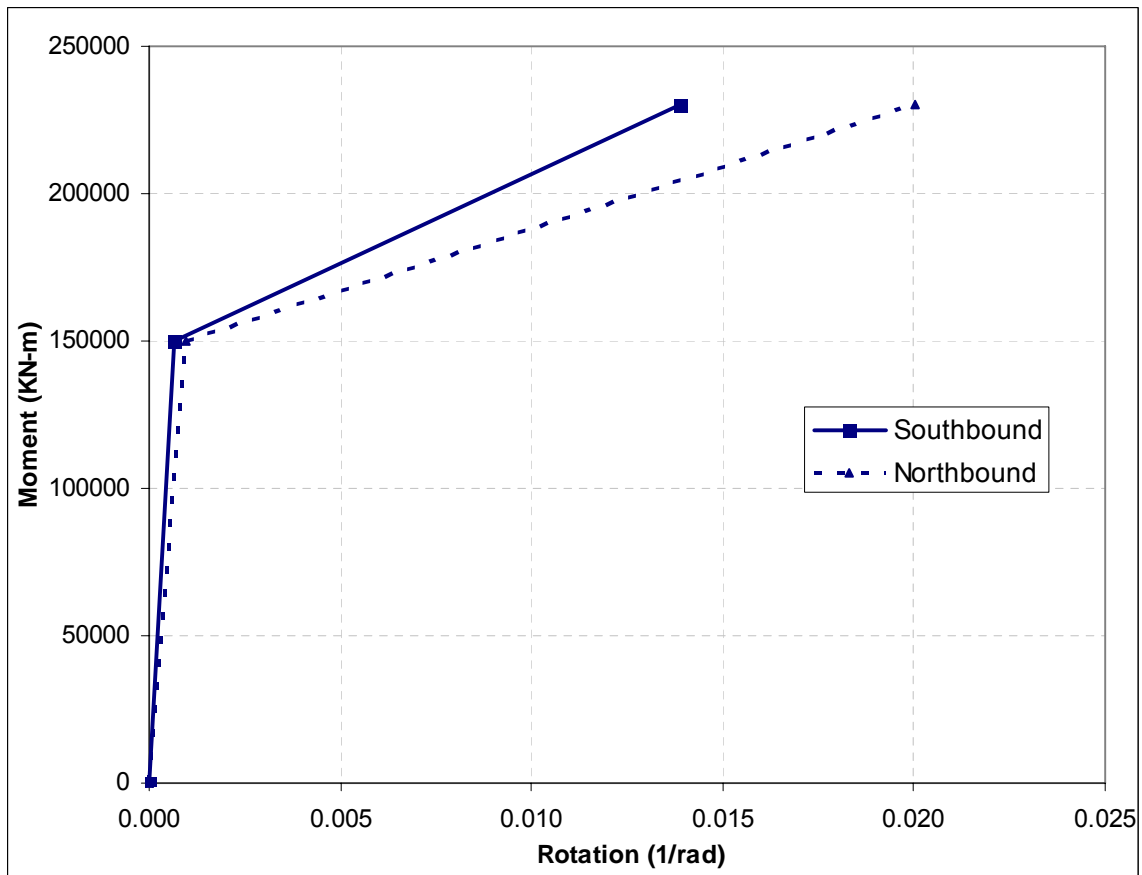


Figure 4-35: Moment-Rotation Response, Pier 4 Top, Y-Axis Bending

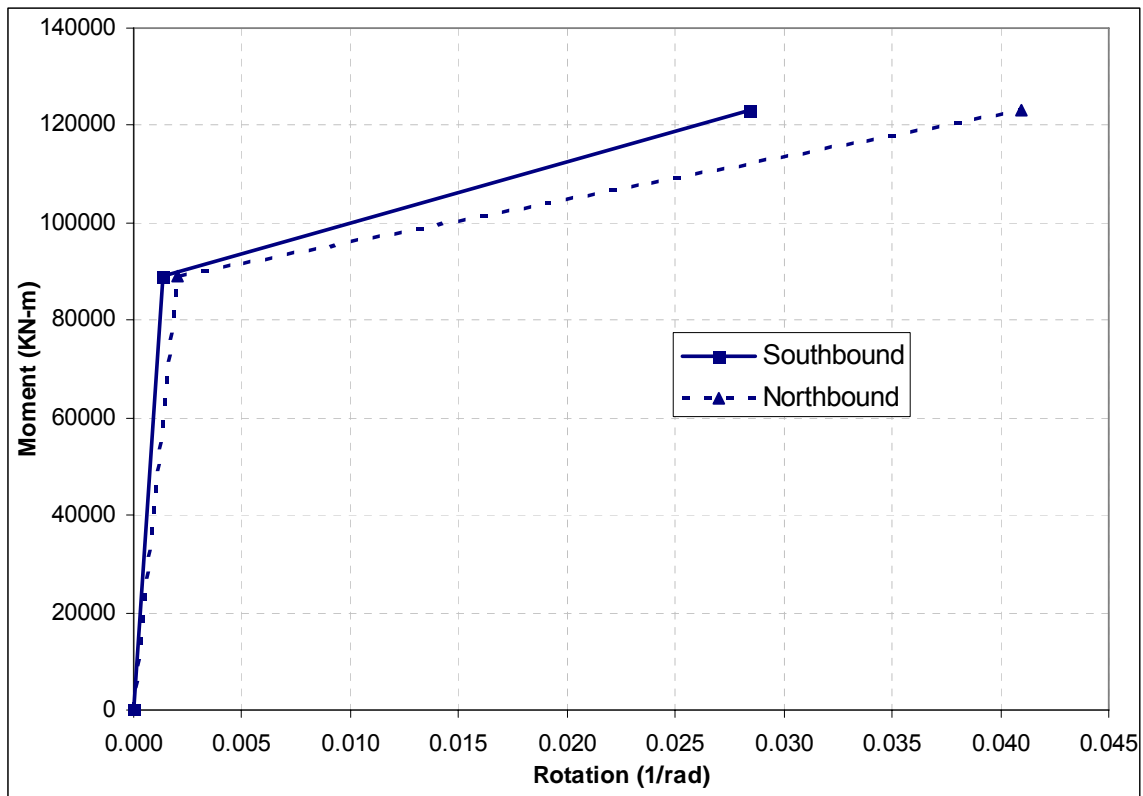


Figure 4-36: Moment-Rotation Response, Pier 4 Bottom, X-Axis Bending

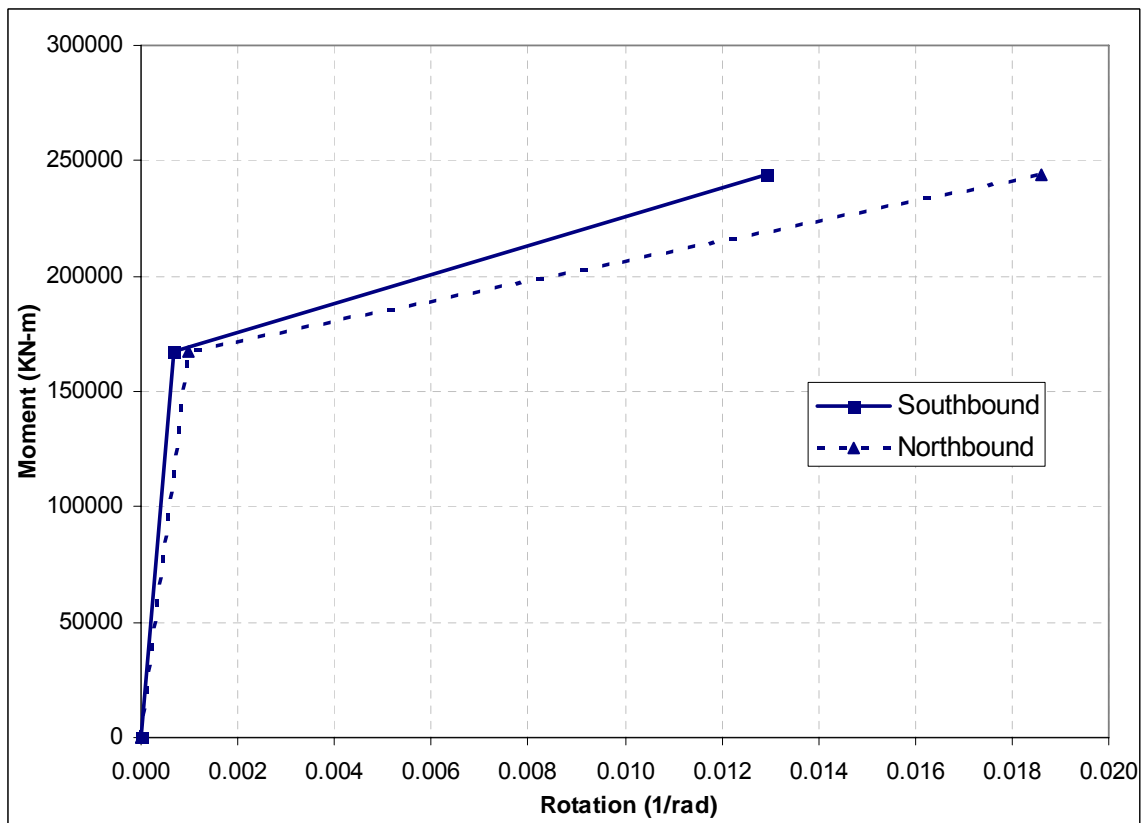


Figure 4-37: Moment-Rotation Response, Pier 4 Bottom, Y-Axis Bending

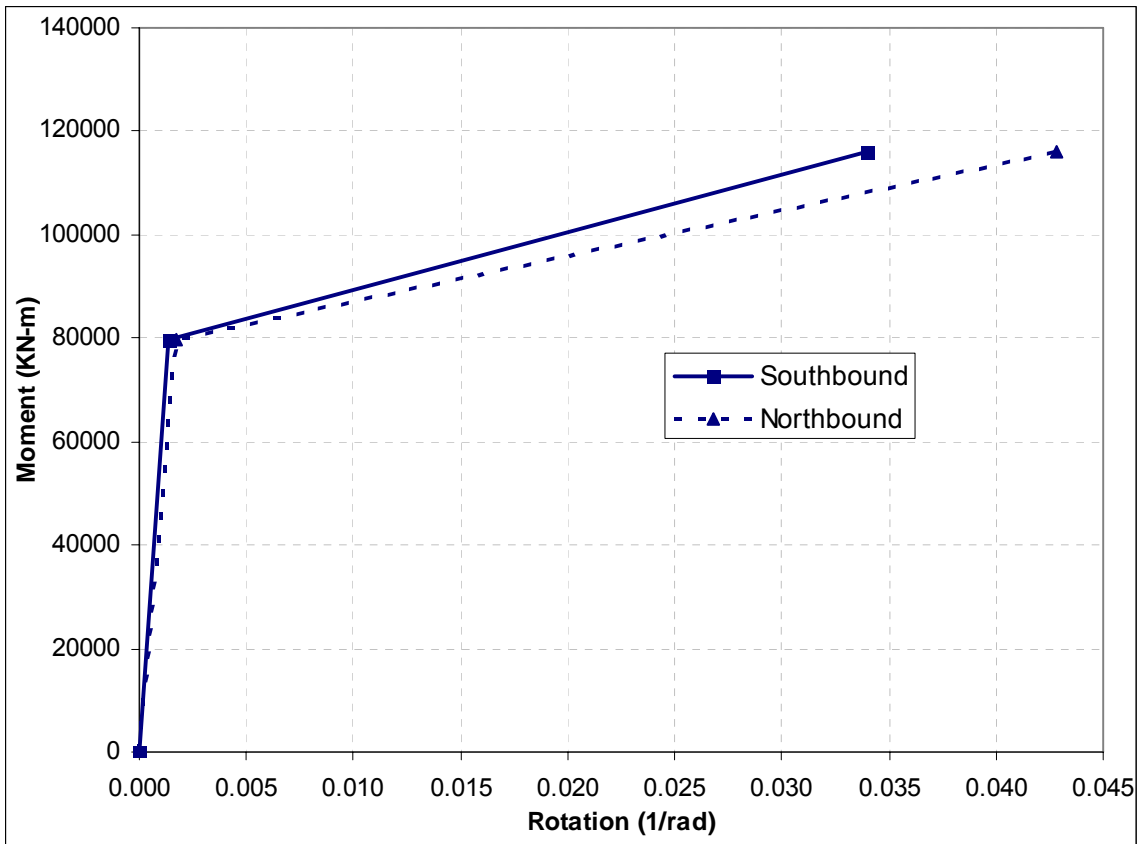


Figure 4-38: Moment-Rotation Response, Pier 5 Top, X-Axis Bending

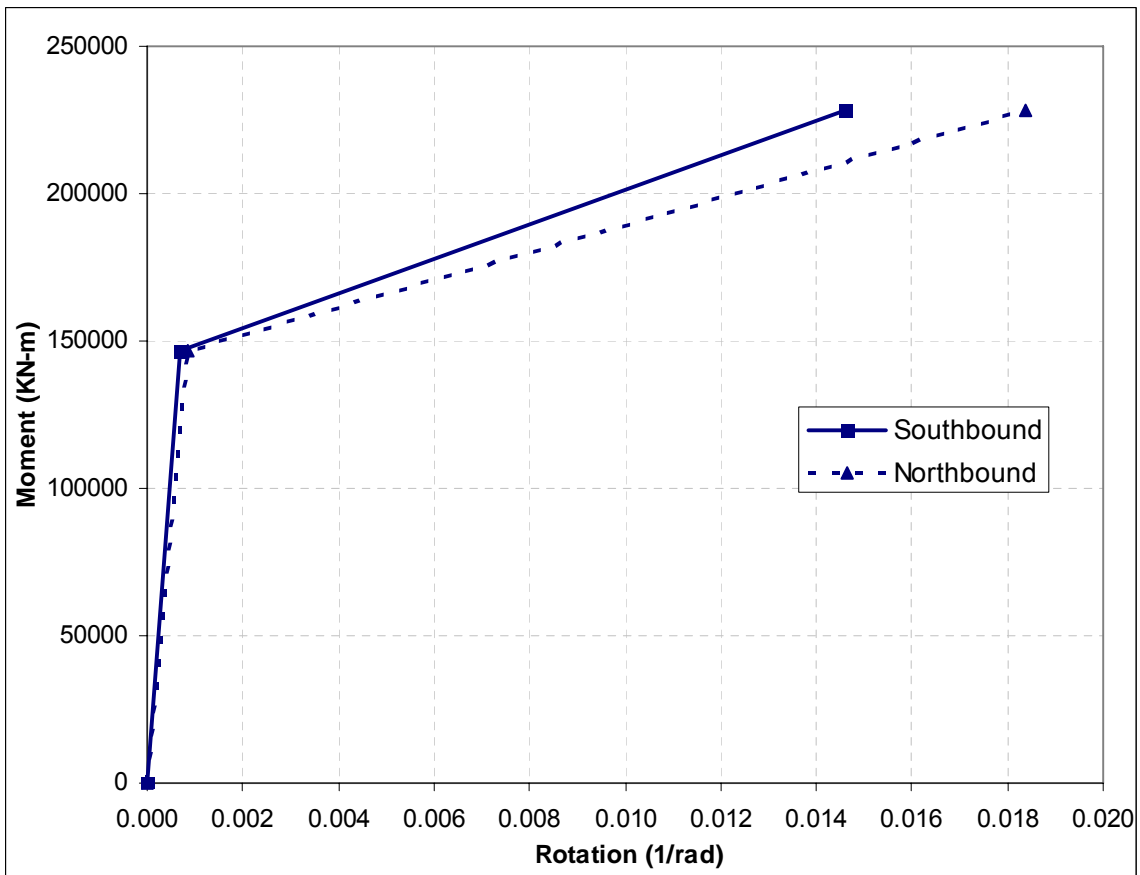


Figure 4-39: Moment-Rotation Response, Pier 5 Top, Y-Axis Bending

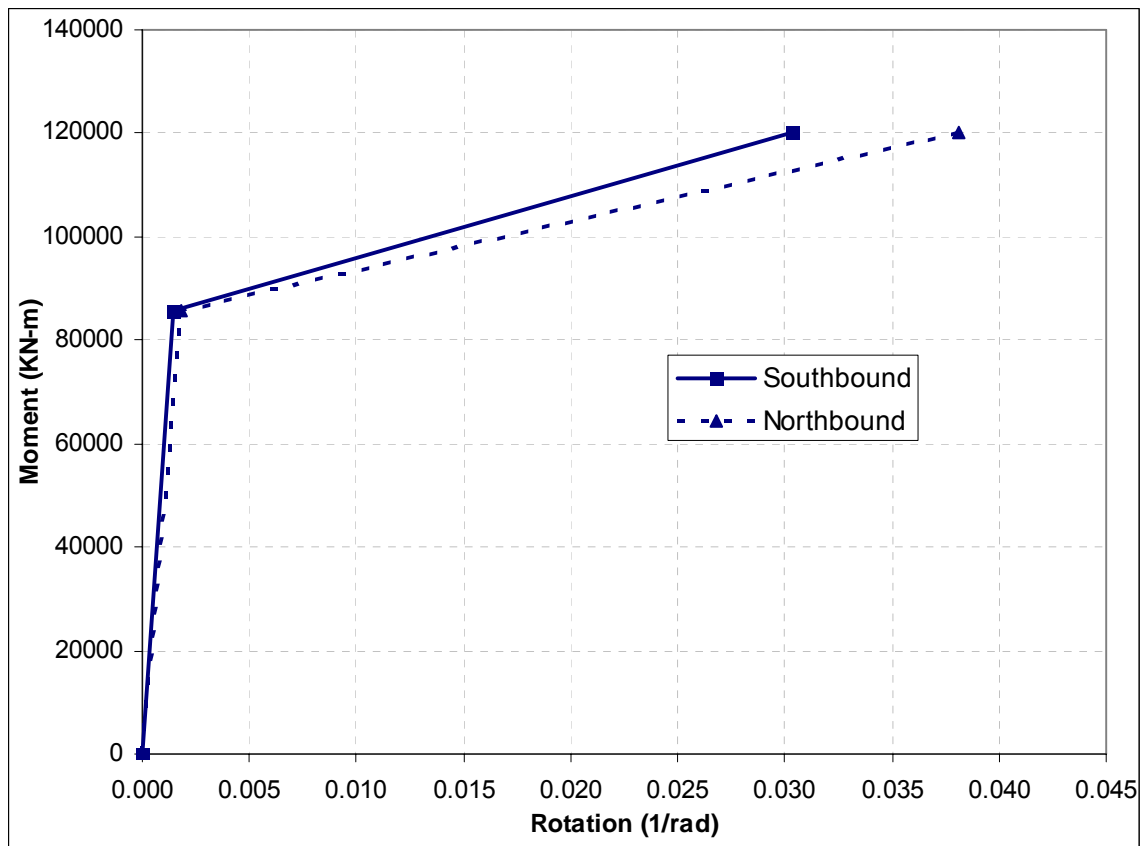


Figure 4-40: Moment-Rotation Response, Pier 5 Bottom, X-Axis Bending

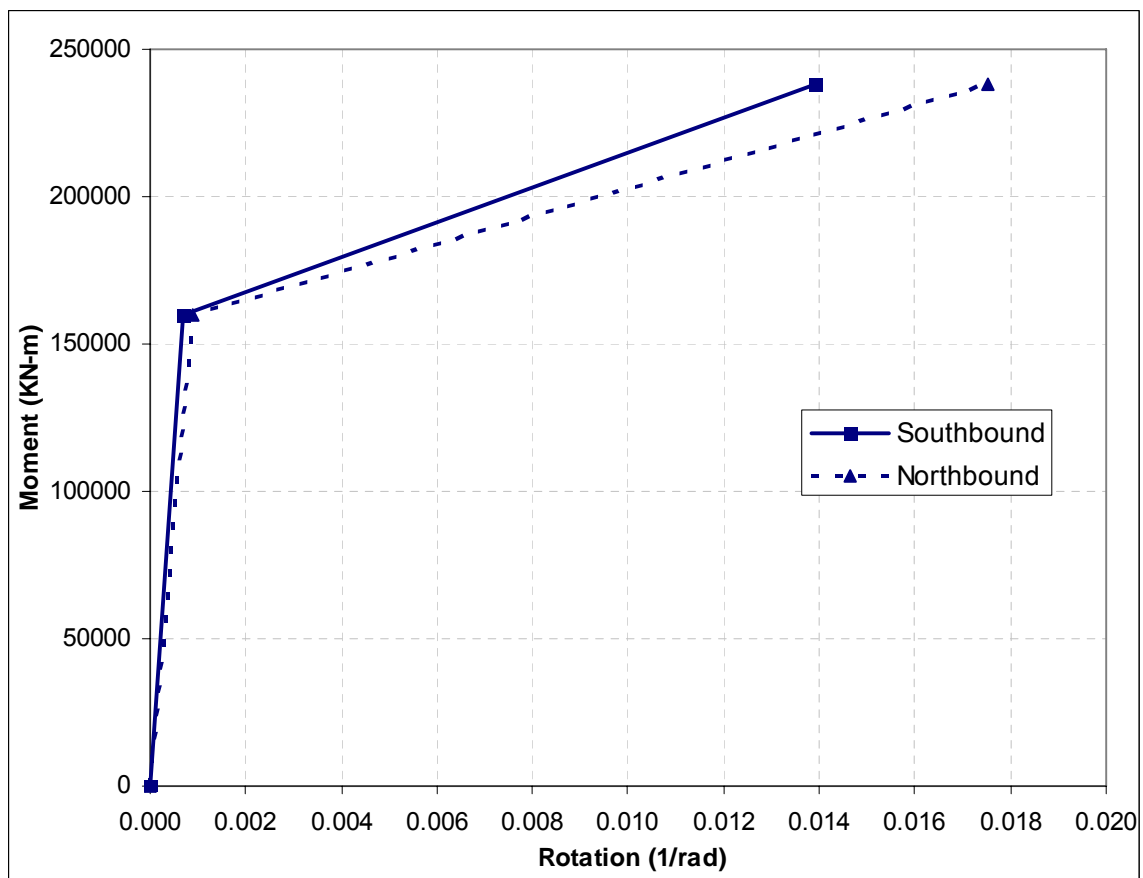


Figure 4-41: Moment-Rotation Response, Pier 5 Bottom, Y-Axis Bending

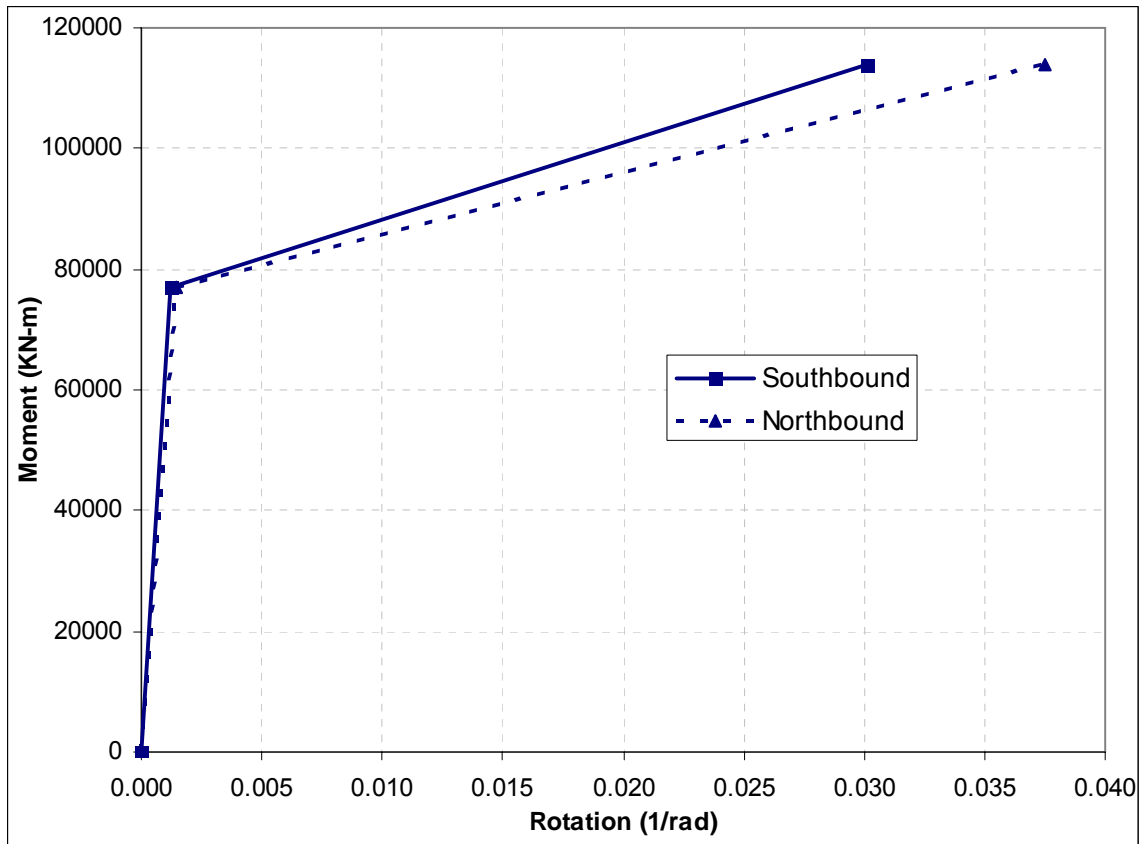


Figure 4-42: Moment-Rotation Response, Pier 6 Top, X-Axis Bending

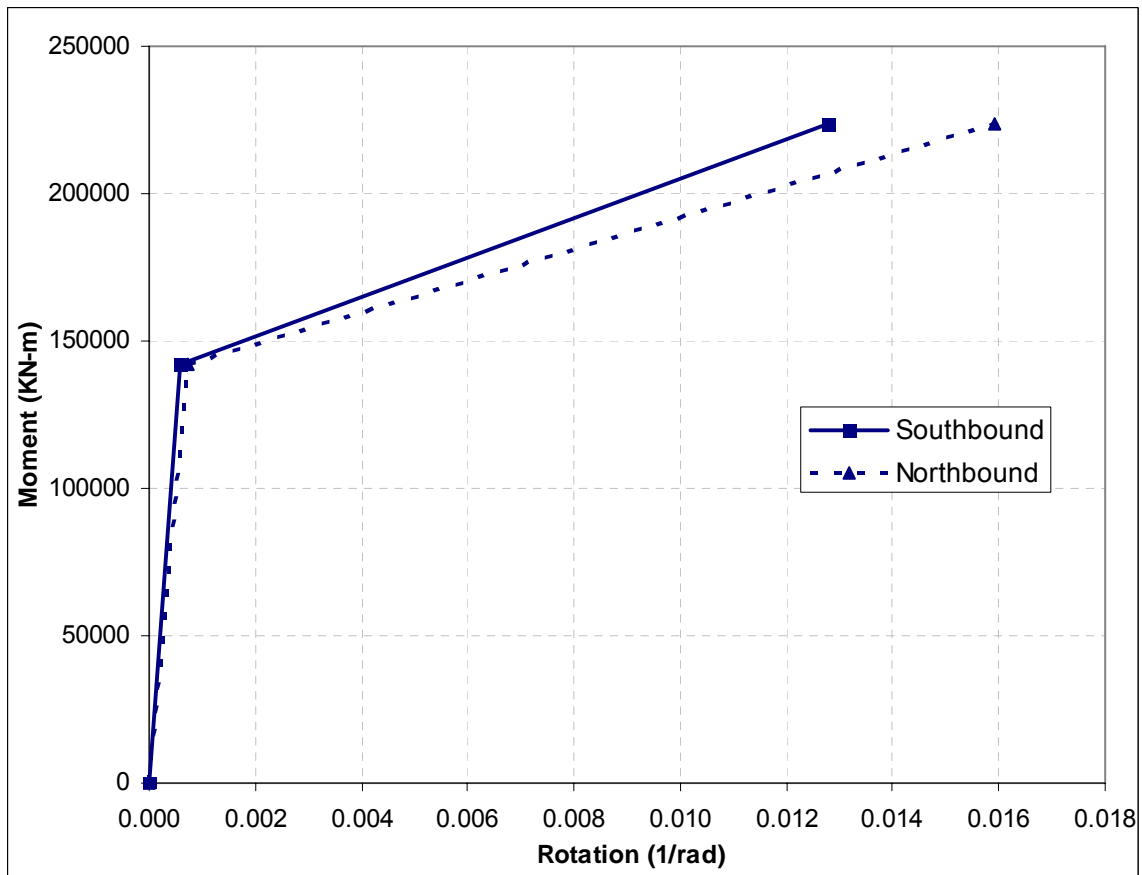


Figure 4-43: Moment-Rotation Response, Pier 6 Top, Y-Axis Bending

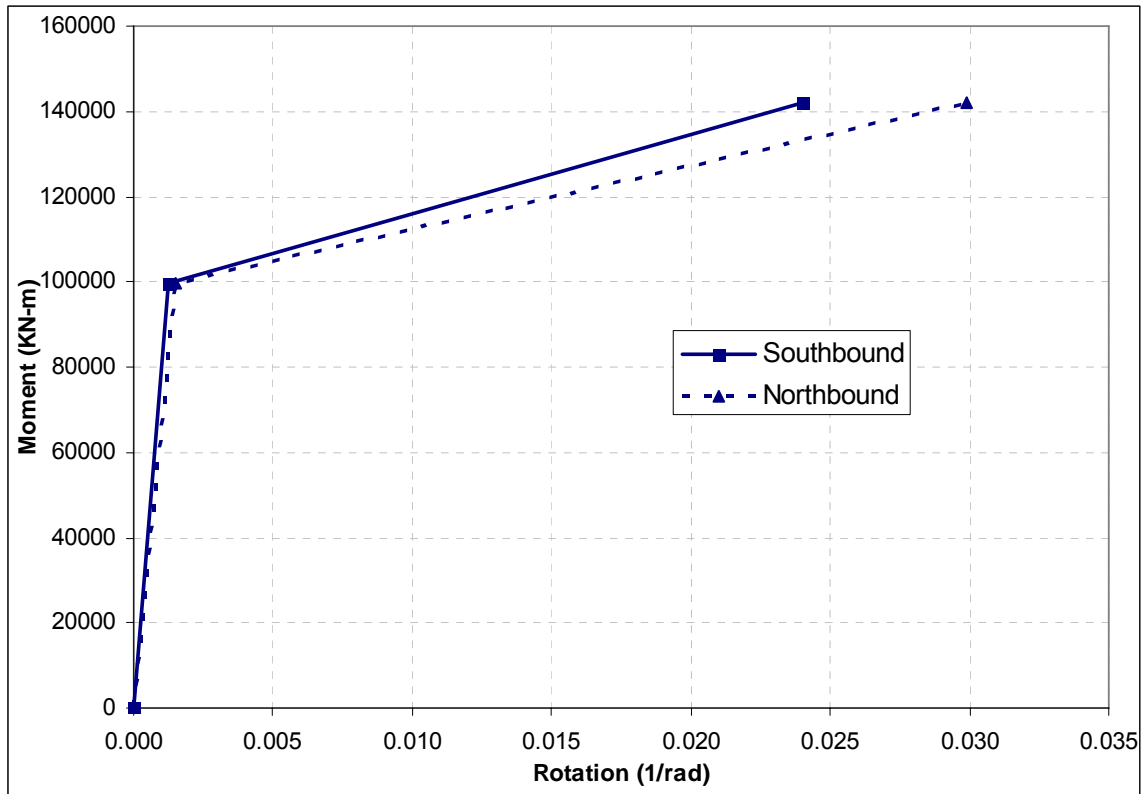


Figure 4-44: Moment-Rotation Response, Pier 6 Bottom, X-Axis Bending

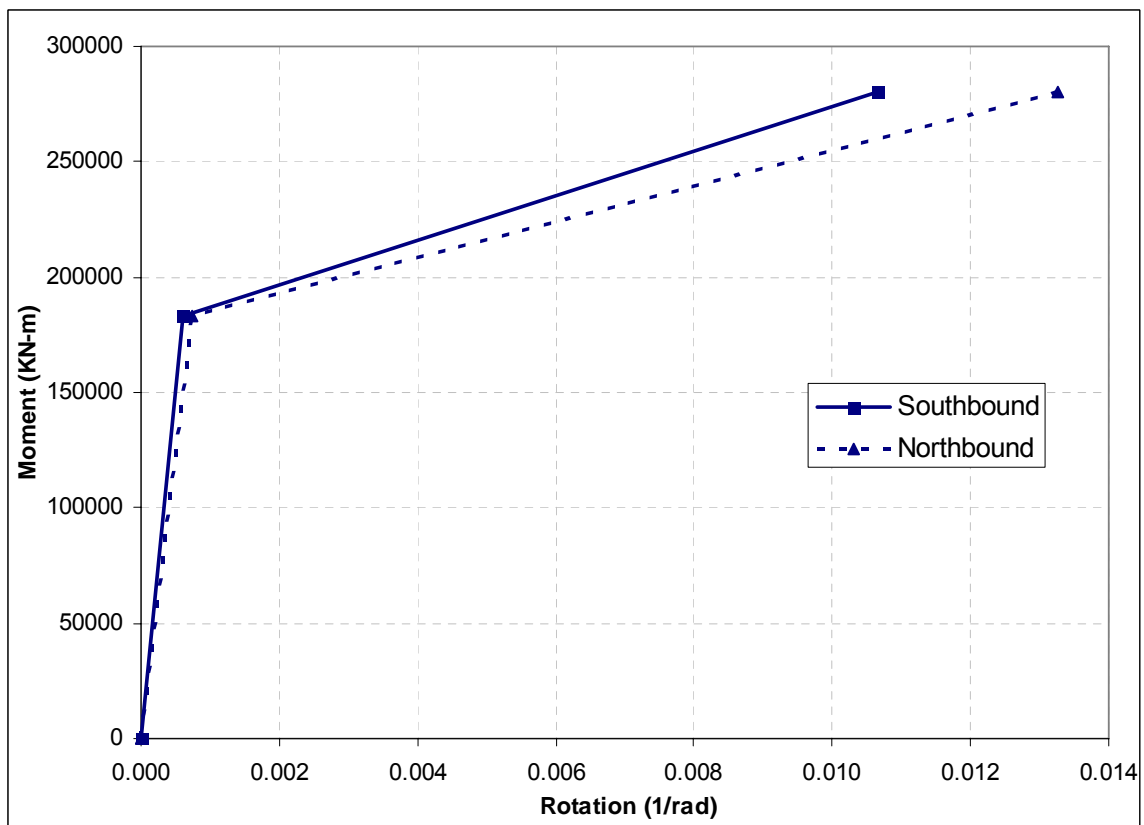


Figure 4-45: Moment-Rotation Response, Pier 6 Bottom, Y-Axis Bending

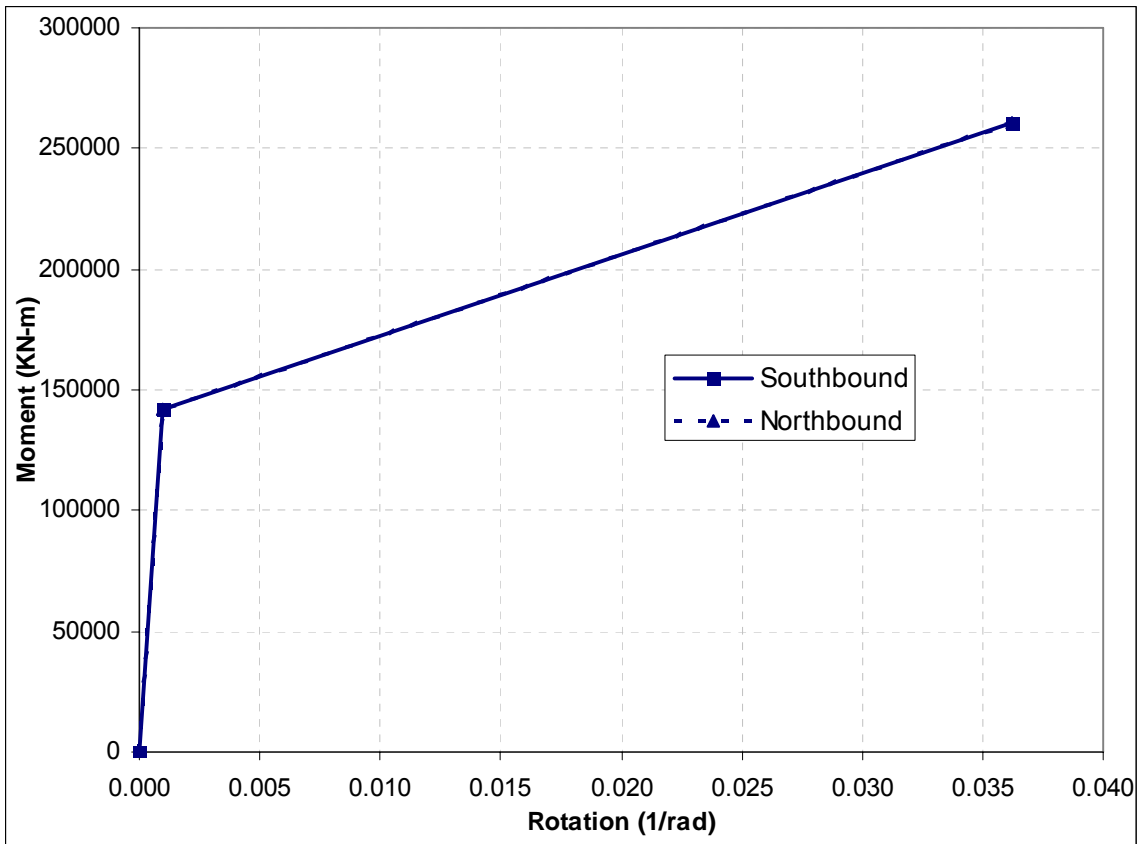


Figure 4-46: Moment-Rotation Response, Arch Crown, X-Axis Bending

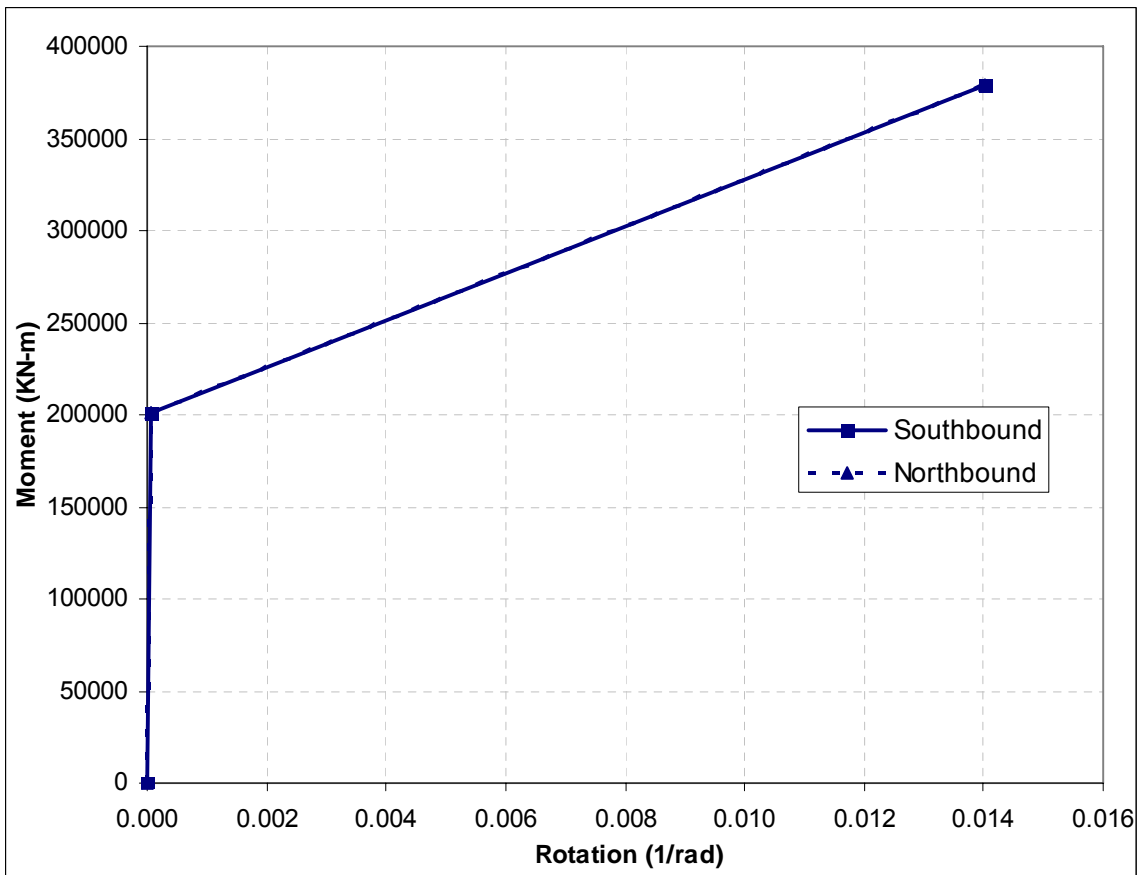


Figure 4-47: Moment Rotation Response, Arch Crown, Y-Axis Bending

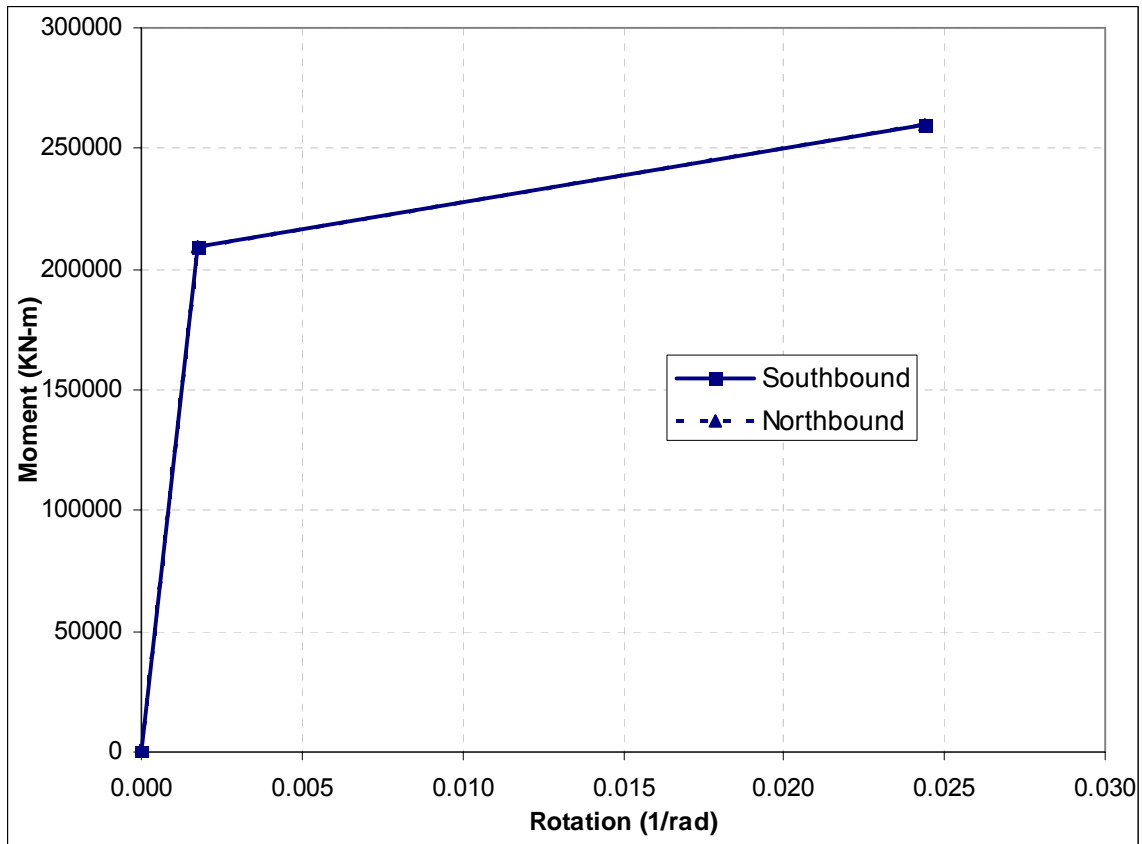


Figure 4-48: Moment-Rotation Response, Arch Segment 0&0A, X-Axis Bending

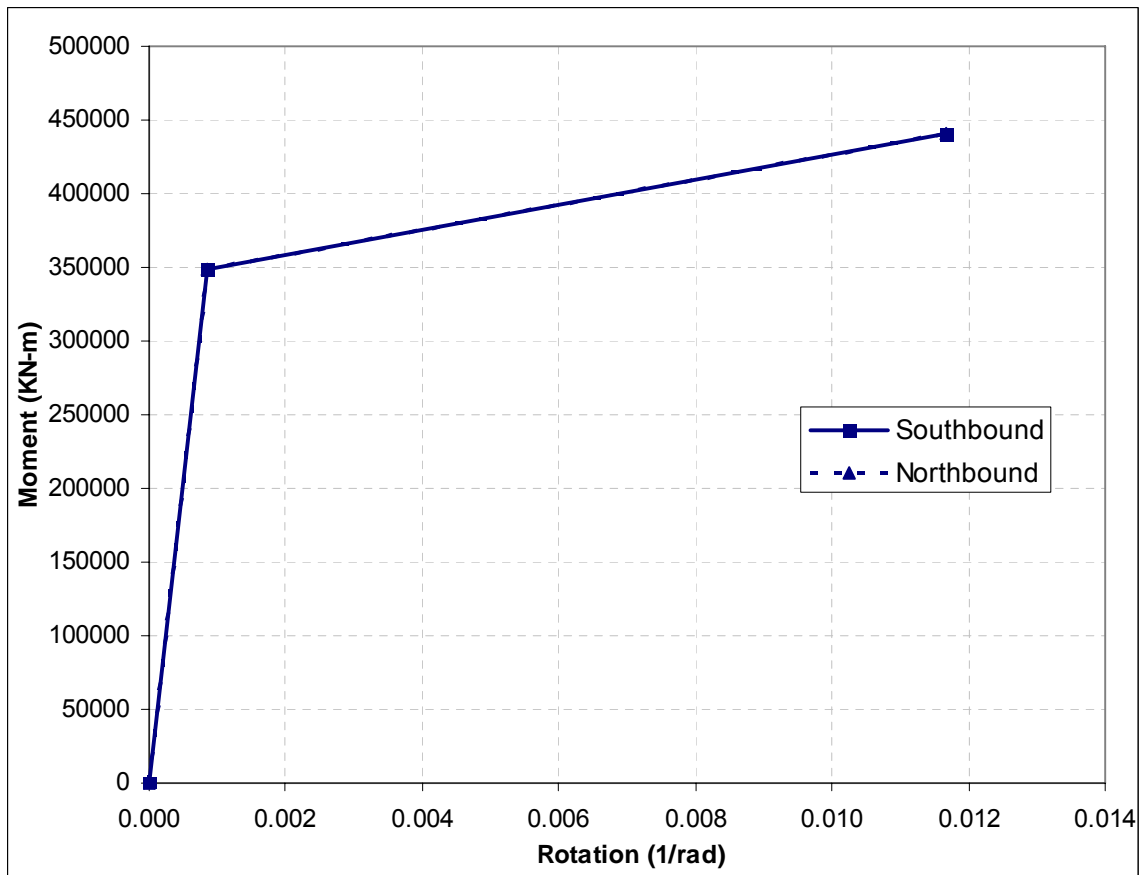
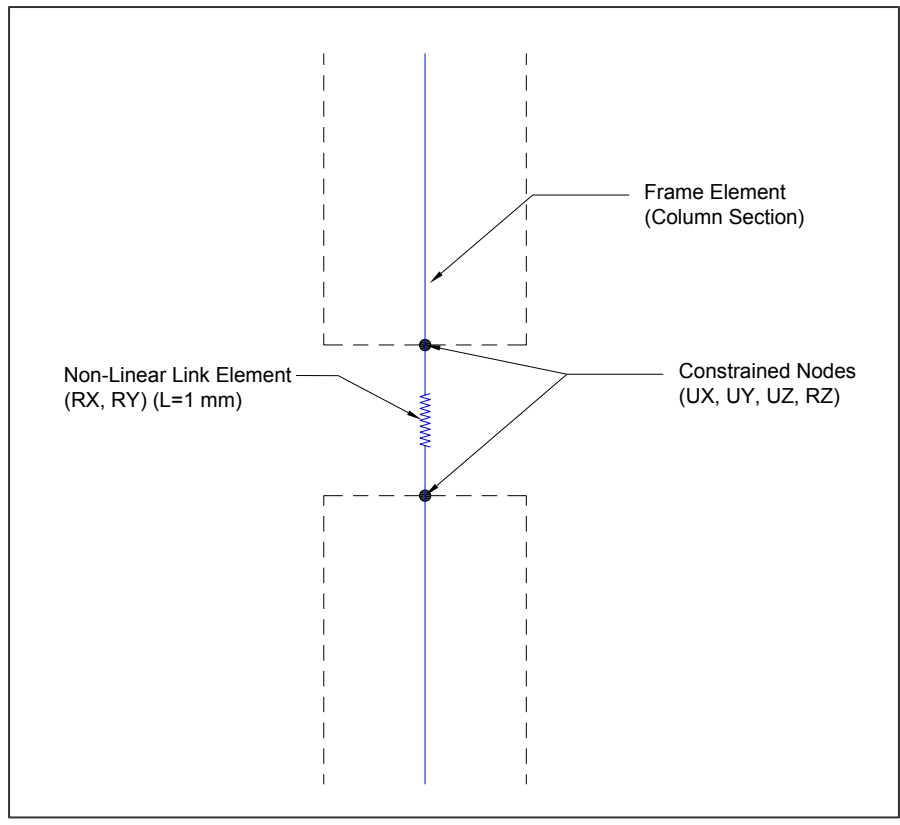
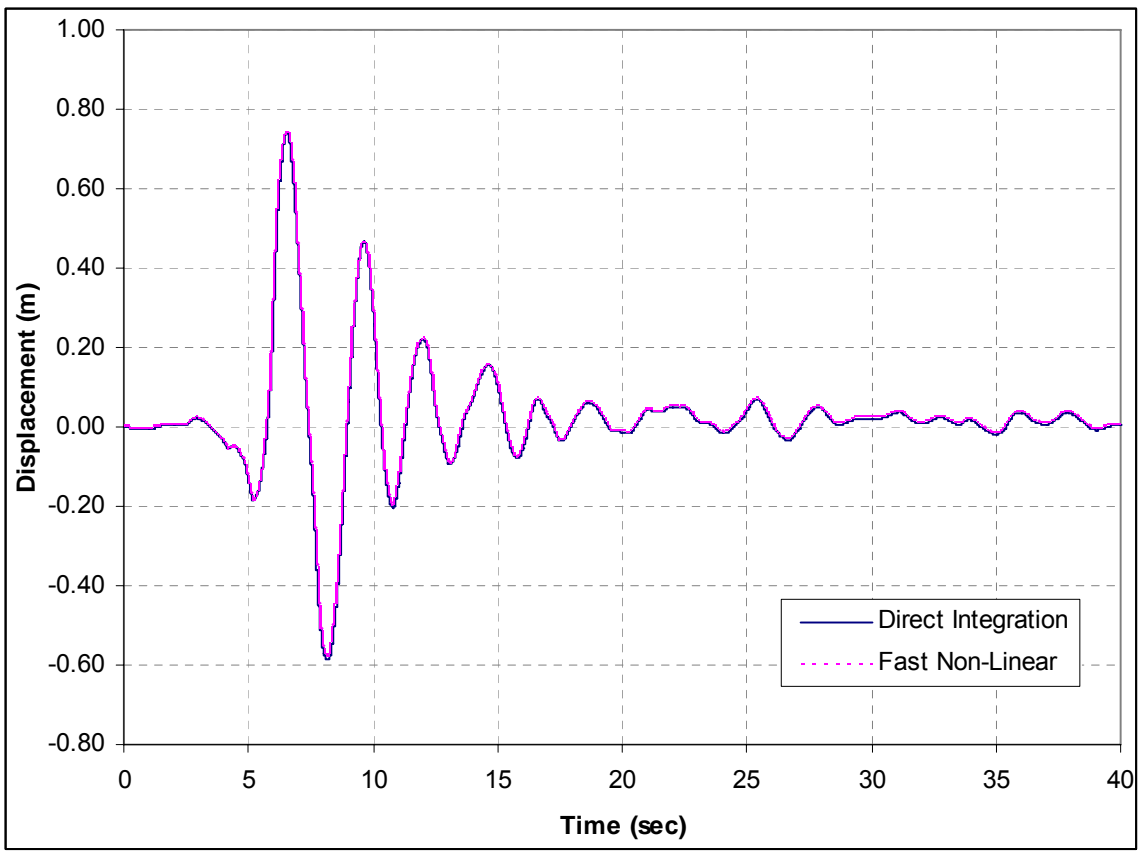


Figure 4-49: Moment-Rotation Response, Arch Segment 0&0A, Y-Axis Bending



**Figure 4-50: Flexural Hinge Modeling Diagram**



**Figure 4-51: Arch Transverse Displacement History, 2500-Year Centro 6 Ground Motion**

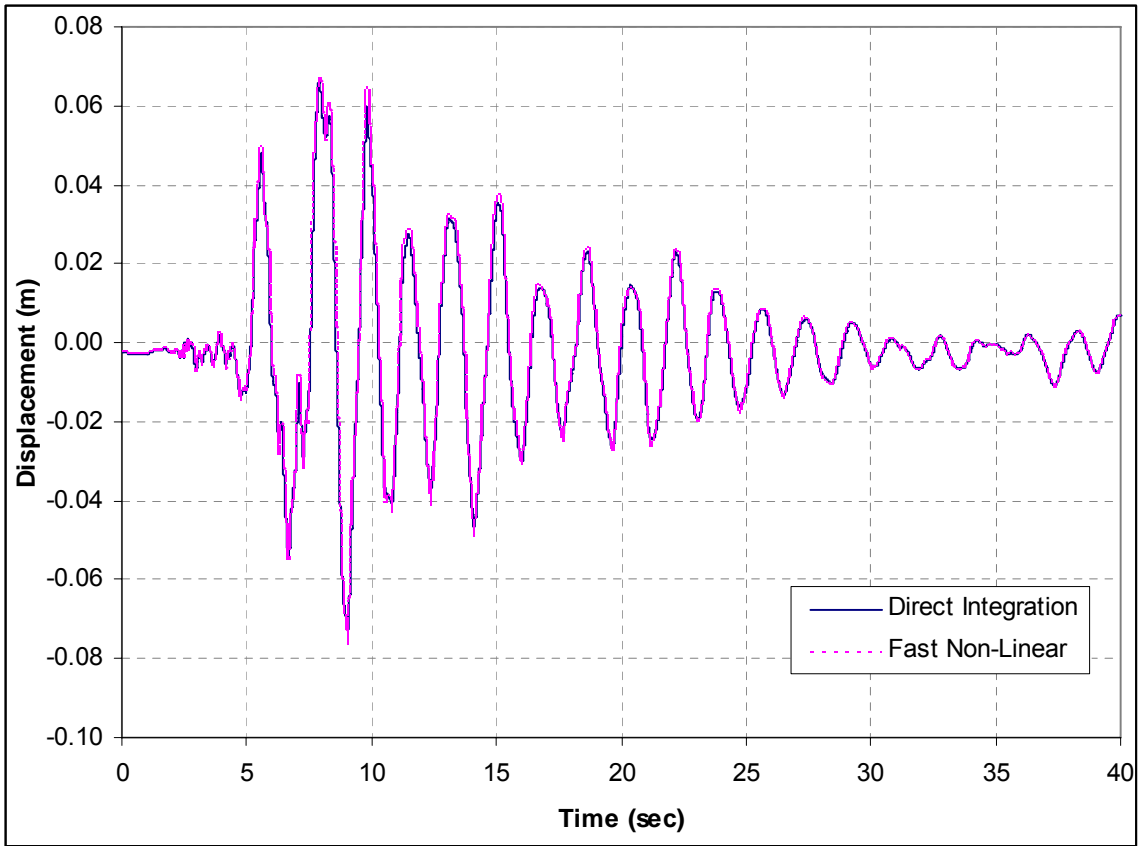


Figure 4-52: Arch Longitudinal Displacement History, 2500-Year Centro 6 Ground Motion

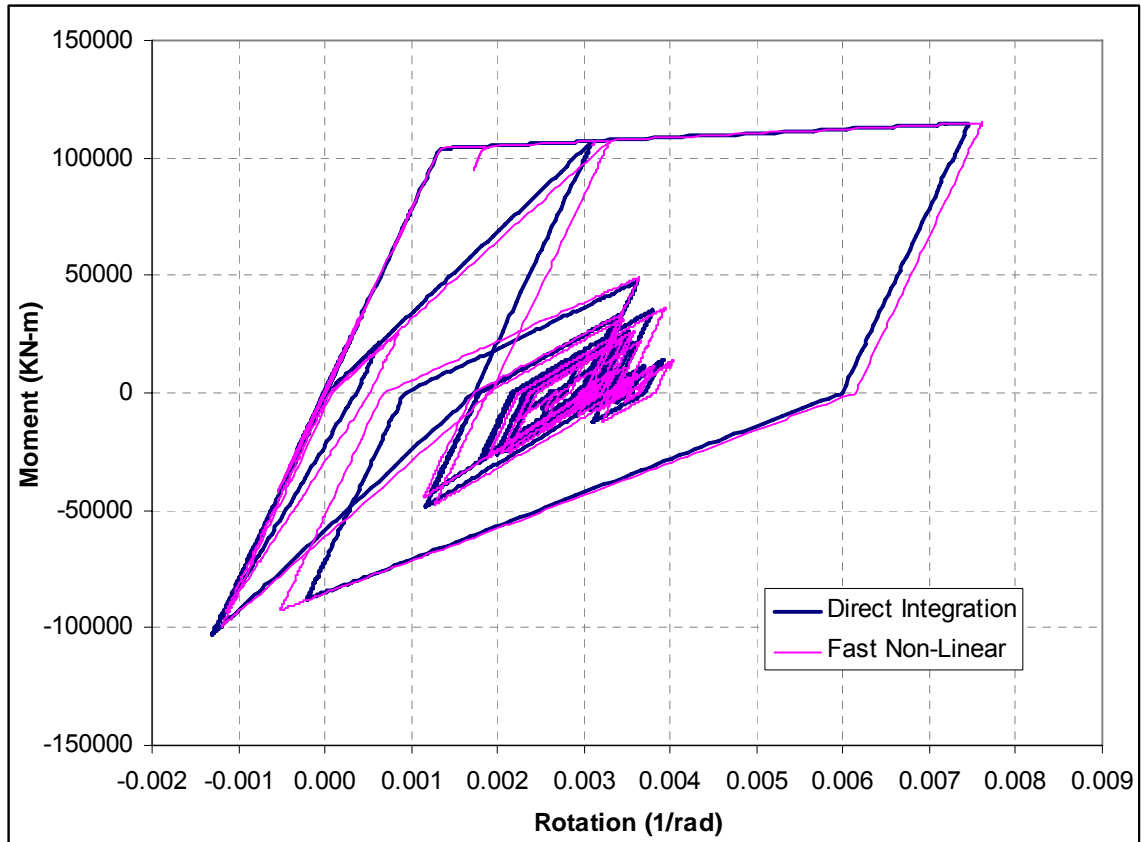
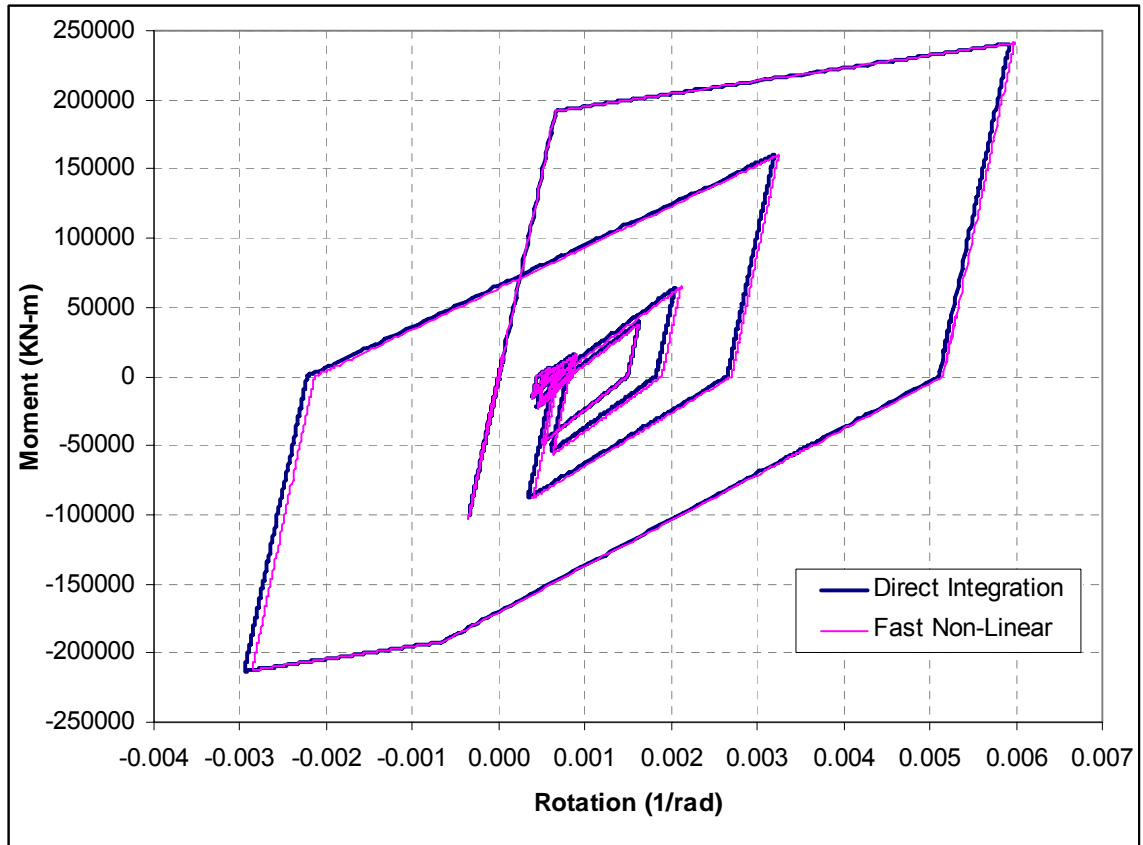


Figure 4-53: Pier 1 NB Longitudinal Moment-Rotation Response, 2500-Year Centro 6 Ground Motion



**Figure 4-54: Pier 1 NB Transverse Moment-Rotation Response, 2500-Year Centro 6 Ground Motion**

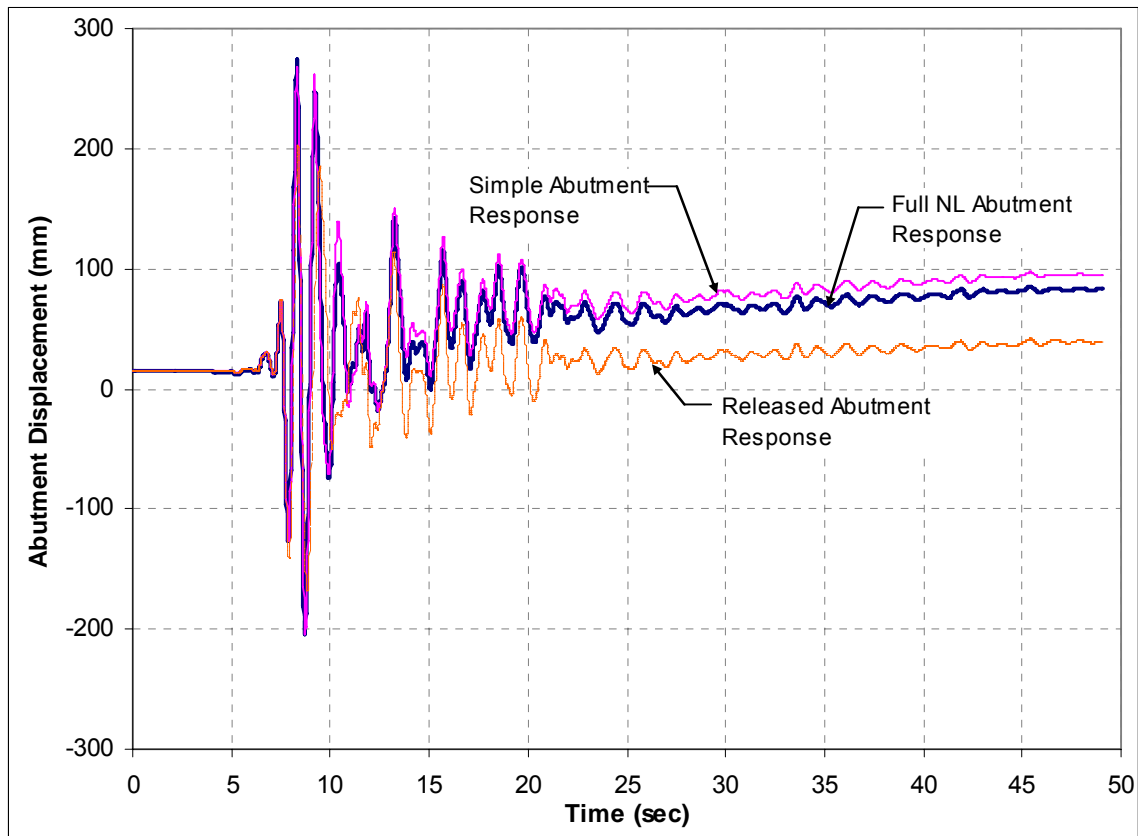


Figure 5-1: Longitudinal Abutment Response Comparison Frame 1 NB, 2500-Year KJMA Motion

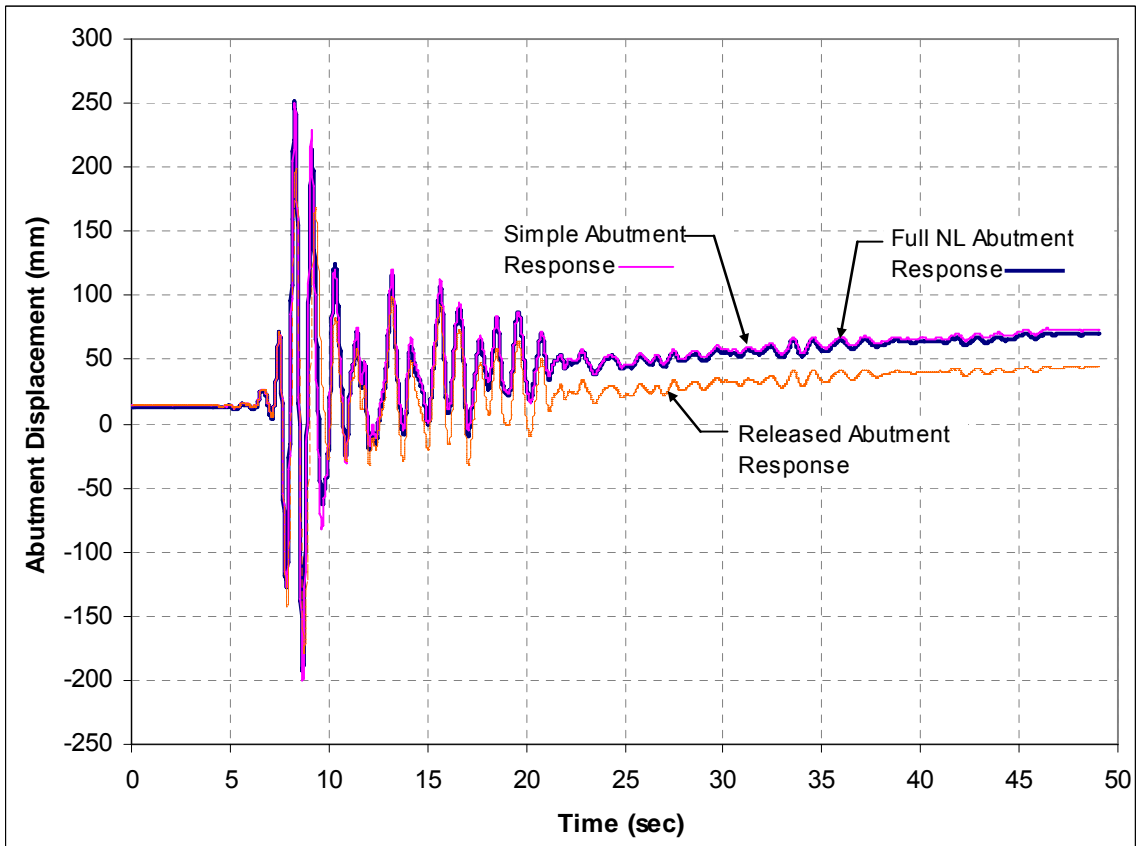


Figure 5-2 Longitudinal Abutment Response Comparison, Frame 1 SB, 2500-Year KJMA Motion

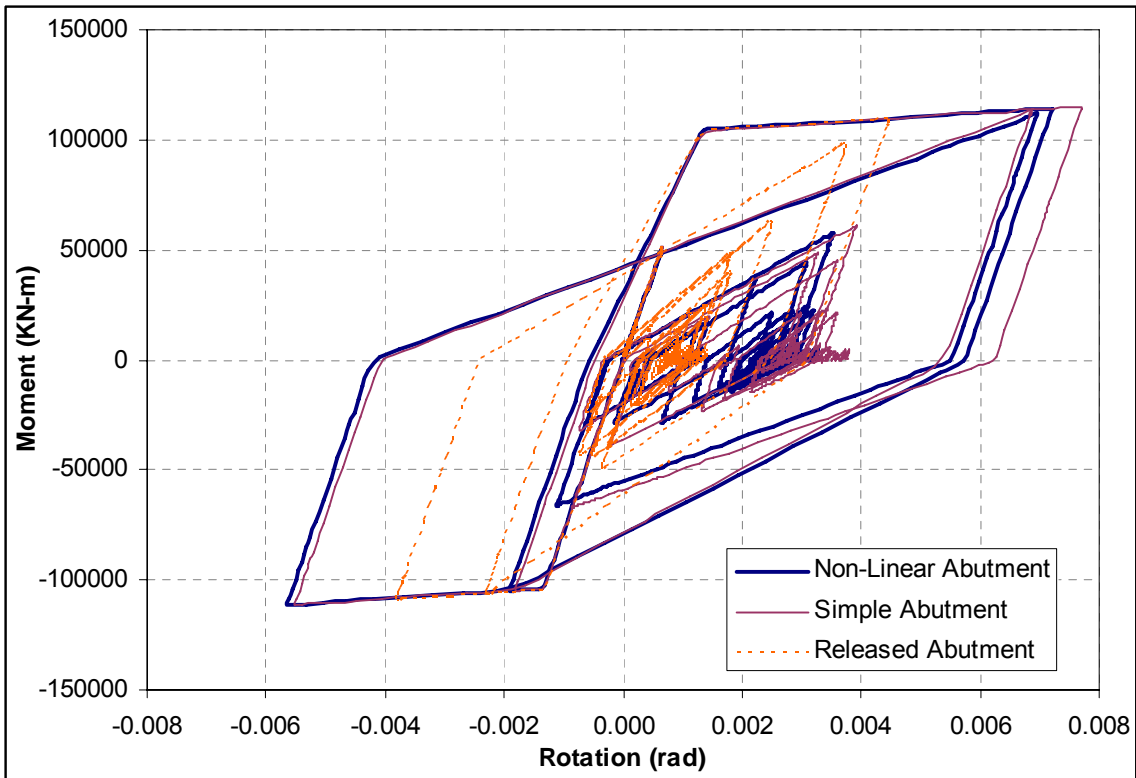


Figure 5-3: Longitudinal Moment-Rotation Response, Pier 1 Northbound, 2500-Year KJMA Motion

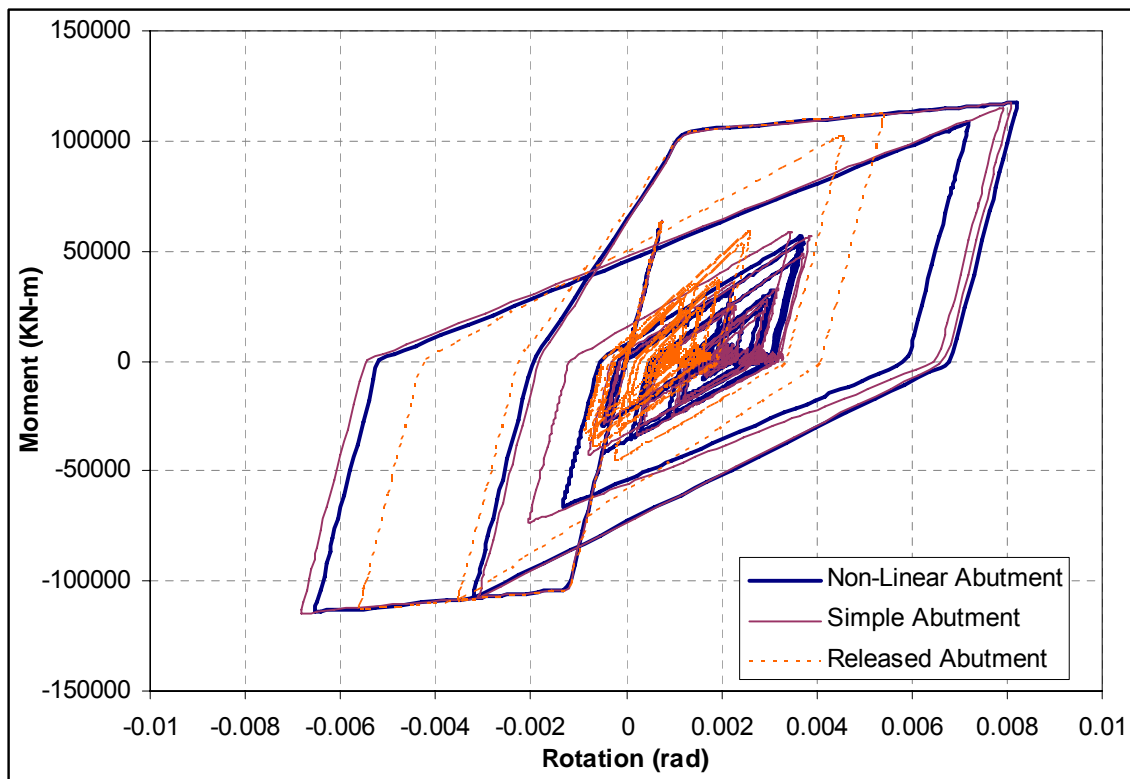


Figure 5-4: Longitudinal Moment-Rotation Response, Pier 1 Southbound, 2500-Year KJMA Motion

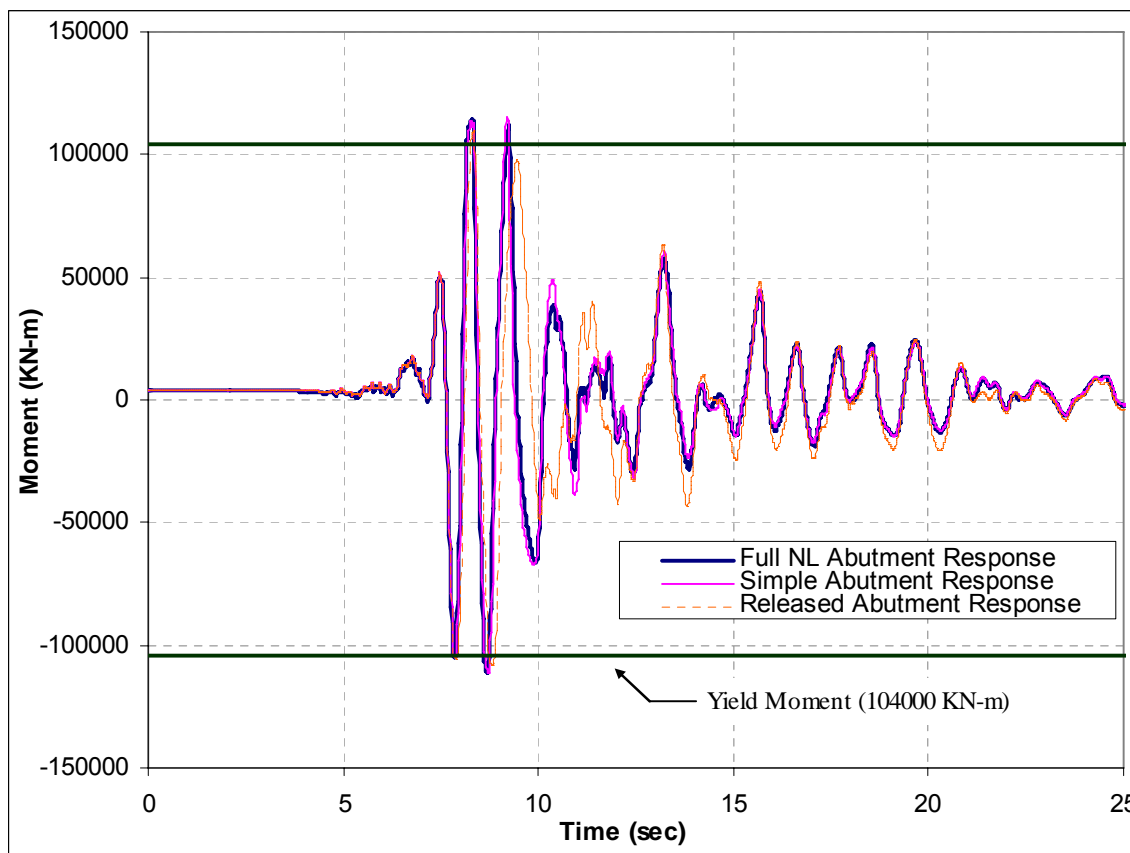


Figure 5-5: Moment Time History, Pier 1 Northbound, 2500-Year KJMA Motion

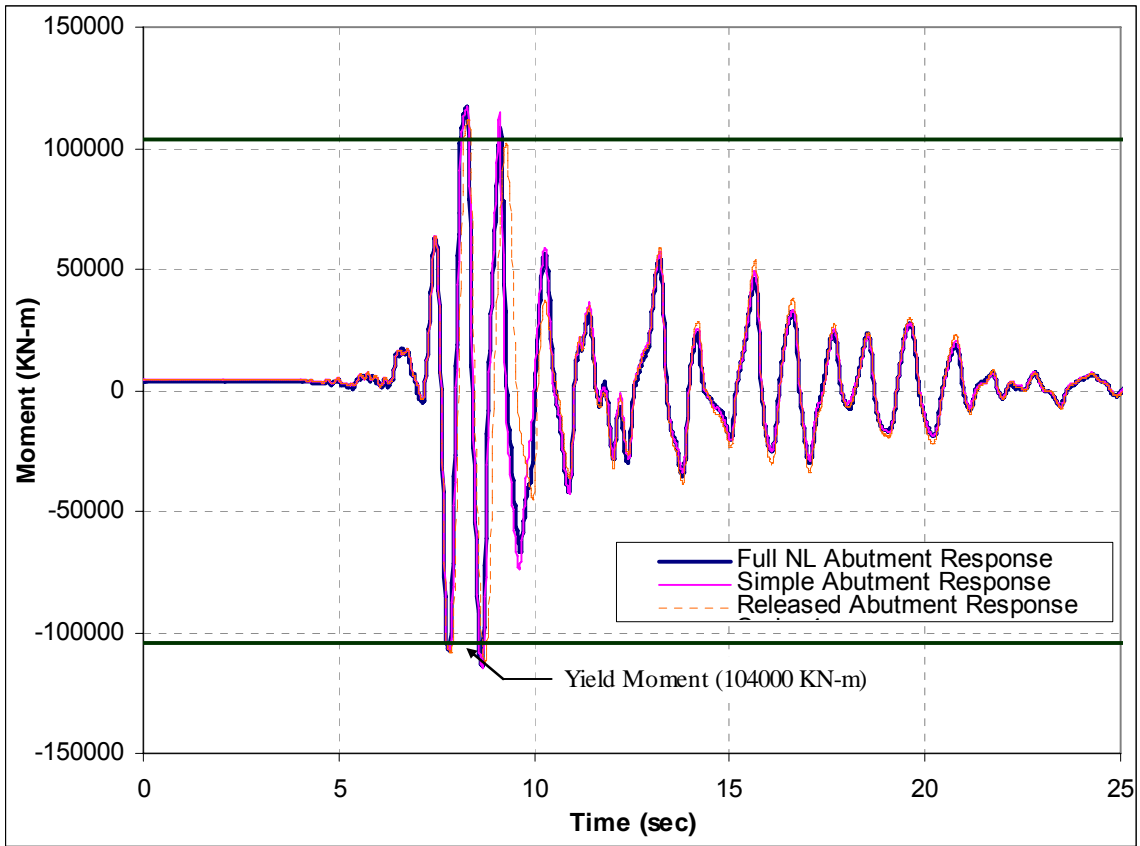


Figure 5-6: Moment Time History, Pier 1 Southbound, 2500-Year KJMA Motion

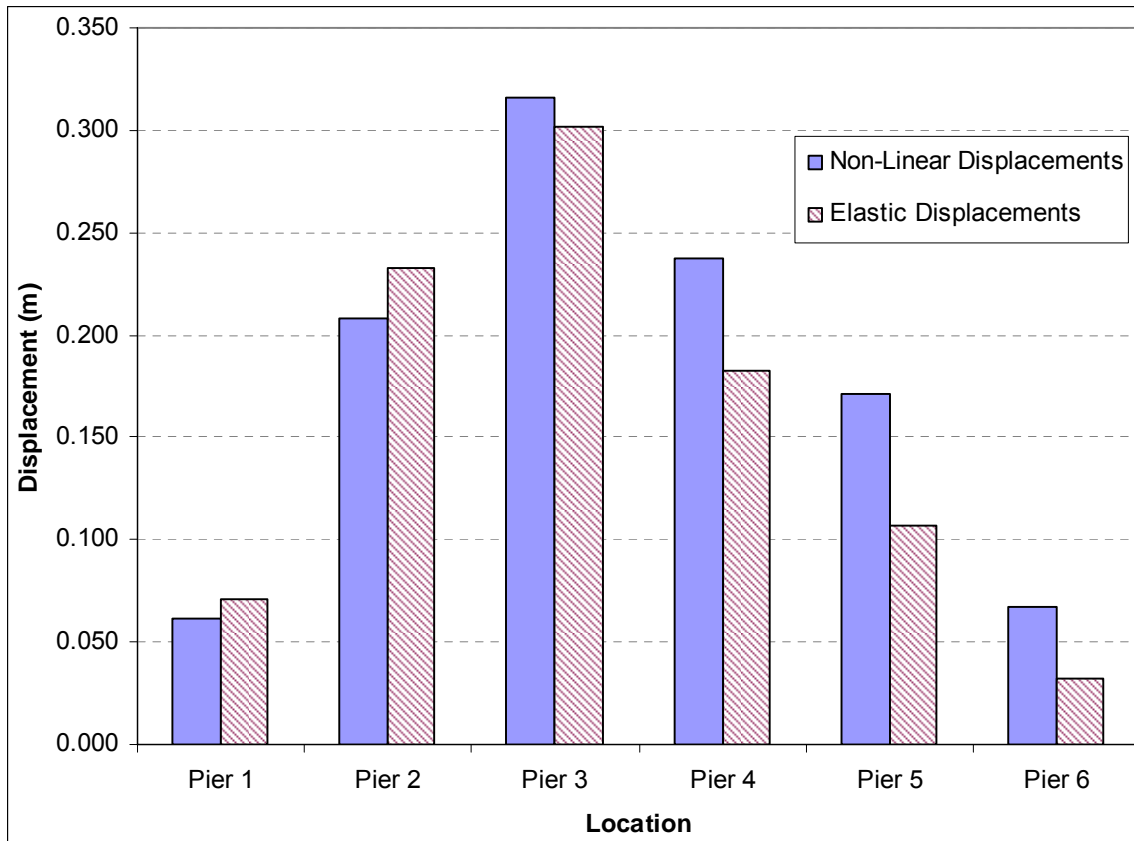


Figure 5-7: Transverse Displacement Comparison, Northbound Structure, 475-Year Earthquake

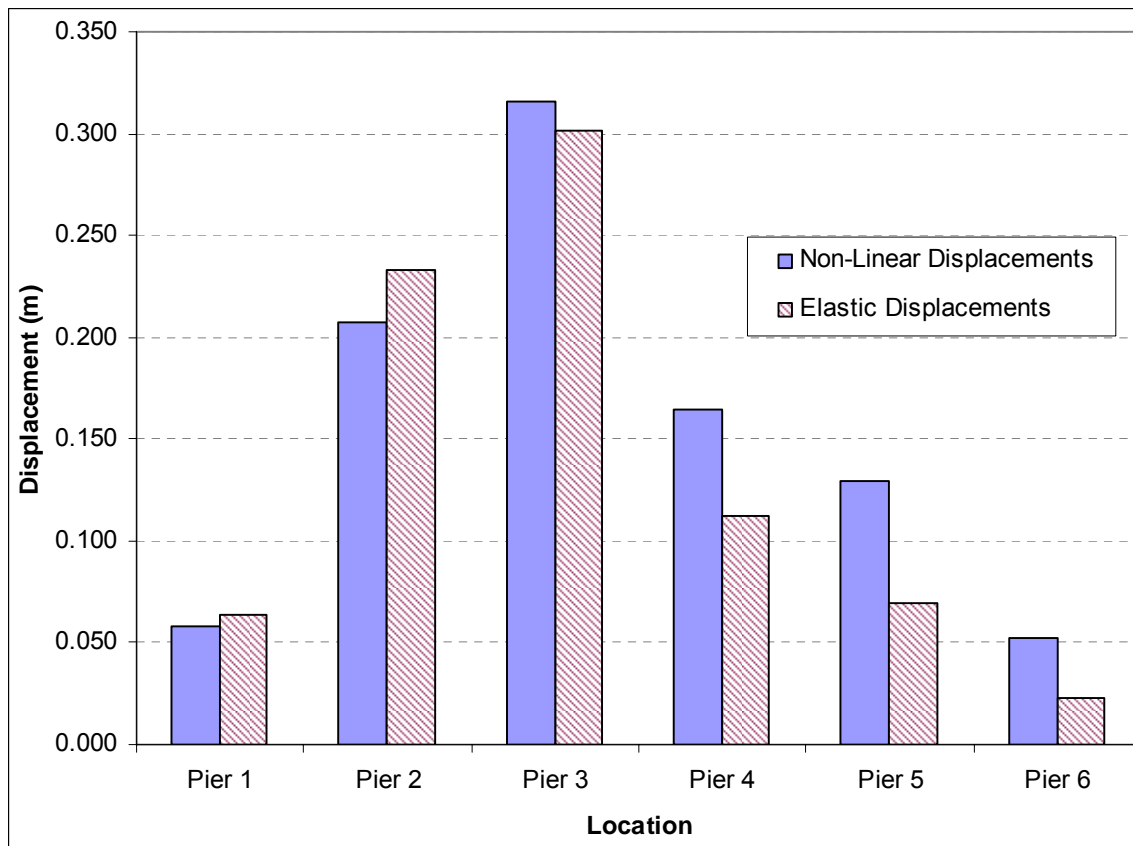
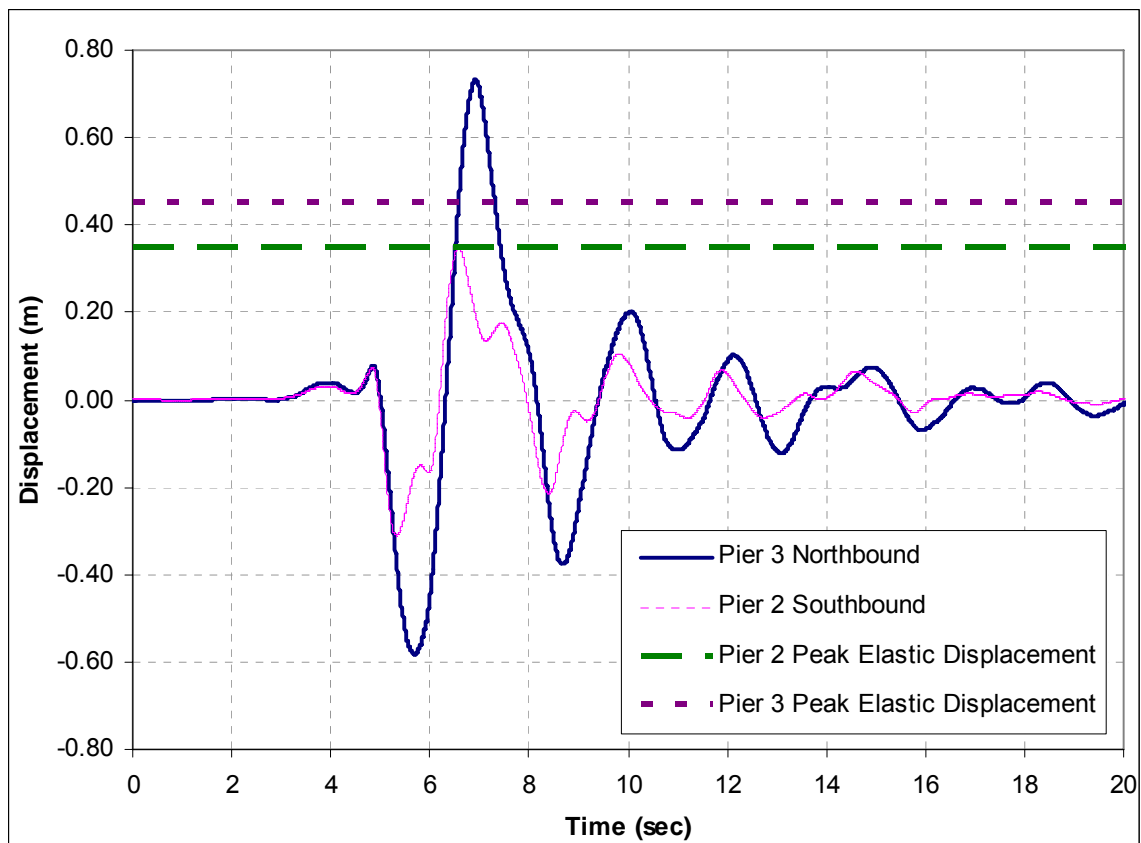


Figure 5-8: Transverse Displacement Comparison, Southbound Structure, 475-Year Earthquake



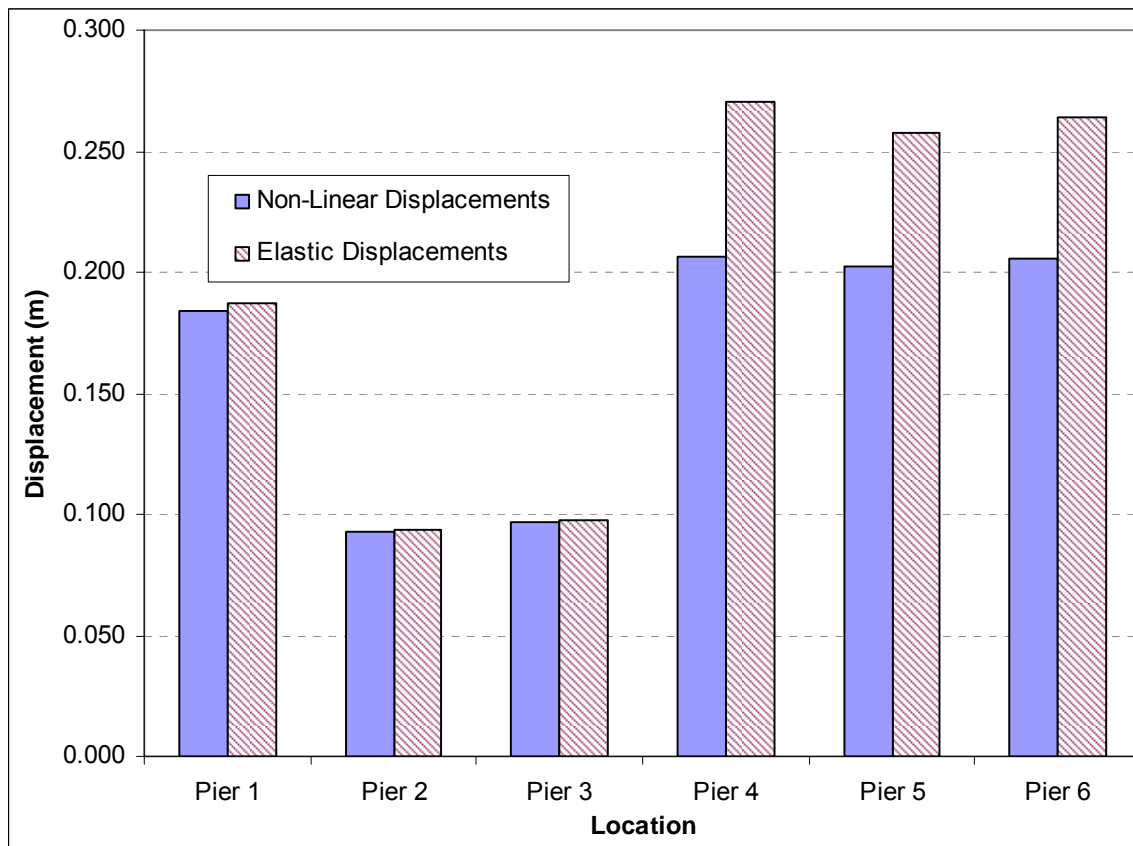


Figure 5-10: Longitudinal Displacement Comparison, Northbound Structure, 475-Year Earthquake

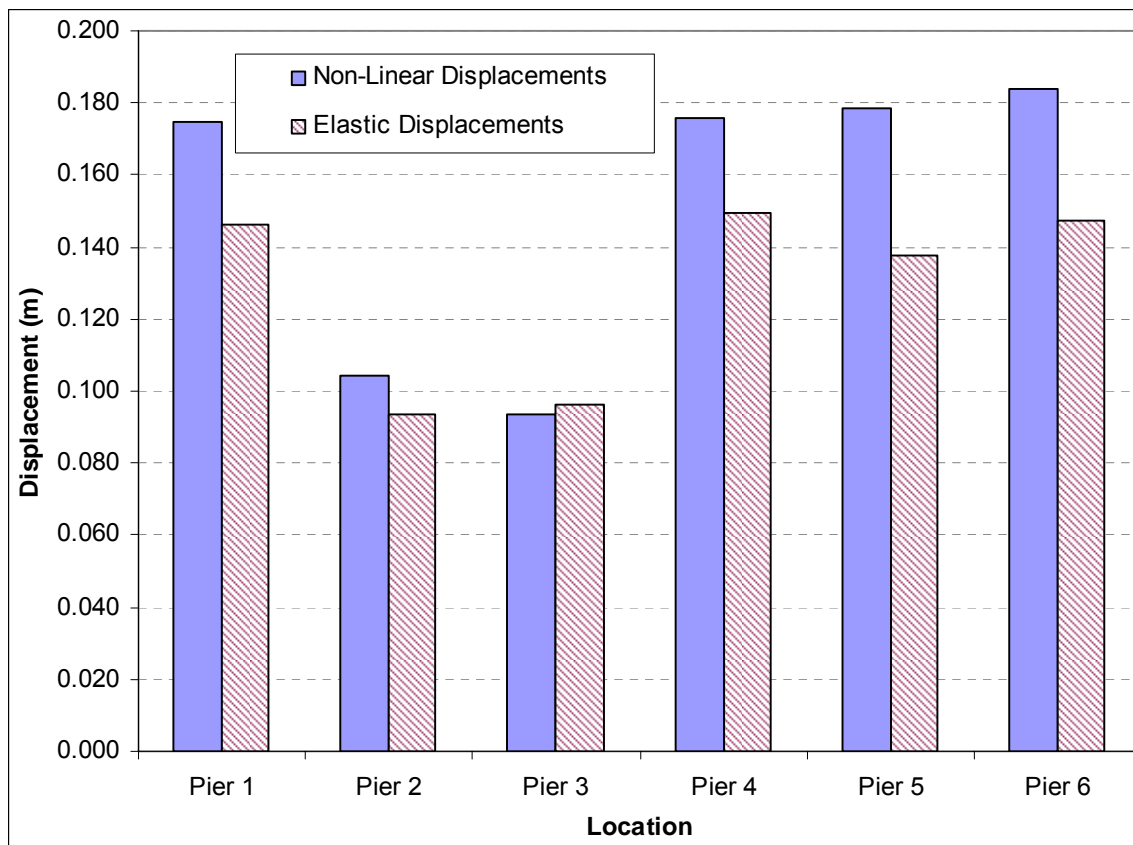


Figure 5-11: Longitudinal Displacement Comparison, Southbound Structure (475-Year Earthquake)

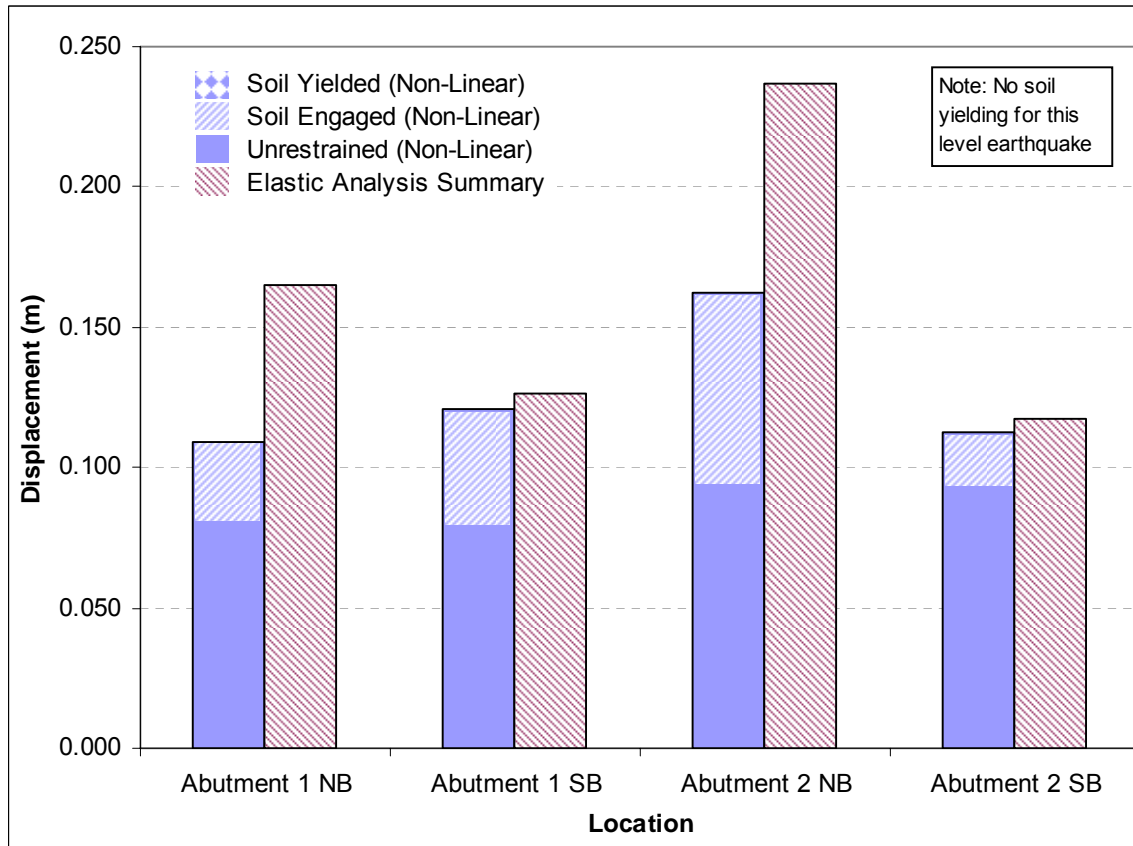


Figure 5-12: Abutment Displacement Comparison (Towards Back-wall), 475-Year Earthquake

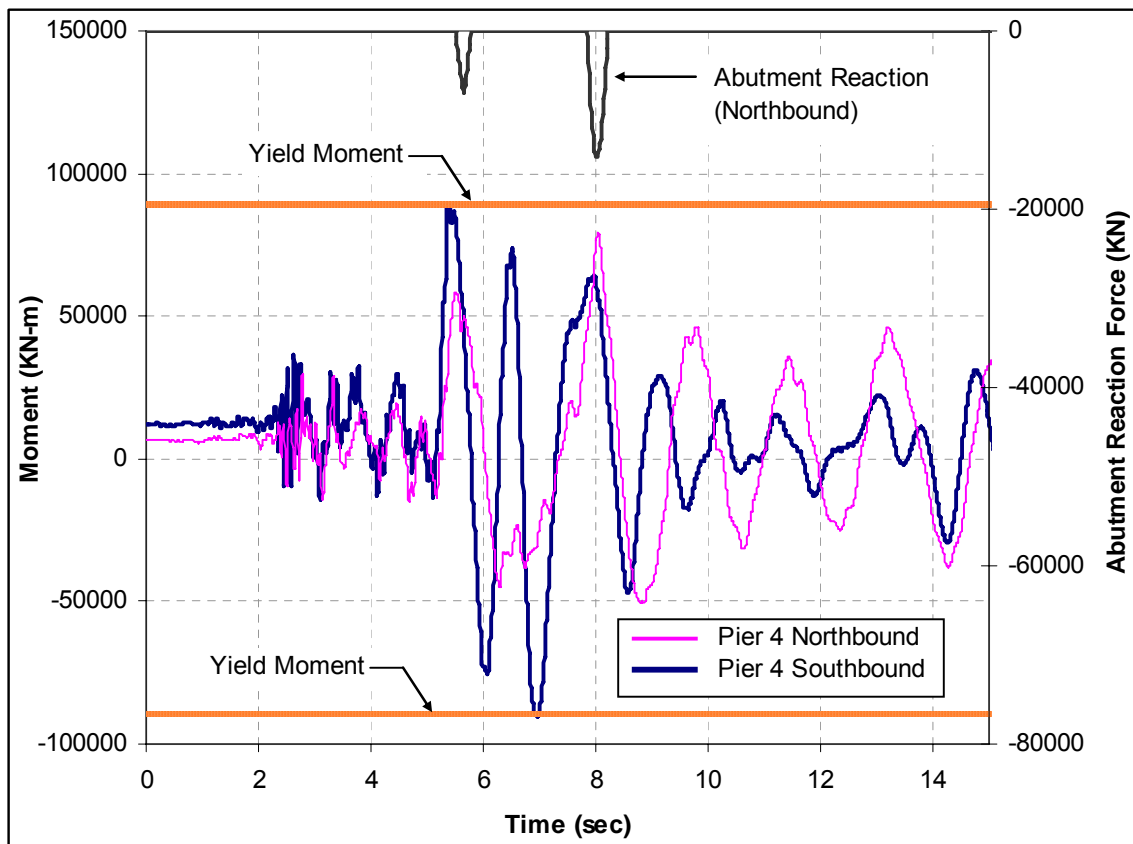


Figure 5-13: Moment Time History (Piers 4 & 5) vs. Abutment Reaction, 475-Year Centro 6 Ground Motion

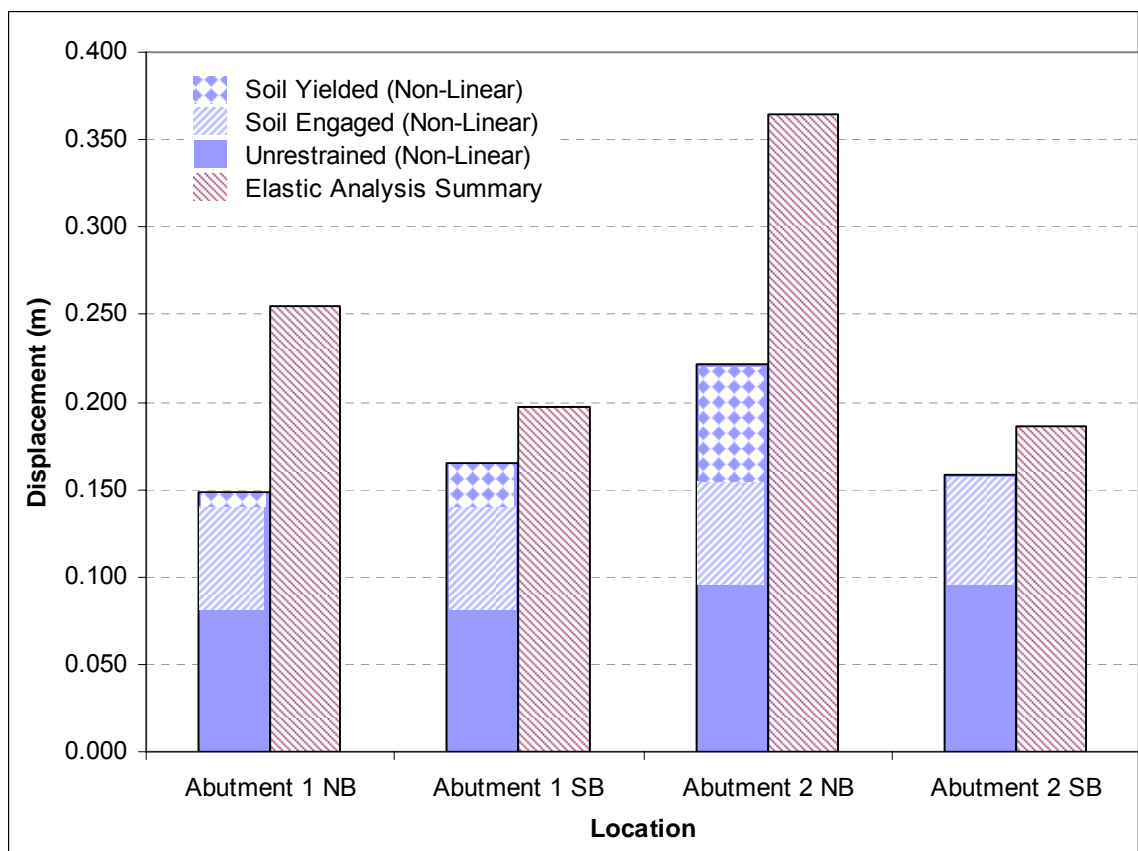


Figure 5-14: Abutment Displacement Comparison (Towards Back-wall), 2500-Year Earthquake

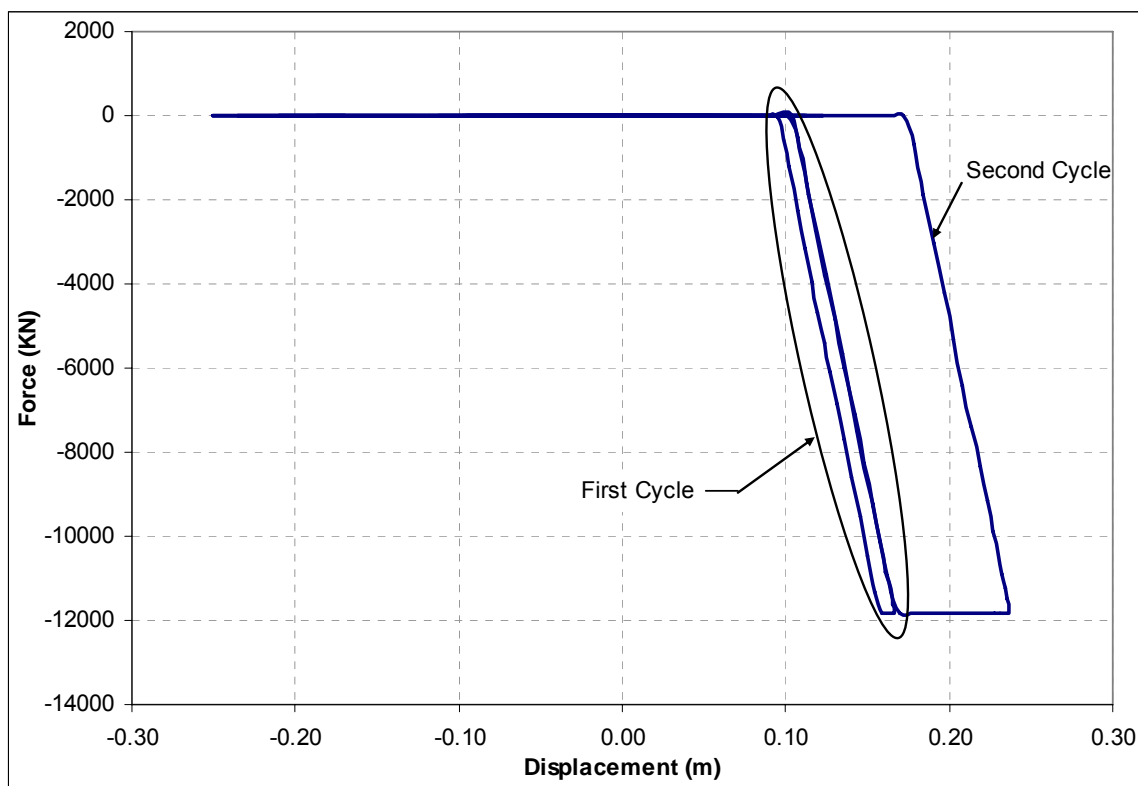


Figure 5-15: Abutment 2 NB Hysteresis Response, 2500-Year Centro 6 Ground Motion

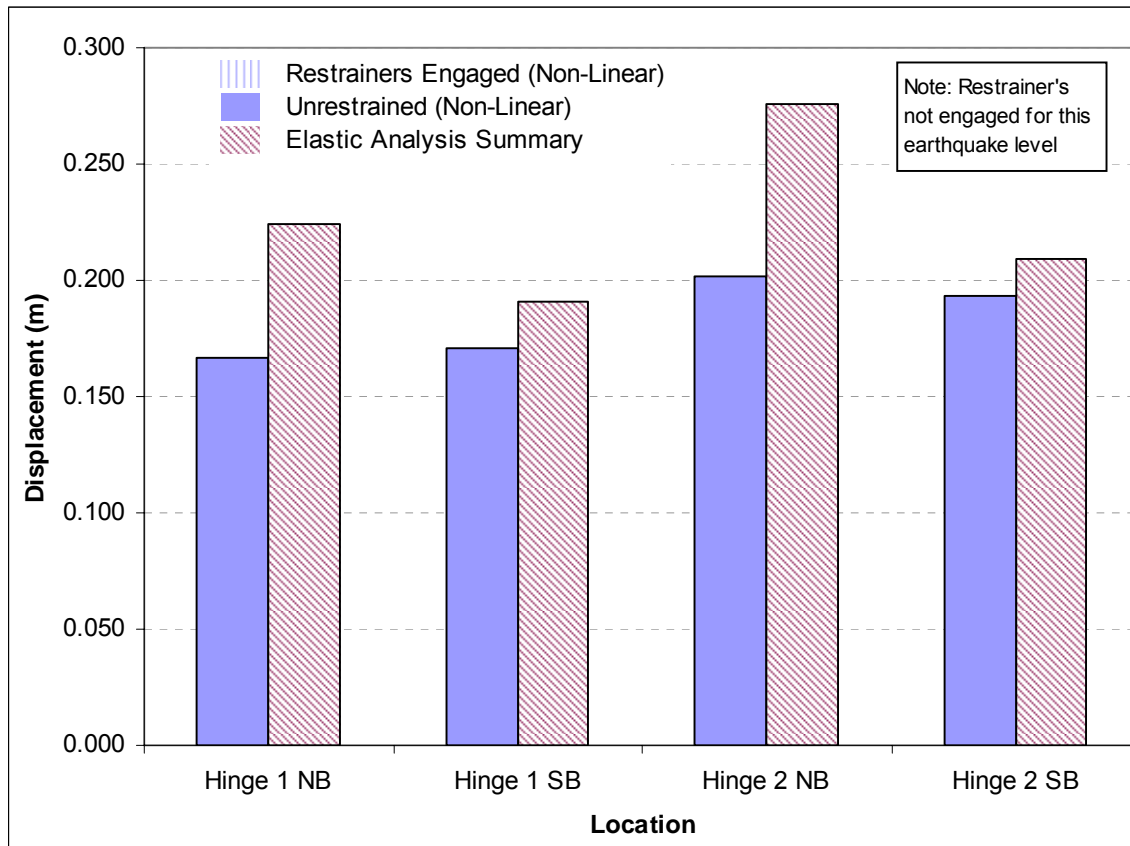


Figure 5-16: Relative Hinge Displacement Comparison (Away), 475-Year Earthquake

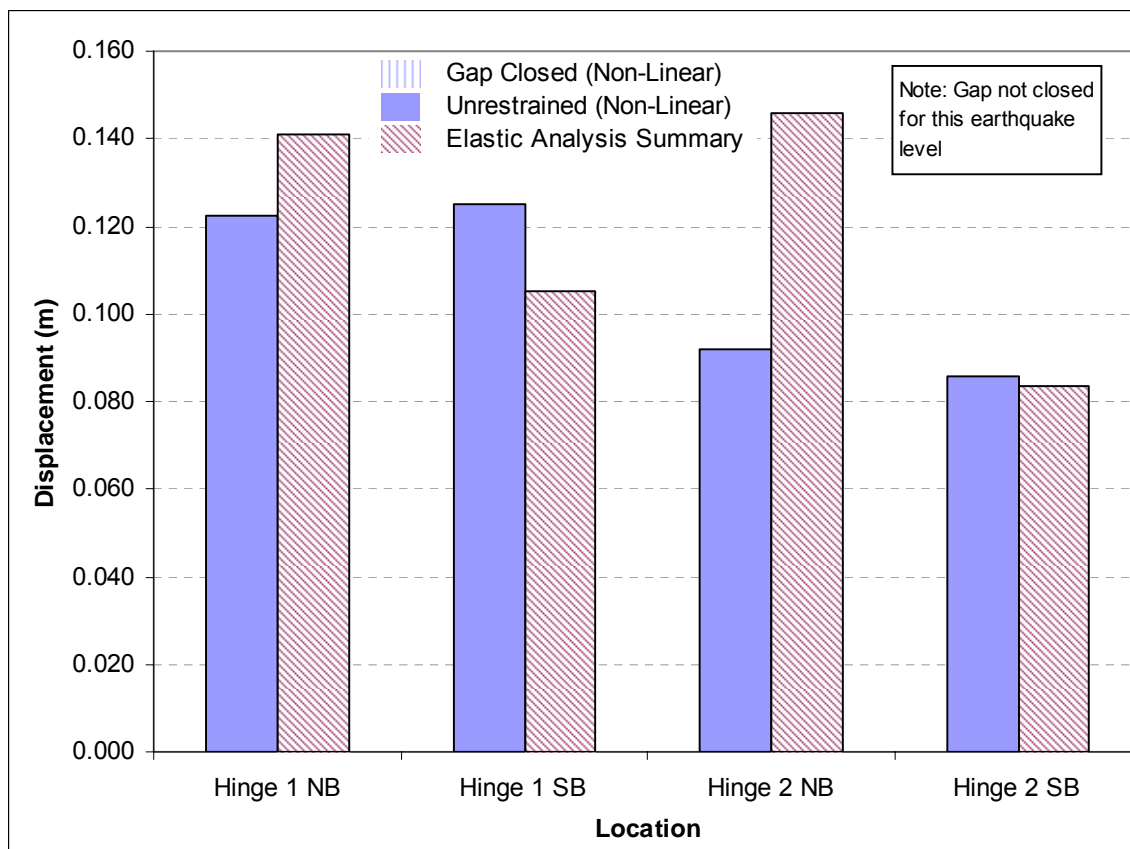


Figure 5-17: Relative Hinge Displacement Comparison (Towards), 475-Year Earthquake

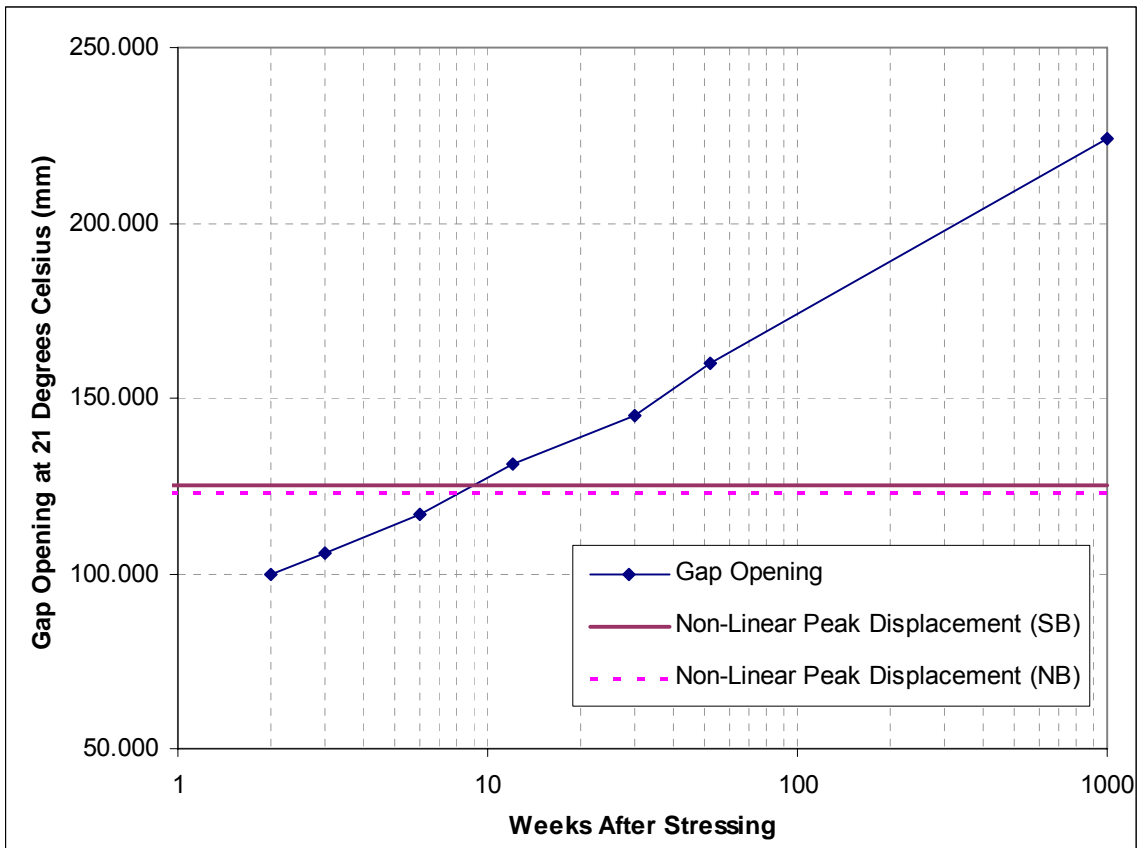


Figure 5-18: Peak Non-Linear Displacements vs. Gap Opening Over Time, Hinge 1

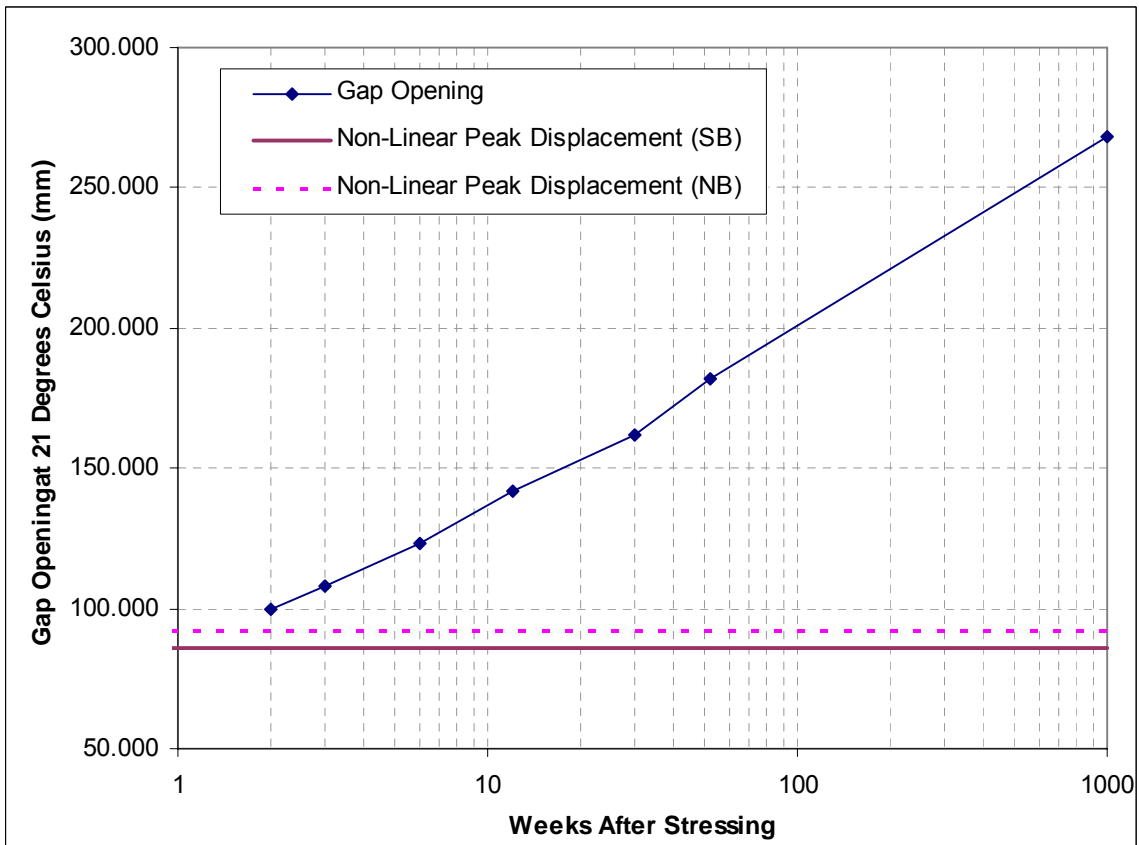


Figure 5-19: Peak Non-Linear Displacements vs. Gap Opening Over Time, Hinge 2

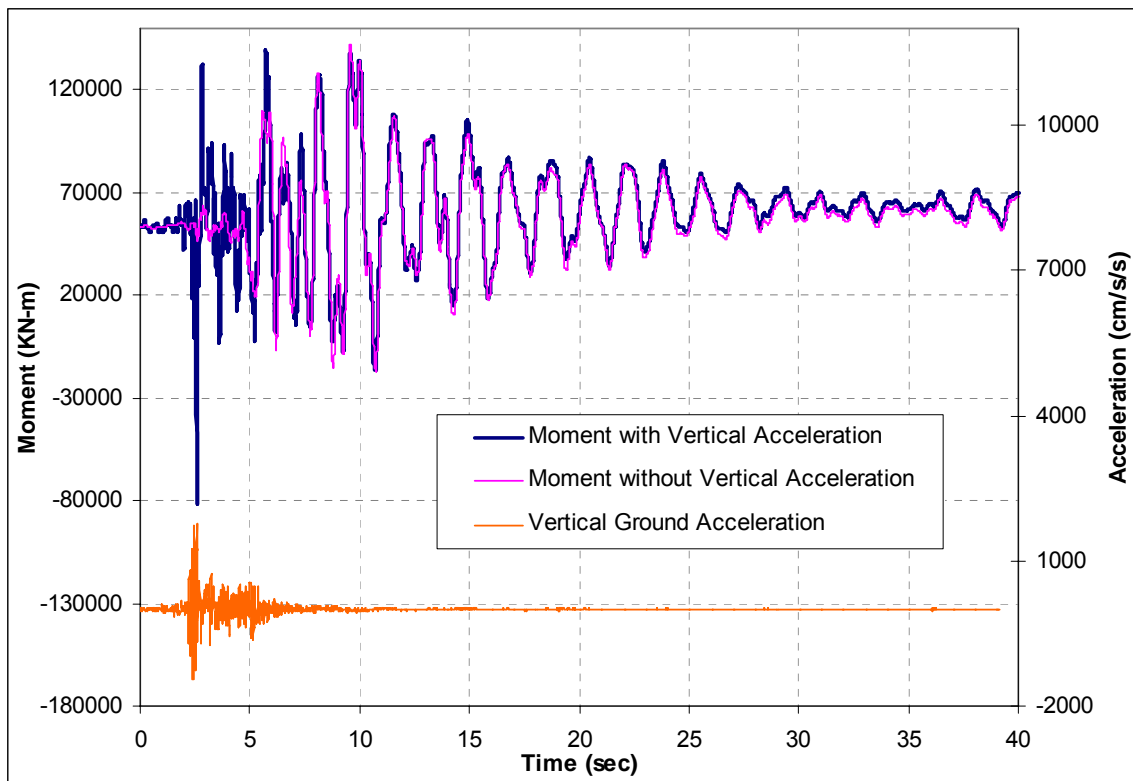


Figure 5-20: Moment Time History for Crown 2 SB, Comparing Effect of Vertical Acceleration

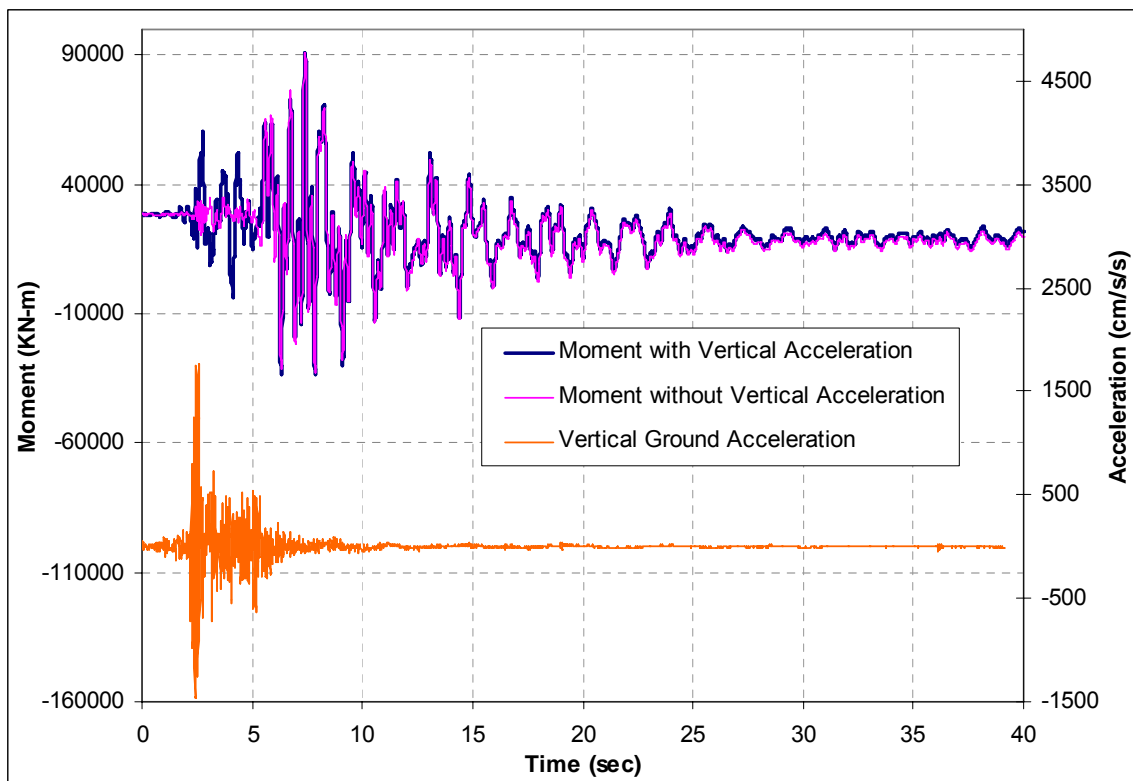


Figure 5-21: Moment Time History, Pier 3 Top SB, Comparing Effect of Vertical Acceleration

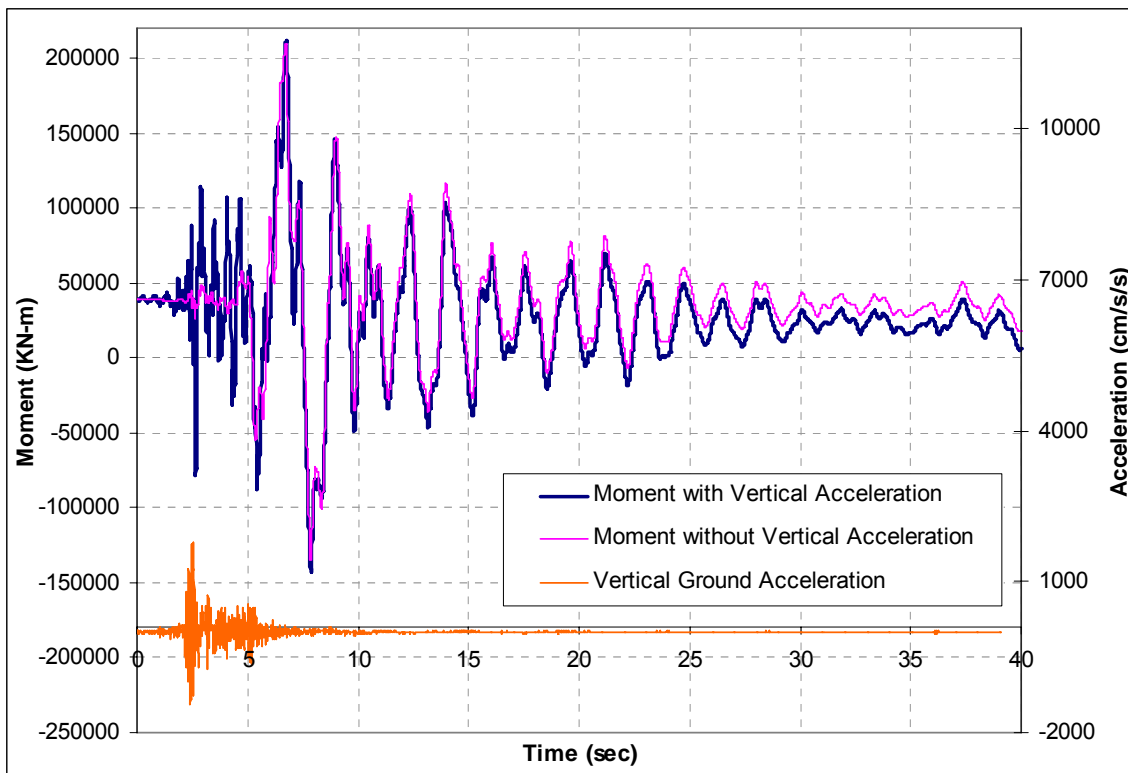


Figure 5-22: Moment Time History, Arch Segment 0 SB, Comparing Effect of Vertical Acceleration

## LIST OF CCEER PUBLICATIONS

Report No.	Publication
CCEER-84-1	Saiidi, M., and R. Lawver, "User's Manual for LZAK-C64, A Computer Program to Implement the Q-Model on Commodore 64," Civil Engineering Department, Report No. CCEER-84-1, University of Nevada, Reno, January 1984.
CCEER-84-1 Reprint	Douglas, B., Norris, G., Saiidi, M., Dodd, L., Richardson, J. and Reid, W., "Simple Bridge Models for Earthquakes and Test Data," Civil Engineering Department, Report No. CCEER-84-1 Reprint, University of Nevada, Reno, January 1984.
CCEER-84-2	Douglas, B. and T. Iwasaki, "Proceedings of the First USA-Japan Bridge Engineering Workshop," held at the Public Works Research Institute, Tsukuba, Japan, Civil Engineering Department, Report No. CCEER-84-2, University of Nevada, Reno, April 1984.
CCEER-84-3	Saiidi, M., J. Hart, and B. Douglas, "Inelastic Static and Dynamic Analysis of Short R/C Bridges Subjected to Lateral Loads," Civil Engineering Department, Report No. CCEER-84-3, University of Nevada, Reno, July 1984.
CCEER-84-4	Douglas, B., "A Proposed Plan for a National Bridge Engineering Laboratory," Civil Engineering Department, Report No. CCEER-84-4, University of Nevada, Reno, December 1984.
CCEER-85-1	Norris, G. and P. Abdollaholiae, "Laterally Loaded Pile Response: Studies with the Strain Wedge Model," Civil Engineering Department, Report No. CCEER-85-1, University of Nevada, Reno, April 1985.
CCEER-86-1	Ghusn, G. and M. Saiidi, "A Simple Hysteretic Element for Biaxial Bending of R/C in NEABS-86," Civil Engineering Department, Report No. CCEER-86-1, University of Nevada, Reno, July 1986.
CCEER-86-2	Saiidi, M., R. Lawver, and J. Hart, "User's Manual of ISADAB and SIBA, Computer Programs for Nonlinear Transverse Analysis of Highway Bridges Subjected to Static and Dynamic Lateral Loads," Civil Engineering Department, Report No. CCEER-86-2, University of Nevada, Reno, September 1986.
CCEER-87-1	Siddharthan, R., "Dynamic Effective Stress Response of Surface and Embedded Footings in Sand," Civil engineering Department, Report No. CCEER-86-2, University of Nevada, Reno, June 1987.
CCEER-87-2	Norris, G. and R. Sack, "Lateral and Rotational Stiffness of Pile Groups for Seismic Analysis of Highway Bridges," Civil Engineering Department, Report No. CCEER-87-2, University of Nevada, Reno, June 1987.
CCEER-88-1	Orie, J. and M. Saiidi, "A Preliminary Study of One-Way Reinforced Concrete Pier Hinges Subjected to Shear and Flexure," Civil Engineering Department, Report No. CCEER-88-1, University of Nevada, Reno, January 1988.
CCEER-88-2	Orie, D., M. Saiidi, and B. Douglas, "A Micro-CAD System for Seismic Design of Regular Highway Bridges," Civil Engineering Department, Report No. CCEER-88-2, University of Nevada, Reno, June 1988.

- CCEER-88-3 Orie, D. and M. Saiidi, "User's Manual for Micro-SARB, a Microcomputer Program for Seismic Analysis of Regular Highway Bridges," Civil Engineering Department, Report No. CCEER-88-3, University of Nevada, Reno, October 1988.
- CCEER-89-1 Douglas, B., M. Saiidi, R. Hayes, and G. Holcomb, "A Comprehensive Study of the Loads and Pressures Exerted on Wall Forms by the Placement of Concrete," Civil Engineering Department, Report No. CCEER-89-1, University of Nevada, Reno, February 1989.
- CCEER-89-2 Richardson, J. and B. Douglas, "Dynamic Response Analysis of the Dominion Road Bridge Test Data," Civil Engineering Department, Report No. CCEER-89-2, University of Nevada, Reno, March 1989.
- CCEER-89-2 Vrontinos, S., M. Saiidi, and B. Douglas, "A Simple Model to Predict the Ultimate Response of R/C Beams with Concrete Overlays," Civil Engineering Department, Report NO. CCEER-89-2, University of Nevada, Reno, June 1989.
- CCEER-89-3 Ebrahimpour, A. and P. Jagadish, "Statistical Modeling of Bridge Traffic Loads - A Case Study," Civil Engineering Department, Report No. CCEER-89-3, University of Nevada, Reno, December 1989.
- CCEER-89-4 Shields, J. and M. Saiidi, "Direct Field Measurement of Prestress Losses in Box Girder Bridges," Civil Engineering Department, Report No. CCEER-89-4, University of Nevada, Reno, December 1989.
- CCEER-90-1 Saiidi, M., E. Maragakis, G. Ghosn, Y. Jiang, and D. Schwartz, "Survey and Evaluation of Nevada's Transportation Infrastructure, Task 7.2 - Highway Bridges, Final Report," Civil Engineering Department, Report No. CCEER 90-1, University of Nevada, Reno, October 1990.
- CCEER-90-2 Abdel-Ghaffar, S., E. Maragakis, and M. Saiidi, "Analysis of the Response of Reinforced Concrete Structures During the Whittier Earthquake 1987," Civil Engineering Department, Report No. CCEER 90-2, University of Nevada, Reno, October 1990.
- CCEER-91-1 Saiidi, M., E. Hwang, E. Maragakis, and B. Douglas, "Dynamic Testing and the Analysis of the Flamingo Road Interchange," Civil Engineering Department, Report No. CCEER-91-1, University of Nevada, Reno, February 1991.
- CCEER-91-2 Norris, G., R. Siddharthan, Z. Zafir, S. Abdel-Ghaffar, and P. Gowda, "Soil-Foundation-Structure Behavior at the Oakland Outer Harbor Wharf," Civil Engineering Department, Report No. CCEER-91-2, University of Nevada, Reno, July 1991.
- CCEER-91-3 Norris, G., "Seismic Lateral and Rotational Pile Foundation Stiffnesses at Cypress," Civil Engineering Department, Report No. CCEER-91-3, University of Nevada, Reno, August 1991.
- CCEER-91-4 O'Connor, D. and M. Saiidi, "A Study of Protective Overlays for Highway Bridge Decks in Nevada, with Emphasis on Polyester-Styrene Polymer Concrete," Civil Engineering Department, Report No. CCEER-91-4, University of Nevada, Reno, October 1991.
- CCEER-91-5 O'Connor, D.N. and M. Saiidi, "Laboratory Studies of Polyester-Styrene Polymer Concrete Engineering Properties," Civil Engineering Department, Report No. CCEER-91-5, University of Nevada, Reno, November 1991.

- CCEER-92-1 Straw, D.L. and M. Saiidi, "Scale Model Testing of One-Way Reinforced Concrete Pier Hinges Subject to Combined Axial Force, Shear and Flexure," edited by D.N. O'Connor, Civil Engineering Department, Report No. CCEER-92-1, University of Nevada, Reno, March 1992.
- CCEER-92-2 Wehbe, N., M. Saiidi, and F. Gordaninejad, "Basic Behavior of Composite Sections Made of Concrete Slabs and Graphite Epoxy Beams," Civil Engineering Department, Report No. CCEER-92-2, University of Nevada, Reno, August 1992.
- CCEER-92-3 Saiidi, M. and E. Hutchens, "A Study of Prestress Changes in A Post-Tensioned Bridge During the First 30 Months," Civil Engineering Department, Report No. CCEER-92-3, University of Nevada, Reno, April 1992.
- CCEER-92-4 Saiidi, M., B. Douglas, S. Feng, E. Hwang, and E. Maragakis, "Effects of Axial Force on Frequency of Prestressed Concrete Bridges," Civil Engineering Department, Report No. CCEER-92-4, University of Nevada, Reno, August 1992.
- CCEER-92-5 Siddharthan, R., and Z. Zafir, "Response of Layered Deposits to Traveling Surface Pressure Waves," Civil Engineering Department, Report No. CCEER-92-5, University of Nevada, Reno, September 1992.
- CCEER-92-6 Norris, G., and Z. Zafir, "Liquefaction and Residual Strength of Loose Sands from Drained Triaxial Tests," Civil Engineering Department, Report No. CCEER-92-6, University of Nevada, Reno, September 1992.
- CCEER-92-7 Douglas, B., "Some Thoughts Regarding the Improvement of the University of Nevada, Reno's National Academic Standing," Civil Engineering Department, Report No. CCEER-92-7, University of Nevada, Reno, September 1992.
- CCEER-92-8 Saiidi, M., E. Maragakis, and S. Feng, "An Evaluation of the Current Caltrans Seismic Restrainer Design Method," Civil Engineering Department, Report No. CCEER-92-8, University of Nevada, Reno, October 1992.
- CCEER-92-9 O'Connor, D., M. Saiidi, and E. Maragakis, "Effect of Hinge Restrainers on the Response of the Madrone Drive Undercrossing During the Loma Prieta Earthquake," Civil Engineering Department, Report No. CCEER-92-9, University of Nevada, Reno, February 1993.
- CCEER-92-10 O'Connor, D., and M. Saiidi, "Laboratory Studies of Polyester Concrete: Compressive Strength at Elevated Temperatures and Following Temperature Cycling, Bond Strength to Portland Cement Concrete, and Modulus of Elasticity," Civil Engineering Department, Report No. CCEER-92-10, University of Nevada, Reno, February 1993.
- CCEER-92-11 Wehbe, N., M. Saiidi, and D. O'Connor, "Economic Impact of Passage of Spent Fuel Traffic on Two Bridges in Northeast Nevada," Civil Engineering Department, Report No. CCEER-92-11, University of Nevada, Reno, December 1992.
- CCEER-93-1 Jiang, Y., and M. Saiidi, "Behavior, Design, and Retrofit of Reinforced Concrete One-way Bridge Column Hinges," edited by D. O'Connor, Civil Engineering Department, Report No. CCEER-93-1, University of Nevada, Reno, March 1993.
- CCEER-93-2 Abdel-Ghaffar, S., E. Maragakis, and M. Saiidi, "Evaluation of the Response of the Aptos Creek Bridge During the 1989 Loma Prieta Earthquake," Civil Engineering Department, Report No. CCEER-93-2, University of Nevada, Reno, June 1993.

- CCEER-93-3 Sanders, D.H., B.M. Douglas, and T.L. Martin, "Seismic Retrofit Prioritization of Nevada Bridges," Civil Engineering Department, Report No. CCEER-93-3, University of Nevada, Reno, July 1993.
- CCEER-93-4 Abdel-Ghaffar, S., E. Maragakis, and M. Saiidi, "Performance of Hinge Restrainers in the Huntington Avenue Overhead During the 1989 Loma Prieta Earthquake," Civil Engineering Department, Report No. CCEER-93-4, University of Nevada, Reno, June 1993 (in final preparation).
- CCEER-93-5 Maragakis, E., M. Saiidi, S. Feng, and L. Flournoy, "Effects of Hinge Restrainers on the Response of the San Gregorio Bridge During the Loma Prieta Earthquake," (in final preparation) Civil Engineering Department, Report No. CCEER-93-5, University of Nevada, Reno.
- CCEER-93-6 Saiidi, M., E. Maragakis, S. Abdel-Ghaffar, S. Feng, and D. O'Connor, "Response of Bridge Hinge Restrainers During Earthquakes -Field Performance, Analysis, and Design," Civil Engineering Department, Report No. CCEER-93-6, University of Nevada, Reno, May 1993.
- CCEER-93-7 Wehbe, N., Saiidi, M., Maragakis, E., and Sanders, D., "Adequacy of Three Highway Structures in Southern Nevada for Spent Fuel Transportation, Civil Engineering Department, Report No. CCEER-93-7, University of Nevada, Reno, August 1993.
- CCEER-93-8 Roybal, J., Sanders, D.H., and Maragakis, E., "Vulnerability Assessment of Masonry in the Reno-Carson City Urban Corridor," Civil Engineering Department, Report No. CCEER-93-8, University of Nevada, Reno, May 1993.
- CCEER-93-9 Zafir, Z. and Siddharthan, R., "MOVLOAD: A Program to Determine the Behavior of Nonlinear Horizontally Layered Medium Under Moving Load," Civil Engineering Department, Report No. CCEER-93-9, University of Nevada, Reno, August 1993.
- CCEER-93-10 O'Connor, D.N., Saiidi, M., and Maragakis, E.A., "A Study of Bridge Column Seismic Damage Susceptibility at the Interstate 80/U.S. 395 Interchange in Reno, Nevada," Civil Engineering Department, Report No. CCEER-93-10, University of Nevada, Reno, October 1993.
- CCEER-94-1 Maragakis, E., B. Douglas, and E. Abdelwahed, "Preliminary Dynamic Analysis of a Railroad Bridge," Report CCEER-94-1, January 1994.
- CCEER-94-2 Douglas, B.M., Maragakis, E.A., and Feng, S., "Stiffness Evaluation of Pile Foundation of Cazenovia Creek Overpass," Civil Engineering Department, Report No. CCEER-94-2, University of Nevada, Reno, March 1994.
- CCEER-94-3 Douglas, B.M., Maragakis, E.A., and Feng, S., "Summary of Pretest Analysis of Cazenovia Creek Bridge," Civil Engineering Department, Report No. CCEER-94-3, University of Nevada, Reno, April 1994.
- CCEER-94-4 Norris, G.M. and Madhu, R., "Liquefaction and Residual Strength of Sands from Drained Triaxial Tests, Report 2," Civil Engineering Department, CCEER-94-4, University of Nevada, Reno, August 1994.

- CCEER-94-5 Saiidi, M., Hutchens, E., and Gardella, D., "Prestress Losses in a Post-Tensioned R/C Box Girder Bridge in Southern Nevada," Civil Engineering Department, CCEER-94-5, University of Nevada, Reno, August 1994.
- CCEER-95-1 Siddharthan, R., El-Gamal, M., and Maragakis, E.A., "Nonlinear Bridge Abutment , Verification, and Design Curves," Civil Engineering Department, CCEER-95-1, University of Nevada, Reno, January 1995.
- CCEER-95-2 Norris, G.M., Madhu, R., Valceschini, R., and Ashour, M., "Liquefaction and Residual Strength of Loose Sands from Drained Triaxial Tests," Report 2, Civil Engineering Department, Report No. CCEER-95-2, University of Nevada, Reno, February 1995.
- CCEER-95-3 Wehbe, N., Saiidi, M., Sanders, D., and Douglas, B., "Ductility of Rectangular Reinforced Concrete Bridge Columns with Moderate Confinement," Civil Engineering Department, Report No. CCEER-95-3, University of Nevada, Reno, July 1995.
- CCEER-95-4 Martin, T., Saiidi, M., and Sanders, D., "Seismic Retrofit of Column-Pier Cap Connections in Bridges in Northern Nevada," Civil Engineering Department, Report No. CCEER-95-4, University of Nevada, Reno, August 1995.
- CCEER-95-5 Darwish, I., Saiidi, M., and Sanders, D., "Experimental Study of Seismic Susceptibility Column-Footing Connections," Civil Engineering Department, Report No. CCEER-95-5, University of Nevada, Reno, September 1995.
- CCEER-95-6 Griffin, G., Saiidi, M., and Maragakis, E., "Nonlinear Seismic Response of Isolated Bridges and Effects of Pier Ductility Demand," Civil Engineering Department, Report No. CCEER-95-6, University of Nevada, Reno, November 1995.
- CCEER-95-7 Acharya, S., Saiidi, M., and Sanders, D., "Seismic Retrofit of Bridge Footings and Column-Footing Connections," Report for the Nevada Department of Transportation, Civil Engineering Department, Report No. CCEER-95-7, University of Nevada, Reno, November 1995.
- CCEER-95-8 Maragakis, E., Douglas, B., and Sandirasegaram, U., "Full-Scale Field Resonance Tests of a Railway Bridge," A Report to the Association of American Railroads, Civil Engineering Department, Report No. CCEER-95-8, University of Nevada, Reno, December 1995.
- CCEER-95-9 Douglas, B., Maragakis, E., and Feng, S., "System Identification Studies on Cazenovia Creek Overpass," Report for the National Center for Earthquake Engineering Research, Civil Engineering Department, Report No. CCEER-95-9, University of Nevada, Reno, October 1995.
- CCEER-96-1 El-Gamal, M.E. and Siddharthan, R.V., "Programs to Computer Translational Stiffness of Seat-Type Bridge Abutment," Civil Engineering Department, Report No. CCEER-96-1, University of Nevada, Reno, March 1996.
- CCEER-96-2 Labia, Y., Saiidi, M., and Douglas, B., "Evaluation and Repair of Full-Scale Prestressed Concrete Box Girders," A Report to the National Science Foundation, Research Grant CMS-9201908, Civil Engineering Department, Report No. CCEER-96-2, University of Nevada, Reno, May 1996.

- CCEER-96-3 Darwish, I., Saiidi, M., and Sanders, D., "Seismic Retrofit of R/C Oblong Tapered Bridge Columns with Inadequate Bar Anchorage in Columns and Footings," A Report to the Nevada Department of Transportation, Civil Engineering Department, Report No. CCEER-96-3, University of Nevada, Reno, May 1996.
- CCEER-96-4 Ashour, M., Pilling, P., Norris, G., and Perez, H., "The Prediction of Lateral Load Behavior of Single Piles and Pile Groups Using the Strain Wedge Model," A Report to the California Department of Transportation, Civil Engineering Department, Report No. CCEER-96-4, University of Nevada, Reno, June, 1996.
- CCEER-97-1-A Rimal, P. and Itani, A. "Sensitivity Analysis of Fatigue Evaluations of Steel Bridges", Center for Earthquake Research, Department of Civil Engineering, University of Nevada, Reno, Nevada Report No. CCEER-97-1-A, September, 1997.
- CCEER-97-1-B Maragakis, E., Douglas, B., and Sandirasegaram, U. "Full-Scale Field Resonance Tests of a Railway Bridge," A Report to the Association of American Railroads, Civil Engineering Department, University of Nevada, Reno, May, 1996.
- CCEER-97-2 Wehbe, N., Saiidi, M., and D. Sanders, "Effect of Confinement and Flares on the Seismic Performance of Reinforced Concrete Bridge Columns," Civil Engineering Department, Report No. CCEER-97-2, University of Nevada, Reno, September 1997.
- CCEER-97-3 Darwish, I., M. Saiidi, G. Norris, and E. Maragakis, "Determination of In-Situ Footing Stiffness Using Full-Scale Dynamic Field Testing," A Report to the Nevada Department of Transportation, Structural Design Division, Carson City, Nevada, Report No. CCEER-97-3, University of Nevada, Reno, October 1997.
- CCEER-97-4 Wehbe, N., and M. Saiidi, "User's manual for RCMC v. 1.2 : A Computer Program for Moment-Curvature Analysis of Confined and Unconfined Reinforced Concrete Sections," Center for Civil Engineering Earthquake Research, Department of Civil Engineering, University of Nevada, Reno, Nevada, Report No. CCEER-97-4, November, 1997.
- CCEER-97-5 Isakovic, T., M. Saiidi, and A. Itani, "Influence of new Bridge Configurations on Seismic Performance," Department of Civil Engineering, University of Nevada, Reno, Report No. CCEER-97-5, September, 1997.
- CCEER-98-1 Itani, A., Vesco, T. and Dietrich, A., "Cyclic Behavior of "as Built" Laced Members With End Gusset Plates on the San Francisco Bay Bridge" Center for Civil Engineering Earthquake Research, Department of Civil Engineering, University of Nevada, Reno, Nevada Report No. CCEER-98-1, March, 1998.
- CCEER-98-2 G. Norris and M. Ashour, "Liqueficiaion and Undraned response evaluation of Sands from Drained Formulation." Center for Civil Engineering Earthquake Research, Department of Civil Engineering, University of Nevada, Reno, Nevada, Report No. CCEER-98-2, May, 1998.
- CCEER-98-3 Qingbin, Chen, B. M. Douglas, E. Maragakis, and I. G. Buckle, "Extraction of Nonlinear Hysteretic Properties of Seismically Isolated Bridges from Quick-Release Field Tests", Center for Civil Engineering Earthquake Research, Department of Civil Engineering, University of Nevada, Reno, Nevada, Report No. CCEER-98-3, June, 1998.

- CCEER-98-4 Maragakis, E., B. M. Douglas, and C. Qingbin, "Full-Scale Field Capacity Tests of a Railway Bridge", Center for Civil Engineering Earthquake Research, Department of Civil Engineering, University of Nevada, Reno, Nevada, Report No. CCEER-98-4, June, 1998.
- CCEER-98-5 Itani, A., Douglas, B., and Woodgate, J., "Cyclic Behavior of Richmond-San Rafael Retrofitted Tower Leg". Center for Civil Engineering Earthquake Research, Department of Civil Engineering, University of Nevada, Reno. Report No. CCEER-98-5, June 1998
- CCEER-98-6 Moore, R., Saiidi, M., and Itani, A., "Seismic Behavior of New Bridges with Skew and Curvature". Center for Civil Engineering Earthquake Research, Department of Civil Engineering, University of Nevada, Reno. Report No. CCEER-98-6, October, 1998.
- CCEER-98-7 Itani, A and Dietrich, A, "Cyclic Behavior of Double Gusset Plate Connections", Center for Civil Engineering Earthquake Research, Department of Civil Engineering, University of Nevada, Reno, Nevada, Report No. CCEER-98-5, December, 1998.
- CCEER-99-1 Caywood, C., M. Saiidi, and D. Sanders, " Seismic Retrofit of Flared Bridge Columns With Steel Jackets," Civil Engineering Department, University of Nevada, Reno, Report No. CCEER-99-1, February 1999.
- CCEER-99-2 Mangoba, N., M. Mayberry, and M. Saiidi, "Prestress Loss in Four Box Girder Bridges in Northern Nevada," Civil Engineering Department, University of Nevada, Reno, Report No. CCEER-99-2, March 1999.
- CCEER-99-3 Abo-Shadi, N., M. Saiidi, and D. Sanders, "Seismic Response of Bridge Pier Walls in the Weak Direction", Civil Engineering Department, University of Nevada, Reno, Report No. CCEER-99-3, April 1999.
- CCEER-99-4 Buzick, A., and M. Saiidi, "Shear Strength and Shear Fatigue Behavior of Full-Scale Prestressed Concrete Box Girders", Civil Engineering Department, University of Nevada, Reno, Report No. CCEER-99-4, April 1999.
- CCEER-99-5 Randall, M., M. Saiidi, E. Maragakis and T. Isakovic, "Restrainer Design Procedures For Multi-Span Simply-Supported Bridges", Civil Engineering Department, University of Nevada, Reno, Report No. CCEER-99-5, April 1999.
- CCEER-99-6 Wehbe, N. and M. Saiidi, "User's Manual for RCMC v. 1.2, A Computer Program for Moment-Curvature Analysis of Confined and Unconfined Reinforced Concrete Sections", Civil Engineering Department, University of Nevada, Reno, Report No. CCEER-99-6, May 1999.
- CCEER-99-7 Burda, J. and A. Itani, "Studies of Seismic Behavior of Steel Base Plates," Civil Engineering Department, University of Nevada, Reno, Report No. CCEER-99-7, May 1999.
- CCEER-99-8 Ashour, M., and G. Norris, "Refinement of the Strain Wedge Model Program," Civil Engineering Department, University of Nevada, Reno, Report No. CCEER-99-8, March 1999.
- CCEER-99-9 Dietrich, A., and A. Itani, "Cyclic Behavior of Laced and Perforated Steel Members on the San Francisco-Oakland Bay Bridge," Civil Engineering Department, University, Reno. December 1999.

- CCEER 99-10 Itani, A., A. Dietrich, "Cyclic Behavior of Built Up Steel Members and their Connections," Civil Engineering Department, University of Nevada, Reno. December 1999.
- CCEER 99-11 Itani, A., J. Woodgate, "Axial and Rotational Ductility of BuiltUp Structural Steel Members," Civil Engineering Department, University of Nevada, Reno December 1999.
- CCEER-99-12 Sgambelluri, M., Sanders, D.H., and Saiidi, M.S., Behavior of One-Way Reinforced Concrete Bridge Column Hinges in the Weak Direction, Report No. Department of Civil Engineering, University of Nevada, Reno, December 1999.
- CCEER-99-13 Laplace, P., Sanders, D.H., Douglas, B, and Saiidi, M, Shake Table Testing of Flexure Dominated Reinforced Concrete Bridge Columns, Report No. Department of Civil Engineering, University of Nevada, Reno, December 1999.
- CCEER-99-14 Ahmad M. Itani, Jose A. Zepeda, and Elizabeth A. Ware "Cyclic Behavior of Steel Moment Frame Connections for the Moscone Center Expansion," December 1999.
- CCEER 00-1 Ashour, M., and Norris, G. "Undrained Lateral Pile and Pile Group Response in Saturated Sand", Civil Engineering Department, University of Nevada, Reno, Report No. CCEER-00-1, May 1999. January 2000.
- CCEER 00-2 Saiidi, M. and Wehbe, N., "A Comparison of Confinement Requirements in Different Codes for Rectangular, Circular, and Double-Spiral RC Bridge Columns," Civil Engineering Department, University of Nevada, Reno, Report No. CCEER-00-2, January 2000.
- CCEER 00-3 McElhaney, B., M. Saiidi, and D. Sanders, "Shake Table Testing of Flared Bridge Columns With Steel Jacket Retrofit," Civil Engineering Department, University of Nevada, Reno, Report No. CCEER-00-3, January 2000.
- CCEER 00-4 Martinovic, F., M. Saiidi, D. Sanders, and F. Gordaninejad, "Dynamic Testing of Non-Prismatic Reinforced Concrete Bridge Columns Retrofitted with FRP Jackets," Civil Engineering Department, University of Nevada, Reno, Report No. CCEER-00-4, January 2000.
- CCEER 00-5 Itani, A., and M. Saiidi, "Seismic Evaluation of Steel Joints for UCLA Center for Health Science Westwood Replacement Hospital," Civil Engineering Department, University of Nevada, Reno, Report No. CCEER-00-5, February 2000.
- CCEER 00-6 Will, J. and D. Sanders, "High Performance Concrete Using Nevada Aggregates," Civil Engineering Department, University of Nevada, Reno, Report No. CCEER-00-6, May 2000.
- CCEER 00-7 French, C., and M. Saiidi, "A Comparison of Static and Dynamic Performance of Models of Flared Bridge Columns ," Civil Engineering Department, University of Nevada, Reno, Report No. CCEER-00-7, October 2000.
- CCEER 00-8 Itani, A., H. Sedarat, "Seismic Analysis of the AISI LRFD Design Example of Steel Highway Bridges," Civil Engineering Department, University of Nevada, Reno, Report No. CCEER 00-08, November 2000.

- CCEER 00-9 Moore, J., D. Sanders, and M. Saiidi, "Shake Table Testing of 1960's Two Column Bent with Hinges Bases," Civil Engineering Department, University of Nevada, Reno, Report No. CCEER 00-09, December 2000.
- CCEER 00-10 Asthana, M., D. Sanders, and M. Saiidi, "One-Way Reinforced Concrete Bridge Column Hinges in the Weak Direction," Civil Engineering Department, University of Nevada, Reno, Report No. CCEER 00-10, April 2001.
- CCEER 01-1 Ah Sha, H., D. Sanders, M. Saiidi, "Early Age Shrinkage and Cracking of Nevada Concrete Bridge Decks," Civil Engineering Department, University of Nevada, Reno, Report No. CCEER 01-01, May 2001.
- CCEER 01-2 Ashour, M. and G. Norris, "Pile Group program for Full Material Modeling an Progressive Failure." Civil Engineering Department, University of Nevada, Reno, Report No. CCEER 01-02, July 2001.
- CCEER 01-3 Itani, A., C. Lanaud, and P. Dusicka, "Non-Linear Finite Element Analysis of Built-Up Shear Links." Civil Engineering Department, University of Nevada, Reno, Report No. CCEER 01-03, July 2001.
- CCEER 01-4 Saiidi, M., J. Mortensen, and F. Martinovic, "Analysis and Retrofit of Fixed Flared Columns with Glass Fiber-Reinforced Plastic Jacketing," Civil Engineering Department, University of Nevada, Reno, Report No. CCEER 01-4, August 2001
- CCEER 01-5 Saiidi, M., A. Itani, I. Buckle, and Z. Cheng," Performance of A Full-Scale Two-Story Wood Frame Structure Supported on Ever-Level Isolators," Civil Engineering Department, University of Nevada, Reno, Report No. CCEER 01-5, October 2001
- CCEER 01-6 Laplace, P., D. Sanders, and M. Saiidi, "Experimental Study and Analysis of Retrofitted Flexure and Shear Dominated Circular Reinforced Concrete Bridge Columns Subjected to Shake Table Excitation," Civil Engineering Department, University of Nevada, Reno, Report No. CCEER 01-6, June 2001.
- CCEER 01-7 Reppi, F., and D. Sanders, "Removal and Replacement of Cast-in-Place, Post-tensioned, Box Girder Bridge," Civil Engineering Department, University of Nevada, Reno, Report No. CCEER 01-7, December 2001.
- CCEER 02-1 Pulido, C., M. Saiidi, D. Sanders, and A. Itani, "Seismic Performance and Retrofitting of Reinforced Concrete Bridge Bents," Civil Engineering Department, University of Nevada, Reno, Report No. CCEER 02-1, January 2002.
- CCEER 02-2 Yang, Q., M. Saiidi, H. Wang, and A. Itani, "Influence of Ground Motion Incoherency on Earthquake Response of Multi-Support Structures," Civil Engineering Department, University of Nevada, Reno, Report No. CCEER 02-2, May 2002.
- CCEER 02-3 M. Saiidi, B. Gopalakrishnan, E. Reinhardt, and R. Siddharthan, A Preliminary Study of Shake Table Response of A Two-Column Bridge Bent on Flexible Footings Civil Engineering Department, University of Nevada, Reno, Report No. CCEER 02-03, June 2002.
- CCEER 02-4 Not Published

- CCEER 02-5 Banghart, A., Sanders, D., Saiidi, M., "Evaluation of Concrete Mixes for Filling the Steel Arches in the Galena Creek Bridge," Civil Engineering Department, University of Nevada, Reno, Report No. CCEER 02-05, June 2002.
- CCEER 02-6 Dusicka, P., Itani, A., Buckle, I. G., "Cyclic Behavior of Shear Links and Tower Shaft Assembly of San Francisco – Oakland Bay Bridge Tower" Civil Engineering Department, University of Nevada, Reno, Report No. CCEER 02-06, July 2002.
- CCEER 02-7 Mortensen, J., and M. Saiidi, " A Performance-Based Design Method for Confinement in Circular Columns," Civil Engineering Department, University of Nevada, Reno, Report No. CCEER 02-07, November 2002.
- CCEER 03-1 Wehbe, N., and M. Saiidi, "User's manual for SPMC v. 1.0 : A Computer Program for Moment-Curvature Analysis of Reinforced Concrete Sections with Interlocking Spirals," Center for Civil Engineering Earthquake Research, Department of Civil Engineering, University of Nevada, Reno, Nevada, Report No. CCEER-03-1, May, 2003.
- CCEER 03-2 Wehbe, N., and M. Saiidi, "User's manual for RCMC v. 2.0 : A Computer Program for Moment-Curvature Analysis of Confined and Unconfined Reinforced Concrete Sections," Center for Civil Engineering Earthquake Research, Department of Civil Engineering, University of Nevada, Reno, Nevada, Report No. CCEER-03-2, June, 2003.
- CCEER 03-3 Nada, H., D. Sanders, and M. Saiidi, " Seismic Performance of RC Bridge Frames with Architectural-Flared Columns," Civil Engineering Department, University of Nevada, Reno, Report No. CCEER 03-3, January 2003.
- CCEER 03-4 Reinhardt, E., M. Saiidi, and R. Siddharthan, " Seismic Performance of a CFRP/Concrete Bridge Bent on Flexible Footings." Civil Engineering Department, University of Nevada, Reno. Report No. CCEER 03-4, August 2003.
- CCEER 03-5 Johnson, N., M. Saiidi, A. Itani, and S. Ladhany, "Seismic Retrofit of Octagonal Columns with Pedestal and One-Way Hinge at the Base," Center for Civil Engineering Earthquake Research, Department of Civil Engineering, University of Nevada, Reno, Nevada, Report No. CCEER-03-5, August 2003.
- CCEER 03-6 Mortensen, C., M. Saiidi, and S. Ladhany, "Creep and Shrinkage Losses in Highly Variable Climates," Center for Civil Engineering Earthquake Research, Department of Civil Engineering, University of Nevada, Reno, Nevada, Report No. CCEER-03-6, September 2003.
- CCEER 03-7 Ayoub, C., M. Saiidi, and A. Itani, "A Study of Shape-Memory-Alloy-Reinforced Beams and Cubes," Center for Civil Engineering Earthquake Research, Department of Civil Engineering, University of Nevada, Reno, Nevada, Report No. CCEER-03-7, October 2003.
- CCEER 03-8 Chandane, S., D. Sanders, and M. Saiidi, "Static and Dynamic Performance of RC Bridge Bents with Architectural-Flared Columns," Center for Civil Engineering Earthquake Research, Department of Civil Engineering, University of Nevada, Reno, Nevada, Report No. CCEER-03-8, November 2003.
- CCEER 04-1 Olaegbe, C., and Saiidi, M., "Effect of Loading History on Shake Table Performance of A Two-Column Bent with Infill Wall," Center for Civil Engineering Earthquake Research, Department of Civil Engineering, University of Nevada, Reno, Nevada, Report No. CCEER-04-1, January 2004.

- CCEER 04-2 Johnson, R., Maragakis, E., Saiidi, M., and DesRoches, R., "Experimental Evaluation of Seismic Performance of SMA Bridge Restrainers," Center for Civil Engineering Earthquake Research, Department of Civil Engineering, University of Nevada, Reno, Nevada, Report No. CCEER-04-2, February 2004.
- CCEER 04-3 Moustafa, K., Sanders, D., and Saiidi, M., "Impact of Aspect Ratio on Two-Column Bent Seismic Performance," Center for Civil Engineering Earthquake Research, Department of Civil Engineering, University of Nevada, Reno, Nevada, Report No. CCEER-04-3, February 2004.
- CCEER 04-4 Maragakis, E., Saiidi, M., Sanchez-Camargo, F., and Elfass, S., "Seismic Performance of Bridge Restrainers At In-Span Hinges," Center for Civil Engineering Earthquake Research, Department of Civil Engineering, University of Nevada, Reno, Nevada, Report No. CCEER-04-4, March 2004.
- CCEER 04-5 Ashour, M., Norris, G. and Elfass, S., "Analysis of Laterally Loaded Long or Intermediate Drilled Shafts of Small or Large Diameter in Layered Soil," Center for Civil Engineering Earthquake Research, Department of Civil Engineering, University of Nevada, Reno, Nevada, Report No. CCEER-04-5, June 2004.
- CCEER 04-6 Correal, J., Saiidi, M. and Sanders, D., "Seismic Performance of RC Bridge Columns Reinforced with Two Interlocking Spirals," Center for Civil Engineering Earthquake Research, Department of Civil Engineering, University of Nevada, Reno, Nevada, Report No. CCEER-04-6, August 2004.
- CCEER 04-7 Dusicka, P., Itani, A. and Buckle, I., "Cyclic Response and Low Cycle Fatigue Characteristics of Plate Steels," Center for Civil Engineering Earthquake Research, Department of Civil Engineering, University of Nevada, Reno, Nevada, Report No. CCEER-04-7, November 2004.
- CCEER 04-8 Dusicka, P., Itani, A. and Buckle, I., "Built-up Shear Links as Energy Dissipaters for Seismic Protection of Bridges," Center for Civil Engineering Earthquake Research, Department of Civil Engineering, University of Nevada, Reno, Nevada, Report No. CCEER-04-8, November 2004.
- CCEER 04-9 Sureshkumar, K., Saiidi, S., Itani, A. and Ladkany, S., "Seismic Retrofit of Two-Column Bents with Diamond Shape Columns," Center for Civil Engineering Earthquake Research, Department of Civil Engineering, University of Nevada, Reno, Nevada, Report No. CCEER-04-9, November 2004.
- CCEER 05-1 Wang, H. and Saiidi, S., "A Study of RC Columns with Shape Memory Alloy and Engineered Cementitious Composites," Center for Civil Engineering Earthquake Research, Department of Civil Engineering, University of Nevada, Reno, Nevada, Report No. CCEER-05-1, January 2005.
- CCEER 05-2 Johnson, R., Saiidi, S. and Maragakis, E., "A Study of Fiber Reinforced Plastics for Seismic Bridge Restrainers," Center for Civil Engineering Earthquake Research, Department of Civil Engineering, University of Nevada, Reno, Nevada, Report No. CCEER-05-2, January 2005.
- CCEER 05-3 Carden, L.P., Itani, A.M., Buckle, I.G., "Seismic Load Path in Steel Girder Bridge Superstructures," Center for Civil Engineering Earthquake Research, Department of Civil Engineering, University of Nevada, Reno, Nevada, Report No. CCEER-05-3, January 2005.

- CCEER 05-4 Carden, L.P., Itani, A.M., Buckle, I.G, "Seismic Performance of Steel Girder Bridge Superstructures with Ductile End Cross Frames and Seismic Isolation," Center for Civil Engineering Earthquake Research, Department of Civil Engineering, University of Nevada, Reno, Nevada, Report No. CCEER-05-4, January 2005.
- CCEER 05-5 Goodwin, E., Maragakis, M., Itani, A. and Luo, S., "Experimental Evaluation of the Seismic Performance of Hospital Piping Subassemblies," Center for Civil Engineering Earthquake Research, Department of Civil Engineering, University of Nevada, Reno, Nevada, Report No. CCEER-05-5, February 2005.
- CCEER 05-6 Zadeh M. S., Saiidi, S, Itani, A. and Ladkany, S., "Seismic Vulnerability Evaluation and Retrofit Design of Las Vegas Downtown Viaduct," Center for Civil Engineering Earthquake Research, Department of Civil Engineering, University of Nevada, Reno, Nevada, Report No. CCEER-05-6, February 2005.
- CCEER 05-7 Phan, V., Saiidi, S. and Anderson, J., "Near Fault (Near Field) Ground Motion Effects on Reinforced Concrete Bridge Columns" Center for Civil Engineering Earthquake Research, Department of Civil Engineering, University of Nevada, Reno, Nevada, Report No. CCEER-05-7, August 2005.
- CCEER 05-8 Carden, L., Itani, A. and Laplace, P., "Performance of Steel Props at the UNR Fire Science Academy subjected to Repeated Fire" Center for Civil Engineering Earthquake Research, Department of Civil Engineering, University of Nevada, Reno, Nevada, Report No. CCEER-05-8, August 2005.
- CCEER 05-9 Yamashita, R. and Sanders, D., "Shake Table Testing and an Analytical Study of Unbonded Prestressed Hollow Concrete Column Constructed with Precast Segments" Center for Civil Engineering Earthquake Research, Department of Civil Engineering, University of Nevada, Reno, Nevada, Report No. CCEER-05-9, August 2005.
- CCEER 05-10 Moustafa, K. Sanders, D., and Saiidi, M., "Seismic Behavior of R/C Bridge Bents with Architectural-Flared Columns Including both Horizontal and Vertical Gaps," Center for Civil Engineering Earthquake Research, Department of Civil Engineering, University of Nevada, Reno, Nevada, Report No. CCEER-05-10, February 2005.
- CCEER 05-11 Carden, L., Itani, A., and Peckan, G., "Recommendations for the Design of Beams and Posts in Bridge Falsework," Center for Civil Engineering Earthquake Research, Department of Civil Engineering, University of Nevada, Reno, Nevada, Report No. CCEER-05-11, October 2005.
- CCEER 06-01 Cheng, Z., Saiidi, M., and Sanders, D., "Development of a Seismic Design Method for Reinforced Concrete Two-Way Bridge Column Hinges," Center for Civil Engineering Earthquake Research, Department of Civil Engineering, University of Nevada, Reno, Nevada, Report No. CCEER-06-01, February 2006.
- CCEER 06-02 Johnson, N., Saiidi, M., and Sanders, D., "Large-Scale Experimental and Analytical Studies of a Two-Span Reinforced Concrete Bridge System," Center for Civil Engineering Earthquake Research, Department of Civil Engineering, University of Nevada, Reno, Nevada, Report No. CCEER-06-02, March 2006.
- CCEER 06-03 Saiidi, M., Ghasemi, H. and Tiras, A., "Seismic Design and Retrofit of Highway Bridges," Proceedings, Second US-Turkey Workshop, Center for Civil Engineering Earthquake Research, Department of Civil Engineering, University of Nevada, Reno, Nevada, Report No. CCEER-06-03, May 2006.

- CCEER 07-01 O'Brien, M., Saiidi, M. and Sadrossadat-Zadeh, M., "A Study of Concrete Bridge Columns Using Innovative Materials Subjected to Cyclic Loading," Center for Civil Engineering Earthquake Research, Department of Civil Engineering, University of Nevada, Reno, Nevada, Report No. CCEER-07-01, January 2007.
- CCEER 07-02 Sadrossadat-Zadeh, M. and Saiidi, M., "Effect of Strain rate on Stress-Strain Properties and Yield Propagation in Steel Reinforcing Bars," Center for Civil Engineering Earthquake Research, Department of Civil Engineering, University of Nevada, Reno, Nevada, Report No. CCEER-07-02, January 2007.
- CCEER 07-03 Sadrossadat-Zadeh, M. and Saiidi, M., " Analytical Study of NEESR-SG 4-Span Bridge Model Using OpenSees," Center for Civil Engineering Earthquake Research, Department of Civil Engineering, University of Nevada, Reno, Nevada, Report No. CCEER-07-03, January 2007.
- CCEER 07-04 Nelson, R., Saiidi, M., and Zadeh, S., "Experimental Evaluation of Performance of Conventional Bridge Systems," Center for Civil Engineering Earthquake Research, Department of Civil and Environmental Engineering, University of Nevada, Reno, Nevada, Report No. CCEER-07-04, October 2007.
- CCEER 07-05 Bahen, N., Sanders, D., "Strut-and-Tie Modeling for Disturbed Regions in Structural Concrete Members with Emphasis on Deep Beams," Center for Civil Engineering Earthquake Research, Department of Civil and Environmental Engineering, University of Nevada, Reno, Nevada, Report No. CCEER-07-05, December 2007.
- CCEER 07-06 Choi, H., Saiidi, M., and Somerville, P., "Effects of Near-Fault Ground Motion and Fault-Rupture on the Seismic Response of Reinforced Concrete Bridges," Center for Civil Engineering Earthquake Research, Department of Civil and Environmental Engineering, University of Nevada, Reno, Nevada, Report No. CCEER-07-06, December 2007.
- CCEER 07-07 Ashour, M., Norris, G., "Report and User Manual on Strain Wedge Model Computer Program for Files and Large Diameter Shafts with LRFD Procedure," Center for Civil Engineering Earthquake Research, Department of Civil and Environmental Engineering, University of Nevada, Reno, Nevada, Report No. CCEER-07-07, October 2007.
- CCEER 08-01 Doyle, K. and Saiidi, M., "Seismic Response of Telescopic Pipe Pin Connections," Center for Civil Engineering Earthquake Research, Department of Civil and Environmental Engineering, University of Nevada, Reno, Nevada, Report No. CCEER-08-01, February 2008.
- CCEER 08-02 Taylor, M. and Sanders, D., "Seismic Time History Analysis and Instrumentation of the Galena Creek Bridge," Center for Civil Engineering Earthquake Research, Department of Civil and Environmental Engineering, University of Nevada, Reno, Nevada, Report No. CCEER-08-02, April 2008.